

6750

NATIONAL LIBRARY
OTTAWA



BIBLIOTHÈQUE NATIONALE
OTTAWA

NAME OF AUTHOR. IN DUPURU KOTA REDDY.....
TITLE OF THESIS. MAGNETOTELLURIC SOUNDING
.....IN CENTRAL ALBERTA.....
.....
UNIVERSITY.....of ALBERTA.....
DEGREE FOR WHICH THESIS WAS PRESENTED...Ph.D.....
YEAR THIS DEGREE GRANTED.....1970.....

Permission is hereby granted to THE NATIONAL LIBRARY
OF CANADA to microfilm this thesis and to lend or sell copies
of the film.

The author reserves other publication rights, and
neither the thesis nor extensive extracts from it may be
printed or otherwise reproduced without the author's
written permission.

(Signed).....*Kota Reddy*.....

PERMANENT ADDRESS:

.....I. K. REDDY.....
.....DEPT. OF PHYSICS
.....UNIVERSITY OF ALBERTA

DATED...*Oct. 5*.....1970

EDMONTON

NL-91 (10-68)

Home address

MODEGUNTA, VEGUR(P.O)
KOVUR (Tq), NELLORE(Dt.)
ANDHRA PRADESH
INDIA

THE UNIVERSITY OF ALBERTA

MAGNETOTELLURIC SOUNDING IN CENTRAL ALBERTA

by



INDUPURU KOTA REDDY

A THESIS

SUBMITTED TO THE FACULTY OF GRADUATE STUDIES
IN PARTIAL FULFILMENT OF THE REQUIREMENTS FOR THE DEGREE
OF DOCTOR OF PHILOSOPHY

DEPARTMENT OF PHYSICS

EDMONTON, ALBERTA

FALL, 1970

UNIVERSITY OF ALBERTA
FACULTY OF GRADUATE STUDIES

The undersigned certify that they have read, and recommend to the Faculty of Graduate Studies for acceptance, a thesis entitled MAGNETOTELLURIC SOUNDING IN CENTRAL ALBERTA submitted by Indupuru Kota Reddy in partial fulfilment of the requirements for the degree of Doctor of Philosophy.

.....*D. Kaulin*.....
Supervisor

.....*J. A. Jacobs*.....

.....*H. A. K. Charlesworth*.....

.....*G. H. Cumming*.....

.....*M. Razavy*.....

.....*Theodore R. Madder*.....
External Examiner

Date September 18, 1970.

ABSTRACT

Magnetotelluric measurements were made in the period range 1 - 1,000 seconds, at sixteen different sites in the plains of central Alberta and in the Rocky Mountains. Tensor impedances, tensor apparent resistivities in principal directions, magnetic and telluric field polarization parameters, and coherencies between the vertical component of the magnetic field and horizontal components of the magnetotelluric fields were computed for each site using digital spectral analyses techniques. The results indicate that the magnetotelluric fields in the Plains of central Alberta are controlled by the strike of the contacts of the undeformed sedimentary rocks of the Plains on the one hand with the crystalline rocks of the underlying Precambrian basement and the deformed sedimentary rocks of the Rocky Mountains on the other. One dimensional models derived from the apparent resistivities for E-polarization are consistent with the known sedimentary section. Magnetotelluric results in the Rocky Mountains and in the foothills are not invariant and are assumed to be affected by local three-dimensional structures.

ACKNOWLEDGEMENTS

I wish to express my sincere thanks to Dr. D. Rankin for suggesting the thesis topic and providing guidance and assistance throughout this project.

I would like to thank Dr. W. J. Peeples for very helpful discussions and his collaboration in many aspects of this work.

I am grateful to Mr. M. D. Burke for his assistance in operating the recording equipment and in digitizing the data.

My thanks to Mr. N. Ouellette who spent many long hours in collecting and digitizing the data. I would also like to acknowledge the assistance of Mr. A. B. Mclellan during the field operations.

During the course of this research the author was supported by a Graduate Teaching Assistantship from the Department of Physics, University of Alberta, and by the National Research Council of Canada.

TABLE OF CONTENTS

	Page
ABSTRACT	i
ACKNOWLEDGEMENTS	iii
LIST OF ILLUSTRATIONS	vi
CHAPTER 1 INTRODUCTION	1
1.1 Purpose of the magnetotelluric sounding	1
1.2 Historical review of the magnetotelluric method	2
1.3 Magnetotelluric source fields	5
1.4 Geology and Geophysics of the area	9
1.5 Outline of the thesis	16
CHAPTER 2 MAGNETOTELLURIC THEORY	
2.1 Basic theory	18
2.2 Magnetotelluric fields over an isotropic, horizontally layered earth	21
2.3 Magnetotelluric fields over a multi-layered anisotropic earth	27
2.4 Magnetotelluric effect of dipping anisotropies	42
2.5 Magnetotelluric effect in the case of lateral inhomogeneities	57

	v
	Page
CHAPTER 3	
DETECTION AND ANALYSES OF THE	
MAGNETOTELLURIC SIGNALS	
3.1 Detection	65
3.2 Digital processing	67
3.3 Spectral computations	69
3.4 Analyses of magnetotelluric	70
signals	
3.5 Polarization parameters of the	75
magnetotelluric fields	
3.6 Vertical magnetic field, H_z	76
CHAPTER 4	
MAGNETOTELLURIC SOUNDING RESULTS	79
FOR CENTRAL ALBERTA	
CHAPTER 5	
INTERPRETATION	
5.1 Interpretation	125
5.2 Summary	148
5.3 Suggestions for future	150
work	
BIBLIOGRAPHY	151
APPENDIX I	
Matrix iteration of magnetotelluric	A1
fields in a multi-layered anisotropic	
earth	
APPENDIX II	
Spectral Analyses	A5

LIST OF ILLUSTRATIONS

Figure	Page
1.1 The geomagnetic pulsation spectrum for the lower frequencies (Campbell, 1966)	7
1.2 Main structural elements of western Canada and magnetotelluric sounding area	10
1.3 Lithology of the Precambrian basement (Garland and Burwash, 1959), Precambrian basement contours and magnetotelluric sounding sites in central Alberta.	12
1.4 Crustal structure under central Alberta (Basham, 1967)	15
2.1 Skin depth as a function of period and resistivity	20
2.2 (n+1) layer earth model	22
2.3 Relationship of conductivity anisotropy to coordinate axes	30
2.4a Tensor impedance elements at the surface of multi-layered anisotropic earth in the measuring directions (x and y)	39

2.4b	Tensor impedance elements at the surface of a multi-layered anisotropic earth in the principal directions (x' and y') at the surface	40
2.5	Relationship of axes of aniso- tropy to the measuring axes in the m^{th} layer	44
2.6a	Tensor apparent resistivity curves for a three layer anisotropic model in the measuring directions for various values of α	51
2.6b	Tensor apparent resistivity curves for a three layer anisotropic model in the strike and dip directions for various values of α	52
2.7a	Tensor apparent resistivity curves for a three layer anisotropic model in the measuring directions for various values of χ	54
2.7b	Tensor apparent resistivity curves for a three layer anisotropic model in the strike and dip directions for various values of χ	55
2.8	Apparent resistivity curves for H and E-polarizations over a two-dimensional structure for three different sounding sites situated along a traverse normal to the strike (after Patrick and Bostick, 1969)	61

2.9	Magnetic and electric field variations along a traverse normal to the strike for the model shown in Fig. 2.8 for 4 seconds period	63
3.1	A block diagram of the magneto- telluric recording system	66
3.2	Calibrated amplitude and phase response for the telluric and magnetic field detection systems	68
4.1	Magnetotelluric results for Alder Flats	83
4.2	Magnetotelluric results for Bonnyville	84
4.2a	Aeromagnetic map of Bonnyville area	85
4.3	Magnetotelluric results for Camp Creek	89
4.4	Magnetotelluric results for Carrot Creek	91
4.5	Magnetotelluric results for Donalda	93
4.6	Magnetotelluric results for Foot Hills	95
4.7	Magnetotelluric results for Fox Creek	97
4.8	Magnetotelluric results for Gregg Lake	99

4.9	Magnetotelluric results for Meanook	101
4.9a	Aeromagnetic map for Meanook area	102
4.10	Magnetotelluric results for Nordegg	105
4.11	Magnetotelluric results for NSR Crossing	108
4.12	Magnetotelluric results for Observatory	110
4.13	Magnetotelluric results for Red Deer	113
4.14	Magnetotelluric results for Smoky Lake	116
4.14a	Aeromagnetic map for Smoky Lake Area	117
4.15	Magnetotelluric results for Two Hills	120
4.15a	Aeromagnetic map for Two Hills Area	121
4.16	Magnetotelluric results for Vermilion	124
5.1	Tensor apparent resistivity curves along the major axis of anisotropy for central Alberta	128
5.2	Tensor apparent resistivity curves along the minor axis of aniso- tropy for central Alberta	129

5.3	The directions of the maximum tensor apparent resistivity for central Alberta	130
5.4	Theoretical apparent resistivity curves for a two layer earth model for various thicknesses and resistivities of the first layer	131
5.5	Electric field polarization angles for central Alberta	134
5.6	Magnetic field polarization angles for central Alberta	135
5.7	A geological cross section along north-east and south-west passing through Edmonton, and approximate location of magnetotelluric sounding sites	138
5.8	Directions of maximum tensor apparent resistivity for central Alberta stations. (Dashed arrows represent the polarization angles for telluric field)	141
5.9	One-dimensional models for four magnetotelluric sounding sites in central Alberta	144

5.10	One-dimensional model apparent resistivity curves and the observed apparent resistivities for E-polarization for four magnetotelluric sounding sites in central Alberta.	146
------	--	-----

CHAPTER 1

INTRODUCTION

1.1 Purpose of the Magnetotelluric Sounding

Since the inception of the magnetotelluric method in 1950, the Province of Alberta has been an important experimental site for this method. Several investigators (Garland and Webster, 1960; Srivastava, et al., 1963; Vozoff et al., 1963; Rankin and Reddy, 1969; Peeples, 1969) conducted magnetotelluric experiments in central and southern Alberta. A considerable ambiguity exists in the published results since, in addition to an expected variation from location to location, there exists a considerable variation in the published results from data obtained at the same site from one investigation to another. In the last decade considerable advances have been made in understanding the problems involved when complex magnetotelluric fields impinge on complex geologic structures. Together with the improvement in statistical methods, this understanding should lead to a better and more consistent interpretation of the subsurface of the earth. A regional magnetotelluric survey has been conducted in central Alberta whose prime objective is to apply these modern developments to investigate the electrical conductivity structure of the Earth's crust in this region.

1.2 Historical Review of the Magnetotelluric Method

Tikhonov (1950), and almost simultaneously, Kato and Kikuchi (1950) and Rikitake (1950, 1951), observing the correlation between the electric and magnetic field variations at the surface of the earth, considered the possibility of using these variations in order to find the conductivity at great depth. Cagniard (1953) showed that the interpretation could be carried out in a practical manner regardless of the depth by applying the law of similitude. This method consists of matching the experimental results, plotted to a suitable scale, with a set of master curves.

The master curves of Cagniard are constructed by solving the boundary value problem for a horizontally stratified earth under the assumption of plane electromagnetic waves incident on the surface of the earth. It is easily shown that in practice, the results are independent of the angle of incidence.

Wait (1954) has developed a first order correction to the simple Cagniard theory for the effect of a finite source, and has concluded that these corrections are required for sources which vary over horizontal distances of the order of, or less than, a skin depth. Price (1962) has developed a more rigorous theory for finite sources from which corrections can be computed in certain cases.

However, Madden and Nelson (1964), considering some realistic earth models, have shown that for cases of practical interest, the plane wave assumption is valid. Srivastava (1965) has shown that the effect of the source dimension can be neglected for periods less than 1000 seconds when determining moderate conductivities to shallow depths (10 - 20 km.) in the earth.

Following Cagniard's paper, magnetotelluric measurements have been made by many investigators (Cantwell, 1960; Wiese, 1962; Srivastava et al., 1963; Vozoff et al., 1963; Tikhonov and Berdichevskii, 1966; Hopkins and Smith, 1966; Swift, 1967; Adam, 1969; Vozoff et al., 1969; Kovtun and Chicherina, 1969; and others). In the last few years attempts have been made by Wu (1968), Chetaev (1966), Nabetani and Rankin (1969) and Patrick and Bostick (1969), to solve the inverse problem for direct interpretation of magnetotelluric data for one dimensional models.

The relationship between magnetic and telluric fields at the surface for various types of anisotropy in conductivity in single or multi-layered earth has been studied by Chetaev (1960, Cantwell (1960), Pokytanski (1961), Bostick and Smith (1962), Mann (1965) O'Brien and Morrison (1967), Praus and Petr (1969), Rankin and Reddy (1970) and others. These authors

expressing surface impedance/admittance as a tensor quantity, have provided methods to find the principal directions of conductivity anisotropy and the conductivity ratio between the major and minor axes of anisotropy in the case of anisotropic half-space, or in the case of multilayered half-space when only one of the layers is anisotropic. Madden and Nelson (1964), Swift (1967), Morrison et al., (1968), Sims and Bostick (1969) have presented methods to compute tensor impedance elements by using statistical and spectral techniques.

The response of the magnetotelluric field to vertical contacts and cylindrical inhomogeneities has also been examined in the last decade. Neves (1957) calculated apparent resistivities over dipping interfaces using finite difference techniques. Kovtun (1961) has discussed, in a general way, the magnetotelluric fields for two-dimensional inhomogeneous structures. d'Erceville and Kunetz (1962) and Rankin (1962) gave the analytical solutions for vertical fault and vertical dyke respectively. In both the cases the fault and dyke is of finite extent underlain by a homogeneous and isotropic half-space, and only the case of H-polarization (magnetic field vector parallel to the strike) is considered. Weaver (1963) solved the problem of infinite depth vertical contact for E- and

H-polarizations, numerically. Blake and Swift (1967) extended the work of Rankin (1962) and Weaver (1963) for a dyke or a long promontory. These latter results are incorrect for E-polarization case because of the improper boundary conditions used at the air-earth boundary in their calculations. Madden (see Swift, 1967) obtained solutions for two-dimensional problems via a transmission line analogy and Patrick and Bostick (1969) developed a finite difference scheme for two-dimensional magnetotelluric models.

Analog model studies for two and three dimensional bodies have been made by Rankin et al., (1965), Dosso (1966), Takaes (1969) and others. These authors suggested that the analog model studies can successfully be used to interpret magnetotelluric measurements over two and three dimensional structures.

1.3 Magnetotelluric Source Fields

The geomagnetic pulsations in the frequency range 1 - .001 Hz are the source fields for the magnetotelluric method presented in this thesis. The pulsations in this range are classified into two main classes; those of regular and continuous appearance called P_c , and those with an irregular form called P_i . The P_c group is further subdivided into five subgroups and the P_i

group into two subgroups (Jacobs et al., 1964). These groups and subgroups are presented in Table 1. The geomagnetic pulsation spectrum is shown in Fig. 1.1.

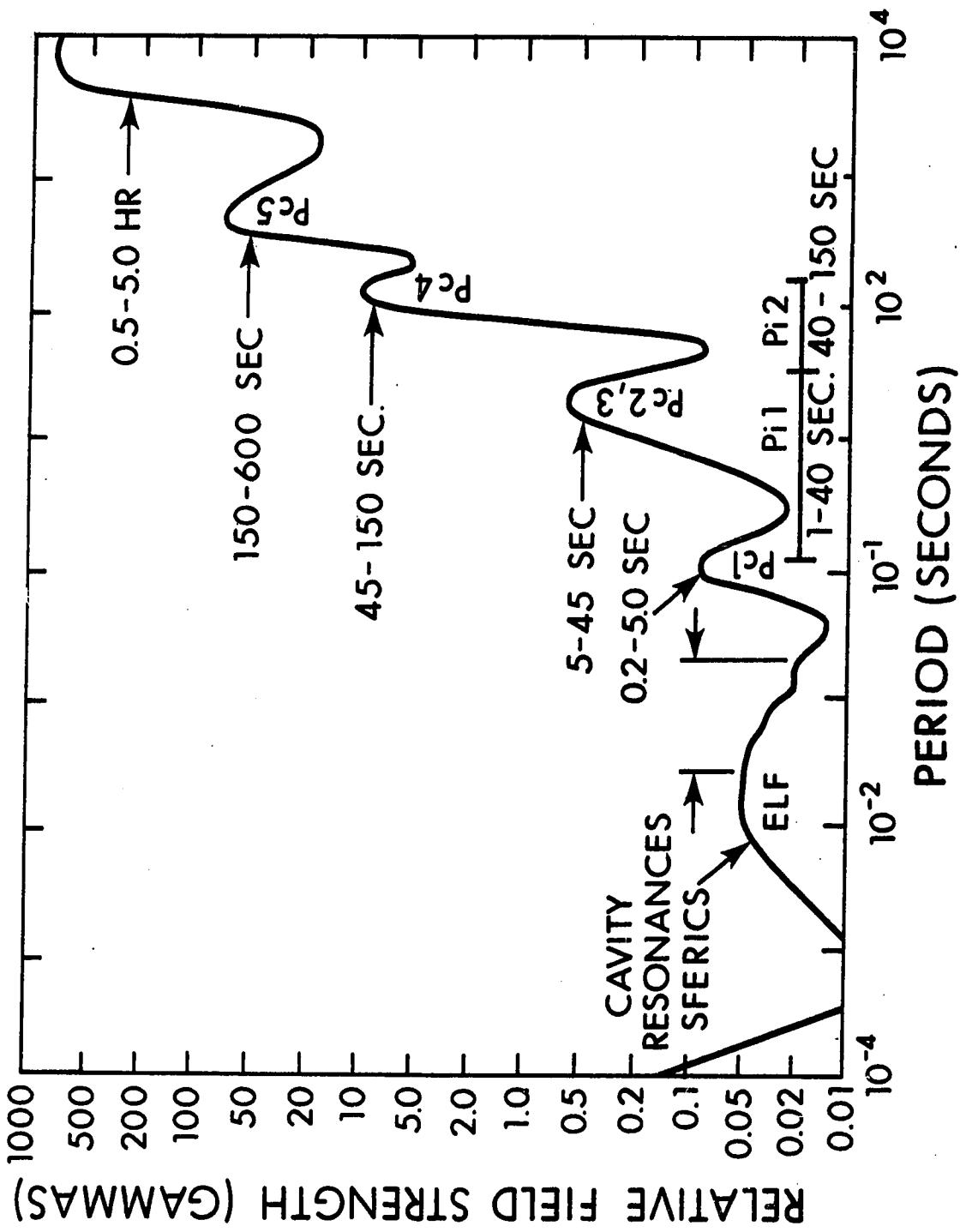
Table 1
Classification of Geomagnetic Micropulsations

Type	Period (Seconds)
Continuous pulsations	
Pc 1	0.2 - 5.0
Pc 2	5.0 - 10.0
Pc 3	10.0 - 45.0
Pc 4	45.0 - 150.0
Pc 5	150.0 - 600.0
Irregular pulsations	
Pi 1	1.0 - 40.0
Pi 2	40.0 - 150.0

It is generally accepted that continuous pulsations, except Pc 1, are generated as resonance oscillations in the magnetosphere of the earth under the influence of solar corpuscular streams. The appearance of different types of Pc depend on the characteristic of solar corpuscular streams which generate them.

Pc 1 pulsations, although they belong to the

Figure 1.1: The geomagnetic pulsation spectrum
for the lower frequencies (Campbell, 1966).



family of continuous pulsations, have completely different origin. They are generated in the interaction of energetic particles with magnetospheric plasma. Pi 2 pulsations are believed to originate by resonance of Alfvén waves in the cavity of the magnetosphere in the region of the beginning of the neutral sheet (Raspopov, 1968).

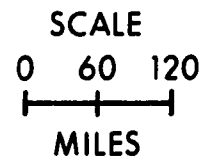
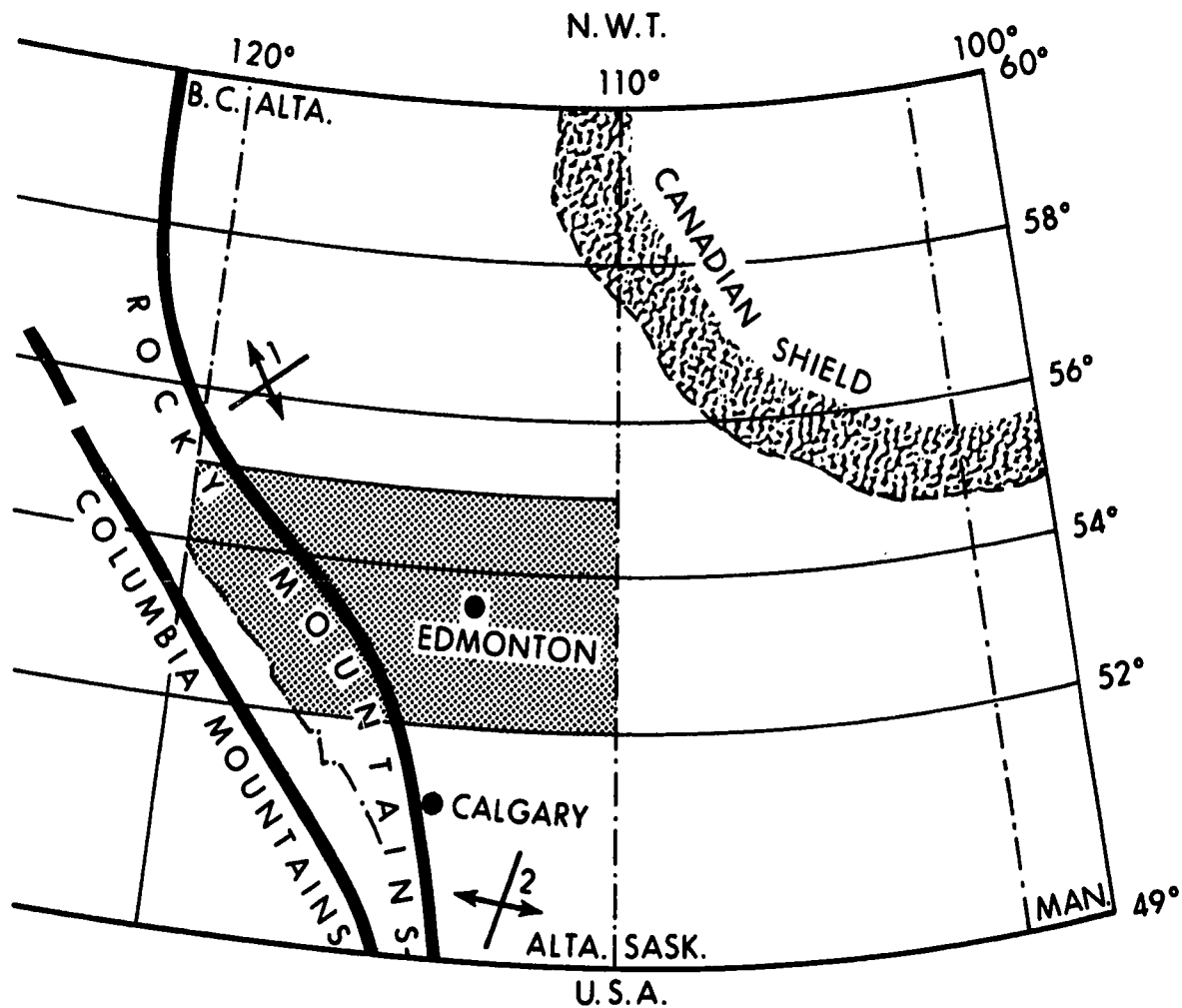
The Pc type pulsations have been found to be more prevalent in the daytime hours (Jacobs and Sinno, 1960). Pc2 and Pc3 pulsations usually have an amplitude of about 0.5 gamma. Campbell (1967) believes that the apparent duration of the signals is related to the sensitivity of the recording device. They are always present but sometimes too small to detect. Pc4 pulsations have an amplitude that ranges from 5 to 20 gammas in the higher latitudes and an event can last from 10 minutes to several hours. These are more active in the morning hours with maximum occurring around 0800 hours local time. Pc5 pulsations have the largest amplitude and are sometimes called pg's or giant pulsations. These pulsations occur most frequently near 0600 hours and 1800 hours local time. Pi 2 pulsations have been found to predominate in the nighttime and have a maximum around local midnight. They have also been detected in the daytime (Volker, 1968). Pi 1 pulsations often appear at the beginning of Pi 2 events and also appear as riders on the long period Pi 2 s'.

1.4 Geology and Geophysics of the Area

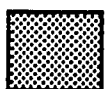
The area investigated during this study covers the central part of the Province of Alberta, bordered by the Rocky Mountains in the west and the Alberta-Saskatchewan provincial border in the east, and lies between the latitudes 52°N and 55°N. Geologically this area is a part of western Canada sedimentary basin. The subsurface geology of the basin has been studied extensively by many petroleum geologists and geophysicists with the help of well logs and geophysical data. A detailed account of the geology is given by McCrossan and Glaister (1966). A brief review of geological and geophysical knowledge of the area and its adjacent areas is given here.

Geologically western Canada may be divided into three distinct units, (1) the Canadian Shield, composed predominantly of crystalline and metamorphic rocks of overall intermediate composition with local areas of sedimentary and basic volcanic rocks, (2) the Interior Plains, underlain by gently dipping sedimentary strata of Phanerozoic age and (3) the Cordillera, a region of complexly folded and faulted sedimentary volcanic and metamorphic rocks of Precambrian and younger age extensively intruded by Mesozoic and Cenozoic plutonic rocks.

Figure 1.2: Main structural elements of western
Canada and magnetotelluric sounding area.



WESTERN BOUNDARY OF PRECAMBRIAN OUTCROP



MAGNETOTELLURIC SOUNDING AREA

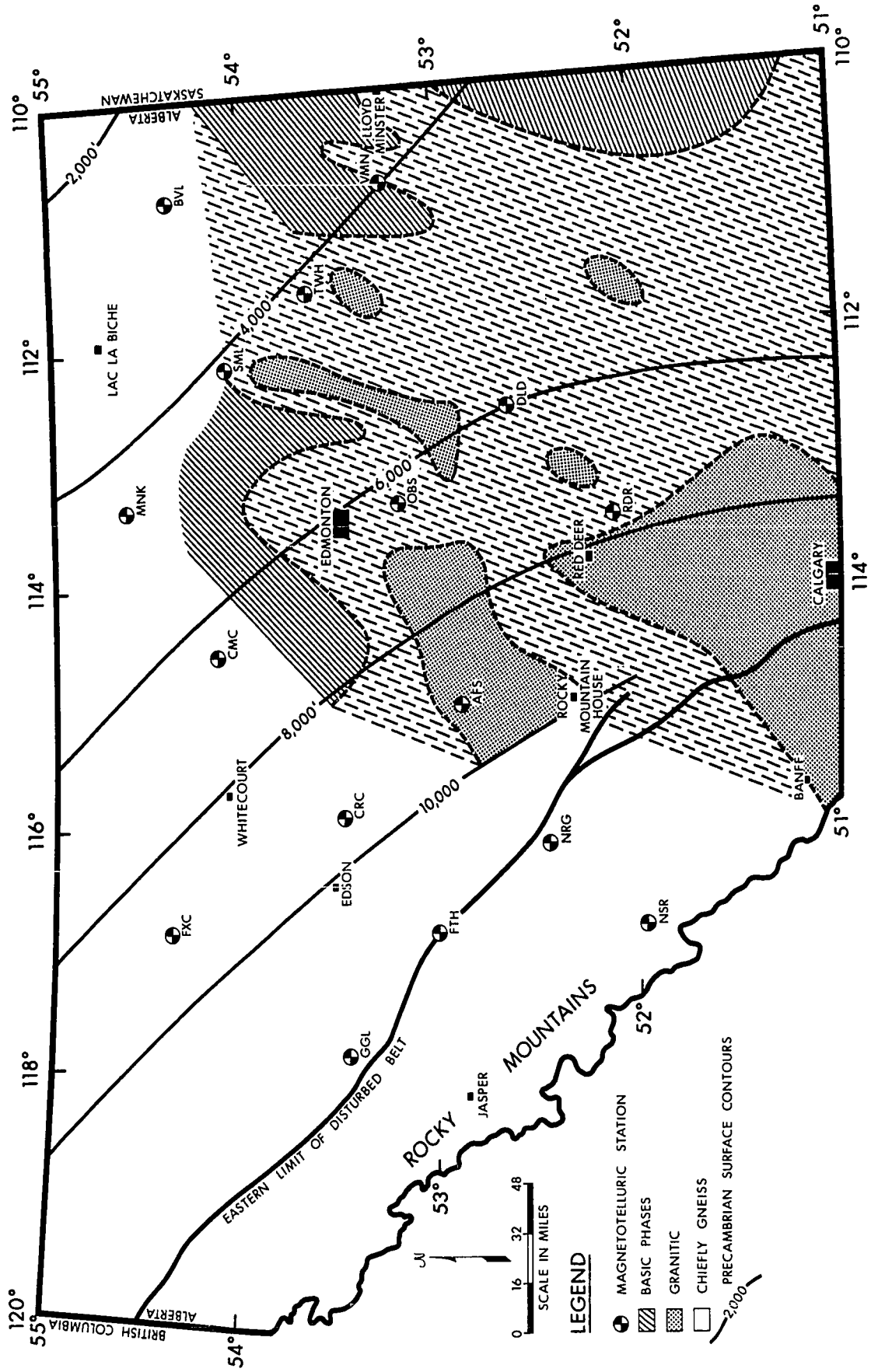
1 PEACE RIVER UPLIFT

2 SWEETGRASS ARCH

Figure 1.2 shows the different important structural elements and the area covered by the magnetotelluric sounding. Relative uplifts in the Precambrian belt extending across the epicontinental basis in the north-east direction are also reported by Sikabonyi (1957). Faults in the basement rocks are known in some areas (Haites, 1960; Burwash, 1965); and in others where faults have affected younger rocks. Faults of probable basement origin in northern Alberta strike northwest and northeast. Garland and Bower (1959) have shown basement faults in northeastern Alberta, on the basis of aeromagnetic data. These faults occur with main orientations, northwest and northeast, which seem parallel to the known direction of faulting in the adjacent shield areas of Alberta and Saskatchewan.

It has been found that the basement rocks in central Alberta are an extension of the Canadian Shield rather than of less metamorphosed predominantly sedimentary rocks of Precambrian age in the Rocky Mountains. Burwash (1957) has published a comprehensive report on the Precambrian based on core

Figure 1.3: Lithology of the Precambrian basement
(Garland and Burwash, 1959), Precambrian
basement contours and magnetotelluric sounding
sites in Central Alberta. (The contours
represent depth to the basement from Sea
level).



samples collected from all over central Alberta and adjoining areas. Garland and Burwash (1959) have interpreted the major part of the Bouguer gravity anomaly over central Alberta in terms of lithological changes in the Precambrian basement beneath the sedimentary section. Their lithological map of the basement based on gravity data and petrological and physical properties of the core samples is shown in Fig. 1.3, on which are superimposed the Precambrian basement contours and the magnetotelluric sounding sites. The geographical coordinates of the magnetotelluric sounding sites are given in Table 2.

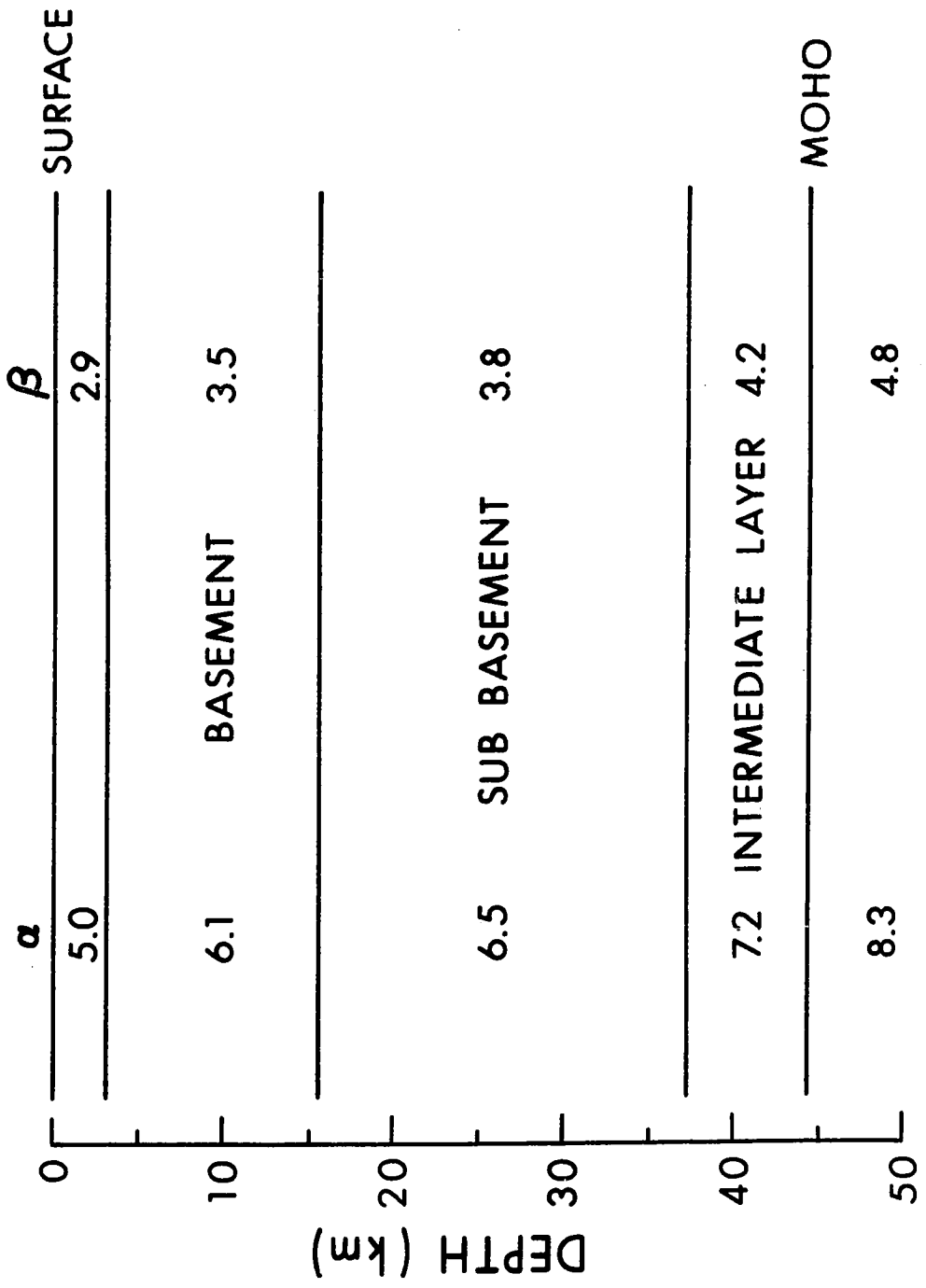
TABLE 2

Magnetotelluric		
Sounding Site	Latitude	Longitude
1. Alder Flats (AFS)	52° 57' N	114° 57' W
2. Bonnyville (BVL)	54° 24' N	110° 47' W
3. Camp Creek (CMC)	54° 13' N	114° 47' W
4. Carrot Creek (CRC)	53° 36' N	115° 52' W
5. Donalda (DLD)	52° 41' N	112° 37' W
6. Foot Hills (FTH)	53° 04' N	116° 48' W
7. Fox Creek (FXC)	54° 26' N	116° 55' W
8. Gregg Lake (GGL)	53° 30' N	117° 50' W
9. Meanook (MNK)	54° 37' N	113° 20' W
10. Nordegg (NRG)	52° 28' N	116° 05' W
11. NSR Crossing (NSR)	51° 56' N	116° 40' W
12. Observatory (OBS)	53° 13' N	113° 21' W
13. Red Deer (RDR)	52° 10' N	113° 27' W
14. Smoky Lake (SML)	54° 07' N	112° 11' W
15. Two Hills (TWH)	53° 44' N	113° 37' W
16. Vermilion (VMN)	53° 16' N	110° 44' W

(Letters in paranthesis represent abbreviations used in this thesis).

The sedimentary rocks, overlying the Precambrian basement have a total thickness varying from less than 4,000 ft. in the northeast corner of the area to greater than 15,000 ft. in the southwest corner (Fig. 1.3). The thicknesses

Figure 1.4: Crustal structure under Central Alberta (Basham 1967). α and β are P and S wave velocities respectively.



and the electrical properties of the individual layers in the sedimentary column differ from sounding site to sounding site. The foothills belt in the western side of the area is highly folded and thrust faulted, the faults dipping generally to the west and striking north or northwest.

Richard and Walker (1959) and Cumming and Kanasewich (1966) have conducted seismic refraction surveys in the plains of Southern Alberta to study the earth's crust in this region. Cumming and Kanasewich estimated the thickness of crust as 45 km. and found evidence for a three layer crust beneath the sediments, with velocities 6.1, 6.5 and 7.2 km/sec. Basham (1967) extrapolated the Cumming and Kanasewich's crustal seismic model to the central region (Rocky Mountain House - Alder Flats area). The extrapolated model is shown in Fig. 1.4. A low velocity channel in the upper mantle in south-central Alberta is at a depth of 120 km. and is approximately 30 km. in thickness (Kanasewich, 1966).

1.5 Outline of the thesis

In Chapter 2, electromagnetic theory applied to an isotropic and an anisotropic layered half-space is studied. A solution is obtained for the magnetotelluric effect in the case of multi-layered earth, each layer containing a dipping anisotropy, and a numerical example is presented. A short review on the effect of lateral inhomogeneities in magnetotelluric sounding is also

given in this chapter.

In Chapter 3, a brief description of the magnetotelluric field recording system and the techniques of handling and analyses of the magnetotelluric data are given.

Chapter 4 contains magnetotelluric sounding results for sixteen sites in central Alberta with a brief description of the results for each site.

In Chapter 5, an attempt is made to interpret magnetotelluric results from central Alberta in terms of local and regional geology. The effect of the source field is discussed. This chapter also contains summary and suggestions for future work.

CHAPTER 2

MAGNETOTELLURIC THEORY2.1 Basic Theory

The basic theory of the magnetotelluric method involves solving Maxwell's equations with appropriate boundary conditions. Maxwell's equations in a source free medium can be written as

$$\nabla \times \tilde{\mathbf{E}} = -\mu \frac{\partial \tilde{\mathbf{H}}}{\partial t} \quad 2.1 - 1a$$

$$\nabla \times \tilde{\mathbf{H}} = \tilde{\mathbf{J}} + \epsilon \frac{\partial \tilde{\mathbf{E}}}{\partial t} \quad 2.1 - 1b$$

$$\nabla \cdot \tilde{\mathbf{B}} = 0 \quad 2.1 - 1c$$

$$\nabla \cdot \tilde{\mathbf{E}} = 0 \quad 2.1 - 1d$$

$$\tilde{\mathbf{J}} = \sigma \tilde{\mathbf{E}}, \quad 2.1 - 1e$$

where the current density vector $\tilde{\mathbf{J}}$, the electrical conductivity σ , the magnetic permeability μ , the permittivity ϵ , the electric and magnetic total field vectors $\tilde{\mathbf{E}}$ and $\tilde{\mathbf{H}}$, are in rationalized MKS units.

Taking the curl of (2.1-1a) and substituting from (2.1-1b) for curl $\tilde{\mathbf{H}}$.

$$\nabla \times \nabla \times \tilde{\mathbf{E}} = -\sigma \mu \frac{\partial \tilde{\mathbf{E}}}{\partial t} - \epsilon \mu \frac{\partial^2 \tilde{\mathbf{E}}}{\partial t^2}. \quad 2.1-2a$$

Similarly taking the curl of (2.1-1b) and substituting for curl $\tilde{\mathbf{E}}$

$$\nabla \times \nabla \times \tilde{\mathbf{H}} = -\sigma \mu \frac{\partial \tilde{\mathbf{H}}}{\partial t} - \epsilon \mu \frac{\partial^2 \tilde{\mathbf{H}}}{\partial t^2}. \quad 2.1-2b$$

Using the vector identity in cartesian coordinate system,

$$\nabla \times \nabla \times \vec{\mathbf{A}} = \nabla(\nabla \cdot \vec{\mathbf{A}}) - \nabla \cdot \nabla \vec{\mathbf{A}} = \nabla(\nabla \cdot \vec{\mathbf{A}}) - \nabla^2 \vec{\mathbf{A}},$$

and equations (2.1-1c) and (2.1-1d), the wave equation can be written as

$$\nabla^2 \tilde{\mathbf{E}} - \sigma \mu \frac{\partial \tilde{\mathbf{E}}}{\partial t} - \epsilon \mu \frac{\partial^2 \tilde{\mathbf{E}}}{\partial t^2} = 0 \quad 2.1-3a$$

and

$$\nabla^2 \tilde{\mathbf{H}} - \sigma \mu \frac{\partial \tilde{\mathbf{H}}}{\partial t} - \epsilon \mu \frac{\partial^2 \tilde{\mathbf{H}}}{\partial t^2} = 0. \quad 2.1-3b$$

Assuming a time variation of the form,

$$\tilde{\mathbf{E}} = \vec{\mathbf{E}} \exp(-i \omega t)$$

$$\tilde{\mathbf{H}} = \vec{\mathbf{H}} \exp(-i \omega t)$$

where $i = \sqrt{-1}$ and ω is angular frequency, equations (2.1-3a) and (2.1-3b) simplify to

$$\nabla^2 \vec{\mathbf{E}} - k^2 \vec{\mathbf{E}} = 0 \quad 2.1-4a$$

$$\nabla^2 \vec{\mathbf{H}} - k^2 \vec{\mathbf{H}} = 0, \quad 2.1-4b$$

where

$$k^2 = -i \mu \omega \sigma + \epsilon \mu \omega^2. \quad 2.1-5$$

The general solution of the wave equation, in cartesian co-ordinate system, takes the form

$$\begin{bmatrix} \vec{\mathbf{H}} \\ \vec{\mathbf{E}} \end{bmatrix} = \begin{bmatrix} H_0 \\ E_0 \end{bmatrix} \exp(\vec{\mathbf{k}} \cdot \vec{\mathbf{r}}), \quad 2.1-6$$

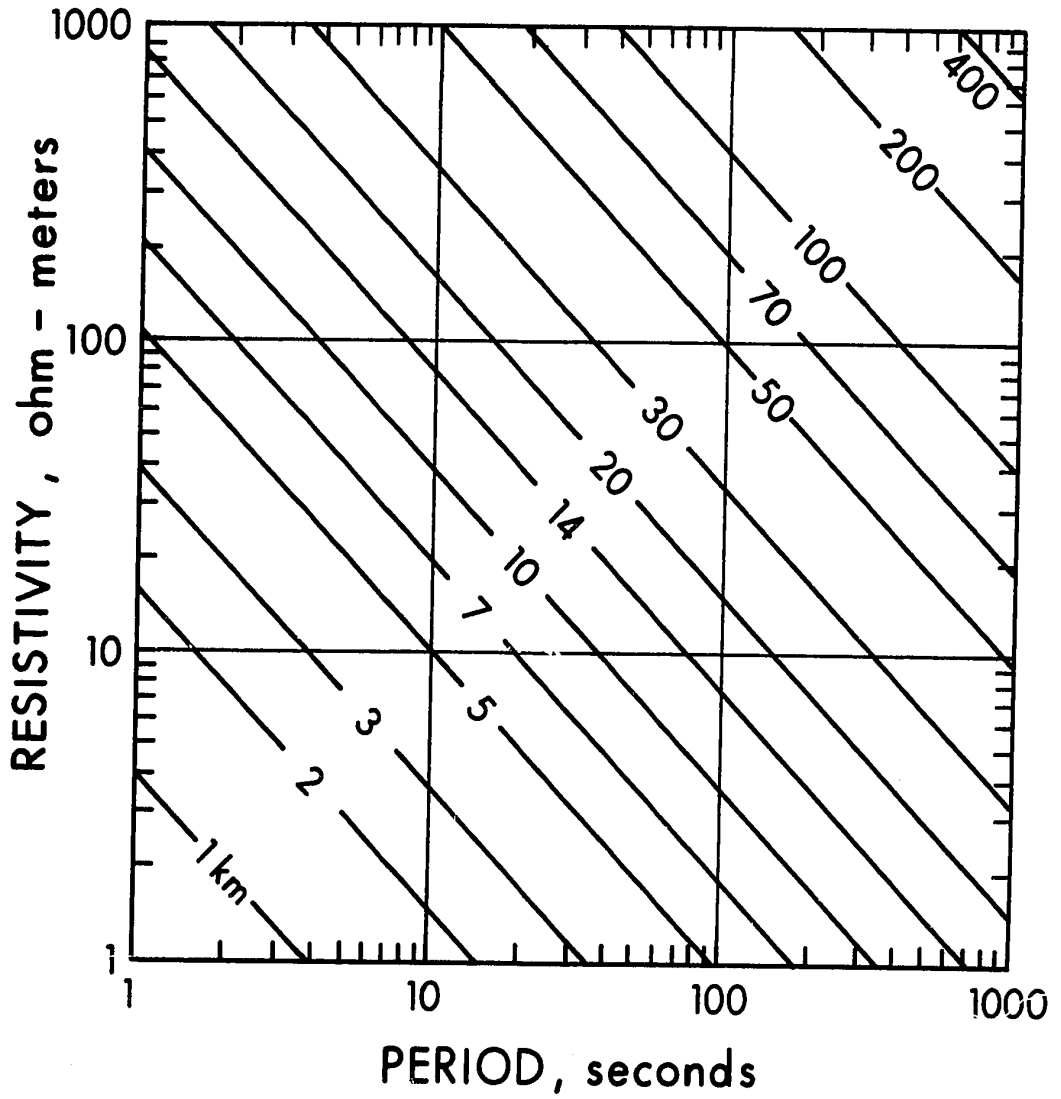
where $\vec{\mathbf{k}} = (k_x, k_y, k_z)$,

$$\vec{\mathbf{r}} = (x, y, z),$$

and H_0 and E_0 are constants.

In the frequency range (0.001 Hz - 1 Hz), which is of interest in the magnetotelluric method, the dis-

Figure 2.1: Skin depth as a function of period
and resistivity.



placement current term is negligible when compared to conduction current terms (i.e., $\epsilon \mu \omega^2 \ll \mu \omega \sigma$), for earth materials, and (2.1-5) reduces to

$$k^2 = -i \mu \omega \sigma. \quad 2.1-7$$

The wave amplitude in a conducting medium decays to $1/e$ in a distance $1/\text{Real}(k)$ where this distance is known as 'skin depth' and is given by

$$\delta = \sqrt{\frac{2}{\mu \omega \sigma}}. \quad 2.1-8$$

A skin depth chart for various periods and conductivities is shown in Figure 2.1.

2.2 Magnetotelluric fields over an isotropic, horizontally layered earth

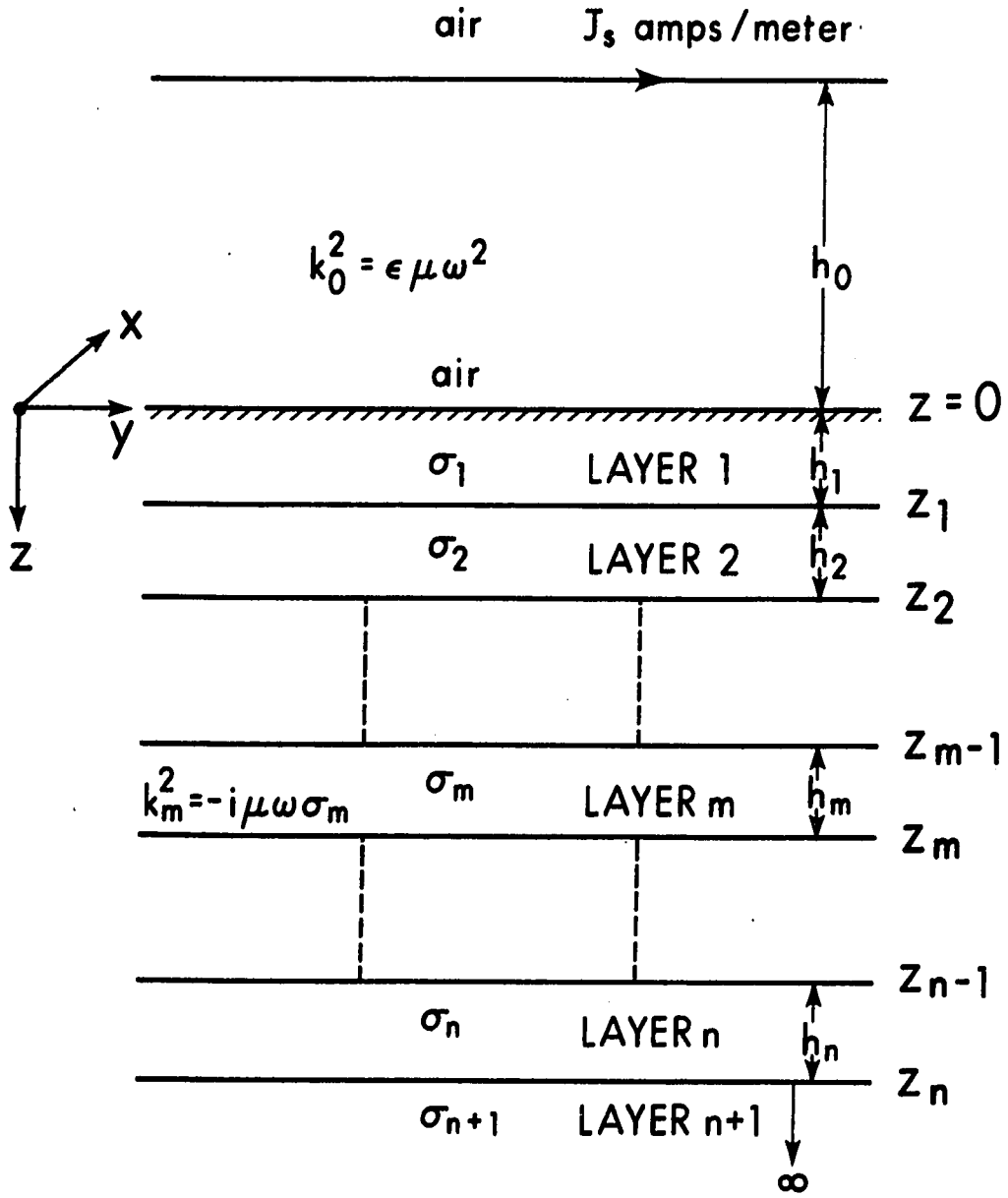
To construct a mathematical model for the magnetotelluric effect in the case of a multi-layered isotropic earth, consider a cartesian co-ordinate system with the following conditions.

1) The origin of the co-ordinate system coincides with the surface of the earth, and the z-axis extends vertically downwards.

2) The earth is divided into $(n+1)$ layers, with the $(n+1)^{\text{th}}$ layer extending downward to infinity.

3) A conductivity value σ_m and a thickness h_m is assigned to each of the $(n+1)$ layers, where m is the layer number.

Figure 2.2: $(n+1)$ layer earth model



4) The permeability μ and the permittivity ϵ are constants within each of the $(n+1)$ layers, and are equal to the permeability and permittivity of free space, μ_0 and ϵ_0 respectively.

5) The source is a current sheet situated at a height h_0 from the surface of the earth. The geometry of the model is depicted in Fig. 2.2.

The boundary conditions to be satisfied are 1) the tangential magnetic and electric fields are continuous at the horizontal interfaces except at the current sheet; 2) at the current sheet the horizontal components of the electric field are continuous but the magnetic field is discontinuous; and 3) the fields must vanish at infinity in the z -direction. The boundary conditions are expressed as follows,

$$\left. \begin{aligned} \vec{n} \times (\vec{H}_m - \vec{H}_{m-1}) &= 0 \\ \vec{n} \times (\vec{E}_m - \vec{E}_{m-1}) &= 0 \end{aligned} \right\} \text{ at } z = z_{m-1}, m = 1, 2, \dots, n$$

$$\left. \begin{aligned} \vec{n} \times (\vec{E}_- - \vec{E}_+) &= 0 \\ \vec{n} \times (\vec{H}_- - \vec{H}_+) &= \vec{J}_s \end{aligned} \right\} \text{ at } z = -h_0$$

$$\left. \begin{aligned} \vec{H} &\rightarrow 0 \\ \vec{E} &\rightarrow 0 \end{aligned} \right\} \text{ as } z \rightarrow \infty,$$

where \vec{n} is a unit vector in the z -direction, \vec{J}_s is the

current density in the sheet, \vec{H}_- , \vec{H}_+ and \vec{E}_- , \vec{E}_+ are the magnetic and electric fields above and below the current sheet, respectively.

For simplicity, let the current in the sheet flow in the y-direction with a surface current density \vec{J}_s amps/meter. A current sheet of this type generates a plane wave parallel to the y-z plane with a magnetic vector normal to the plane of incidence. With these assumptions the wave equation in the m^{th} layer can be written

$$\frac{\partial^2 H_{x,m}}{\partial z^2} - k_m^2 H_{x,m} = 0. \quad 2.2-1$$

The general solution of which takes the form

$$H_{x,m} = A_m \exp(\vec{k}_m \cdot \vec{r}) + B_m \exp(-\vec{k}_m \cdot \vec{r}). \quad 2.2-2$$

Since the source is assumed to be uniform

$$\vec{k} \cdot \vec{r} = k(z) \cdot z,$$

and equation (2.2-2) reduces to

$$H_{x,m} = A_m \exp(k_m [z - z_{m-1}]) + B_m \exp(-k_m [z - z_{m-1}]),$$

2.2-3

where A_m and B_m are complex constants which can be evaluated by the proper application of the boundary conditions. The corresponding equation for the electric field can be written, using (2.1-1b) and (2.1-1c),

$$\begin{aligned}
 E_{y,m} &= \frac{1}{\sigma_m} \frac{\partial H_{x,m}}{\partial z} \\
 &= \frac{k_m}{\sigma_m} \{A_m \exp(k_m [z-z_{m-1}]) - B_m \exp(-k_m [z-z_{m-1}])\}.
 \end{aligned}
 \tag{2.2-4}$$

Applying the boundary condition, that the tangential magnetic and electric fields are continuous at $z=z_m$, one gets from (2.2-3) and (2.2-4)

$$A_m = \left[\frac{1+\gamma_{m,m+1}}{2} A_{m+1} + \frac{1-\gamma_{m,m+1}}{2} B_{m+1} \right] \exp(-k_m h_m), \tag{2.2-5a}$$

$$B_m = \left[\frac{1-\gamma_{m,m+1}}{2} A_{m+1} + \frac{1+\gamma_{m,m+1}}{2} B_{m+1} \right] \exp(k_m h_m), \tag{2.2-5b}$$

where

$$\gamma_{m,m+1} = \frac{\sigma_m}{\sigma_{m+1}} \frac{k_{m+1}}{k_m}. \tag{2.2-6}$$

Since the lower boundary of the $(n+1)^{\text{th}}$ layer extends to infinity ($h_{n+1} \rightarrow \infty$), one can write

$$A_{n+1} = 0 \quad B_{n+1} = 1;$$

and the constants A_n and B_n for the n th layer can then be written as

$$A_n = \frac{1-\gamma_{n,n+1}}{2} \exp(-k_n h_n)$$

$$B_n = \frac{1+\gamma_{n,n+1}}{2} \exp(k_n h_n).$$

Iterating to the surface of the model, matching

tangential electric and magnetic fields at each horizontal interface, the constants A_1 and B_1 can be written,

$$A_1 = \left[\frac{1+\gamma_{1,2}}{2} A_2 + \frac{1-\gamma_{1,2}}{2} B_2 \right] \exp(-k_1 h_1) \quad 2.2-7a$$

$$B_1 = \left[\frac{1-\gamma_{1,2}}{2} A_2 + \frac{1+\gamma_{1,2}}{2} B_2 \right] \exp(k_1 h_1). \quad 2.2-7b$$

At the air earth interface ($z=0$), where the measurements are made, the magnetic and electric field vectors can be expressed in terms of A_1 and B_1 ,

$$H_{x,1} = H_{x,0} = A_1 + B_1 \quad 2.2-8a$$

$$E_{y,1} = E_{y,0} = \frac{k_1}{\sigma_1} [A_1 - B_1]. \quad 2.2-8b$$

The intrinsic impedance of the earth Z , can be defined

$$Z = \left. \frac{E_y}{H_x} \right|_{z=0} = \frac{k_1}{\sigma_1} \frac{A_1 - B_1}{A_1 + B_1}, \quad 2.2-9$$

and the apparent resistivity ρ^a is defined,

$$\rho^a = \frac{T}{2\pi\mu} \left| \frac{E_y}{H_x} \right|^2 = \frac{T}{2\pi\mu} |Z|^2 \quad 2.2-10$$

where

ρ^a = apparent resistivity in ohm-meters,

T = period of magnetotelluric disturbance in seconds,

E_y, H_x = electric and magnetic field disturbances in
rationalized MKS units

Z = intrinsic impedance in ohms

μ = magnetic permeability of the medium.

The intrinsic impedance at the surface of a multi-layered earth was obtained by Wait (1962), who defined the impedance in the lowest, $(n+1)^{th}$ layer, as

$$Z_{n+1} = \frac{\omega\mu}{k_{n+1}} \quad 2.2-11$$

and wrote the impedance of any intermediate layer

$$Z_m = \rho_m k_m \frac{Z_{m+1} + \rho_m k_m \tanh(k_m h_m)}{\rho_m k_m + Z_{m+1} \tanh(k_m h_m)} \quad 2.2-12$$

$$\text{where } \rho_m = \frac{1}{\sigma_m}.$$

Matching the impedance at each boundary, the impedance, at the surface, in this case takes the form

$$Z = Z_1 \Big|_{z=0} = \rho_1 k_1 \frac{Z_2 + \rho_1 k_1 \tanh(k_1 h_1)}{\rho_1 k_1 + Z_2 \tanh(k_1 h_1)}. \quad 2.2-13$$

2.3 Magnetotelluric fields over a multi-layered anisotropic earth.

The scalar impedance as defined in the previous section, allows interpretations only for homogeneous and isotropic layered earth models. In this section, the theory developed in section 2.2 will be extended to an anisotropic layered earth model in which one or

more layers are anisotropic in the horizontal (x-y) plane. Anisotropy in the horizontal plane may be due to banded structure of the rocks of which the medium is composed and/or due to two dimensional structures which allow the current to flow more freely in one direction than the other. In such cases the electric field in a particular direction may depend on magnetic field variations parallel to, as well as perpendicular to, its direction.

Cantwell (1960) developed a technique to determine the effect of anisotropy and/or two dimensional structures on magnetotelluric fields using the tensor relationships between the magnetic and electric fields,

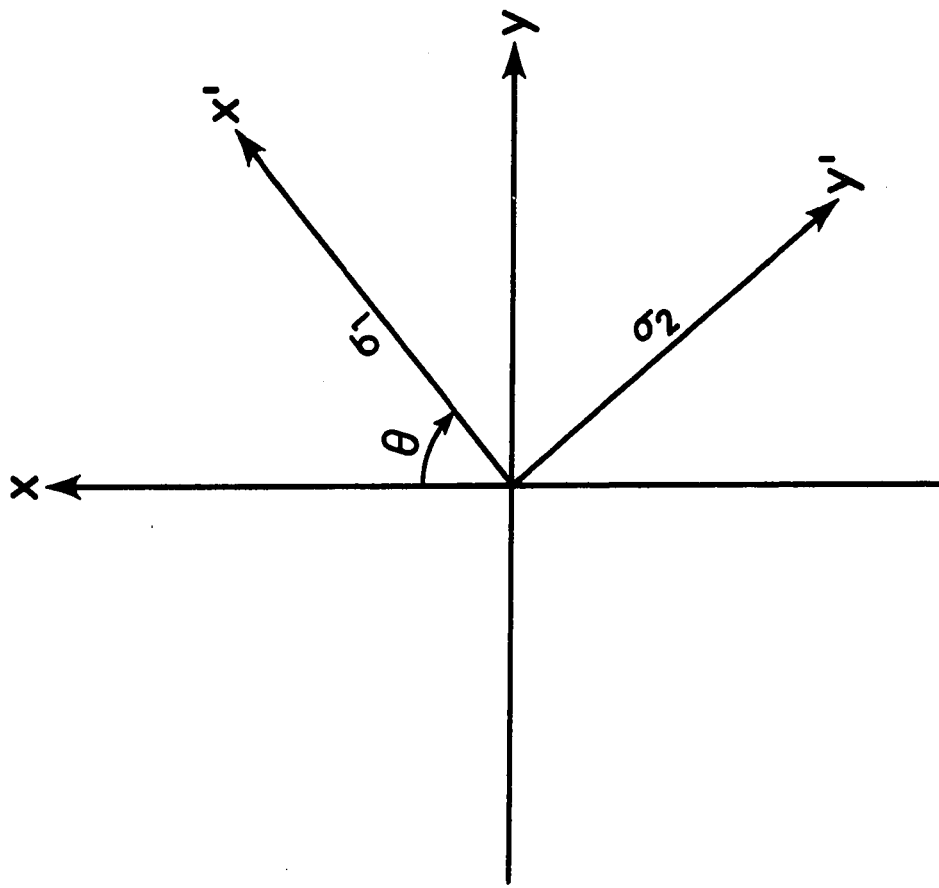
$$\begin{bmatrix} H_x \\ H_y \end{bmatrix} = \begin{bmatrix} Y_{xx} & Y_{xy} \\ Y_{yx} & Y_{yy} \end{bmatrix} \begin{bmatrix} E_x \\ E_y \end{bmatrix} \quad 2.3-1$$

where Y_{xx} , Y_{xy} , Y_{yx} and Y_{yy} are complex admittance elements. Bostick and Smith (1962) presented a computational technique for admittance elements. Pokityanski (1961) developed a method to determine azimuth and coefficient of anisotropy using tensor impedances rather than admittances. The tensor relationship between the magnetic and electric fields in terms of the impedance elements is

$$\begin{bmatrix} E_x \\ E_y \end{bmatrix} = \begin{bmatrix} Z_{xx} & Z_{xy} \\ Z_{yx} & Z_{yy} \end{bmatrix} \begin{bmatrix} H_x \\ H_y \end{bmatrix} \quad 2.3-2$$

where Z_{xy} , Z_{yx} are the principal impedances and Z_{xx} , Z_{yy} are the additional impedances caused by anisotropy and/or inhomogeneity. Madden and Nelson (1964), Swift (1967) and Bostick and Sims (1969) have studied the properties of these impedance elements and presented computational techniques for their computation from the measured electromagnetic fields. Mann (1965) has analyzed the problem of a plane wave incident on an anisotropic half-space and showed that there exist two skin depths corresponding to two principal directions of anisotropy. O'Brien and Morrison (1967) and Praus and Petr (1969) developed theory for multilayered anisotropic half-space and presented numerical examples for single layer anisotropy in a multi-layered earth. Rankin and Reddy (1970) studied the polarization properties of magnetotelluric fields in the case of single layer anisotropy and presented a technique to interpret magnetotelluric data from the polarization characteristics of the surface magnetotelluric fields. A brief derivation of the formulae for impedance elements in the case of multi-layered anisotropies is given below.

Figure 2.3: Relationship of conductivity anisotropy
to coordinate axes.



Using similar assumptions to those in Section 2.2 and assuming further that the current flows in an arbitrary direction in the current sheet, and that each layer is anisotropic in the horizontal plane with the principal axes x' and y' , and that the major conductivity axis is oriented at an angle θ to the x -axis (Fig. 2.3), the wave equations in the anisotropic layer, in the two principal directions of anisotropy can be written

$$\frac{\partial H_{x',m}}{\partial z^2} - k_{2,m}^2 H_{x',m} = 0 \quad 2.3-1a$$

$$\frac{\partial H_{y',m}}{\partial z^2} - k_{1,m}^2 H_{y',m} = 0, \quad 2.3-1b$$

where $H_{x',m}$ and $H_{y',m}$ are the magnetic field components in the two principal directions of anisotropy in the m th layer, and

$$k_{1,m}^2 = -i \omega \mu \sigma_{1,m} \quad 2.3-2a$$

$$k_{2,m}^2 = -i \omega \mu \sigma_{2,m} \quad 2.3-2b$$

$\sigma_{1,m}$ and $\sigma_{2,m}$ are the conductivities in the two principal directions x' and y' respectively. The general solutions of equations 2.3-1 are

$$H_{x',m} = A_{1,m} \exp(-k_{2,m}[z-z_{m-1}]) + B_{1,m} \exp(k_{2,m}[z-z_{m-1}]) \quad 2.3-3a$$

$$H_{y',m} = A_{2,m} \exp(-k_{1,m}[z-z_{m-1}]) + B_{2,m} \exp(k_{1,m}[z-z_{m-1}])$$

2.3-3b

and the corresponding electric field components are then given by

$$\begin{aligned} E_{x',m} &= \frac{-1}{\sigma_{1,m}} \frac{\partial H_{y',m}}{\partial z} \\ &= \frac{k_{1,m}}{\sigma_{1,m}} \left\{ A_{2,m} \exp(-k_{2,m}[z-z_{m-1}]) - B_{2,m} \right. \\ &\quad \left. \exp(k_{2,m}[z-z_{m-1}]) \right\} \end{aligned}$$

2.3-3c

$$\begin{aligned} E_{y',m} &= \frac{1}{\sigma_{2,m}} \frac{\partial H_{x',m}}{\partial z} \\ &= \frac{-k_{2,m}}{\sigma_{2,m}} \left\{ A_{1,m} \exp(-k_{1,m}[z-z_{m-1}]) - B_{1,m} \right. \\ &\quad \left. \exp(k_{1,m}[z-z_{m-1}]) \right\} \end{aligned}$$

2.3-3d

The magnetic and electric field components in the measuring directions, x and y are given in terms of

$H_{x',m}$, $H_{y',m}$, $E_{x',m}$ and $E_{y',m}$ as

$$H_{x,m} = H_{x',m} \cos \theta_m - H_{y',m} \sin \theta_m$$

$$H_{y,m} = H_{x',m} \sin \theta_m + H_{y',m} \cos \theta_m$$

$$E_{x,m} = E_{x',m} \cos \theta_m - E_{y',m} \sin \theta_m$$

2.3-4

$$E_{y,m} = E_{x',m} \sin \theta_m + E_{y',m} \cos \theta_m$$

where θ_m is the direction of the major axis of conductivity (azimuth), as measured in clockwise direction from x-axis. These magnetic and electric fields can be extended to the surface ($z=0$) satisfying the boundary conditions at each horizontal interface and the surface components can be written as

$$H_{x,0} = [A_{1,1} + B_{1,1}] \cos \theta_1 - [A_{2,1} + B_{2,1}] \sin \theta_1 \quad 2.3-5a$$

$$H_{y,0} = [A_{1,1} + B_{1,1}] \sin \theta_1 + [A_{2,1} + B_{2,1}] \cos \theta_1 \quad 2.3-5b$$

$$E_{x,0} = \frac{k_{1,1} \cos \theta_1}{\sigma_{1,1}} [A_{2,1} - B_{2,1}] + \frac{k_{2,1} \sin \theta_1}{\sigma_{2,1}} [A_{1,1} - B_{1,1}] \quad 2.3-5c$$

$$E_{y,0} = \frac{k_{1,1} \sin \theta_1}{\sigma_{1,1}} [A_{2,1} - B_{2,1}] - \frac{k_{2,1} \cos \theta_1}{\sigma_{2,1}} [A_{1,1} - B_{1,1}] \quad 2.3-5d$$

The coefficients $A_{1,1}$, $B_{1,1}$, $A_{2,1}$ and $B_{2,1}$, defined in Appendix I, contain the unknowns $A_{1,n+1}$ and $A_{2,n+1}$, which depend on the magnetic field polarization in the (n+1) layer. These coefficients, $A_{1,n+1}$ and $A_{2,n+1}$ can be evaluated by the technique described below.

Assuming the magnetic field in the incident plane wave to be elliptically polarized, its components in the measuring directions, x and y, at the surface, normalizing to $H_{y,0}$ can be written as

$$H_{x,0} = G \exp (i \alpha) \quad 2.3-6a$$

$$H_{y,0} = 1, \quad 2.3-6b$$

where α is the phase difference in degrees and G is the amplitude ratio. From 2.3-5a, 2.3-5b, 2.3-6a and 2.3-6b, using the matrix $[R]$, defined in Appendix I

$$G \exp (i\alpha) = (R_1 \cos \theta_1 - R_3 \sin \theta_1) A_{1,n+1} + (R_2 \cos \theta_1 - R_4 \sin \theta_1) A_{2,n+1} \quad 2.3-7a$$

$$1 = (R_1 \sin \theta_1 + R_3 \cos \theta_1) A_{1,n+1} + (R_2 \sin \theta_1 + R_4 \cos \theta_1) A_{2,n+1} \quad 2.3-7b$$

$$R_1 = r_{11} + r_{21}$$

$$R_2 = r_{31} + r_{41}$$

$$R_3 = r_{13} + r_{23}$$

$$R_4 = r_{33} + r_{43}$$

where $r_{11}, r_{21} \dots r_{43}$ are the elements of the matrix $[R]$. Thus $A_{1,n+1}$ and $A_{2,n+1}$ can be obtained.

If one attempts to define scalar apparent resistivities in the two measuring directions, one can write

$$\rho_x^a = \frac{T}{2\pi\mu} \left| \frac{E_{x,0}}{H_{y,0}} \right|^2 \quad 2.3-8a$$

$$\rho_y^a = \frac{T}{2\pi\mu} \left| \frac{E_{y,0}}{H_{x,0}} \right|^2, \quad 2.3-8b$$

which are not invariant and indeed depend on the polarization parameters of the incoming wave. O'Brien

and Morrison (1967) computed apparent resistivities and developed an interpretation based on the presumed knowledge of the polarization characteristics, which in fact vary with local time, season and place apart from local conductivity structures in the earth.

An interpretation independent of source polarization characteristics can be obtained by solving tensor relation 2.3-2, which can be written out

$$E_x = Z_{xx} H_x + Z_{xy} H_y$$

$$E_y = Z_{yx} H_x + Z_{yy} H_y. \quad 2.3-9$$

To solve 2.3-11, let α_1 and G_1 be the polarization parameters of the incident magnetic field at one instant and α_2 and G_2 the parameters at some other instant. Then 2.3-11 can be written for these two instances

$$E_x^I = Z_{xx} G_1 \exp(i \alpha_1) + Z_{xy}$$

$$E_y^I = Z_{yx} G_1 \exp(i \alpha_1) + Z_{yy}$$

$$E_x^{II} = Z_{xx} G_2 \exp(i \alpha_2) + Z_{xy} \quad 2.3-10$$

$$E_y^{II} = Z_{yx} G_2 \exp(i \alpha_2) + Z_{yy}.$$

These four equations can be used to solve for the four unknowns Z_{xx} , Z_{xy} , Z_{yx} and Z_{yy} . Here, G_1 , G_2 , α_1 and α_2 are arbitrary.

The four tensor apparent resistivities can then be obtained from the four tensor impedances.

$$\rho_{xy}^a = \frac{T}{2\pi\mu} |z_{xy}|^2$$

$$\rho_{yx}^a = \frac{T}{2\pi\mu} |z_{yx}|^2$$

2.3-11

$$\rho_{xx}^a = \frac{T}{2\pi\mu} |z_{xx}|^2$$

$$\rho_{yy}^a = \frac{T}{2\pi\mu} |z_{yy}|^2$$

For a theoretical anisotropic layered earth $z_{xx} = -z_{yy}$ and hence $\rho_{xx}^a = \rho_{yy}^a$.

The properties of these tensor elements as summarized by Swift (1967) are as follows.

For an isotropic or layered earth

$$z_{xx} = z_{yy} = 0$$

2.3-12

$$z_{xy} = -z_{yx}$$

when the earth layers contain anisotropy or lateral inhomogeneity of two dimensional type

$$z_{xx} = -z_{yy}$$

$$z_{xy} \neq z_{yx}$$

2.3-13

For a rotation in cartesian coordinate system the rotated impedance tensor must satisfy the relation

$$Z' = \beta Z \beta^T \quad 2.3-14$$

where

$$\beta = \begin{bmatrix} \cos \phi & \sin \phi \\ -\sin \phi & \cos \phi \end{bmatrix}$$

β^T is the transpose of β and ϕ is the angle to which the axes are rotated in the clockwise direction.

Equation (2.3-15) can be written in expanded form

$$Z'_{xx} = Z_{xx} \cos^2 \phi + (Z_{xy} + Z_{yx}) \sin \phi \cos \phi + Z_{yy} \sin^2 \phi \quad 2.3-15a$$

$$Z'_{xy} = Z_{xy} \cos^2 \phi + (Z_{yy} - Z_{xx}) \sin \phi \cos \phi - Z_{yx} \sin^2 \phi \quad 2.3-15b$$

$$Z'_{yx} = Z_{yx} \cos^2 \phi + (Z_{yy} - Z_{xx}) \sin \phi \cos \phi - Z_{xy} \sin^2 \phi \quad 2.3-15c$$

$$Z'_{yy} = Z_{yy} \cos^2 \phi - (Z_{xy} + Z_{yx}) \sin \phi \cos \phi + Z_{xx} \sin^2 \phi \quad 2.3-15d$$

When the measuring axes are aligned with the axes of anisotropy

$$Z'_{xx} = Z'_{yy} = 0$$

$$Z'_{xy} \neq Z'_{yx}$$

and for any other orientation of measuring axes

$$Z'_{xx} = -Z'_{yy} .$$

The magnitude of one off-diagonal element is always greater than the magnitude of diagonal elements, and

$$Z'_{xx} + Z'_{yy} = Z_{xx} + Z_{yy}$$

$$Z'_{xy} - Z'_{yx} = Z_{xy} - Z_{yx}$$

2.3-16

The quantities $(Z'_{xx} + Z'_{yy})$ and $(Z'_{xy} - Z'_{yx})$ are invariant under rotational transformation.

For an anisotropic half-space or for a single layer anisotropy in a multi-layered medium, the direction that maximizes $\{|Z_{xx}|^2 + |Z_{yx}|^2\}$ or minimizes the quantity $\{|Z_{xx}|^2 + |Z_{yy}|^2\}$ defines the direction of the principal axes, or in the case of two dimensional structures the direction of the strike with 90° uncertainty.

In the case of multi-layered anisotropies, where the principal axes or conductivity are oriented in different directions in each layer, the direction obtained by the above criteria is defined as the "apparent azimuth" or "apparent strike direction" with 90° uncertainty. This direction is a weighted average direction depending on the electrical and geometrical parameters of the layers.

Numerical example for two-layer anisotropy in a multi-layered medium

A simple four-layer model is used to demonstrate the effect of anisotropy on the tensor impedances at

Figure 2.4a: Tensor impedance elements at the surface of a multi-layered anisotropic earth in the measuring directions (x and y).

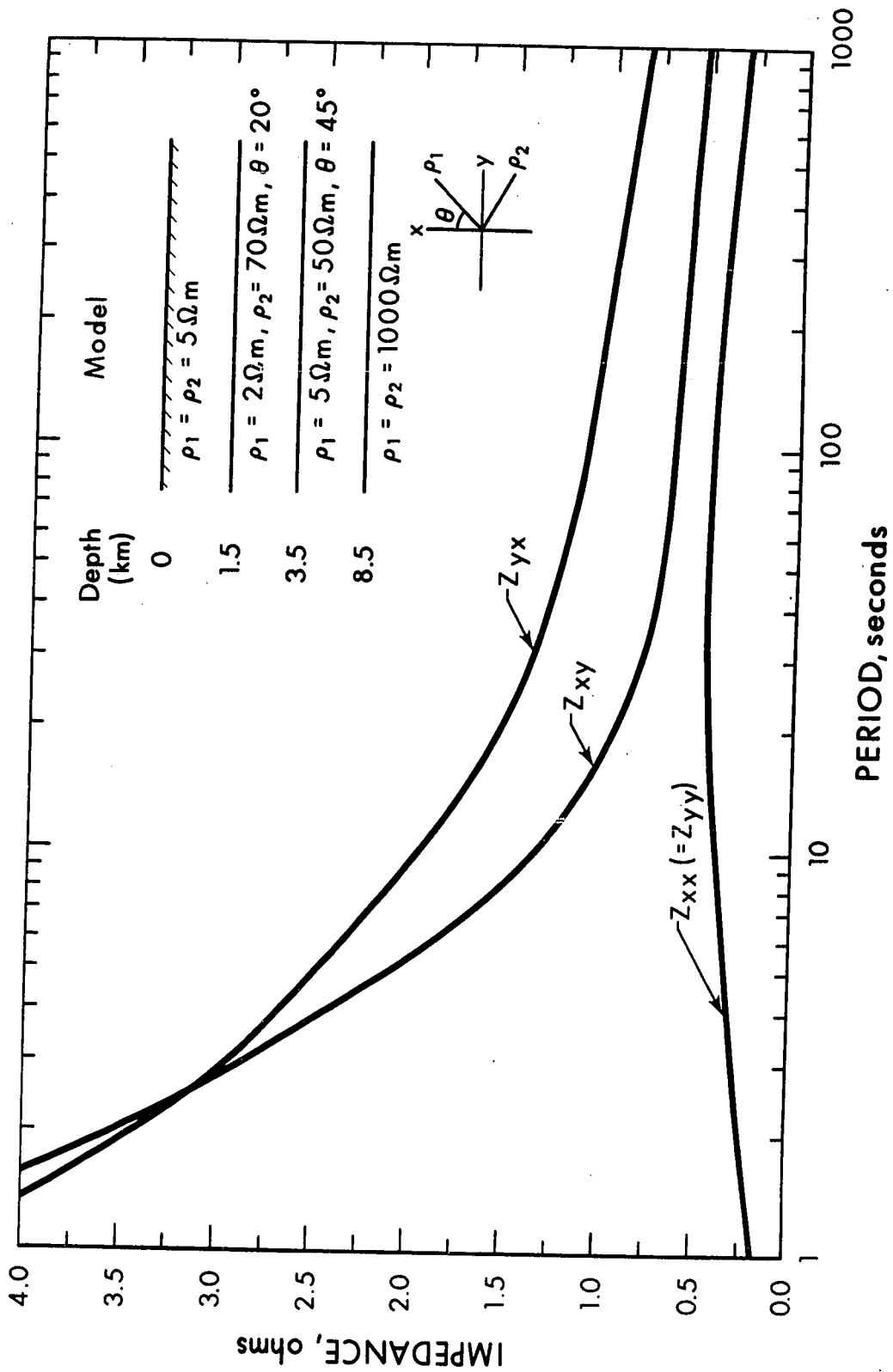
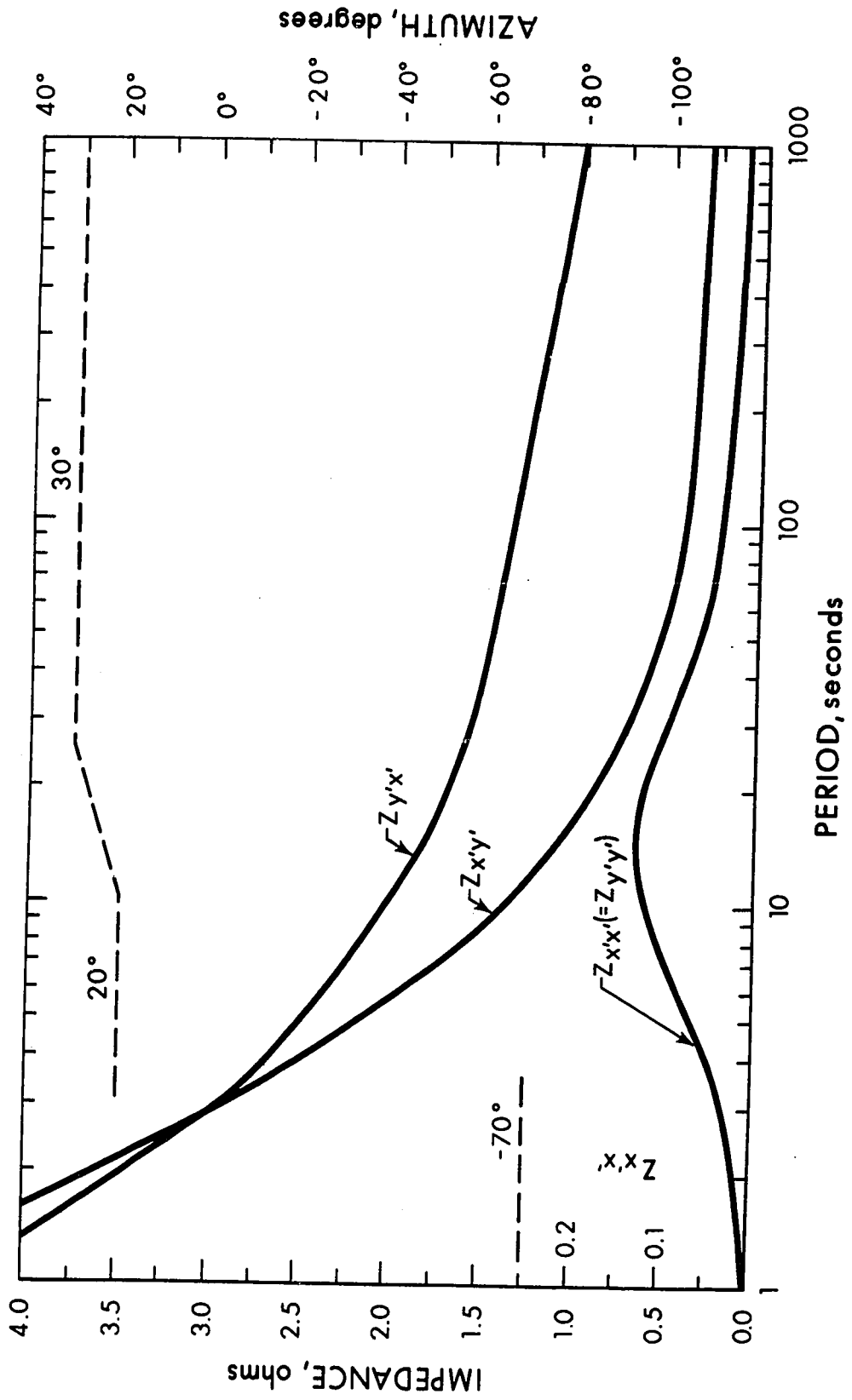


Figure 2.4b: Tensor impedance elements at the surface of a multi-layered anisotropic earth (model shown in Fig. 2.4a) in the principal directions (x' and y') at the surface.



the surface. The top and bottom layers of the earth model (Fig. 2-4a) are anisotropic with the principal axes oriented in different directions in each layer. In Fig. 2.4a the absolute values of the four tensor impedances are plotted as a function of period at the surface, in the measuring directions (x and y directions). As expected the diagonal impedance elements Z_{xx} and Z_{yy} are identical and small compared to off-diagonal elements.

The absolute values of the tensor impedances in the apparent principal directions (x' and y') and the apparent azimuth are presented in Fig. 2.4b. In the apparent principal directions, the diagonal elements $Z_{x'x'}$ and $Z_{y'y'}$ reached their minimum values (note the scale change for $Z_{x'x'}$ and $Z_{y'y'}$ in Fig. 2.4b). The maximum separation is observed between the two off-diagonal elements in the apparent principal directions. For short periods the apparent azimuth approaches to the azimuth in the second layer but for longer periods the apparent azimuth approaches 30° , which is less than azimuth in the third layer, 45° . This effect is due to the fact that for longer periods both individual anisotropies are effective. The transition region between 20° and 30° in apparent azimuth is marked by the maximum in the diagonal impedances. The presence of diagonal elements

even for very long periods is due to the fact that the apparent azimuth is significantly different from the azimuth in the second layer, for these periods.

2.4 Magnetotelluric effect of dipping anisotropies

Dipping anisotropies are encountered in sedimentary strata which contain unconformities. The anisotropy may be due to the microstructure of the rock.

Sedimentary rocks for example, are generally more resistant in the direction normal to the bedding plane than parallel to the bedding plane. When large volumes are involved, there may also be present another kind of anisotropy called 'macroanisotropy', which is caused by a succession of beds with varying

resistivities which appear to have higher resistivity normal to the bedding plane. For example, consider a sedimentary column with a number of horizontal beds, each with its own characteristic resistivity ρ_m and thickness h_m . For a current flowing vertically through a unit cross-sectional column, the transverse resistance R_{tr} is the sum of resistances met in each of the individual layers.

$$R_{tr} = \sum_{m=1}^m \rho_m h_m.$$

The average transverse resistivity, which is seen by the current flowing vertically through the column is

$$\rho_{tr} = \frac{R_{tr}}{H} = \frac{\sum_{m=1}^m \rho_m h_m}{\sum_{m=1}^n h_m} \quad 2.4-1$$

where H is the total thickness of the layers. For current flowing laterally through the column, which is the case in magnetotelluric method when applied to horizontal layering, the longitudinal conductance, which is reciprocal of resistance is

$$S_l = \sum_{m=1}^n \frac{h_m}{\rho_m}$$

and the apparent longitudinal resistivity is

$$\rho_l = \frac{H}{S_l} = \frac{\sum_{m=1}^n h_m}{\sum_{m=1}^n \frac{h_m}{\rho_m}} \quad 2.4-2$$

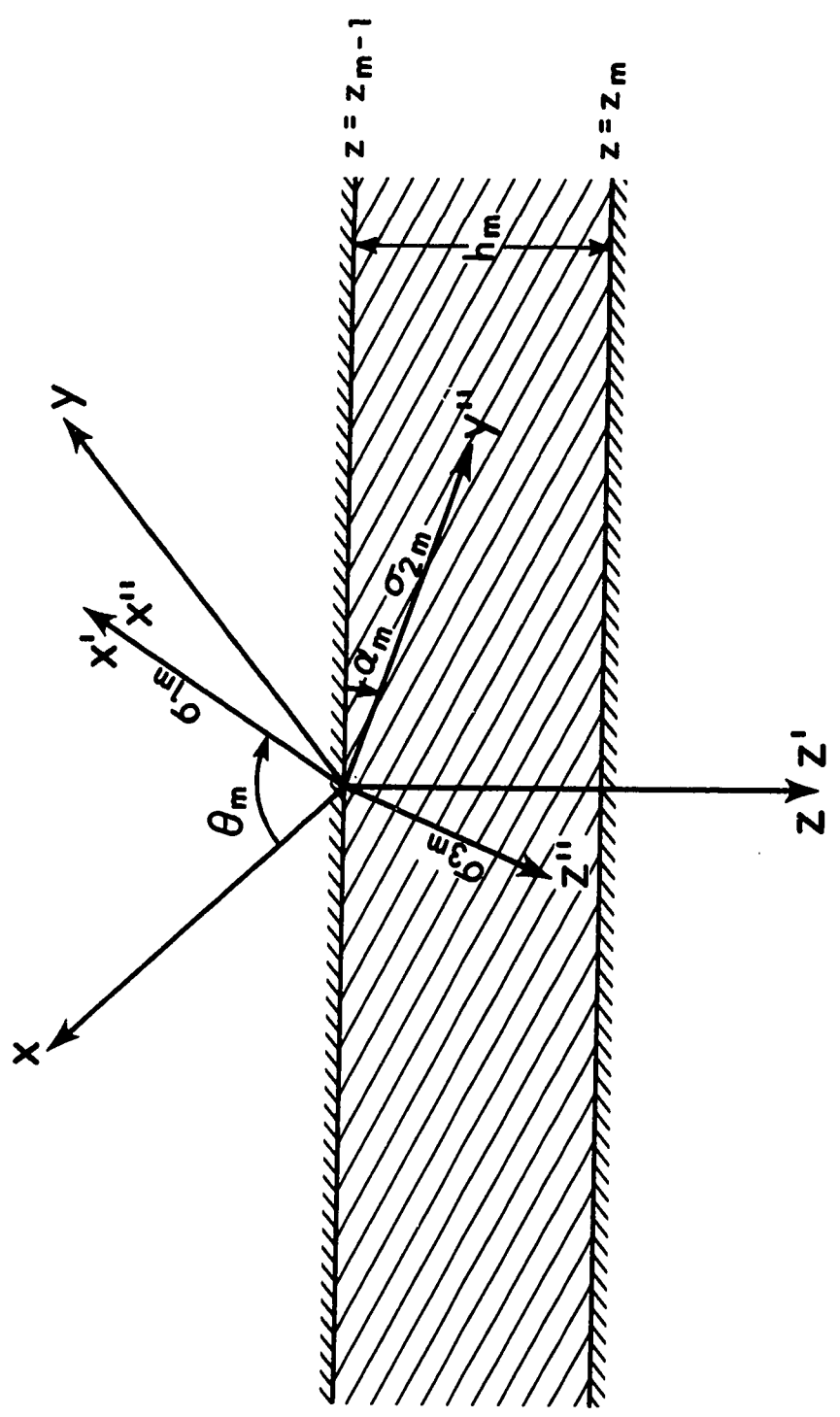
Unless the resistivity of the individual layers are exactly the same, the longitudinal resistivity is smaller than the transverse resistivity. This dependence of resistivity on the direction of current flow constitutes anisotropy, and the coefficient of anisotropy for layered sequence of rocks is defined as

$$\lambda = \sqrt{\rho_{tr}/\rho_l} \quad 2.4-3$$

This kind of anisotropy may be important in studying dipping sedimentary strata by the magnetotelluric method.

This problem can be solved by considering a layered

Figure 2.5: Relationship of axes of anisotropy
to the measuring axes in the m^{th} layer.



half-space in which each layer has a dipping anisotropy as shown in Fig. 2.5. Ohm's law for the anisotropic medium shown in Fig. 2.5 takes the form

$$\begin{bmatrix} J_{x''} \\ J_{y''} \\ J_{z''} \end{bmatrix} = \begin{bmatrix} \sigma_1 & 0 & 0 \\ 0 & \sigma_2 & 0 \\ 0 & 0 & \sigma_3 \end{bmatrix} \begin{bmatrix} E_{x''} \\ E_{y''} \\ E_{z''} \end{bmatrix} \quad 2.4-4$$

An incident plane wave can be resolved into components in mutually orthogonal directions with magnetic field vector oriented along (H-polarization) and normal (E-polarization) to the strike direction (x'' -axis). Since an arbitrary disturbance can be resolved into Fourier components of angular frequency ω with an $\exp(-i \omega t)$ time dependence, the electromagnetic field relationship can be written in rationalized MKS units (neglecting displacement currents), for the two polarization cases as follows:

E-polarization

$$\sigma_1 E_{x'} = \frac{\partial H_{z'}}{\partial y'} - \frac{\partial H_{y'}}{\partial z'} \quad 2.4-5a$$

$$i \omega \mu H_{y'} = \frac{\partial E_{x'}}{\partial z'} \quad 2.4-5b$$

$$-i \omega \mu H_{z'} = \frac{\partial E_{x'}}{\partial y'} \quad 2.4-5c$$

where these equations are expressed directly in the singly primed system of coordinates.

H-polarization

$$i \omega \mu H_{x''} = \frac{\partial E_{2''}}{\partial y''} - \frac{\partial E_{y''}}{\partial z''} \quad 2.4-6a$$

$$\sigma_2 E_{y''} = \frac{\partial H_{x''}}{\partial z''} \quad 2.4-6b$$

$$\sigma_3 E_{2''} = - \frac{\partial H_{x''}}{\partial y''} \quad 2.4-6c$$

where σ_1 , σ_2 and σ_3 are the conductivities in x'' , y'' and z'' directions respectively. Expressing these in the doubly primed system results in an independent set of equations. The solutions can later be transformed into the singly primed system as will be done below.

Since the medium chosen is free from lateral inhomogeneities, E_x , must be constant with respect to y -direction and hence no vertical component, H_z of the magnetic field exists. The equations for E-polarization are similar to the equations for an isotropic, homogeneous earth with conductivity σ_1 . H_y , and E_x , being thus the solutions of the Helmholtz equation:

$$\frac{\partial^2 H_{y'}}{\partial z'^2} - k^2 H_{y'} = 0 \quad 2.4-7$$

where

$$k^2 = - i \mu \omega \sigma_1 \quad 2.4-8$$

$H_{y'}$, and $E_{x'}$, in the m^{th} layer are written as the solutions of Helmholtz equations in that layer,

$$H_{y',m} = A_{1,m} \exp(-k_{1,m}[Z-Z_{m-1}]) + B_{1,m} \exp(k_{1,m}[Z-Z_{m-1}])$$

2.4-9

$$E_{x',m} = \frac{k_{1,m}}{\sigma_{1,m}} \{A_{1,m} \exp(-k_{1,m}[Z-Z_{m-1}]) - B_{1,m} \exp(k_{1,m}[Z-Z_{m-1}])\}$$

2.4-10

where

$$k_{1,m} = \sqrt{-i \mu \omega \sigma_{1,m}}, \text{ and}$$

$A_{1,m}$ and $B_{1,m}$ are the complex coefficients.

Solutions for the electric and magnetic fields in the case of H-polarization are complicated by the fact that they depend on σ_2 as well as σ_3 . Chetaev (1960) solved the H-polarization case for a half-space. Sinha (1969) extended Chetaev's work to a two-layer model, in which only the bottom layer contained a dipping anisotropy. Both Chetaev and Sinha studied the case in which no anisotropy exists in the dipping plane. In this thesis, a more general model is considered, consisting of a multilayered medium, each layer containing a dipping anisotropy, with the strike of the anisotropy oriented at an arbitrary angle to the measuring directions, but with one of the principal directions, e.g. x' , with its associated resistivity $\sigma_{1,m}$, lying in the horizontal plane.

For a source free medium

$$\text{Div } \vec{J} = \frac{\partial J_x''}{\partial x''} + \frac{\partial J_y''}{\partial y''} + \frac{\partial J_z''}{\partial z''} \quad 2.4-11$$

Since there is no gradient of current density in the x'' direction, by using Ohm's law (2.4-4), the above equation reduces to

$$\sigma_2 \frac{\partial E_y''}{\partial y''} + \sigma_3 \frac{\partial E_z''}{\partial z''} = 0 \quad 2.4-12$$

From (2.4-6) and (2.4-12) the Helmholtz equation in the m^{th} layer for the H-polarization case, can be written:

$$\frac{1}{\sigma_{3,m}} \frac{\partial^2 H_{x'',m}}{\partial y''^2} + \frac{1}{\sigma_{2,m}} \frac{\partial^2 H_{x'',m}}{\partial z''^2} + i \mu \omega H_{x''} = 0 \quad 2.4-13$$

The general solution of (2.4-13) in the m^{th} layer is

$$H_{x'',m} = H_{x',m} = A_{2,m} \exp(-\alpha_m [z' - z'_{m-1}]) + B_{2,m}$$

$$\exp(\alpha_m [z' - z'_{m-1}]) \quad 2.4-14$$

where

$$z' = z'' \cos \alpha + y'' \sin \alpha \quad 2.4-15$$

Substituting for $H_{x''}$ from (2.4-14) into (2.4-13) yields

$$\alpha_m^2 = i \mu \omega \sigma_{2,m} \left[\frac{1}{1 + \sin^2 \alpha_m (\lambda_m^2 - 1)} \right] \quad 2.4-16$$

$$\text{where } \lambda_m^2 = \frac{\sigma_{2,m}}{\sigma_{3,m}} .$$

From (2.4-14), (2.4-15) and (2.4-9), $E_{y'',m}$ and $E_{z'',m}$ can be written as

$$E_{y'' , m} = \frac{-q_m \cos \alpha_m}{\sigma_{2, m}} \{A_{2, m} \exp(-q_m [z' - z'_{m-1}]) - B_{2, m} \exp(q_m [z' - z'_{m-1}])\} \quad 2.4-17$$

$$E_{z'' , m} = \frac{-q_m \sin \alpha_m}{\sigma_{2, m}} \{A_{2, m} \exp(-q_m [z' - z'_{m-1}]) - B_{2, m} \exp(q_m [z' - z'_{m-1}])\} \quad 2.4-18$$

From the geometry in Fig. 2.4

$$E_{y', m} = E_{y'' , m} \cos \alpha_m - E_{z'' , m} \sin \alpha_m \quad 2.4-19$$

Therefore,

$$E_{y', m} = \frac{-q_m}{\sigma_{2, m}} [1 + \sin^2 \alpha_m (\lambda_{m-1}^2)] \{A_{2, m} \exp(-q_m [z - z_{m-1}]) - B_{2, m} \exp(q_m [z - z_{m-1}])\} \quad 2.4-20$$

Equations (2.4-9), (2.4-10), (2.4-14) and (2.4-20) specify the electric and magnetic field components in the m^{th} layer, in the strike and dip directions of the anisotropy.

If the strike of the anisotropy is oriented at an angle θ_m to the measuring axis, x , the magnetic and electric field components in the measuring directions are written, using (2.3-4), as

$$H_{x, m} = P_{2, m} \cos \theta_m - P_{1, m} \sin \theta_m \quad 2.4-21a$$

$$H_{y, m} = P_{2, m} \sin \theta_m + P_{1, m} \cos \theta_m \quad 2.4-21b$$

$$E_{x,m} = \frac{k_{1,m}}{\sigma_{1,m}} P_{3,m} \cos \theta_m + \frac{q_m}{\sigma_{2,m}} P_{4,m} \sin \theta_m$$

$$[1 + \sin^2 \alpha_m (\lambda_{m-1}^2)] \quad 2.4-21c$$

$$E_{y,m} = \frac{k_{1,m}}{\sigma_{1,m}} P_{3,m} \sin \theta_m - \frac{q_m}{\sigma_{2,m}} P_{4,m} \cos \theta_m$$

$$[1 + \sin^2 \alpha_m (\lambda_{m-1}^2)] \quad 2.4-21d$$

where

$$P_{1,m} = A_{1,m} \exp(-k_{1,m} [z-z_{m-1}]) + B_{1,m} \exp(k_{1,m} [z-z_{m-1}])$$

$$P_{2,m} = A_{2,m} \exp(-q_m [z-z_{m-1}]) + B_{2,m} \exp(q_m [z-z_{m-1}])$$

$$P_{3,m} = A_{1,m} \exp(-k_{1,m} [z-z_{m-1}]) - B_{1,m} \exp(k_{1,m} [z-z_{m-1}])$$

2.4-22

$$(k_{1,m} [z-z_{m-1}])$$

$$P_{4,m} = A_{2,m} \exp(-q_m [z-z_{m-1}]) - B_{2,m} \exp(q_m [z-z_{m-1}])$$

Equations (2.4-21a) to (2.4-21d) are similar to equations in 2.3-5, hence the magnetic and electric field components at the surface of the earth can be computed by using the same iterative technique given in Appendix I and in Section 2.3, by matching the electric and magnetic fields at each horizontal

Figure 2.6a: Tensor apparent resistivity curves
for a three layer anisotropic model in the
measuring directions for various values
of α .

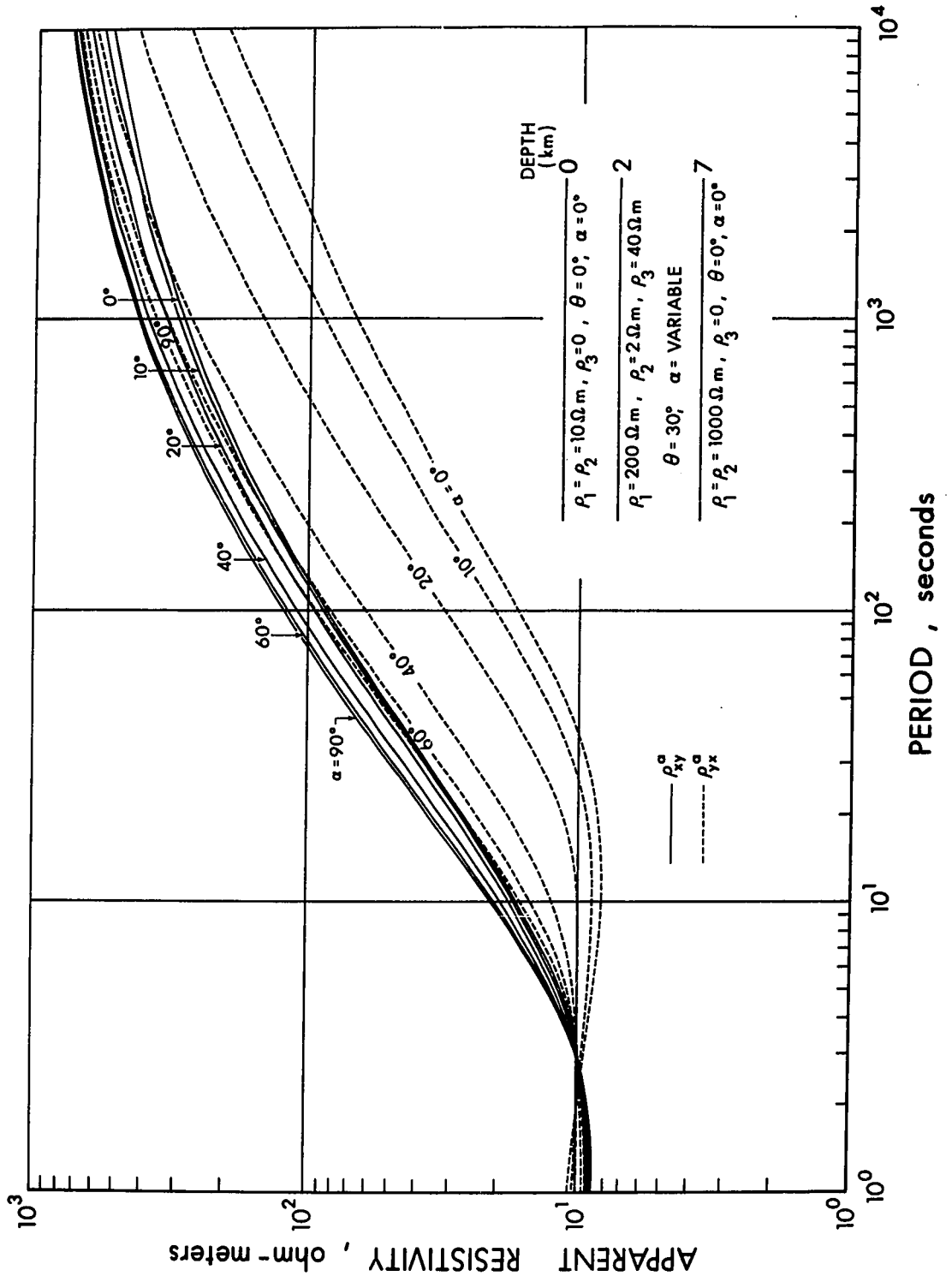
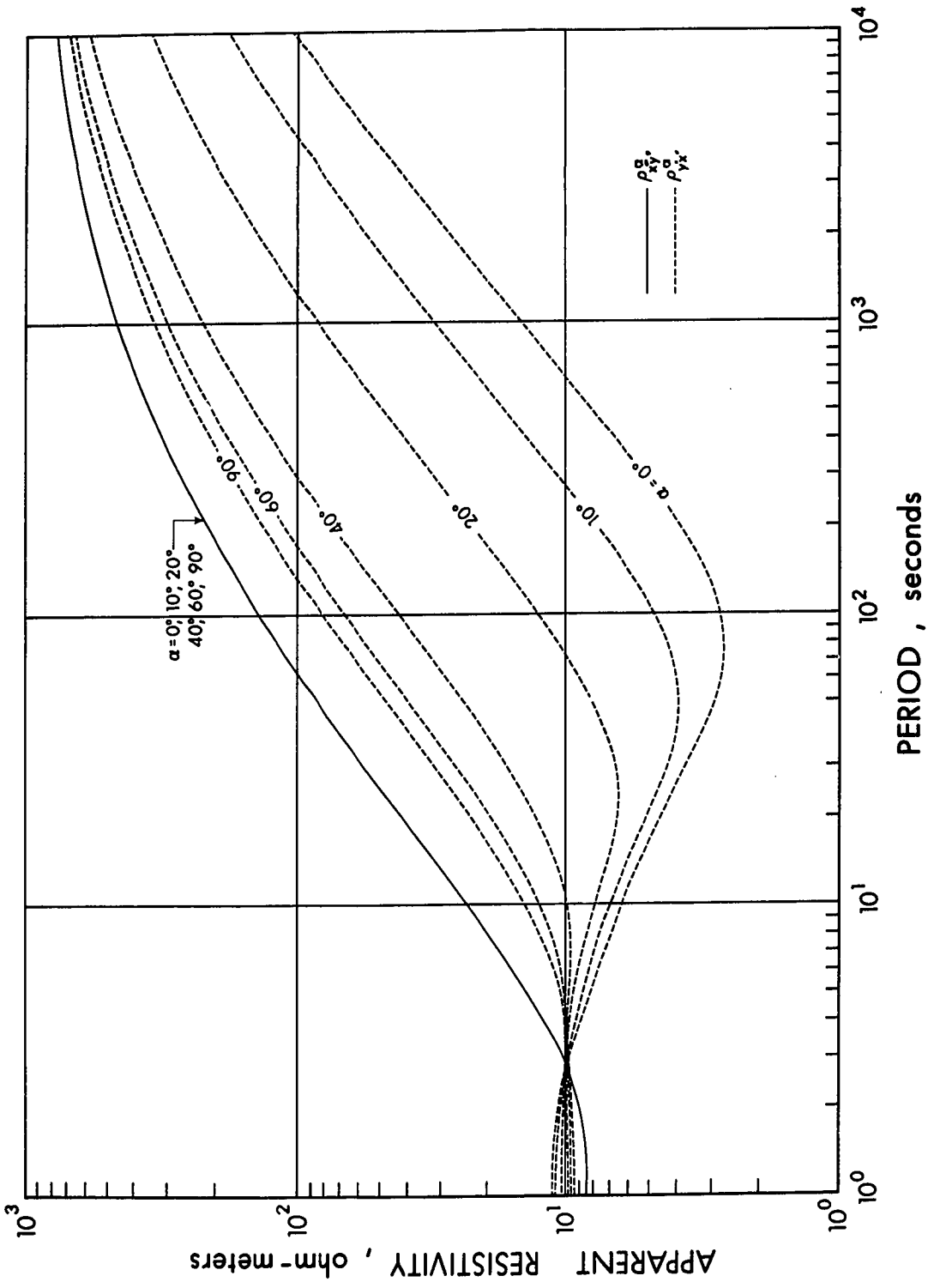


Figure 2.6b: Tensor apparent resistivity curves
for a three layer anisotropic model (shown
in Fig. 2.6a) in the strike and dip directions
for various values of α .



interface. The tensor impedance elements and the apparent resistivities can also be obtained by the same formulae given in section 2.3.

Numerical Example

A simple three layer model is used to demonstrate the effect of dipping anisotropy on the magnetotelluric apparent resistivity. Both the upper and lower layers contain a dipping anisotropy. A set of tensor apparent resistivity curves in the measuring directions corresponding to dip angles varied in steps 0° to 90° , is shown in Fig. 2.6a. The model and its parameters are also shown in the same diagram. Fig. 2.6b shows another set of curves for the same dip angles computed in the strike and dip directions of the intermediate layer. Figure 2.7a illustrates the model and a set of tensor apparent resistivity curves in measuring directions for a fixed dip angle $\alpha = 40^\circ$, but varying $\chi = \rho_3/\rho_2$. Figure 2.7b shows the tensor apparent resistivity curves for the same model in strike and dip directions of the anisotropy of the intermediate layer. In both the models the strike of the anisotropy is fixed at 30° to the measuring axis, x , and the resistivity along the strike is constant.

Figure 2.7a: Tensor apparent resistivity curves
for a three layer anisotropic model in the
measuring directions for various values of
 χ .

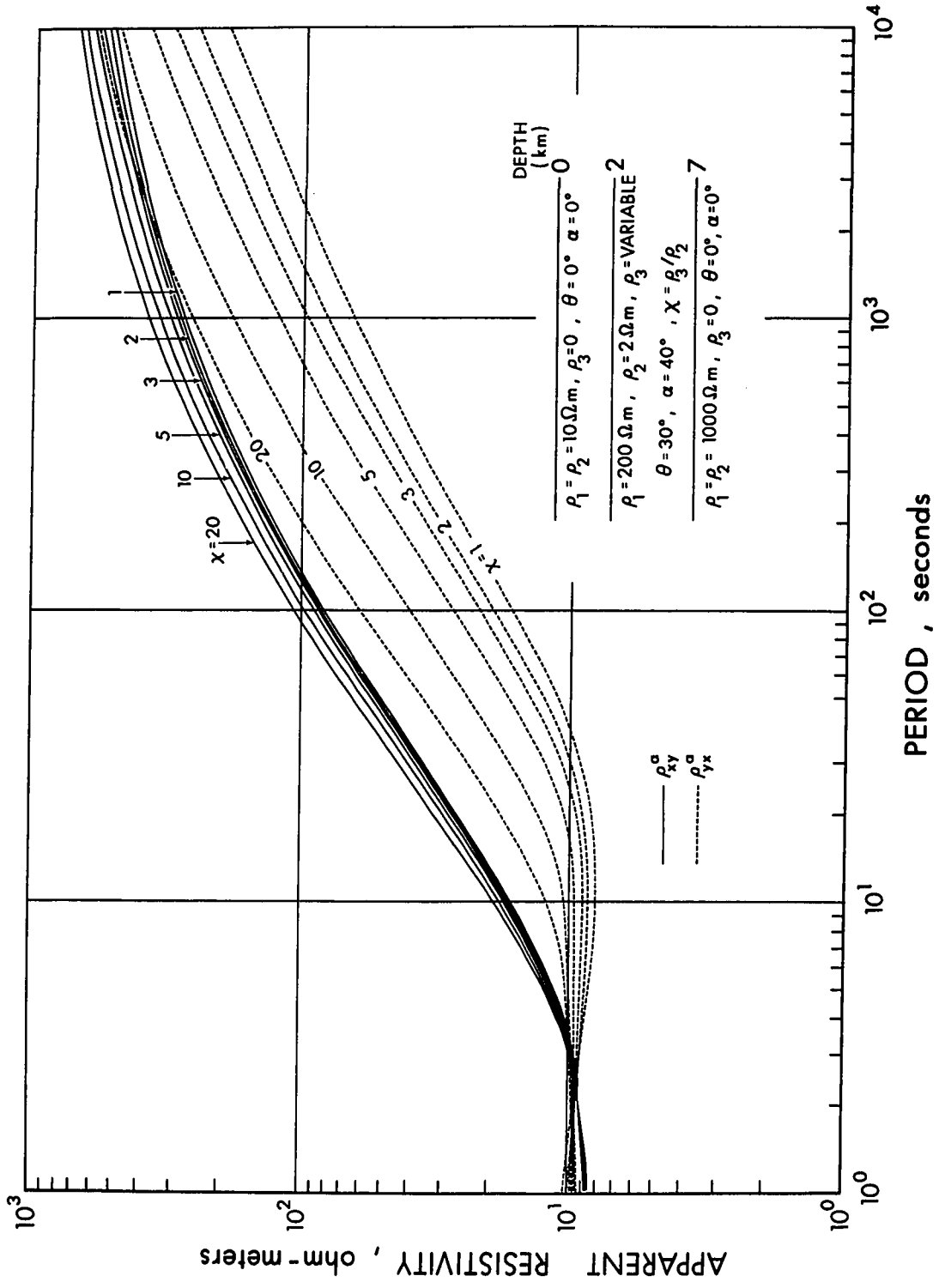
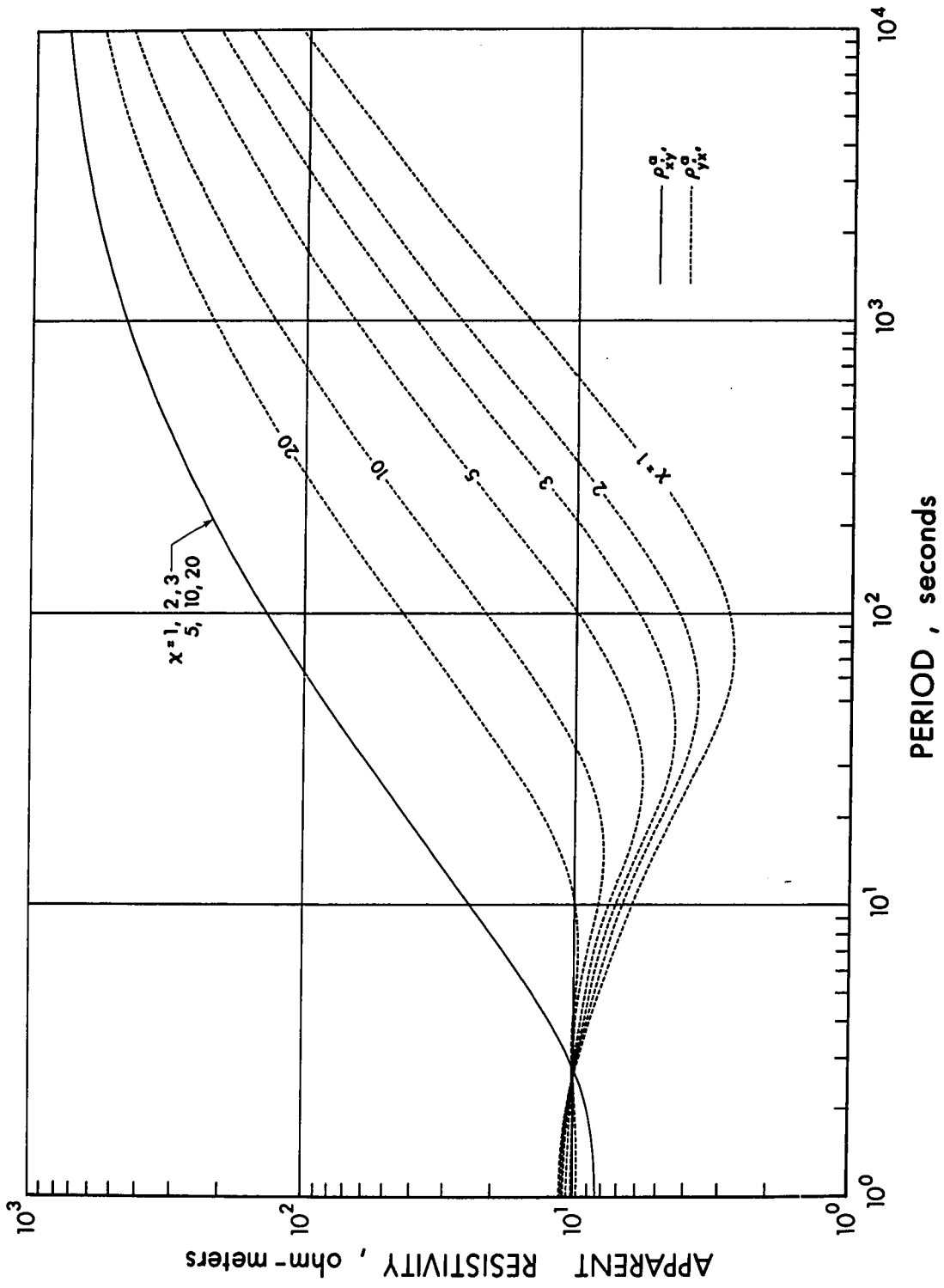


Figure 2.7b: Tensor apparent resistivity curves for a three layer anisotropic model (shown in Fig. 2.7a) in the strike and dip directions for various values of χ .



When $\alpha = 0$, the results correspond to that of horizontal anisotropy with resistivity ρ_1 and ρ_2 along x' and y' directions respectively. The resistivity ρ_3 along z' -direction has no effect since the flow of current is horizontal. A similar situation arises when $\alpha = 90^\circ$, the apparent resistivity is independent of ρ_2 . When $\chi = 1$ (i.e. $\rho_2 = \rho_3$) the apparent resistivity curves are independent of dip angle α . The apparent resistivity in the strike direction is independent of resistivities ρ_2 and ρ_3 and dip angle α (Figs. 2.6b and 2.7b). The apparent resistivities in measuring directions depend on all three resistivities in addition to strike and dip angles of the anisotropy.

2.5 Magnetotelluric effect in the case of lateral inhomogeneities

Solutions of Maxwell's equations in the case of lateral inhomogeneities have been obtained for certain two-dimensional geometries. The condition for the validity of two dimensional solutions is that the extension of electrical structure should be large compared to a skin depth for the frequencies of interest. Further the source is considered to be uniform over a similar distance along the strike of the inhomogeneity.

The electromagnetic field vectors can be resolved into components, such that the electric field component and the associated currents are parallel to (E-polarization) and perpendicular to (H-polarization) the strike direction.

In a cartesian coordinate system, with the x-axis parallel to the strike, y-axis perpendicular to the strike and the z-axis vertically downwards, Maxwell's equations for the two cases can be written in MKS units, assuming a $e^{-i\omega t}$ time dependency, as follows.

E-polarization

$$\sigma E_x = \frac{\partial H_z}{\partial y} - \frac{\partial H_y}{\partial z}$$

$$i\omega\mu H_y = \frac{\partial E_x}{\partial z}$$

$$-i\omega\mu H_z = \frac{\partial E_x}{\partial y} \quad 2.5-1$$

H-polarization

$$i\omega\mu H_x = \frac{\partial E_z}{\partial y} - \frac{\partial E_y}{\partial z}$$

$$\sigma E_y = \frac{\partial H_x}{\partial z} \quad 2.5-2$$

$$\sigma E_z = -\frac{\partial H_x}{\partial y}$$

The scalar Helmholtz equation to be solved then reduces to the form

$$\frac{\partial^2 F}{\partial x^2} + \frac{\partial^2 F}{\partial y^2} - i\omega\mu\sigma F = 0 \quad 2.5-3$$

where $F = E_x$ for E-polarization and $F = H_x$ for H-polarization.

Analytical solutions in the H-polarization case of equation (2.5-3), for some simple geometries such as faults and dykes were obtained by d'Erceville and Kunetz (1962), and Rankin (1962). Weaver (1963), Blake and Swift (1967), and others obtained solutions for E-polarization which were incorrect due to improper boundary conditions

used at the air-earth interface. The source problem for the H-polarization case is simple due to the infinite conductivity contrast across the air-earth boundary. Thus

$$I_z = 0, E_z = 0 \text{ at } z = 0.$$

From (2.5-2)

$$\frac{\partial H_x}{\partial y} = 0$$

or

$$H_x(y) = \text{constant at } z = 0.$$

At the surface of the earth the magnetic field component parallel to the strike is constant with respect to the y-direction even in the presence of lateral inhomogeneities. For the case of E-polarization the air layer must be included in the Calculations and for a solution to be found, this layer must be thick enough so that the field in the region of the source is relatively uninfluenced by the inhomogeneity.

Neves (1957) first applied finite difference techniques to solve some two-dimensional problems but unfortunately his solutions suffered from errors associated with incorrect boundary conditions. In recent years numerical techniques have been developed by Madden and Swift (1969), Wright (1969), Patrick and Bostick (1969), and

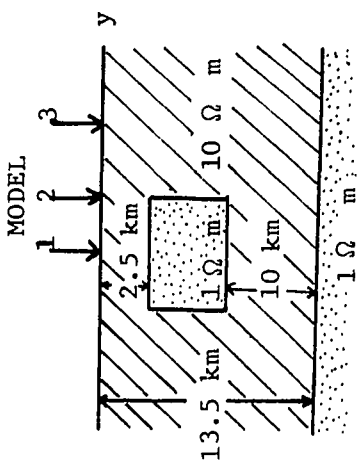
Jones and Price (1970a, b), to study the effect of lateral inhomogeneities of two-dimensional type on magnetotelluric fields. Madden and Swift (1969) and Wright (1969) used the transmission line analogy to solve the magnetelluric problem, whereas Patrick and Bostick (1969), and Jones and Price (1970a) used direct finite difference techniques. A numerical example is presented below to show the effect of a two dimensional conductivity structure within the earth on the apparent resistivities and the magnetotelluric fields at the surface.

Numerical example for lateral inhomogeneity

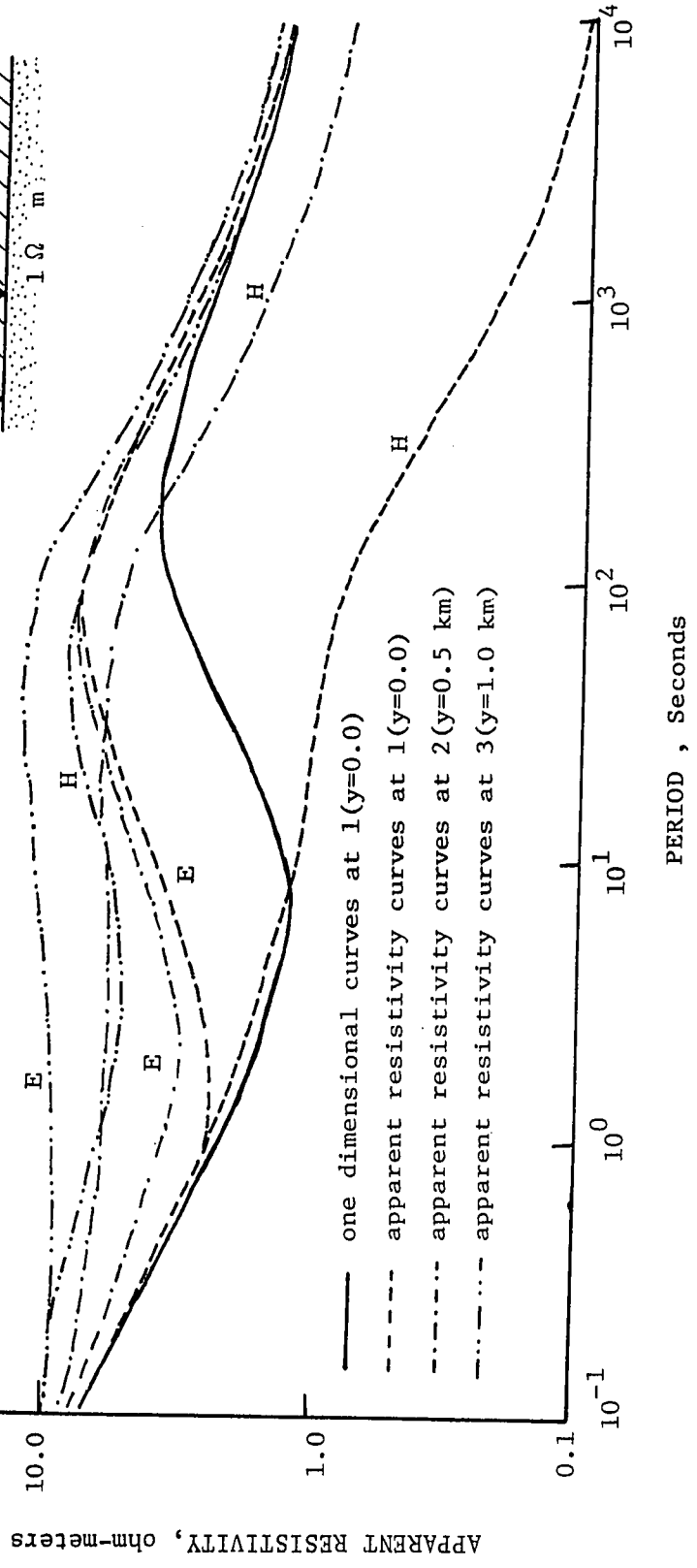
This example is taken from Patrick and Bostick (1969). The two-dimensional model consists of a conductive prism buried in the first layer of a two-layered earth. The dimensions of the prism are 1 km x 1 km, the thickness of the first-layer is 11.25 km and the top of the prism is 0.25 km from the surface of the earth. The first-layer resistivity is 10 ohm-meters, the prism and the semi-infinite second layer have a resistivity of 1 ohm-meter.

The apparent resistivity curves for three different sounding sites and the model are presented in Fig. 2.8. For the sounding site

Figure 2.8: Apparent resistivity curves for H and E-polarizations over a two-dimensional structure for three different sounding sites situated along a traverse normal to the strike (after Patrick and Bostick, 1969).



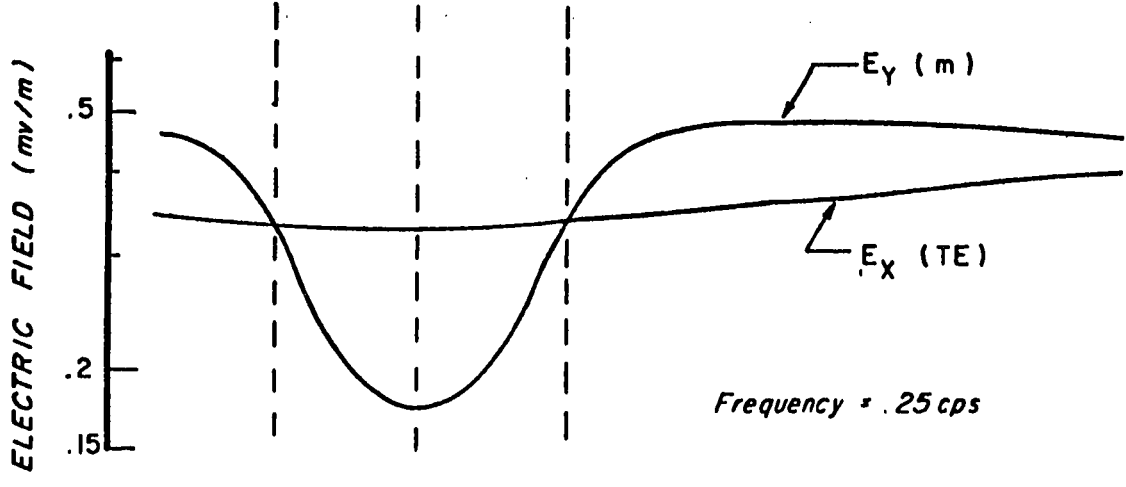
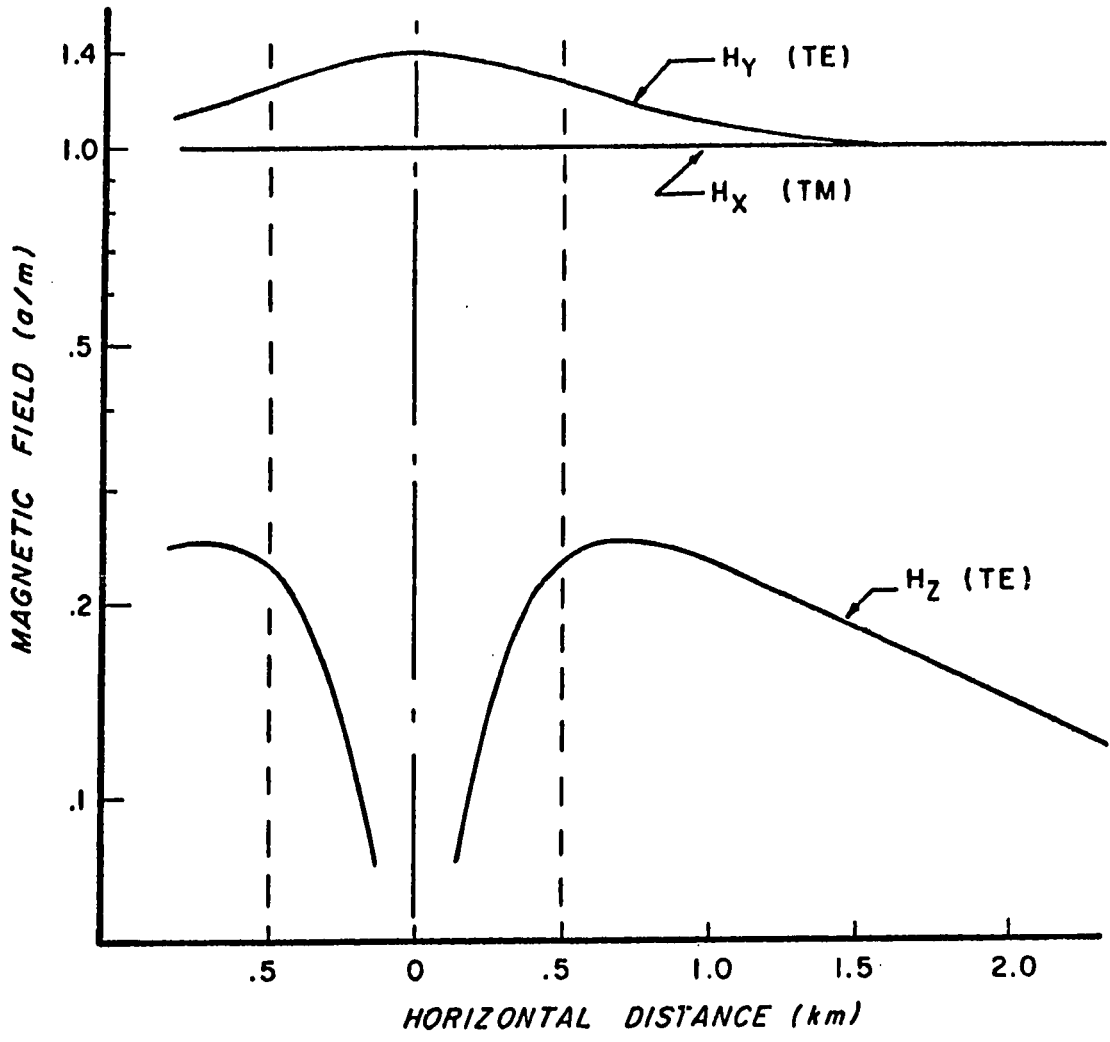
H = H-polarization
 E = E-polarization



above the middle of the prism, the apparent resistivity curves for H-polarization and E-polarization approach the same limit for short periods. As the period increases to about 1 sec. the curves diverge and remain separated over the entire period range above this point. The solid curve in Fig. 2.8 is the apparent resistivity curve for the one-dimensional model which would be obtained if the prism were infinitely wide. The apparent resistivity curve for E-polarization and the one-dimensional curve approach the same limit for long periods. For a sounding site located at the edge of the prism (sounding site #2), and 0.5 km away from the edge of the prism (sounding site #3), the apparent resistivity curves show a constant off-set at longer periods but to a lesser extent. As the sounding site moved away from the anomaly the apparent resistivity for H-polarization becomes larger than for E-polarization.

The field components computed at the surface of the earth show that the magnetic field is constant for H-polarization (Fig. 2.9). The electric field for E-polarization varies slowly across the strike while H-polarization varies rapidly. This implies that for 4 sec. period,

Figure 2.9: Magnetic and electric field variations along a traverse normal to the strike for the model shown in Fig. 2.8 for 4 second period. TE corresponds to E-polarization case and TM corresponds to H-polarization case. (after Patric and Bostick, 1969).



for which the field components are computed, the anomalies in the apparent resistivity are reflected in magnetic field for E-polarization and in the electric field for H-polarization. Due to symmetry H_z vanishes along the center of the anomaly. The peak H_z occurs close to the contacts.

CHAPTER 3
DETECTION AND ANALYSES OF THE MAGNETOTELLURIC
SIGNALS

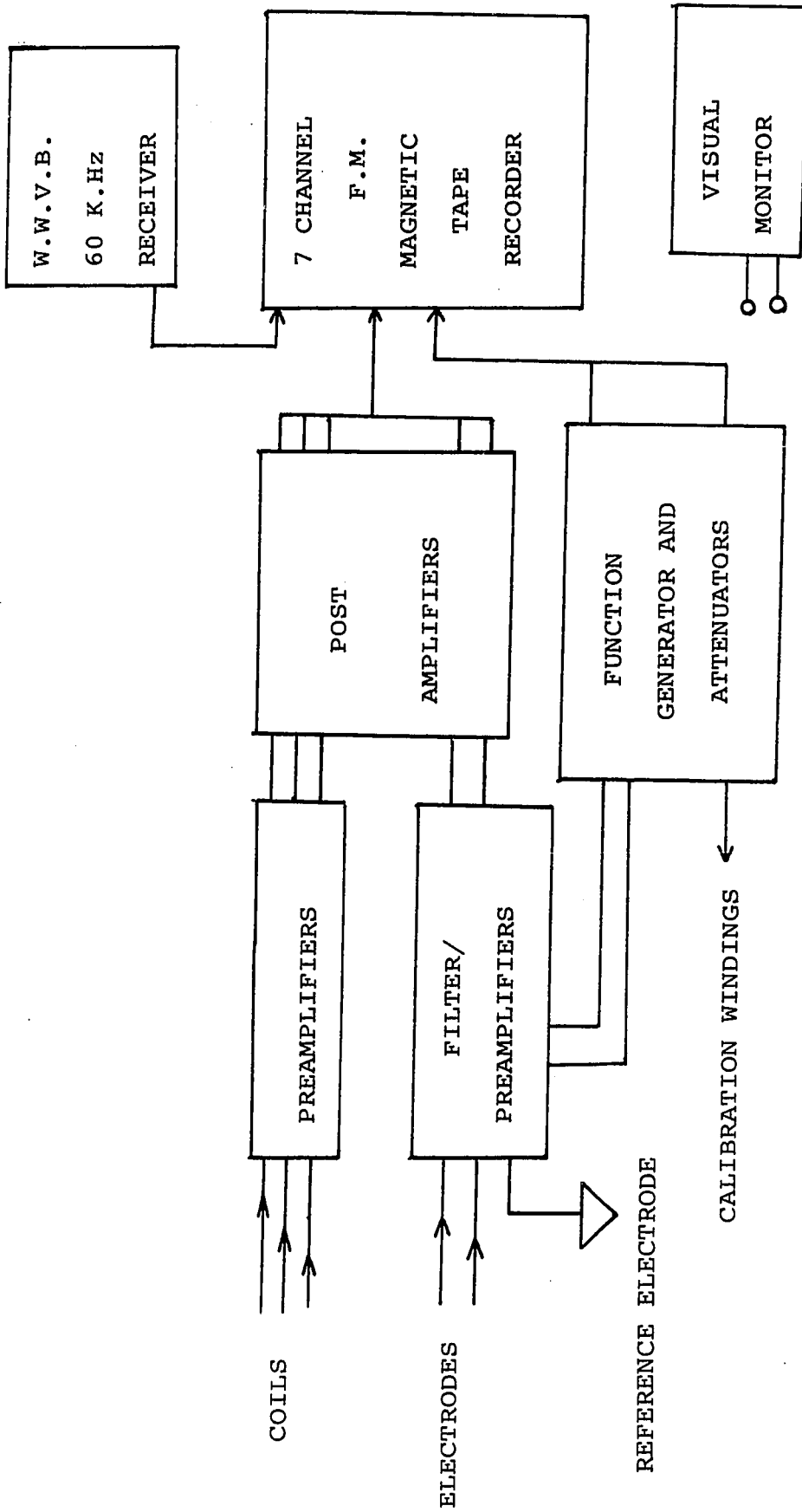
3.1 Detection

Variations in the telluric and geomagnetic field are measured at each station using mobile magnetotelluric signal detection system designed and built at the University of Alberta (Vozoff et al., 1964).

The telluric field variations are derived from potential differences between two copper electrodes driven into the ground. The electrodes are spaced at 350 feet apart in each of two orthogonal directions, generally geographic north-south and geographic east-west. A 100 μ f capacitor is used to block the D.C. potentials due to the polarization at the electrodes.

The sensors for magnetic variations are induction coils. Three coils are buried in mutually orthogonal directions to measure the variations in the vertical (H_z), the geographic north-south (H_x) and the geographic east-west (H_y) components of the magnetic field. Each coil consists of 32,000 turns of #28GA enamelled copper wire on a 60 inches by 0.75 inch high permeability core.

Figure 3.1: A block diagram of the magnetotelluric recording system.

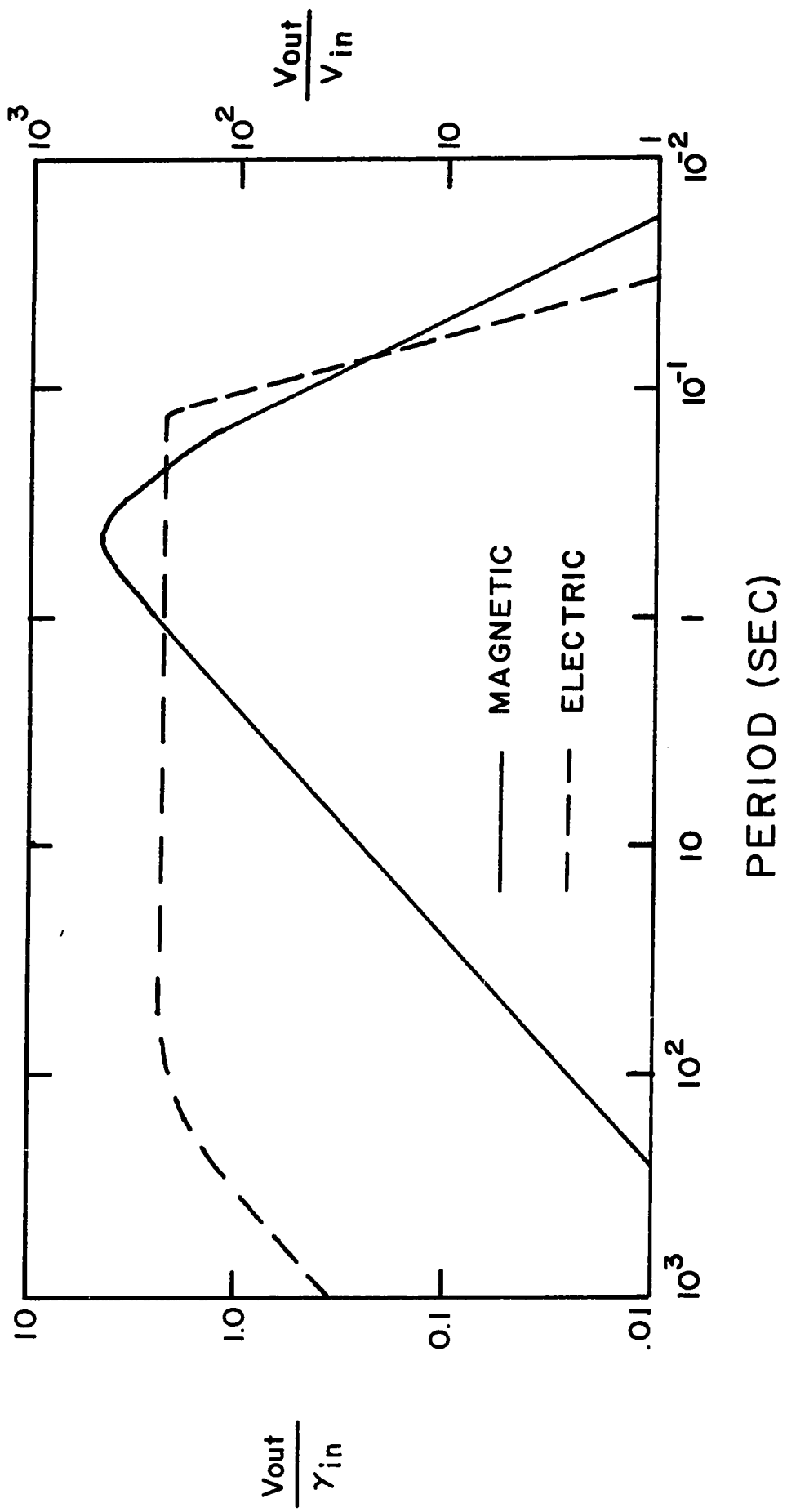


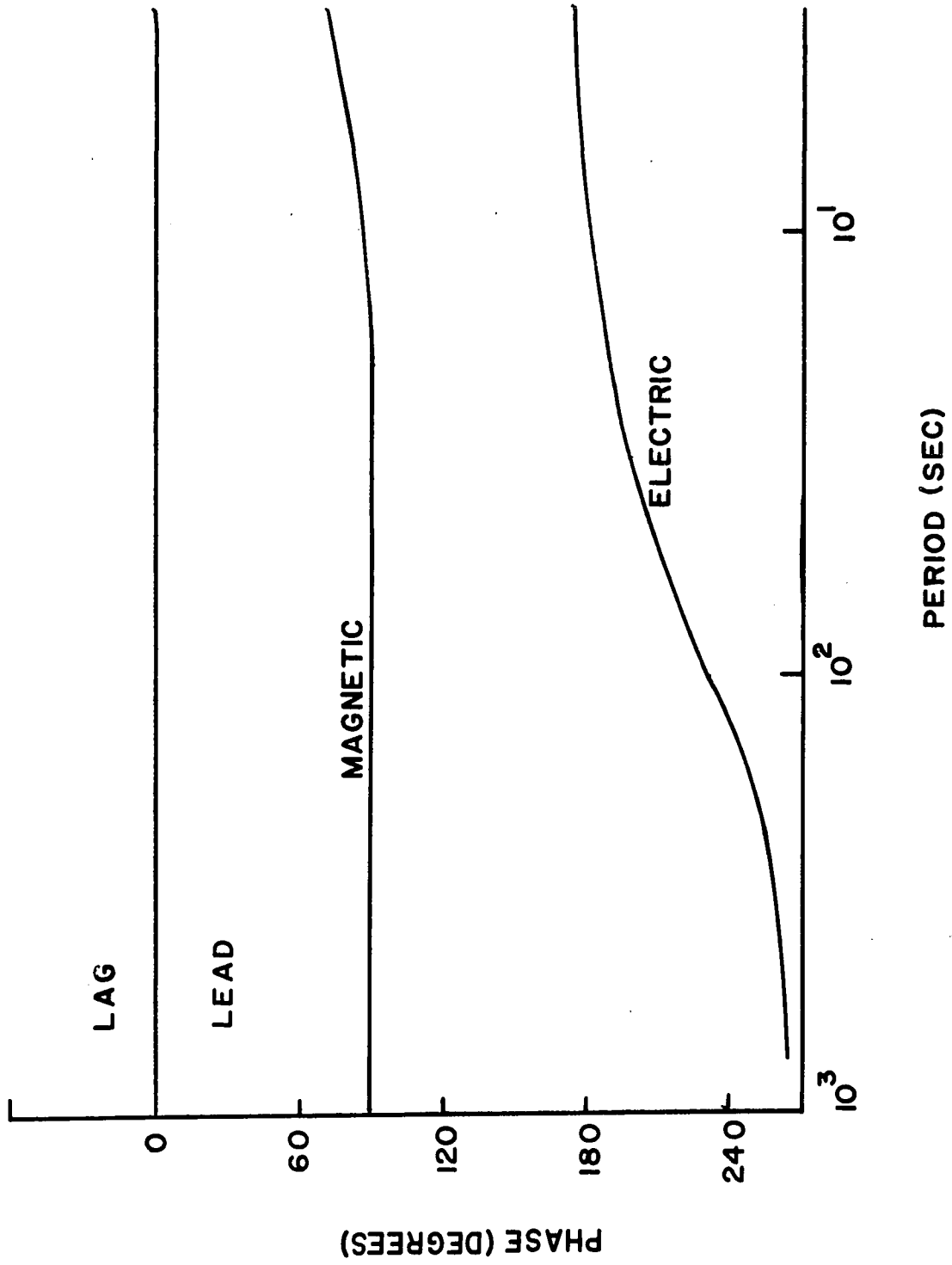
The signals from the coils and the electrodes are fed into a preamplifier and post-amplifier system. The post-amplifiers have discrete gain settings from -20 db to +20 db in steps of 10 db to permit recording of various signal levels. The amplified signals are then recorded on magnetic tape in analog form using a seven channel Precision Instruments analog FM tape recorder with a recording speed of 15/16 inch/second. WWVB time signals were also recorded. A block diagram of the magneto-telluric recording system is shown in Figure 3.1. The amplitude and phase responses of the magnetic and telluric systems are shown in Figure 3.2.

3.2 Digital Processing

Records approximately three hours in length and free from discontinuities were selected for digital conversion. The analog signals were alias filtered and sampled by an Analog to Digital Converter at a digitizing rate of 15 samples per second per channel. The analog tape is played back at a speed of 30 inches/second. This gave a digitizing interval of 32/15 seconds. Digitized data in 11 bit binary form in blocks of 7200 two character words were recorded on two seven channel asynchronous, incremental, Kennedy digital tape

Figure 3.2: Calibrated amplitude and phase response for the telluric and magnetic field detection systems.





recorders. The data from the two seven track tapes were read and stored on nine track tape in IBM 360/67 Fortran compatible format.

3.3 Spectral Computations

Assuming that the magnetotelluric signals are samples of stationary random process, the auto- and cross-power spectral density estimates for the five components, H_x , H_y , H_z , E_x and E_y of the magnetotelluric fields were computed using the Fast Fourier Transform and the technique described in Appendix II. The following notation will be used to represent auto and cross power spectral density estimates and the coherency.

If X and Y are two time sequences produced by measurements on stationary random process, then

$PX(\omega) = \langle X^*(\omega) X(\omega) \rangle =$ time averaged auto power spectral density estimate of the X series for angular frequency ω ,

$PY(\omega) = \langle Y^*(\omega) Y(\omega) \rangle =$ time averaged auto power spectral density estimate of Y series for angular frequency ω ,

$PXY(\omega) = \langle X^*(\omega) Y(\omega) \rangle =$ time averaged cross power spectral density estimate of series X and Y for angular frequency ω ,

$\text{Coh } XY(\omega) = \frac{PXY(\omega)}{[PX(\omega)PY(\omega)]^{1/2}} =$ coherency between

X and Y series for angular frequency ω ,

where * represents the complex conjugate. The

symbol ω of the spectral densities will be omitted in the remainder of this work.

Digital time sequences containing 4096 points consisting of 3,000 data points and 1096 zeros were used for most of the spectral computations. The maximum lag number was 512. Digital phase shift corrections and the removal of instrument phase and amplitude responses were carried out in the frequency domain. The smoothed spectral density estimates were obtained by applying a Parzen window in the lag domain.

3.4 Analyses of Magnetotelluric Signals

Using the definitions of the preceding section, the Cagniard-type resistivities (scalar resistivities) can be expressed in terms of autopower spectral density estimates of E_x , H_y , E_y and H_x , as

$$\rho_x^a = \frac{T}{2\pi\mu} \frac{PE_x}{PH_y} \quad 3.4-1$$

$$\rho_y^a = \frac{T}{2\pi\mu} \frac{PE_y}{PH_x} \quad 3.4-2$$

Phase differences of E_x-H_y and E_y-H_x can be obtained from the cross power spectral density estimates,

$$\tan \phi_x = \frac{\text{Im}(PE_x H_y)}{\text{Re}(PE_x H_y)} \quad 3.4-3$$

$$\tan \phi_y = \frac{\text{Im}(PE_{yx})}{\text{Re}(PE_{yx})} \quad 3.4-4$$

As it has been pointed out in Chapter 2, the scalar apparent resistivities are valid only under very limited conditions for the interpretation of magnetotelluric data. For this reason tensor impedances and tensor resistivities were computed.

Swift (1967), Morrison et al., (1968) and Sims and Bostick (1969) have presented methods to solve the impedance relation (2.3-2) for the measured magnetotelluric fields. Consider for example the equation

$$E_x = Z_{xx}H_x + Z_{xy}H_y \quad 3.4-5$$

from which four distinct equations can be obtained involving the various spectral estimates. In terms of the auto and cross power spectral estimates, these are

$$PE_{xx} = Z_{xx}PE_{xx} + Z_{xy}PE_{xy} \quad 3.4-6a$$

$$PE_{yx} = Z_{xx}PE_{yx} + Z_{xy}PE_{yy} \quad 3.4-6b$$

$$PH_{xx} = Z_{xx}PH_{xx} + Z_{xy}PH_{xy} \quad 3.4-6c$$

$$PH_{yx} = Z_{xx}PH_{yx} + Z_{xy}PH_{yy} \quad 3.4-6d$$

Any two of these equations can be solved simultaneously for Z_{xx} and Z_{xy} . Since there are six possible pairs

of equations, there are six ways to solve for Z_{xx} and Z_{xy} . Similarly, Z_{yx} and Z_{yy} can be estimated in six different ways. For example, the six estimates of Z_{xx} are

$$Z_{xx} = \frac{PE_x PE_y H_y - PE_y E_x PE_x H_y}{PE_x H_x PE_y H_y - PE_y H_x PE_x H_y} \quad 3.4-7a$$

$$Z_{xx} = \frac{PE_x PH_x H_y - PH_x E_x PE_x H_y}{PE_x H_y PH_x H_y - PH_x PE_x H_y} \quad 3.4-7b$$

$$Z_{xx} = \frac{PE_x PH_y - PH_y E_x PE_x H_y}{PE_x H_x PH_y - PH_y H_x PE_x H_y} \quad 3.4-7c$$

$$Z_{xx} = \frac{PE_y E_x PH_x H_y - PH_x PE_y H_y}{PE_y H_x PH_x H_y - PH_x PE_y H_y} \quad 3.4-7d$$

$$Z_{xx} = \frac{PE_y E_x PH_y - PH_y E_x PE_y H_y}{PE_y H_x PH_y - PH_y H_x PE_y H_y} \quad 3.4-7e$$

$$Z_{xx} = \frac{PH_x E_x PH_y - PH_y E_x PH_x H_y}{PH_x PH_y - PH_y H_x PH_x H_y} \quad 3.4-7f$$

Of these six possible estimates, two tend to be relatively unstable, for the one dimensional case, particularly when the incident fields are unpolarized. For this case $PE_y E_x$, $PE_x H_x$, $PE_y H_y$ and $PH_x H_y$ tend toward zero, so the equations (3.4-7c) and (3.4-7d) are indeterminate. The other four estimates are stable and correctly predict Z_{xx} , provided the incident fields are not too highly polarized.

The four stable estimates of each impedance element were computed using the cross and auto power spectral density estimates and an arithmetic mean of the four estimates of each tensor element was obtained. These mean values were used in subsequent computations.

The mean impedance elements are rotated through 90° in steps of 5° to find the principle directions of conductivity. The direction that maximizes $\{|Z'_{xy}|^2 + |Z'_{yx}|^2\}$ corresponds to the strike direction with 90° uncertainty, since the geologic strike may coincide either with the maximum conductivity or with minimum conductivity. For the case of a one or two-dimensional conductivity structures, $(Z'_{xx} + Z'_{yy})$ vanishes if there is a unique direction of anisotropy. In this case the normalized ratio

$$\text{SKEW} = \frac{Z'_{xx} + Z'_{yy}}{Z'_{xy} - Z'_{yx}} \quad 3.4-8$$

must be small compared to unity in order that the data fit a two-dimensional model. Sims and Bostick (1969) used impedance ellipses as a criterion for distinguishing between two- and three-dimensional magnetotelluric structures. Each impedance element traces an ellipse in the complex plane as the measuring axes are rotated and for

two-dimensional models the ellipses degenerate to straight lines, which in the case of the diagonal elements Z_{xx} and Z_{yy} pass through the origin.

The quality measure generally used for magnetotelluric field data over one-dimensional structures is the coherency between orthogonal electric and magnetic field components. However, in the case of anisotropic and/or two-dimensional structures, the electric field component in any one direction (other than in the strike direction) is affected by magnetic field components both perpendicular and parallel. Hence the coherencies between orthogonal components of the electric and magnetic fields may not be a true indication of data reliability. In such cases "predicted coherency" (Swift, 1967) can be used as a measure of the quality of the data. The predicted coherency is the coherency between the measured E-field component and the E-field component predicted from the magnetic field components and the average value of the impedance elements. The predicted coherencies for both the components of the electric field can be expressed as

$$\text{coh } E_x E_x^p = \frac{Z_{xx} P E_x H_x + Z_{xy} P E_x H_y}{|Z_{xx}|^2 P H_x + |Z_{xy}|^2 P H_y + 2 \text{Re}(Z_{xx}^* Z_{xy} P H_x H_y)}$$

$$\text{coh } E_Y E_Y^P = \frac{Z_{YX} P_{E_Y H_X} + Z_{YY} P_{E_Y H_Y}}{|Z_{YX}|^2 P_{H_X} + |Z_{YY}|^2 P_{H_Y} + 2 \text{Re}(Z_{YX}^* Z_{YY} P_{H_X H_Y})}$$

3.4-9b

when the predicted coherencies are high, the signal to noise ratio is high.

3.5 Polarization Parameters of the Magnetotelluric Fields

Fowler et al., (1967), Paulson (1968) and Rankin and Kurtz (1970) have studied the polarization characteristics of micropulsations using auto and cross spectral density estimates. The technique used by these authors is applied here, to obtain the polarization parameters (viz. the degree of polarization, the angle of polarization and the ellipticity) of the magnetotelluric fields.

For quasi-monochromatic signals, the degree of polarization (ratio of the polarized intensity to the total intensity) is given by

$$R = [1 - \frac{4|J|}{(P_X + P_Y)^2}]^{1/2} \quad 3.4-10$$

where $J = P_X P_Y - P_{XY} P_{YX}$ and the X and Y series refer to the components of either the electric or magnetic fields. For completely polarized signal $J \rightarrow 0$, $R \rightarrow 1$ and the mutual coherency between X and Y series must be 1. For completely unpolarized

signal the coherency between X and Y series must be zero.

The angle of polarization of the field (the angle through which the coordinate axes must be rotated to align with the major and minor axes of the ellipse) is given by

$$\theta = \frac{1}{2} \tan^{-1} \frac{2 \operatorname{Re} PXY}{(PX - PY)} \quad 3.4-11$$

For positive θ values the angle is measured clockwise from x-axis.

The ellipticity of the field ellipse (the ratio of minor to major axis of the ellipse) is given by

$$\psi = \tan \left[\frac{1}{2} \sin^{-1} \left\{ \frac{2 \operatorname{Im} PXY}{((PX-PY)^2 + 4 PXY PYX)^{1/2}} \right\} \right] \quad 3.4-12$$

The ellipticity ranges from 1 for a circularly polarized signal, to zero for a linearly polarized signal. If ψ is positive the sense of polarization is counterclockwise when looking into the propagating wave and the rotation sense is clockwise if ψ is negative.

3.6 Vertical Magnetic Field, H_z

The presence of vertical magnetic field (assuming plane wave incidence), implies that the underlying medium is laterally inhomogeneous, from (2.4-5c),

$$H_z = \frac{-1}{i\omega\mu} \frac{\partial E_{x'}}{\partial y'}$$

That is, the vertical magnetic field at a given frequency is directly proportional to the gradient in the direction normal to the strike of the electric field component parallel to the strike. Hence, a maximum coherency is expected between H_z and the electric field component parallel to the strike, or the direction that gives maximum coherency between the electric field component and H_z gives the strike of a two dimensional conductivity structure.

The coherencies between the vertical magnetic field and the four horizontal components of the magnetotelluric field were computed for various rotation angles using the expressions

$$\text{coh } H_z E_{x'} = \frac{PH_z E_x \cos \theta + PH_z E_y \sin \theta}{PH_z [PE_x \cos^2 \theta + PE_y \sin^2 \theta + \text{Re}(PE_x E_y) \sin 2\theta]}$$

3.4-13a

$$\text{coh } H_z E_{y'} = \frac{-PH_z E_x \sin \theta + PH_z E_y \cos \theta}{PH_z [PE_x \sin^2 \theta + PE_y \cos^2 \theta - \text{Re}(PE_x E_y) \sin 2\theta]}$$

3.4-13b

(Similar expressions can be written for $\text{coh } H_z H_x$, and $\text{coh } H_z H_y$), where θ is the rotation angle measured in clockwise direction from the measuring axis x , and E_x , and E_y , are the electric field components along the rotated axes.

The amplitude ratios between the vertical and horizontal components of the magnetic field are also obtained for each rotation angle, to determine the relative amplitude of the vertical field which depends on the conductivity contrast across the lateral discontinuity.

CHAPTER 4
MAGNETOTELLURIC SOUNDING RESULTS FOR
CENTRAL ALBERTA

In this chapter the magnetotelluric results for the 16 sounding sites, listed in Table 2 of Chapter 1, are presented in alphabetical order. For each station, unless otherwise noted, will be shown the curves and tables as follows:

- a) curves of rotated tensor apparent resistivities in principal directions;
- b) curves of azimuth, the direction of minimum resistivity measured positive clockwise from north;
- c) polarization angles of the electric and magnetic fields;
- d) table of values of the coherencies H_z-E_x , H_z-E_y , H_z-H_x , H_z-H_y and the ratios H_z/H_x and H_z/H_y in the measuring directions and for the direction in which one of the electric field components exhibits maximum coherency with H_z . Aeromagnetic maps are also presented where available.

The selection criteria used to edit the tensor apparent resistivities and the azimuths were:

- a) the predicted coherencies for the electric field components greater than 0.95,
- b) the skew values less than or equal to 0.2.

The angles of polarization presented are for the degree of polarization greater than 0.5 and the ellipticity less than 0.5. The second selection criteria for tensor apparent resistivities was relaxed for the Donalda station for which the data was slightly lower in quality and also for Nordegg and Observatory where the high skew probably indicates a more complex geology.

The tensor apparent resistivities were computed, by the methods outlined in Chapter 3, for time sequences for which the original data produced high coherencies between E_x-H_y and E_y-H_x . Coherencies greater than 0.9 for the magnetotelluric components generally resulted in high predicted coherencies for E_x and E_y , as well as low skew values and also smooth tensor apparent resistivity curves. For good magnetotelluric data the coherencies H_x-H_y and E_x-E_y were generally lower (<0.8) than the coherencies E_x-H_y and E_y-H_x . High coherency between E_x and E_y reaching its theoretical limit of unity occurred for the stations in mountains and in foothills, which were characterized, in most cases, by low coherency for the orthogonal magnetotelluric components as well as low coherency between H_x and H_y .

The degree of polarization, angle of polarization and the ellipticity of magnetic and telluric fields were computed using the techniques described in Chapter 3. In the polarization plots the number of data sets used for the analyses is indicated by the number following the station name. An attempt was made to obtain a uniform distribution of the polarization angles over the day.

Aeromagnetic maps (published by the Geological Survey of Canada) are available for some of the sounding sites. These depict contours of total magnetic field intensity. The flight altitude was 1000 ft. above the ground level. No correction is made for regional variation, which increases between 0.5γ to 3γ /mile from north to south and 2.8γ /mile from west to east.

The anomalies expressed by the magnetic contours are generally believed to be dependent on variations in the magnetic intensities of the basement rocks, which are, for the most part due to changes in composition of the basement rocks. While strong anomalies are probably due to an increased magnetic content in the rocks, weak anomalies may well be due to changes in the basement topography.

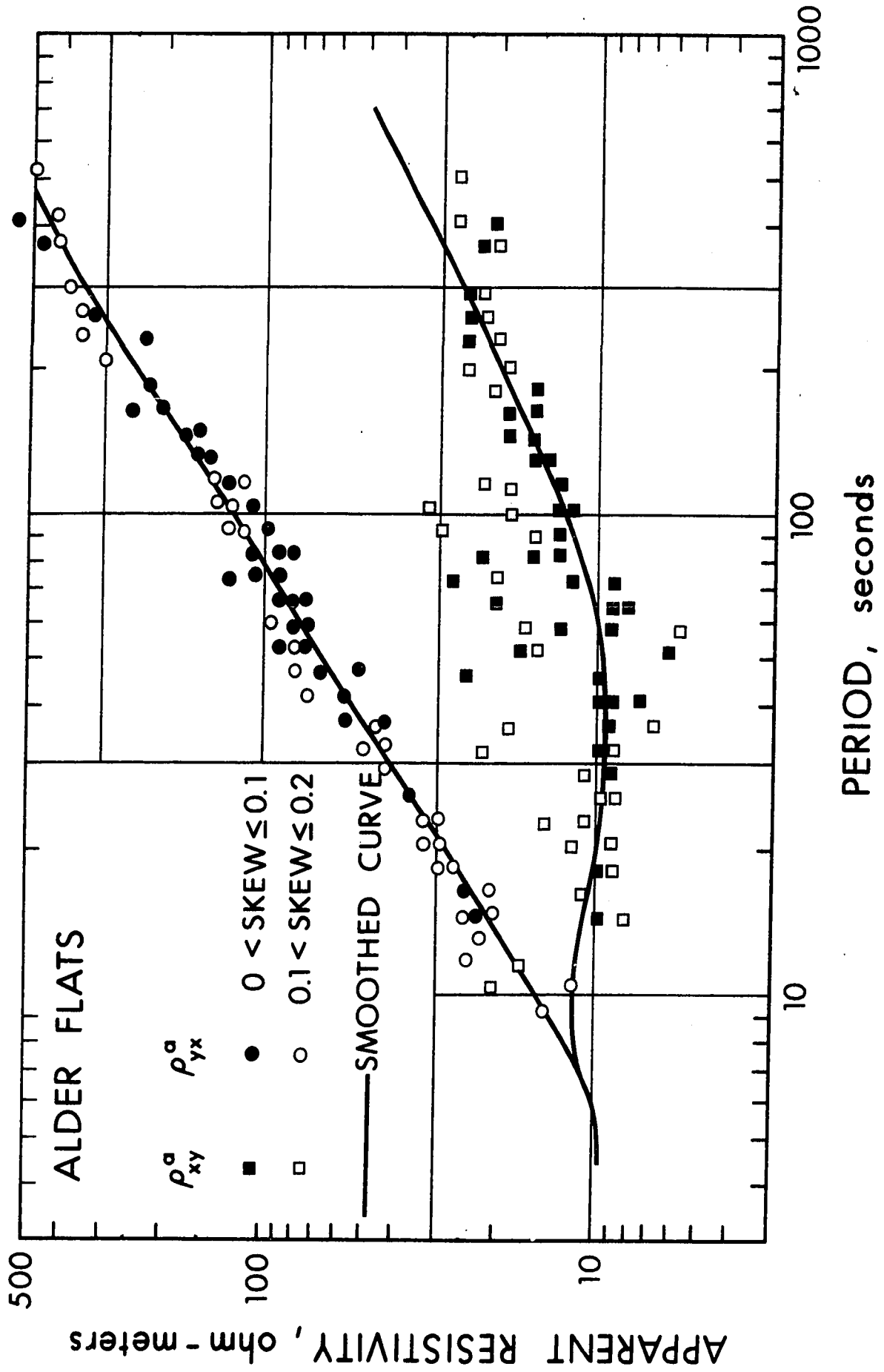
1. Alder flats (fig. 4.1)

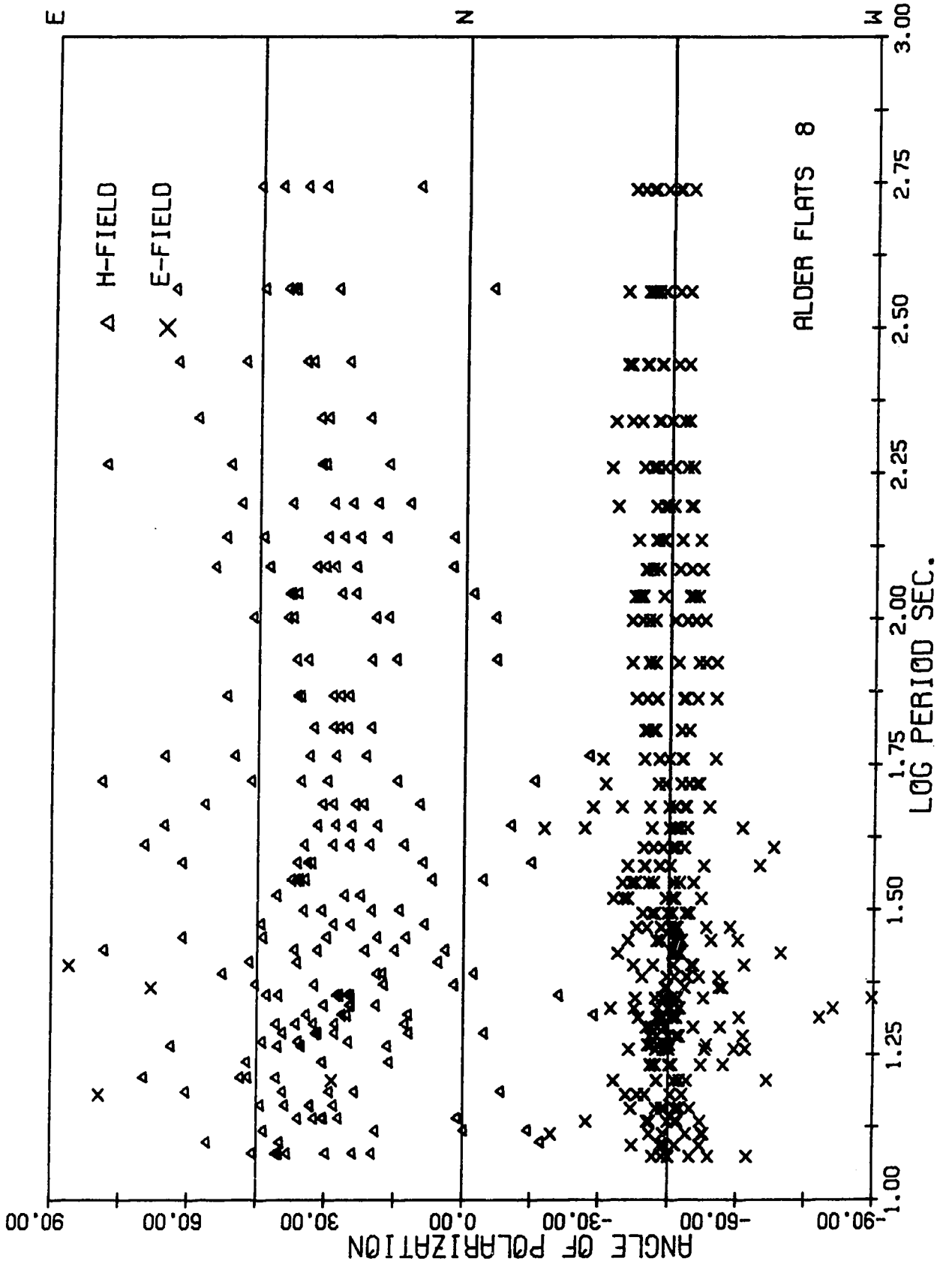
The tensor apparent resistivities show anisotropic behaviour for the periods greater than 10 seconds. The curves seem to converge for periods less than 10 seconds and approach asymptotically to the resistivity of the sedimentary strata, which is over 4 km thick at this location. The ρ_{xy}^a values show much scatter when compared to the ρ_{yx}^a values. The skewness coefficient less than 0.2 indicates a good approximation to a one or two dimensional structure. The azimuth of minimum resistivity is about $+50^\circ$. The telluric field is polarized in the north-westerly direction.

Since there is no significant vertical component at this station poor coherencies are obtained between H_z and the other four components of the magnetotelluric field. However, $\text{coh } H_z E_y$ and $\text{coh } H_z H_y$ are significantly greater than $\text{coh } H_z E_x$ and $\text{coh } H_z H_x$ for $N40^\circ E$ rotation.

Figure 4.1: Magnetotelluric results for Alder Flats

- i. Tensor apparent resistivities in the principal directions.
- ii. Azimuth (the direction of minimum tensor apparent resistivity).
- iii. Polarization angles for telluric and magnetic fields.
- iv. Vertical magnetic field analyses' results.





ROTATION ANGLE = N 0.0F

PERIOD SEC.	COH			HZ/HY
	HZ-EX	HZ-EY	HZ-HX	
546.13	0.15	0.22	0.56	0.85
364.09	0.35	0.40	0.41	0.63
273.07	0.58	0.63	0.60	0.52
218.45	0.31	0.51	0.68	0.50
182.04	0.23	0.41	0.66	0.49
156.04	0.26	0.37	0.60	0.44
136.53	0.39	0.44	0.51	0.40
121.36	0.54	0.58	0.60	0.36
109.23	0.66	0.66	0.64	0.33
99.30	0.81	0.82	0.77	0.32
84.02	0.76	0.87	0.82	0.30
72.82	0.72	0.87	0.82	0.25
64.25	0.75	0.82	0.74	0.22
57.49	0.71	0.69	0.57	0.20
52.01	0.67	0.62	0.47	0.20
47.49	0.66	0.66	0.67	0.22
43.69	0.66	0.66	0.67	0.21
40.45	0.52	0.66	0.66	0.21
37.66	0.71	0.77	0.69	0.17
35.23	0.60	0.80	0.82	0.16
33.10	0.57	0.75	0.54	0.14
31.21	0.60	0.75	0.73	0.18
29.52	0.77	0.89	0.73	0.20
28.01	0.80	0.86	0.70	0.18
26.64	0.46	0.67	0.60	0.11
25.40	0.52	0.68	0.57	0.39
24.27	0.66	0.74	0.54	0.53
23.24	0.53	0.72	0.58	0.67
22.29	0.75	0.78	0.54	0.77
21.42	0.62	0.67	0.43	0.62
20.61	0.47	0.90	0.84	0.43
19.86	0.71	0.95	0.92	0.68
19.16	0.76	0.95	0.91	0.72
18.51	0.57	0.94	0.92	0.20
18.20	0.57	0.94	0.94	0.18
17.07	0.67	0.97	0.95	0.19
16.06	0.63	0.95	0.94	0.16
15.17	0.81	0.93	0.88	0.23
14.37	0.80	0.93	0.90	0.15
13.65	0.32	0.87	0.85	0.13
13.00	0.79	0.79	0.64	0.14
12.41	0.72	0.91	0.79	0.15
11.87	0.82	0.88	0.80	0.13

ALDER FLATS 12 SEPT 1968 AM A 2

ROTATION ANGLE = N 40.0E

PERIOD SEC.	COH			HZ/HX	HZ/HY
	HZ-EX	HZ-EY	HZ-HX		
546.13	0.00	0.19	0.19	1.12	0.65
364.09	0.26	0.38	0.31	0.63	0.55
273.07	0.40	0.62	0.57	0.51	0.52
218.45	0.28	0.60	0.58	0.55	0.51
182.04	0.38	0.41	0.44	0.58	0.46
156.04	0.38	0.29	0.37	0.50	0.43
136.53	0.35	0.30	0.37	0.40	0.42
121.36	0.36	0.42	0.46	0.33	0.39
109.23	0.46	0.57	0.60	0.31	0.37
99.30	0.59	0.67	0.69	0.32	0.38
84.02	0.64	0.83	0.82	0.28	0.42
72.82	0.43	0.84	0.83	0.26	0.37
64.25	0.21	0.84	0.82	0.26	0.27
57.49	0.46	0.82	0.78	0.23	0.22
52.01	0.71	0.70	0.60	0.21	0.22
47.49	0.59	0.66	0.55	0.22	0.14
43.69	0.73	0.64	0.54	0.17	0.14
40.45	0.59	0.55	0.42	0.16	0.12
37.66	0.73	0.73	0.65	0.16	0.12
35.23	0.74	0.69	0.56	0.17	0.11
33.10	0.69	0.64	0.52	0.16	0.13
31.21	0.57	0.67	0.58	0.17	0.13
29.52	0.78	0.82	0.74	0.16	0.12
28.01	0.81	0.83	0.77	0.19	0.15
26.64	0.40	0.56	0.52	0.16	0.16
25.40	0.59	0.57	0.47	0.09	0.15
24.27	0.74	0.62	0.49	0.12	0.08
23.24	0.64	0.54	0.47	0.11	0.08
22.29	0.79	0.74	0.67	0.13	0.12
21.42	0.66	0.62	0.50	0.15	0.14
20.61	0.52	0.73	0.66	0.16	0.14
19.86	0.70	0.85	0.81	0.20	0.18
19.16	0.73	0.86	0.83	0.17	0.26
18.51	0.76	0.78	0.73	0.17	0.25
18.20	0.83	0.82	0.78	0.22	0.19
17.07	0.60	0.92	0.90	0.25	0.21
16.06	0.66	0.91	0.88	0.16	0.21
15.17	0.52	0.89	0.87	0.15	0.18
14.37	0.65	0.91	0.88	0.12	0.20
13.65	0.52	0.65	0.62	0.11	0.20
13.00	0.73	0.83	0.79	0.14	0.13
12.41	0.73	0.84	0.72	0.13	0.11
11.87	0.82	0.86	0.78	0.14	0.12

ALDER FLATS 12 SEPT 1968 AM A 2

2. Bonnyville (Fig. 4.2)

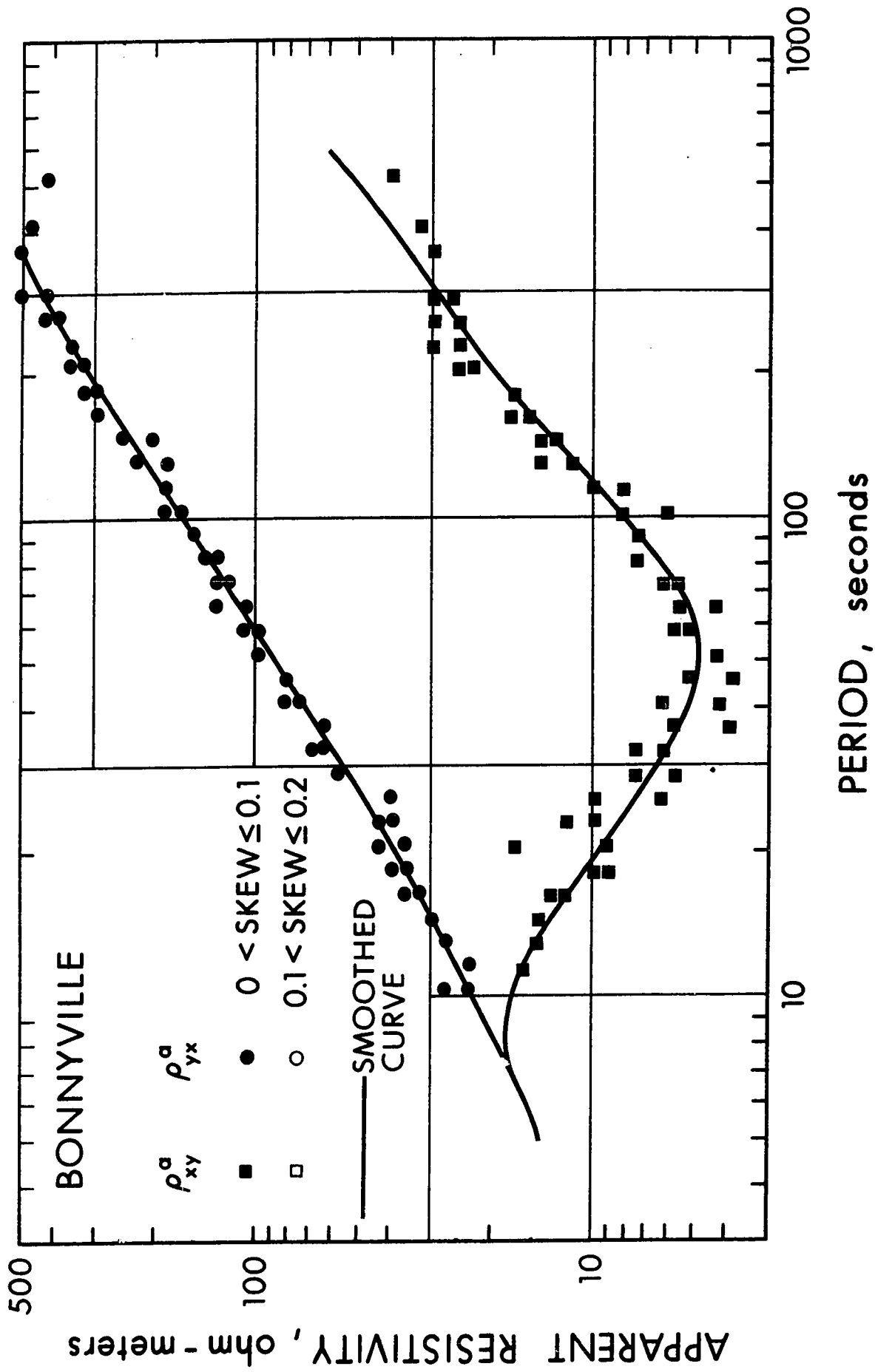
Bonnyville is the closest station to the Canadian Shield. The thickness of the sedimentary section is about 1.5 km. The rotated tensor apparent resistivity curves show anisotropic behaviour for periods greater than 10 seconds. The maximum difference between the two curves occurs between 30 seconds and 100 seconds. The curves seem to converge for shorter periods. Relatively smooth resistivity estimates are obtained in both the minimum and maximum directions of the resistivity.

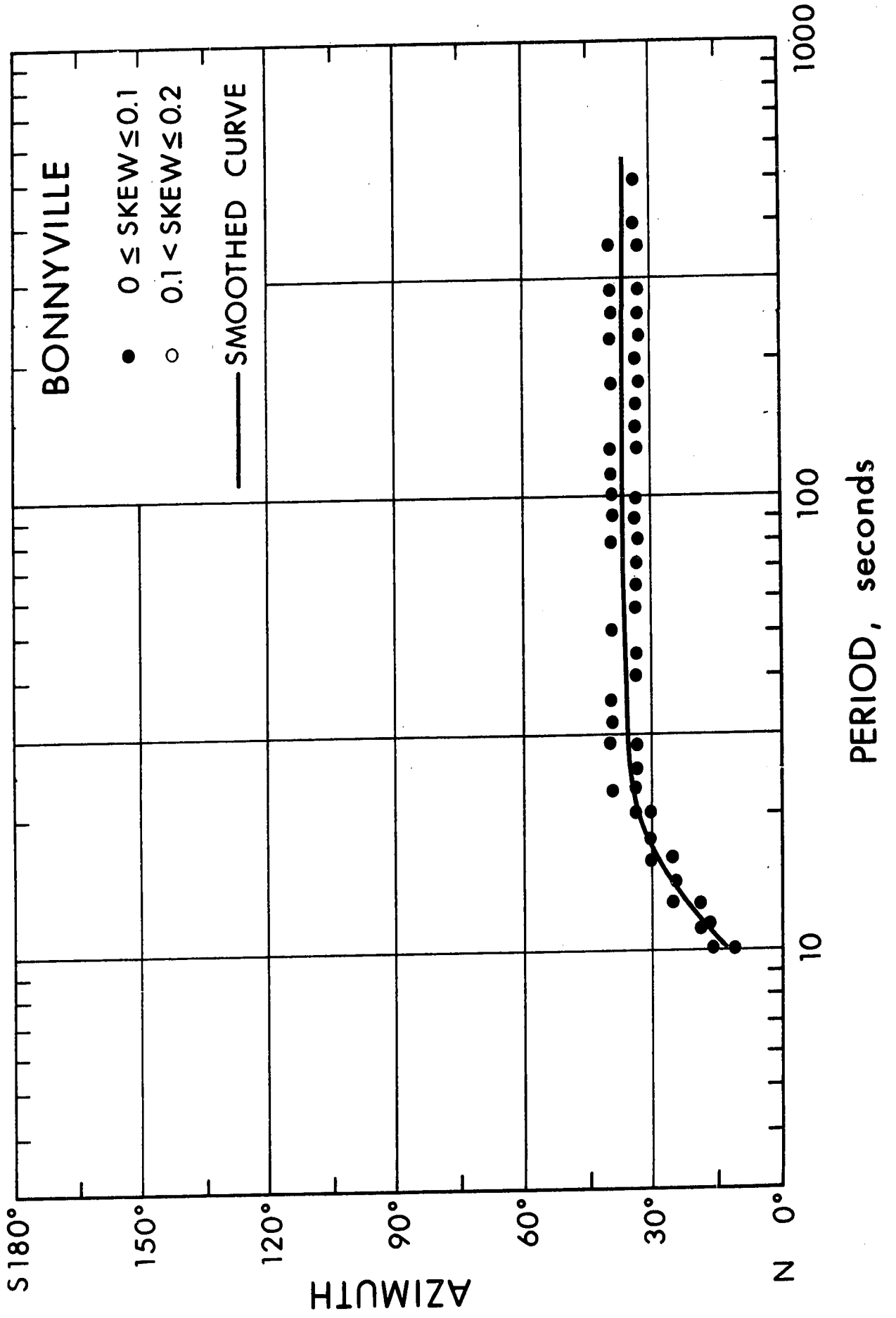
The azimuth for the minimum apparent resistivity is about $+35^\circ$ for periods greater than 20 seconds and tends towards zero for shorter periods. The telluric field is polarized about $N55^\circ W$ direction. The magnetic and telluric fields are non-orthogonal for most of the spectrum except at short period end. There is much variation in the angle of polarization of the magnetic field for periods less than 30 seconds.

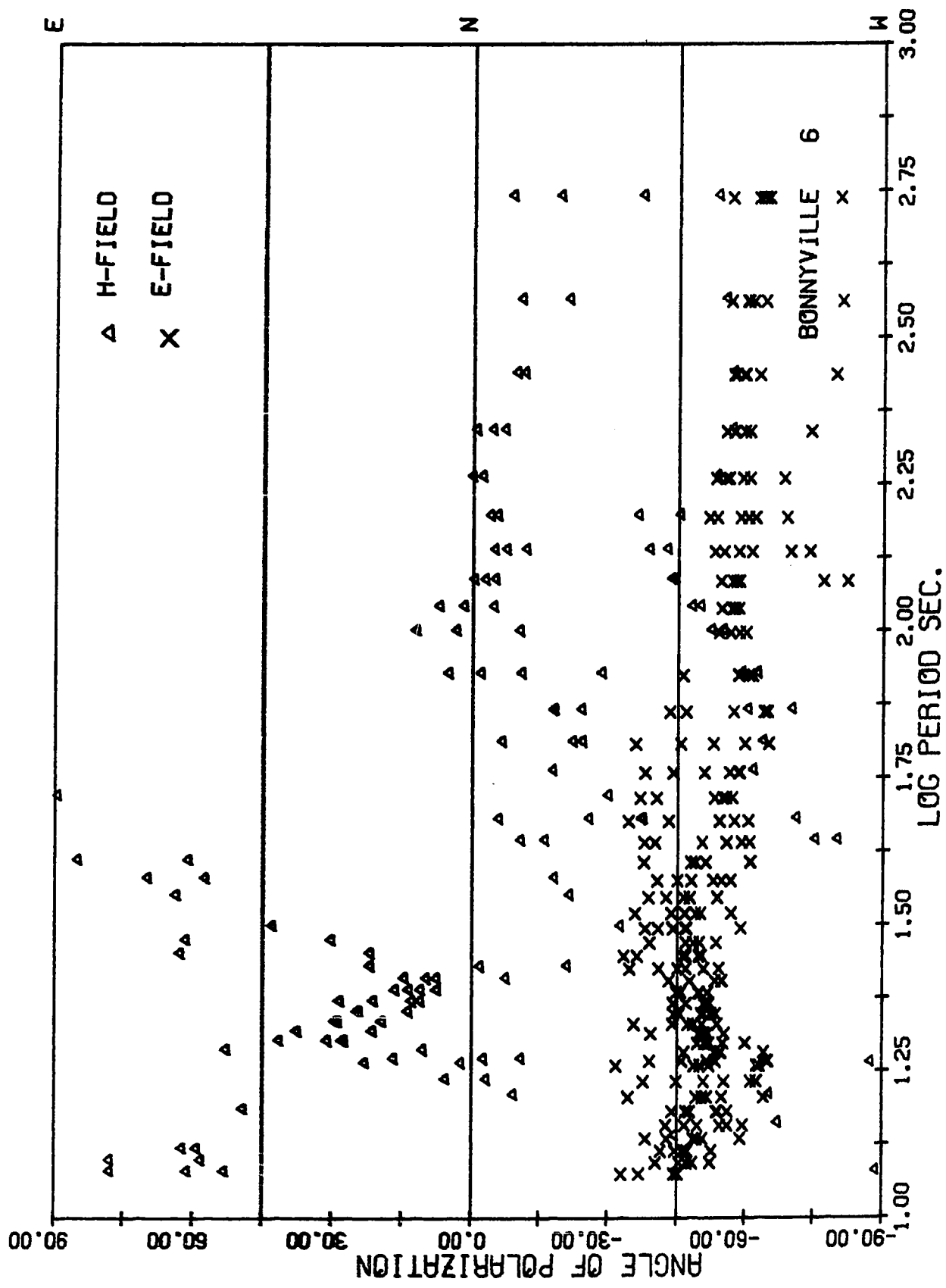
A significant H_z component is observed in some sections of the data, particularly during times of high magnetic activity. $\text{coh } H_z E_x$, $\text{coh } H_z E_y$ and $\text{coh } H_z H_x$ are high in the measuring directions. However, the $\text{coh } H_z E_x$ drops to

Figure 4.2: Magnetotelluric results for Bonnyville

- i. Tensor apparent resistivities in the principal directions.
- ii. Azimuth (the direction of minimum tensor apparent resistivity).
- iii. Polarization angles for telluric and magnetic fields.
- iv. Vertical magnetic field analyses' results.







ROTATION ANGLE = N 0.0E

PERIOD SEC.	COH		COH		COH		HZ/HY	HZ/HX	HZ/HY	COH	COH		COH		HZ/HX	HZ/HY
	HZ-EX	HZ-EY	HZ-HX	HZ-HY	HZ-EX	HZ-EY					HZ-HX	HZ-HY	HZ-EX	HZ-EY		
546.13	0.62	0.83	0.73	0.42	0.99	1.32	0.99	1.32	0.62	0.80	0.80	0.29	1.04	1.21		
364.03	0.62	0.89	0.85	0.30	0.81	1.05	0.81	1.05	0.60	0.84	0.81	0.56	0.93	0.89		
273.07	0.59	0.91	0.94	0.26	0.80	0.97	0.80	0.97	0.48	0.85	0.88	0.66	0.85	0.79		
218.45	0.72	0.94	0.97	0.24	0.67	1.05	0.67	1.05	0.40	0.90	0.91	0.70	0.76	0.85		
182.04	0.85	0.97	0.98	0.42	0.63	1.23	0.63	1.23	0.56	0.95	0.95	0.79	0.69	0.87		
156.04	0.91	0.98	0.98	0.63	0.60	1.28	0.60	1.28	0.75	0.97	0.97	0.87	0.69	0.87		
136.53	0.90	0.98	0.99	0.64	0.58	1.13	0.58	1.13	0.72	0.97	0.96	0.86	0.67	0.81		
121.36	0.87	0.97	0.99	0.68	0.57	1.04	0.57	1.04	0.53	0.96	0.96	0.77	0.59	0.82		
109.23	0.89	0.97	0.98	0.33	0.55	1.08	0.55	1.08	0.33	0.95	0.96	0.69	0.59	0.91		
99.30	0.92	0.97	0.97	0.39	0.51	1.12	0.51	1.12	0.31	0.96	0.96	0.66	0.53	1.00		
84.02	0.86	0.95	0.97	0.15	0.39	0.82	0.39	0.82	0.16	0.94	0.95	0.70	0.42	0.65		
72.82	0.77	0.91	0.97	0.06	0.38	0.61	0.38	0.61	0.20	0.88	0.91	0.69	0.41	0.51		
64.25	0.73	0.86	0.94	0.23	0.40	0.42	0.40	0.42	0.27	0.84	0.87	0.47	0.42	0.41		
57.49	0.73	0.89	0.95	0.25	0.39	0.43	0.39	0.43	0.27	0.85	0.89	0.56	0.43	0.39		
52.01	0.75	0.91	0.98	0.19	0.38	0.54	0.38	0.54	0.16	0.87	0.91	0.66	0.44	0.45		
47.49	0.80	0.93	0.97	0.32	0.34	0.47	0.34	0.47	0.19	0.91	0.92	0.65	0.37	0.41		
43.69	0.74	0.88	0.94	0.19	0.32	0.47	0.32	0.47	0.19	0.91	0.92	0.65	0.37	0.41		
40.45	0.72	0.88	0.94	0.52	0.33	0.32	0.33	0.32	0.31	0.85	0.89	0.34	0.32	0.32		
37.66	0.72	0.77	0.91	0.29	0.32	0.28	0.32	0.28	0.54	0.76	0.80	0.39	0.29	0.31		
35.23	0.72	0.82	0.93	0.29	0.27	0.27	0.27	0.27	0.59	0.79	0.82	0.52	0.28	0.26		
33.10	0.62	0.81	0.90	0.09	0.27	0.25	0.27	0.25	0.32	0.77	0.83	0.45	0.31	0.23		
31.21	0.49	0.65	0.75	0.12	0.29	0.18	0.29	0.18	0.32	0.62	0.61	0.24	0.26	0.19		
29.52	0.64	0.87	0.92	0.20	0.28	0.29	0.28	0.29	0.35	0.82	0.81	0.52	0.29	0.28		
28.01	0.76	0.85	0.93	0.20	0.28	0.36	0.28	0.36	0.65	0.84	0.86	0.62	0.32	0.31		
26.64	0.81	0.82	0.93	0.43	0.23	0.34	0.23	0.34	0.80	0.82	0.89	0.74	0.29	0.25		
25.40	0.86	0.87	0.96	0.57	0.20	0.34	0.20	0.34	0.85	0.87	0.92	0.80	0.23	0.26		
24.27	0.91	0.92	0.96	0.65	0.19	0.32	0.19	0.32	0.81	0.93	0.96	0.71	0.20	0.30		
23.24	0.89	0.88	0.93	0.65	0.18	0.24	0.18	0.24	0.69	0.90	0.93	0.43	0.16	0.29		
22.29	0.88	0.91	0.93	0.60	0.16	0.24	0.16	0.24	0.65	0.92	0.94	0.33	0.15	0.28		
21.42	0.35	0.84	0.90	0.56	0.17	0.18	0.17	0.18	0.68	0.88	0.92	0.40	0.16	0.20		
20.61	0.84	0.82	0.96	0.61	0.15	0.15	0.15	0.15	0.51	0.85	0.92	0.12	0.13	0.18		
19.86	0.83	0.85	0.90	0.62	0.14	0.15	0.14	0.15	0.52	0.87	0.92	0.07	0.12	0.20		
19.16	0.68	0.81	0.90	0.66	0.16	0.14	0.16	0.14	0.61	0.84	0.91	0.26	0.13	0.19		
18.51	0.68	0.64	0.73	0.39	0.16	0.12	0.16	0.12	0.44	0.70	0.79	0.11	0.14	0.13		
18.20	0.57	0.54	0.68	0.26	0.15	0.10	0.15	0.10	0.36	0.59	0.68	0.09	0.13	0.11		
17.07	0.68	0.38	0.71	0.56	0.18	0.18	0.18	0.18	0.82	0.84	0.86	0.06	0.19	0.17		
16.06	0.35	0.16	0.45	0.44	0.16	0.16	0.16	0.16	0.55	0.44	0.58	0.53	0.18	0.12		
15.17	0.39	0.58	0.64	0.16	0.17	0.16	0.17	0.16	0.28	0.53	0.53	0.28	0.15	0.20		
14.37	0.57	0.63	0.68	0.32	0.16	0.13	0.16	0.13	0.44	0.62	0.68	0.20	0.14	0.14		
13.65	0.40	0.32	0.60	0.35	0.12	0.12	0.12	0.12	0.62	0.27	0.38	0.58	0.12	0.13		
13.00	0.35	0.24	0.31	0.26	0.09	0.07	0.09	0.07	0.41	0.28	0.29	0.26	0.07	0.09		
12.41	0.71	0.49	0.30	0.76	0.17	0.11	0.17	0.11	0.72	0.59	0.62	0.70	0.13	0.12		
11.87	0.79	0.55	0.59	0.78	0.17	0.12	0.17	0.12	0.77	0.70	0.74	0.70	0.12	0.17		

BONNYVILLE 15 JUNE 1969 AM B

BONNYVILLE 15 JUNE 1969 AM B

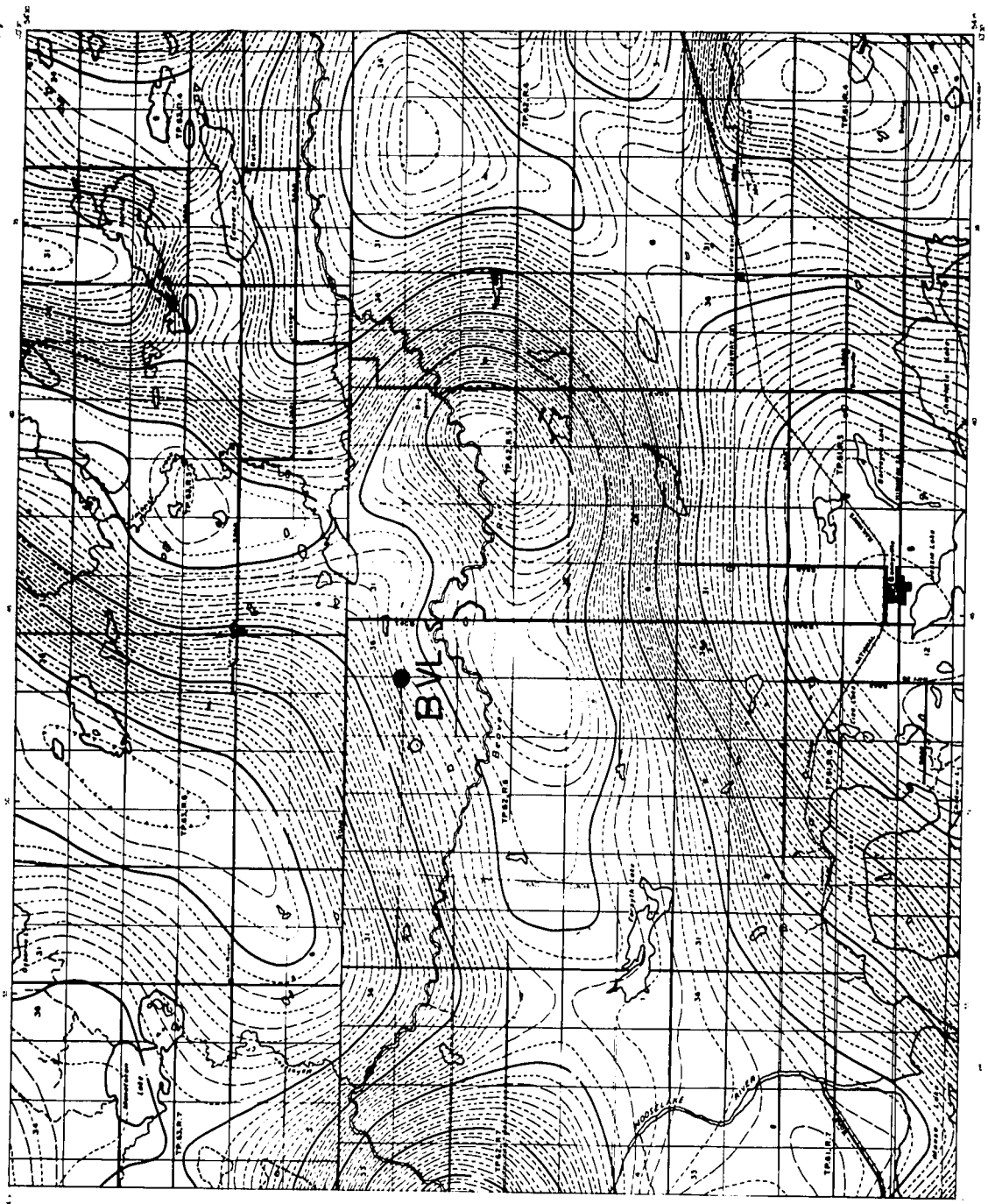
minimum for the rotation angle $N30^{\circ}E$ and $\text{coh } H_z E_y$ and $\text{coh } H_z H_x$ continue to show a maximum indicating a possible strike direction of $N60^{\circ}W$. The amplitude ratio between H_z and H_x varies between 0.1 and 0.6. The high value for the ratio H_z/H_y is a consequence of low power in the H_y component.

Figure 4.2a: Aeromagnetic map of Bonnyville area

Canada
DEPARTMENT
OF
MINES AND TECHNICAL SURVEYS
GEOLOGICAL SURVEY OF CANADA

AEROMAGNETIC SERIES

SHEET 724



Scale 1:50,000

3. Camp Creek (Fig. 4.3)

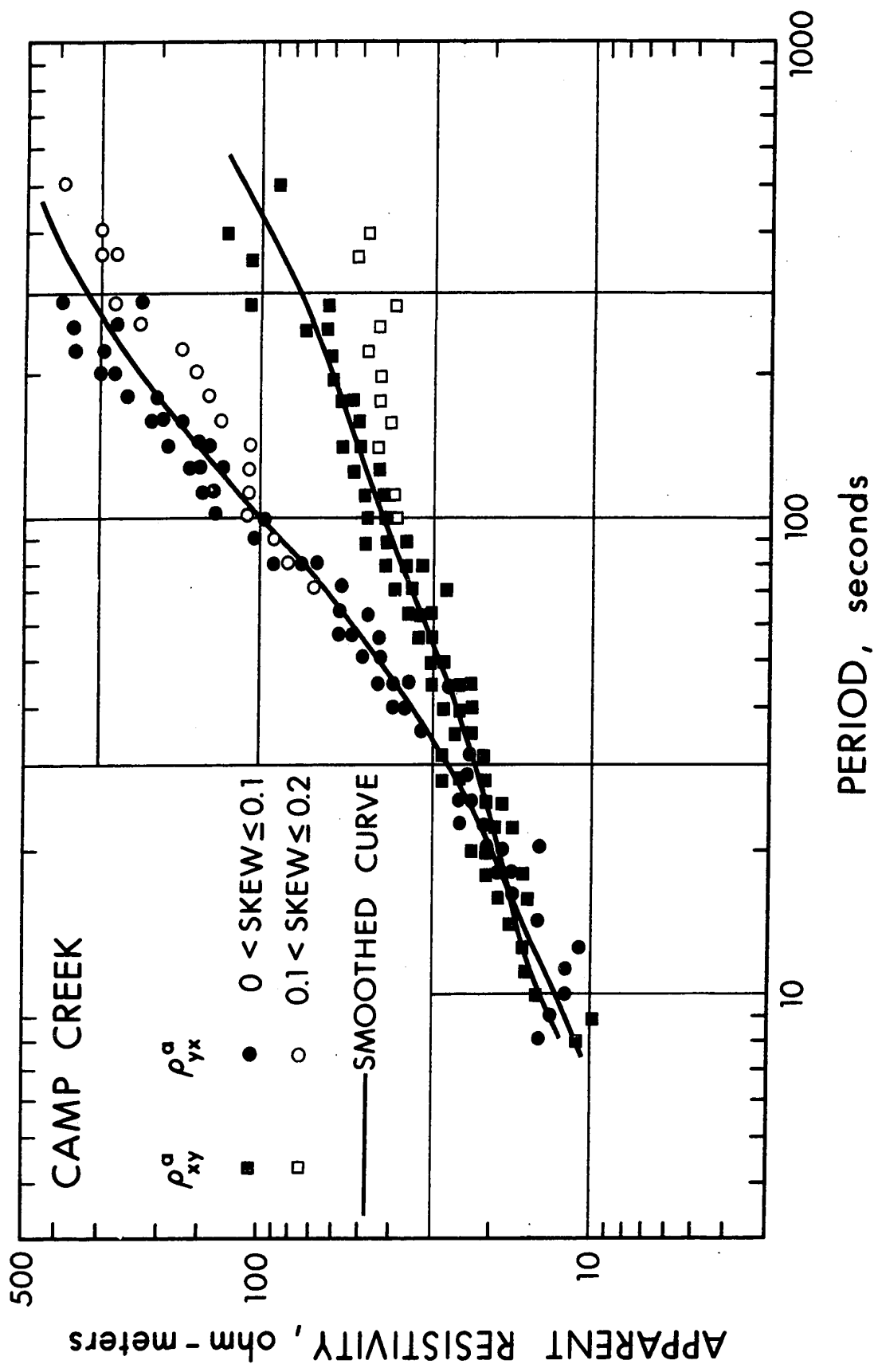
The tensor apparent resistivity curves show anisotropic behaviour for the periods greater than 40 seconds. The degree of anisotropy is less than that of Alder Flats or Bonnyville. The apparent resistivity estimates are relatively smooth for skew less than 0.1.

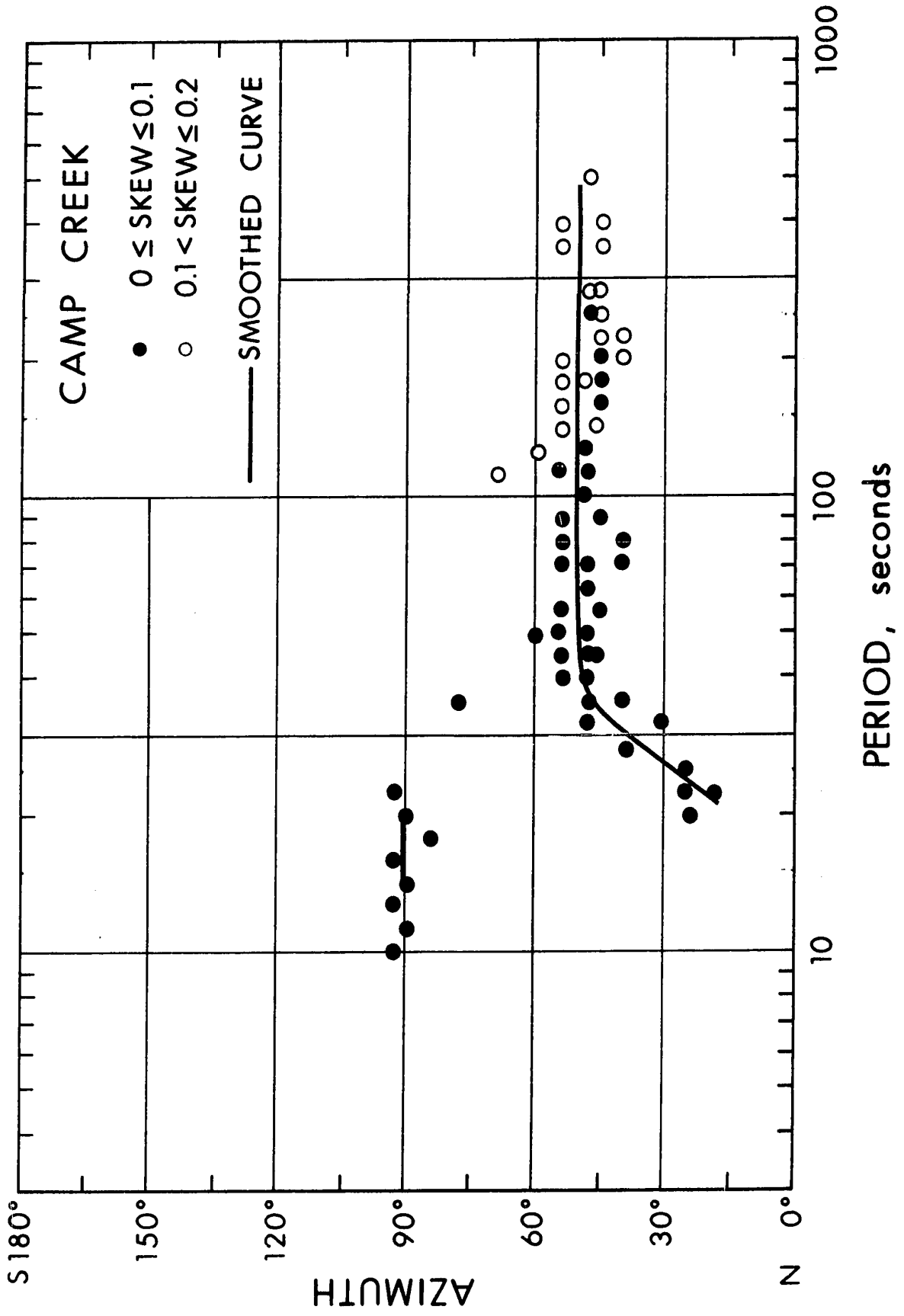
The azimuth for minimum apparent resistivity is about $+45^\circ$ for periods greater than 40 seconds and tends to 0° or 90° for shorter periods. The telluric and magnetic fields are orthogonal for shorter periods indicating a possible isotropic nature of the surface layers. The angle of polarization of the telluric field is about $N50^\circ W$ which corresponds closely to the direction of maximum apparent resistivity.

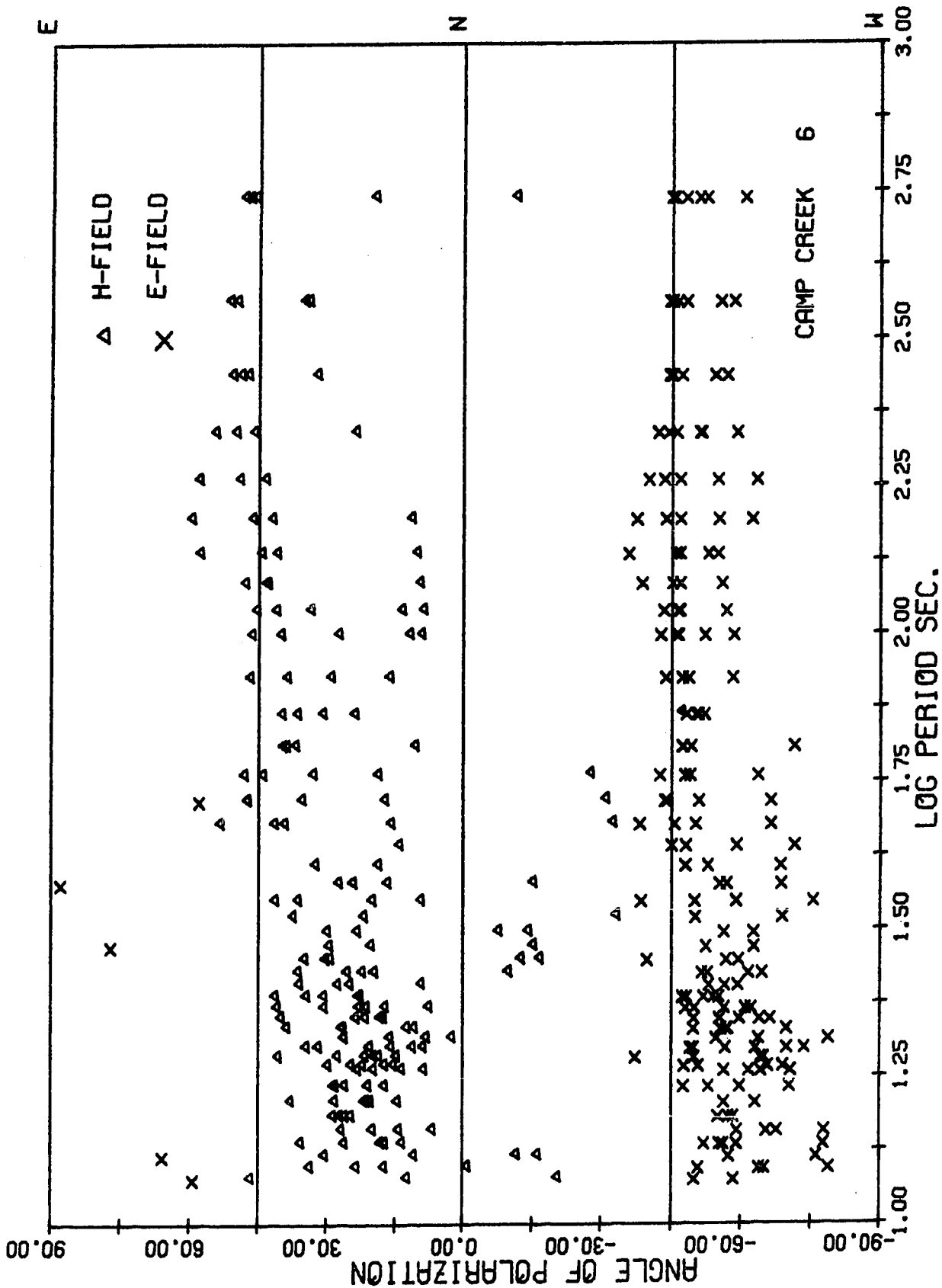
The coherencies between the vertical magnetic field component and the other four components of the horizontal magnetic and telluric fields are low, however, the $\text{coh } H_z E_x$ and $\text{coh } H_z H_y$ drops to a minimum for a rotation angle of $N40^\circ E$.

Figure 4.3: Magnetotelluric results for Camp Creek

- i. Tensor apparent resistivities in the principal directions.
- ii. Azimuth (the direction of minimum tensor apparent resistivity).
- iii. Polarization angles for telluric and magnetic fields.
- iv. Vertical magnetic field analyses' results.







ROTATION ANGLE = N 0.0E				ROTATION ANGLE = N 40.0E			
PERIOD SEC.	COH HZ-EX	COH HZ-EY	COH HZ-HX	COH HZ-HY	COH HZ-HX	COH HZ-HY	HZ/HV
546.13	0.84	0.85	0.88	0.83	0.54	0.50	0.39
364.09	0.94	0.95	0.93	0.92	0.47	0.41	1.18
273.07	0.95	0.96	0.93	0.91	0.42	0.38	1.12
218.45	0.92	0.92	0.89	0.84	0.38	0.38	1.07
182.04	0.84	0.84	0.81	0.73	0.37	0.40	1.00
156.04	0.73	0.74	0.69	0.56	0.38	0.42	0.96
136.53	0.72	0.74	0.70	0.59	0.34	0.39	0.94
121.36	0.80	0.81	0.78	0.74	0.31	0.33	0.92
109.23	0.79	0.81	0.78	0.77	0.29	0.29	0.83
99.30	0.76	0.79	0.74	0.76	0.28	0.27	0.83
84.02	0.71	0.78	0.74	0.72	0.29	0.28	0.65
72.82	0.82	0.87	0.83	0.83	0.26	0.31	0.64
64.25	0.82	0.82	0.79	0.84	0.26	0.31	0.58
57.49	0.74	0.73	0.70	0.77	0.32	0.33	0.54
52.01	0.83	0.80	0.78	0.85	0.30	0.28	0.51
47.49	0.82	0.72	0.62	0.82	0.28	0.24	0.35
43.69	0.72	0.60	0.48	0.73	0.21	0.22	0.25
40.45	0.77	0.69	0.55	0.80	0.23	0.27	0.19
37.66	0.60	0.56	0.38	0.62	0.23	0.26	0.32
35.23	0.68	0.21	0.07	0.70	0.20	0.24	0.23
33.10	0.70	0.24	0.14	0.72	0.22	0.28	0.20
31.21	0.57	0.25	0.15	0.55	0.22	0.34	0.24
29.52	0.44	0.27	0.15	0.42	0.20	0.29	0.27
28.01	0.50	0.26	0.16	0.46	0.23	0.31	0.23
26.64	0.27	0.39	0.31	0.29	0.21	0.33	0.28
25.40	0.44	0.37	0.29	0.47	0.23	0.37	0.32
24.27	0.54	0.49	0.43	0.55	0.24	0.34	0.43
23.24	0.64	0.63	0.58	0.63	0.27	0.40	0.47
22.29	0.64	0.56	0.52	0.59	0.30	0.42	0.42
21.42	0.68	0.44	0.42	0.63	0.29	0.38	0.35
20.61	0.55	0.15	0.17	0.46	0.25	0.40	0.31
19.86	0.58	0.26	0.13	0.52	0.27	0.47	0.28
19.16	0.56	0.37	0.26	0.52	0.28	0.52	0.29
18.51	0.48	0.45	0.38	0.41	0.35	0.44	0.45
18.20	0.40	0.39	0.36	0.39	0.34	0.48	0.51
17.07	0.49	0.19	0.32	0.46	0.28	0.45	0.48
16.06	0.47	0.42	0.35	0.40	0.35	0.51	0.60
15.17	0.51	0.08	0.23	0.41	0.38	0.54	0.52
14.37	0.38	0.25	0.10	0.15	0.36	0.82	0.61
13.65	0.52	0.30	0.36	0.38	0.32	0.57	0.55
13.00	0.56	0.35	0.14	0.44	0.42	0.63	0.53
12.41	0.47	0.37	0.37	0.33	0.46	0.58	0.56
11.87	0.43	0.29	0.32	0.26	0.33	0.62	0.64

CAMP CREEK 04 SEPT 1968 PM2 A 1

CAMP CREEK 04 SEPT 1968 PM2 A 1

4. Carrot Creek (Fig. 4.4)

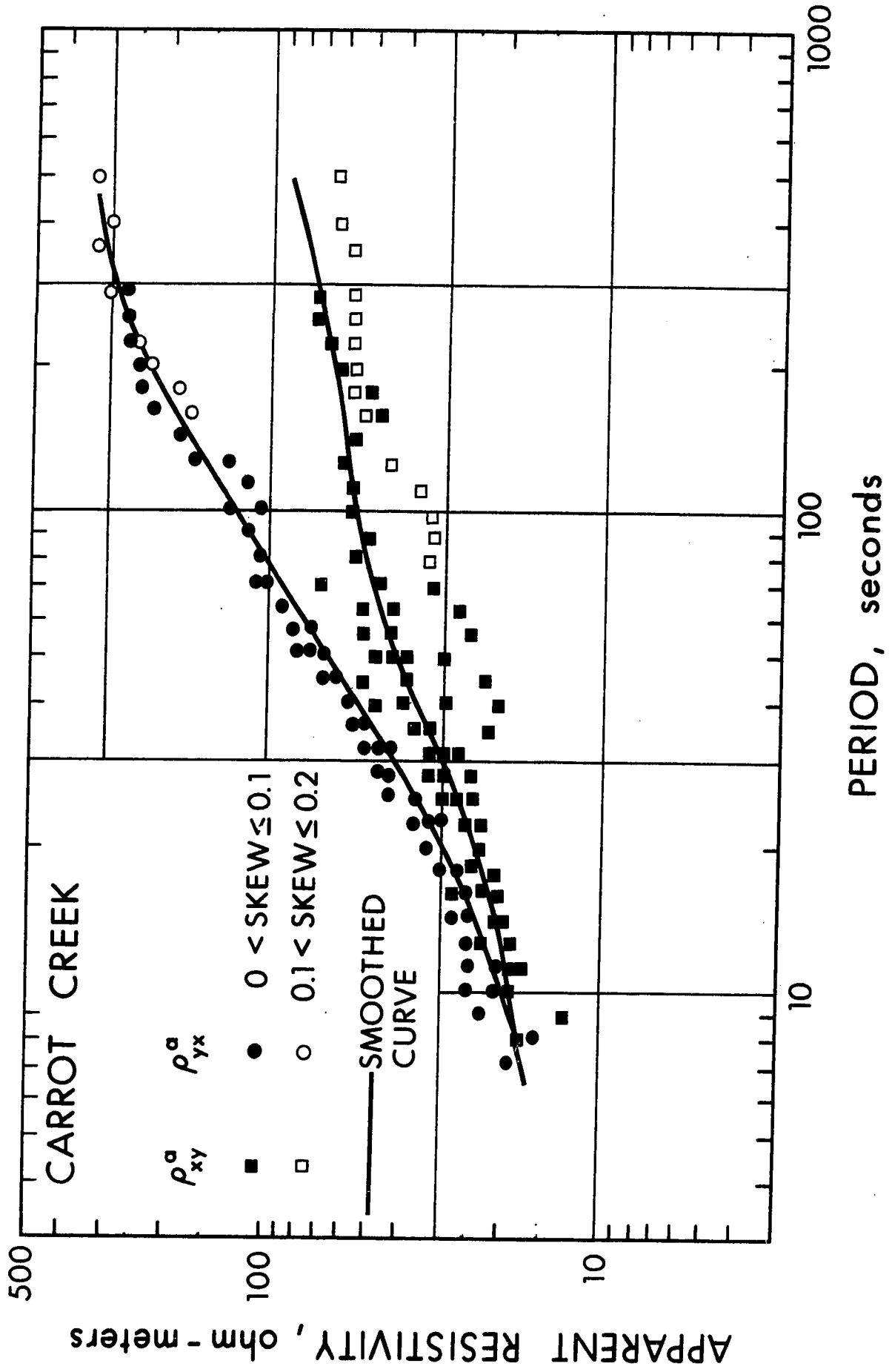
The tensor apparent resistivity curves for this station are similar to the curves for Camp Creek. The anisotropic effect is pronounced for periods greater than 80 seconds, although the presence of it is noticeable for periods greater than 20 seconds. There is a considerable amount of scatter in ρ_{xy}^a , even for skew values less than 0.1.

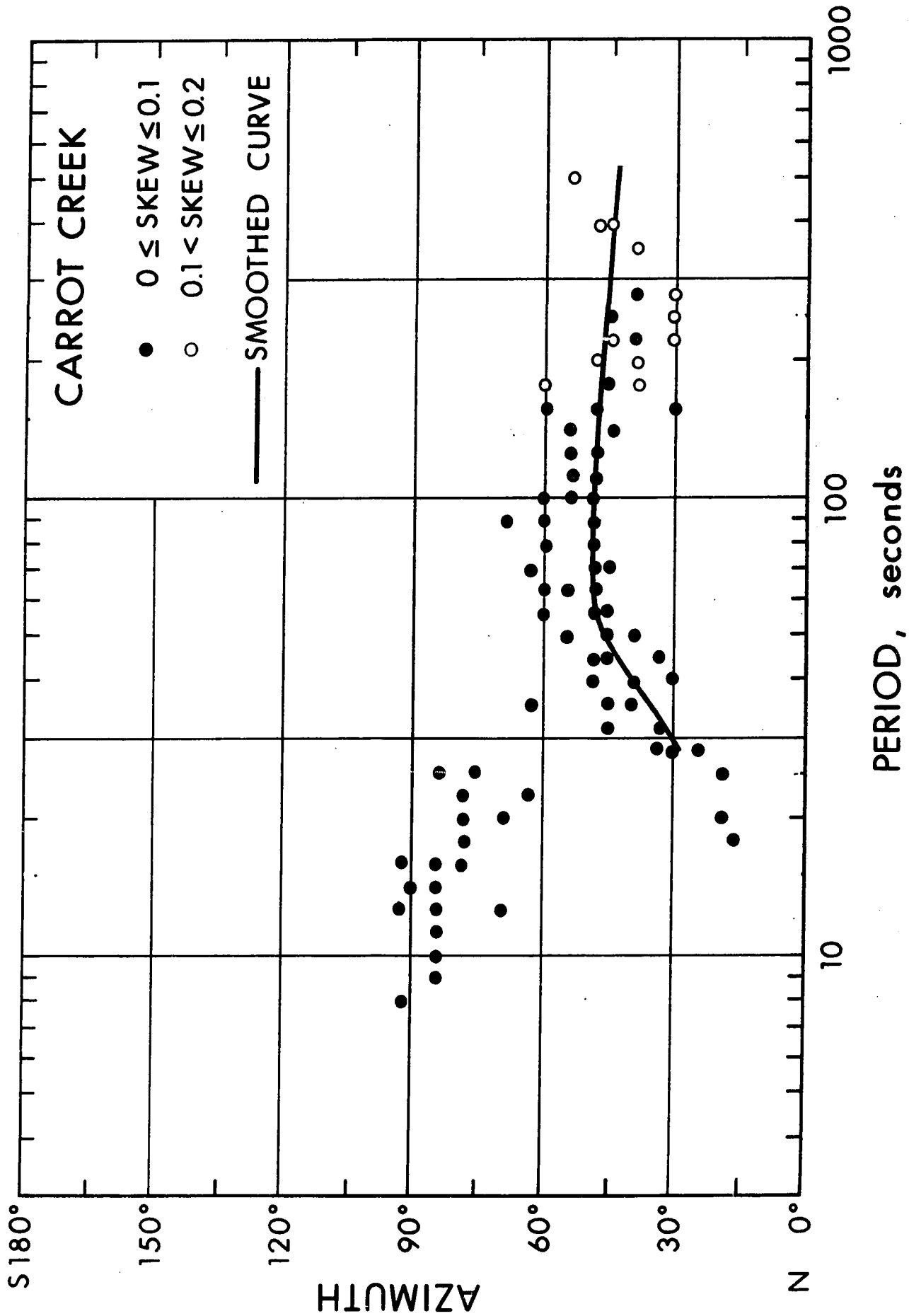
Rotation of tensor impedances gave $+50^\circ$ azimuth for minimum apparent resistivity for longer periods and tends to 90° for shorter periods. There is a considerable amount of scatter in azimuth. The angle of polarization of the telluric field distributed around $N45^\circ W$ for long periods and close to east-west for short periods. Magnetic and telluric fields are orthogonal for shorter periods. There is a considerable variation in the angle of polarization of the magnetic field, although it is mainly oriented along the $N20^\circ E$ direction.

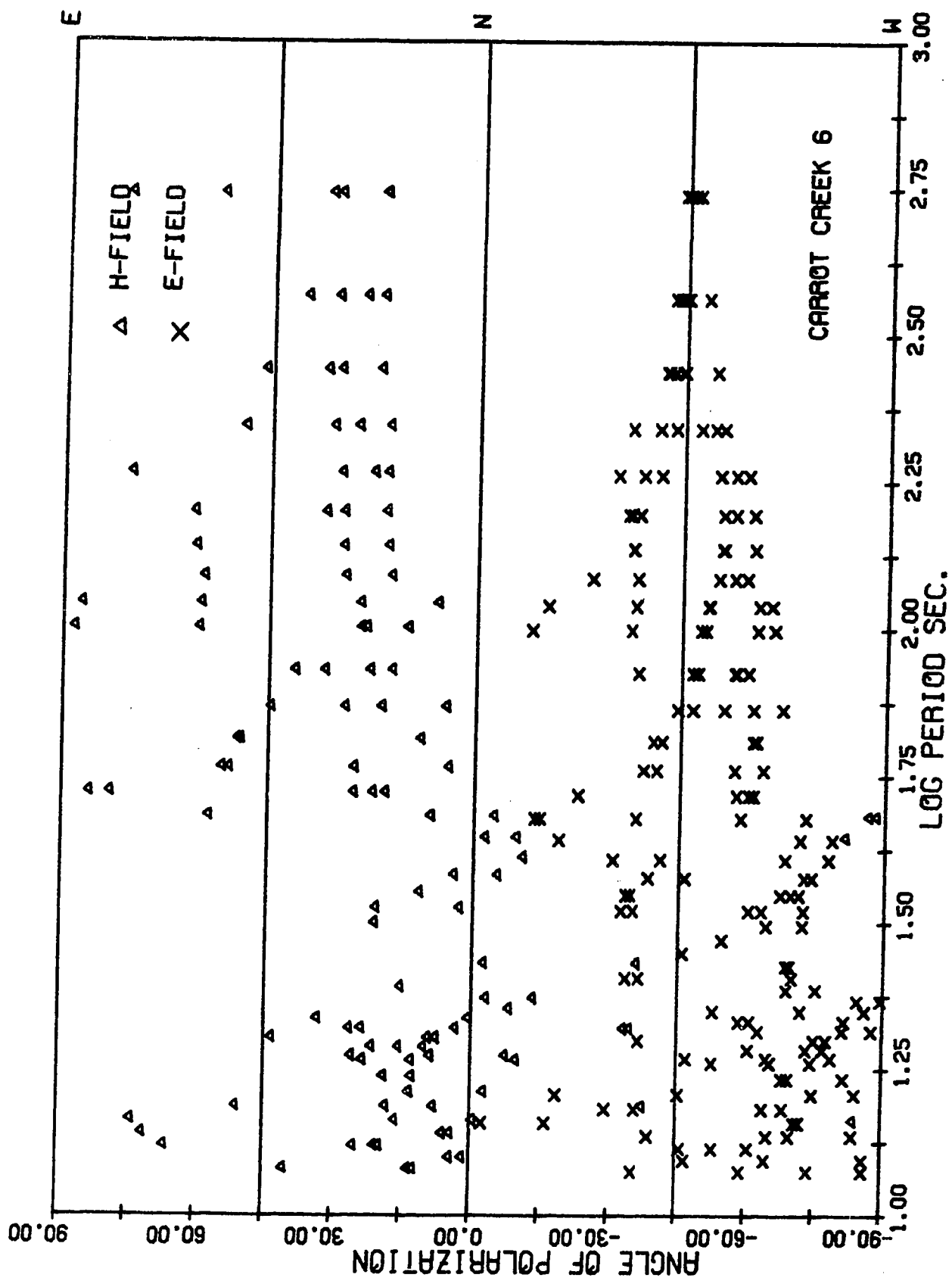
Significant level of H_z activity is observed at this site. Coherency analyses show that $\text{coh } H_z E_y$ and $\text{coh } H_z H_x$ are greater than $\text{coh } H_z E_x$ and $\text{coh } H_z H_y$, further $\text{coh } H_z E_x$ and $\text{coh } H_z H_y$ drops to a minimum for a rotation angle of $N30^\circ E$, giving a probable strike direction of $N60^\circ W$. The amplitude ratio between H_z and H_x varies between 0.7 and 0.5 for this rotation angle.

Figure 4.4: Magnetotelluric results for Carrot Creek

- i. Tensor apparent resistivities in the principal directions.
- ii. Azimuth (the direction of minimum tensor apparent resistivity).
- iii. Polarization angles for telluric and magnetic fields.
- iv. Vertical magnetic field analyses' results.







ROTATION ANGLE = N 0.0E				ROTATION ANGLE = N 30.0E			
PERIOD SEC.	COH HZ-EX	COH HZ-EY	COH HZ-HX	COH HZ-HY	COH HZ-HX	COH HZ-HY	HZ/HY
546.13	0.47	0.51	0.45	0.39	0.38	0.50	0.92
364.09	0.71	0.78	0.73	0.46	0.46	0.77	0.81
273.07	0.77	0.84	0.82	0.65	0.43	0.84	1.28
218.45	0.70	0.83	0.78	0.56	0.25	0.82	1.16
182.04	0.59	0.78	0.70	0.41	0.10	0.77	0.72
156.04	0.61	0.81	0.75	0.55	0.14	0.79	1.05
136.53	0.62	0.83	0.79	0.65	0.32	0.81	0.97
121.36	0.62	0.84	0.80	0.66	0.49	0.82	0.70
109.23	0.78	0.85	0.82	0.70	0.54	0.84	0.89
99.30	0.78	0.85	0.82	0.77	0.54	0.84	0.99
84.02	0.91	0.91	0.86	0.87	0.49	0.86	1.13
72.82	0.87	0.86	0.80	0.78	0.59	0.94	1.29
64.25	0.80	0.84	0.80	0.65	0.65	0.89	0.93
57.49	0.80	0.97	0.93	0.65	0.53	0.96	0.83
52.01	0.88	0.96	0.91	0.77	0.59	0.98	0.81
47.49	0.85	0.94	0.86	0.71	0.51	0.98	0.93
43.69	0.76	0.91	0.85	0.57	0.23	0.97	0.86
40.45	0.72	0.93	0.87	0.60	0.47	0.95	0.67
37.66	0.71	0.87	0.78	0.55	0.60	0.97	0.56
35.23	0.74	0.86	0.78	0.55	0.38	0.94	0.58
33.10	0.75	0.89	0.83	0.67	0.48	0.94	0.55
31.21	0.57	0.73	0.64	0.47	0.49	0.94	0.70
29.52	0.73	0.52	0.25	0.69	0.21	0.89	0.48
28.01	0.83	0.76	0.56	0.82	0.53	0.82	0.41
26.64	0.81	0.87	0.78	0.80	0.73	0.84	0.62
25.40	0.80	0.91	0.86	0.77	0.69	0.91	0.49
24.27	0.82	0.91	0.86	0.80	0.73	0.94	0.62
23.24	0.69	0.91	0.86	0.73	0.76	0.92	0.66
22.29	0.80	0.94	0.91	0.79	0.84	0.95	0.58
21.42	0.70	0.93	0.89	0.63	0.77	0.94	0.77
20.61	0.74	0.91	0.88	0.59	0.67	0.94	0.54
19.86	0.77	0.84	0.79	0.72	0.47	0.89	0.90
19.16	0.77	0.73	0.71	0.74	0.47	0.89	0.58
18.51	0.57	0.80	0.82	0.50	0.14	0.80	1.24
18.20	0.67	0.84	0.86	0.60	0.47	0.82	1.08
17.07	0.77	0.86	0.86	0.67	0.46	0.86	1.23
16.06	0.70	0.83	0.80	0.65	0.35	0.87	1.36
15.17	0.66	0.80	0.67	0.65	0.50	0.86	1.36
14.37	0.68	0.61	0.71	0.65	0.47	0.73	1.14
13.65	0.15	0.54	0.57	0.09	0.31	0.70	1.28
13.00	0.55	0.28	0.48	0.52	0.41	0.53	1.99
12.41	0.50	0.24	0.12	0.54	0.48	0.33	1.97
11.87	0.35	0.27	0.25	0.17	0.13	0.33	1.14
							1.07

CARROT CREEK 17 AUG 1968 AMI A2

CARROT CREEK 17 AUG 1968 AMI A2

5. Donalda (Fig. 4.5)

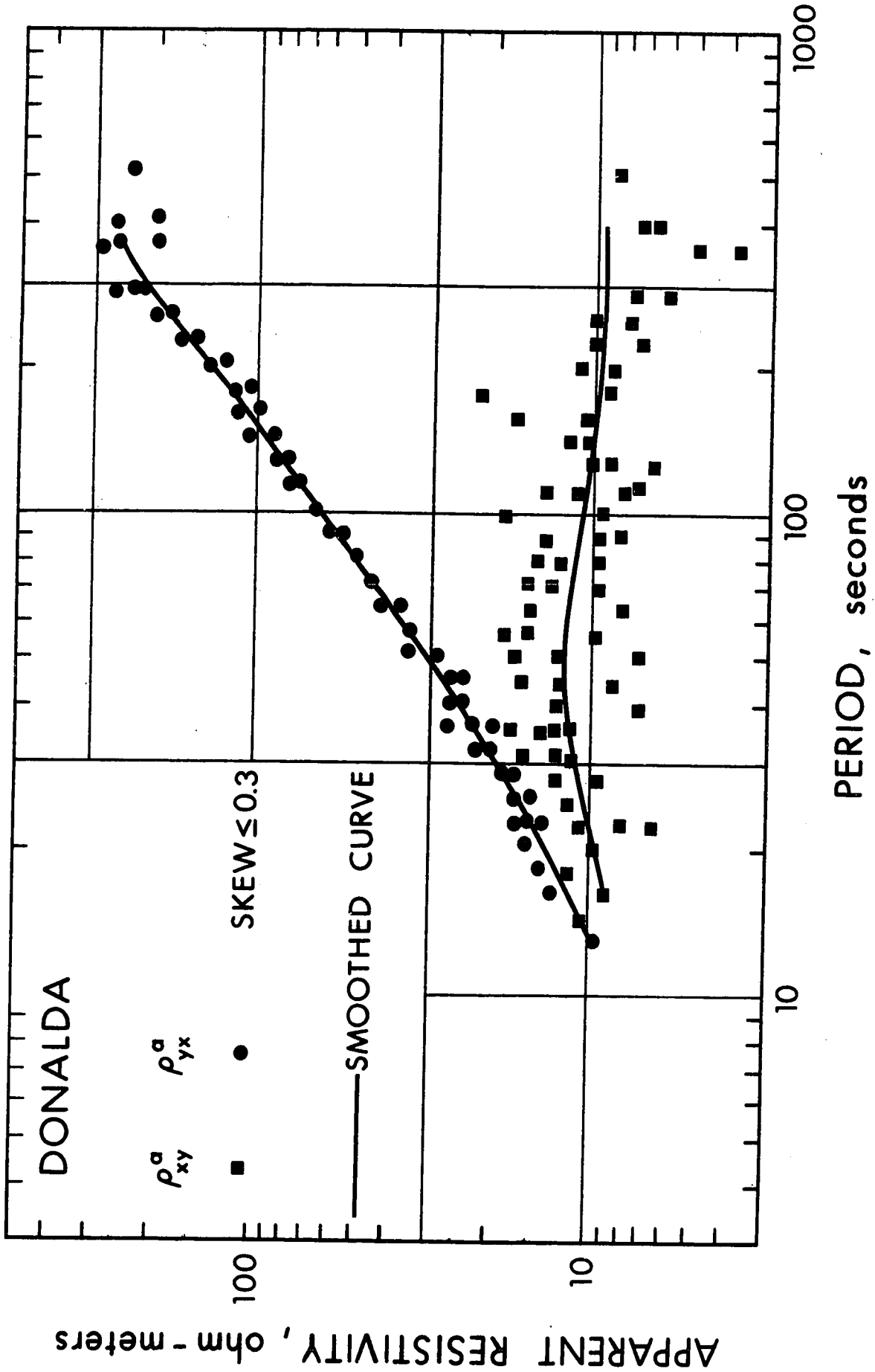
The quality of the data for Donalda was not very good and did not meet some of the editing requirements. The skew values for all most all of the data sets analysed were greater than 0.1, although the predicted coherencies were greater than 0.95 for some data sets for certain period bands. Rotated tensor apparent resistivities for skew values less than or equal to 0.3 are smooth along the maximum apparent resistivity direction. There is a considerable amount of scatter in ρ_{xy}^a values and they continue to drop even for very long periods.

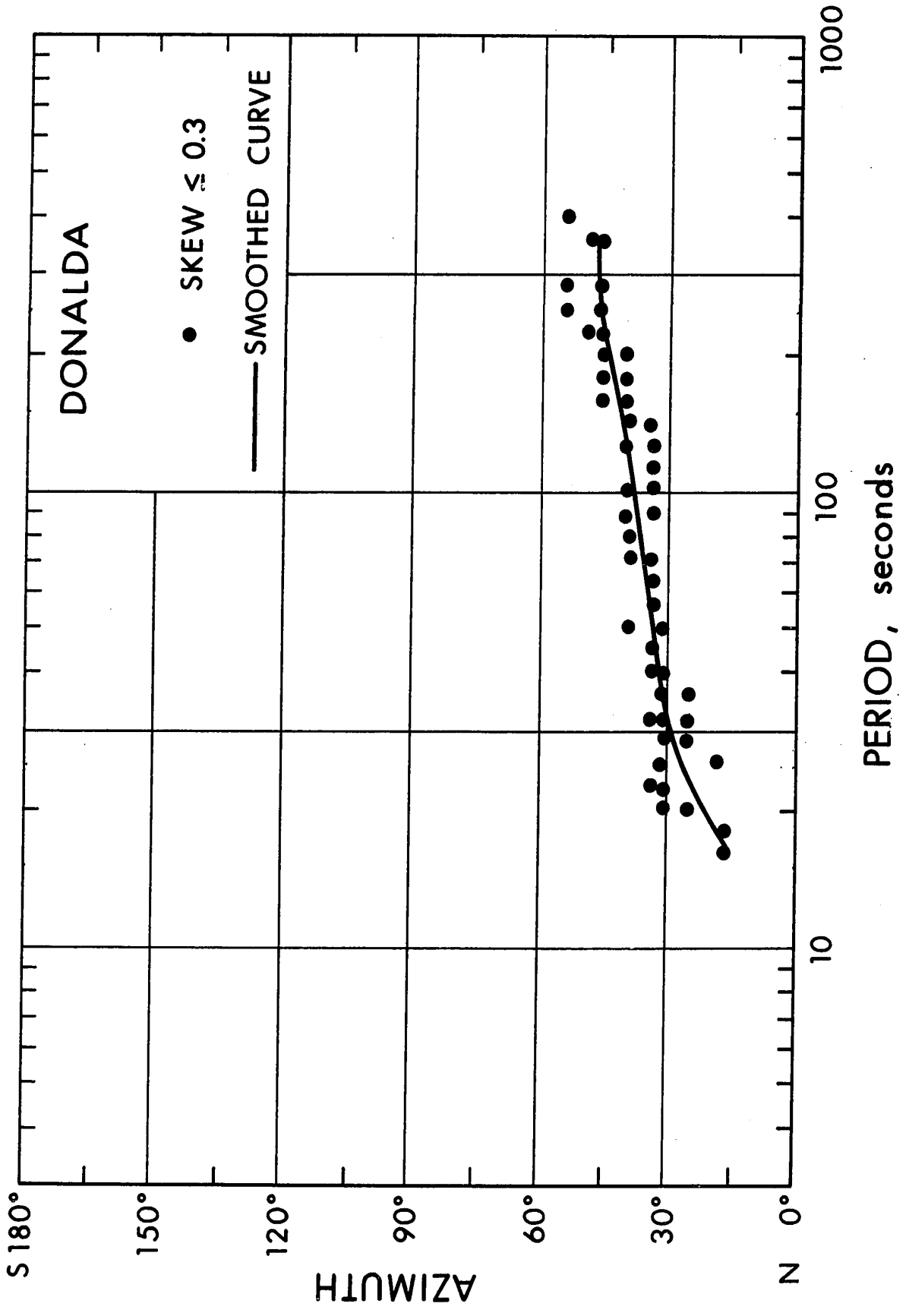
Rotation of tensor impedances gave an azimuth between $+30^\circ$ and $+50^\circ$ for periods greater than 20 seconds and evidence of decreasing for shorter periods. The angle of polarization of the telluric field is about $N40^\circ W$ and there is much scatter for shorter periods. The degree of polarization of the magnetic field was less than 0.5 in most cases.

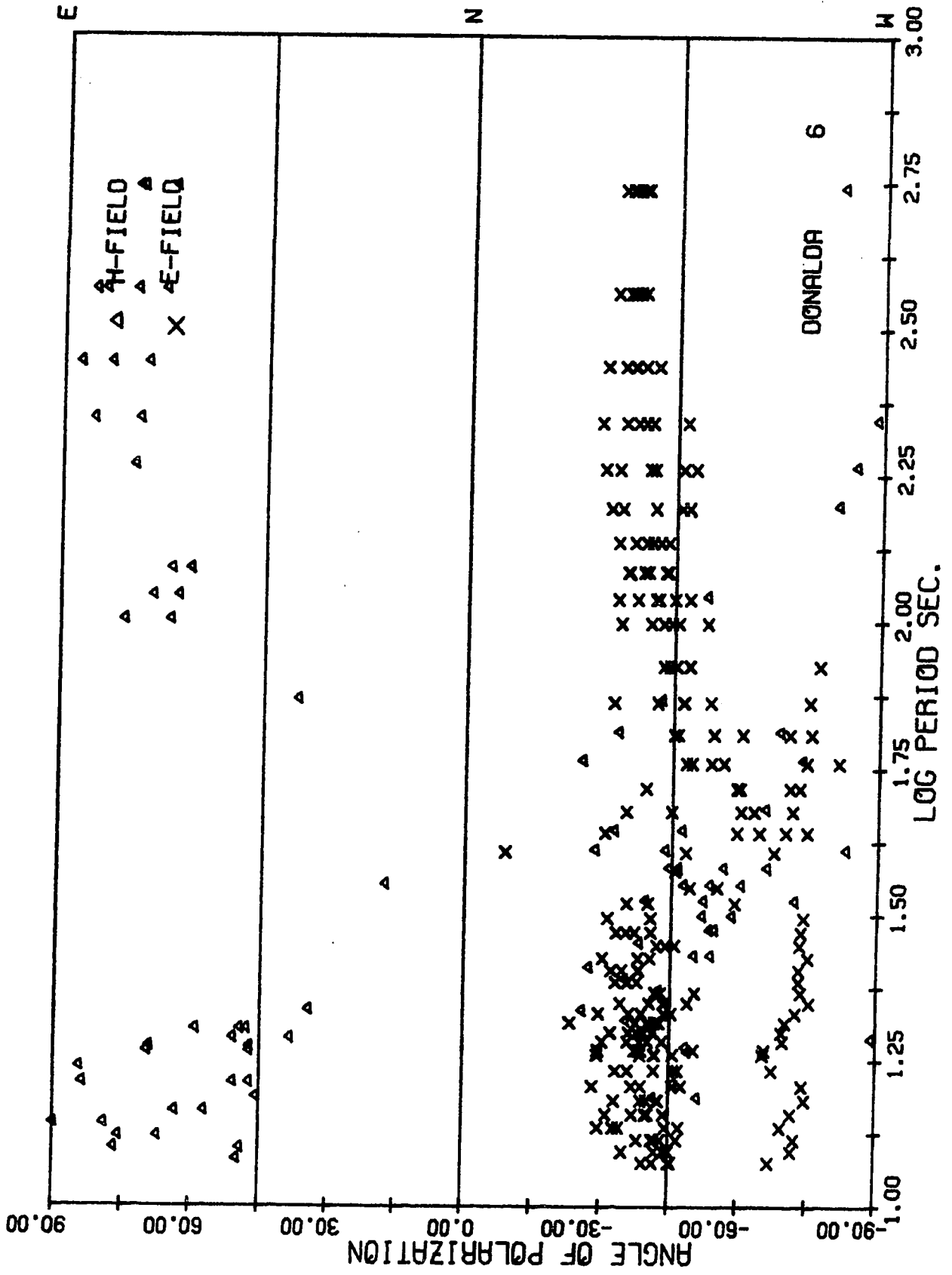
Coherencies between the vertical magnetic field and the electric field components are low, however, good coherency is obtained between H_z and H_y for longer periods for some data sets for the rotation angle about $N40^\circ E$.

Figure 4.5: Magnetotelluric results for Donalda

- i. Tensor apparent resistivities in the principal directions.
- ii. Azimuth (the direction of minimum tensor apparent resistivity).
- iii. Polarization angles for telluric and magnetic fields.
- iv. Vertical magnetic field analyses results.







ROTATION ANGLE = N 0.0E

PERIOD SEC.	COH HZ-EX	COH HZ-EY	COH HZ-HX	COH HZ-HY	HZ/HX	HZ/HY
546.13	0.66	0.66	0.59	0.73	0.87	0.59
364.09	0.59	0.62	0.61	0.73	0.86	0.60
273.07	0.32	0.30	0.46	0.79	0.87	0.64
218.45	0.35	0.04	0.46	0.86	0.85	0.62
182.04	0.38	0.10	0.52	0.90	0.82	0.60
156.04	0.23	0.26	0.54	0.90	0.77	0.61
136.53	0.07	0.52	0.62	0.89	0.72	0.61
121.36	0.06	0.65	0.72	0.91	0.69	0.62
109.23	0.09	0.72	0.77	0.91	0.67	0.58
99.30	0.21	0.73	0.74	0.89	0.61	0.58
84.02	0.30	0.71	0.69	0.91	0.48	0.52
72.82	0.32	0.49	0.61	0.89	0.56	0.48
64.25	0.13	0.66	0.69	0.89	0.44	0.49
57.49	0.13	0.65	0.61	0.83	0.43	0.54
52.01	0.10	0.60	0.57	0.76	0.43	0.44
47.49	0.29	0.47	0.46	0.76	0.30	0.42
43.69	0.50	0.51	0.53	0.83	0.38	0.47
40.45	0.49	0.56	0.58	0.77	0.29	0.40
37.66	0.54	0.54	0.74	0.74	0.33	0.32
35.23	0.49	0.67	0.70	0.68	0.33	0.46
33.10	0.40	0.58	0.66	0.64	0.47	0.53
31.21	0.37	0.22	0.45	0.45	0.59	0.52
29.52	0.29	0.37	0.65	0.13	0.52	0.49
28.01	0.17	0.34	0.34	0.14	0.48	0.51
26.64	0.25	0.25	0.29	0.34	0.72	0.73
25.40	0.25	0.17	0.23	0.41	0.95	0.88
24.27	0.35	0.33	0.43	0.34	1.51	1.11
23.24	0.32	0.37	0.25	0.26	1.56	1.10
22.29	0.05	0.16	0.10	0.33	1.49	1.25
21.42	0.10	0.19	0.37	0.29	1.76	1.43
20.61	0.52	0.52	0.14	0.32	1.68	1.59
19.86	0.36	0.13	0.46	0.42	1.84	1.77
19.16	0.20	0.08	0.41	0.40	1.59	1.87
18.51	0.21	0.19	0.28	0.36	1.58	2.03
18.20	0.20	0.15	0.24	0.42	1.64	1.90
17.07	0.08	0.16	0.26	0.11	1.78	1.76
16.06	0.17	0.02	0.43	0.25	1.87	1.82
15.17	0.29	0.16	0.21	0.04	2.39	1.63
14.37	0.36	0.32	0.19	0.31	2.46	1.74
13.65	0.40	0.46	0.53	0.21	2.64	2.13
13.00	0.15	0.06	0.53	0.40	2.09	2.13
12.41	0.22	0.40	0.55	0.25	2.03	1.90
11.07	0.46	0.46	0.24	0.45	3.33	2.89

DONALDA 22 JUNE 1969 PM D 2

ROTATION ANGLE = N 40.0E

PERIOD SEC.	COH HZ-EX	COH HZ-EY	COH HZ-HX	COH HZ-HY	HZ/HX	HZ/HY
546.13	0.73	0.65	0.55	0.85	0.64	0.76
364.09	0.67	0.60	0.53	0.86	0.65	0.75
273.07	0.58	0.27	0.31	0.94	0.72	0.74
218.45	0.64	0.21	0.41	0.96	0.73	0.69
182.04	0.66	0.24	0.45	0.95	0.76	0.63
156.04	0.62	0.04	0.33	0.94	0.81	0.59
136.53	0.60	0.25	0.39	0.94	0.77	0.58
121.36	0.66	0.37	0.48	0.97	0.78	0.58
109.23	0.68	0.45	0.53	0.97	0.77	0.56
99.30	0.62	0.51	0.57	0.96	0.77	0.55
84.02	0.66	0.55	0.59	0.94	0.65	0.55
72.82	0.84	0.12	0.33	0.94	0.52	0.48
64.25	0.82	0.38	0.46	0.93	0.61	0.45
57.49	0.77	0.39	0.41	0.93	0.53	0.42
52.01	0.62	0.43	0.49	0.83	0.56	0.42
47.49	0.67	0.21	0.28	0.71	0.40	0.32
43.69	0.79	0.16	0.26	0.77	0.38	0.31
40.45	0.76	0.29	0.14	0.78	0.54	0.35
37.66	0.81	0.14	0.19	0.83	0.43	0.28
35.23	0.75	0.14	0.12	0.78	0.50	0.26
33.10	0.68	0.32	0.26	0.71	0.81	0.39
31.21	0.50	0.06	0.05	0.52	0.79	0.45
29.52	0.45	0.25	0.45	0.45	0.55	0.47
28.01	0.17	0.28	0.29	0.23	0.48	0.51
26.64	0.10	0.32	0.43	0.13	0.71	0.74
25.40	0.18	0.23	0.27	0.39	0.94	0.89
24.27	0.18	0.38	0.43	0.31	1.23	1.23
23.24	0.31	0.35	0.23	0.29	1.24	1.30
22.29	0.21	0.05	0.15	0.39	1.20	1.30
21.42	0.24	0.11	0.35	0.24	1.36	1.93
20.61	0.23	0.55	0.30	0.18	1.56	1.72
19.86	0.49	0.26	0.42	0.50	1.50	2.46
19.16	0.28	0.13	0.45	0.13	1.34	2.82
18.51	0.16	0.20	0.04	0.52	1.55	2.10
18.20	0.21	0.17	0.11	0.55	1.51	2.18
17.07	0.21	0.13	0.11	0.29	1.52	2.12
16.06	0.35	0.07	0.40	0.11	1.52	2.52
15.17	0.30	0.22	0.29	0.07	1.90	1.90
14.37	0.31	0.36	0.29	0.23	1.69	2.59
13.65	0.42	0.43	0.21	0.49	2.30	2.40
13.00	0.20	0.09	0.33	0.36	2.10	1.76
12.41	0.33	0.32	0.45	0.30	1.60	2.79
11.07	0.23	0.47	0.40	0.34	3.12	3.05

DONALCA 22 JUNE 1969 PM D 2

6. Foot Hills (Fig. 4.6)

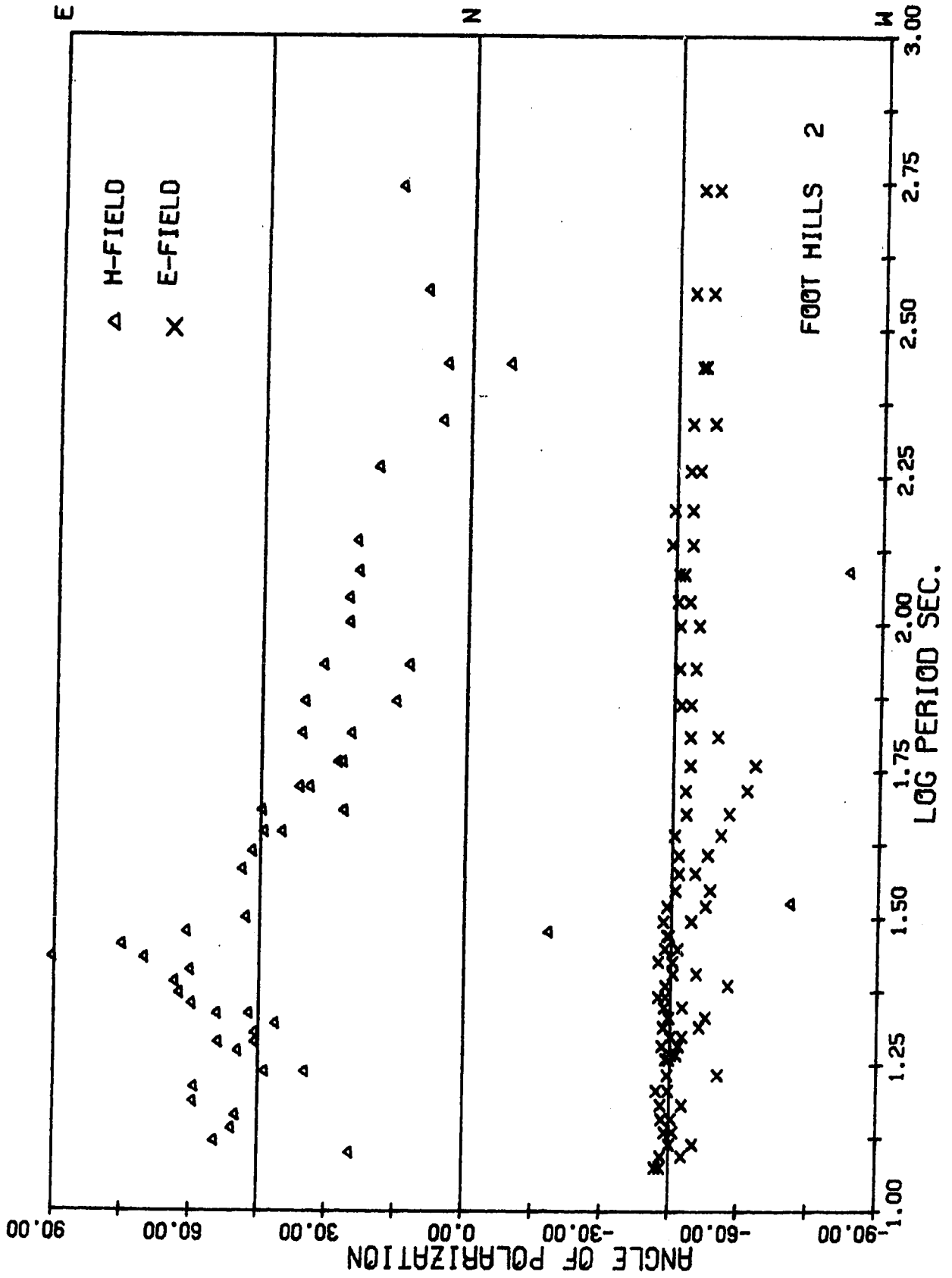
Foot Hills station is situated in the Rocky Mountain foothills belt. The basement depth is unknown in this area. The tensor apparent resistivities showed too much scatter and did not satisfy the selection criteria and hence they are not presented here. The power level in the magnetic and telluric signals was reasonably good for several records but the coherency between magnetic and telluric fields was low (<0.8). The skew values were greater than 0.5 and the predicted coherencies were less than 0.9. Rotation of tensor impedances gave an azimuth about $+50^\circ$, but significant amplitudes for diagonal impedance elements were obtained even for this angle.

The degree of polarization of the magnetic field for one of the two records chosen for polarization analyses is less than 0.5 for most of the periods. The electric field is linearly polarized in the north-westerly direction.

The coherency analyses with the vertical magnetic field show that there is a considerable band of coherencies greater than 0.8, between H_z-H_x and H_z-H_y for the unrotated data. A rotation of $N50^\circ E$ improved $\text{coh } H_z H_x$ at the expense of $\text{coh } H_z H_y$. An anomalously high value for $\text{coh } H_z E_x$ appeared over most of the range of periods in the rotated direction.

Figure 4.6: Magnetotelluric results for Foot Hills

- i. Polarization angles for the telluric and magnetic fields.
- ii. Vertical magnetic field analyses results.



ROTATION ANGLE = N 0.0E

PERIOD SEC.	COH		COH		COH		HZ/HV
	HZ-EX	HZ-EY	HZ-HX	HZ-HY	HZ-HX	HZ-HY	
546.13	0.19	0.36	0.70	0.27	0.47	0.48	
364.09	0.09	0.44	0.83	0.51	0.40	0.47	
273.07	0.09	0.55	0.91	0.74	0.39	0.58	
218.45	0.09	0.62	0.90	0.83	0.38	0.66	
182.04	0.09	0.48	0.82	0.84	0.38	0.57	
156.04	0.21	0.13	0.63	0.84	0.42	0.41	
136.53	0.23	0.19	0.56	0.87	0.53	0.37	
121.36	0.24	0.38	0.72	0.87	0.55	0.40	
109.23	0.23	0.50	0.87	0.87	0.45	0.49	
99.30	0.22	0.56	0.92	0.89	0.39	0.53	
84.02	0.29	0.62	0.84	0.89	0.38	0.47	
72.82	0.13	0.51	0.82	0.81	0.32	0.40	
64.25	0.26	0.70	0.95	0.90	0.35	0.46	
57.49	0.27	0.81	0.94	0.83	0.40	0.57	
52.01	0.30	0.77	0.88	0.84	0.46	0.52	
47.49	0.62	0.84	0.93	0.94	0.53	0.54	
43.69	0.52	0.81	0.94	0.91	0.48	0.54	
40.45	0.40	0.75	0.88	0.75	0.43	0.44	
37.66	0.14	0.55	0.86	0.63	0.39	0.49	
35.23	0.50	0.70	0.82	0.65	0.39	0.40	
33.10	0.56	0.69	0.82	0.73	0.41	0.29	
31.21	0.28	0.71	0.84	0.58	0.34	0.33	
29.52	0.15	0.61	0.81	0.53	0.25	0.41	
28.01	0.07	0.49	0.67	0.33	0.22	0.26	
26.64	0.58	0.61	0.36	0.79	0.33	0.19	
25.40	0.54	0.68	0.47	0.67	0.28	0.20	
24.27	0.22	0.71	0.83	0.67	0.24	0.33	
23.24	0.43	0.65	0.74	0.76	0.28	0.20	
22.29	0.45	0.73	0.87	0.78	0.34	0.32	
21.42	0.26	0.68	0.90	0.81	0.36	0.35	
20.61	0.41	0.67	0.77	0.76	0.35	0.31	
19.86	0.42	0.70	0.71	0.76	0.29	0.28	
19.16	0.15	0.38	0.73	0.67	0.32	0.28	
18.51	0.18	0.21	0.76	0.73	0.31	0.28	
18.20	0.22	0.13	0.76	0.66	0.28	0.27	
17.07	0.43	0.77	0.95	0.85	0.29	0.30	
16.06	0.08	0.22	0.88	0.64	0.34	0.25	
15.17	0.22	0.28	0.70	0.83	0.41	0.29	
14.37	0.26	0.44	0.85	0.88	0.40	0.36	
13.65	0.11	0.33	0.89	0.85	0.45	0.36	
13.00	0.43	0.49	0.78	0.73	0.37	0.32	
12.41	0.12	0.31	0.90	0.87	0.41	0.41	
11.87	0.24	0.13	0.72	0.74	0.43	0.40	

FOOT HILLS 15 AUG 1968 AP1 A2

ROTATION ANGLE = N 50.0E

PERIOD SEC.	COH		COH		COH		HZ/HX	HZ/HY
	HZ-EX	HZ-EY	HZ-HX	HZ-HY	HZ-HX	HZ-HY		
546.13	0.54	0.27	0.46	0.60	0.47	0.48		
364.09	0.84	0.24	0.66	0.74	0.48	0.39		
273.07	0.93	0.33	0.86	0.86	0.51	0.42		
218.45	0.92	0.43	0.89	0.88	0.47	0.47		
182.04	0.86	0.23	0.85	0.78	0.40	0.51		
156.04	0.70	0.09	0.79	0.67	0.38	0.48		
136.53	0.68	0.19	0.78	0.42	0.43	0.43		
121.36	0.81	0.29	0.82	0.82	0.46	0.45		
109.23	0.99	0.36	0.90	0.84	0.45	0.48		
84.02	0.92	0.38	0.94	0.88	0.46	0.46		
72.82	0.91	0.45	0.91	0.74	0.36	0.51		
64.25	0.88	0.32	0.89	0.50	0.28	0.52		
57.49	0.96	0.51	0.96	0.73	0.30	0.76		
52.01	0.92	0.63	0.95	0.77	0.39	0.61		
47.49	0.95	0.59	0.94	0.66	0.42	0.60		
43.69	0.97	0.72	0.98	0.76	0.41	0.87		
40.45	0.92	0.66	0.97	0.76	0.41	0.76		
37.66	0.85	0.60	0.92	0.65	0.40	0.49		
35.23	0.86	0.57	0.90	0.67	0.45	0.41		
33.10	0.90	0.58	0.93	0.67	0.44	0.36		
31.21	0.89	0.58	0.93	0.77	0.44	0.31		
29.52	0.83	0.46	0.80	0.68	0.39	0.30		
28.01	0.71	0.27	0.80	0.72	0.40	0.25		
26.64	0.54	0.27	0.69	0.43	0.22	0.24		
25.40	0.77	0.60	0.87	0.46	0.22	0.22		
24.27	0.87	0.49	0.79	0.59	0.25	0.24		
23.24	0.88	0.45	0.76	0.79	0.29	0.25		
22.29	0.89	0.53	0.88	0.71	0.29	0.26		
21.42	0.83	0.47	0.93	0.72	0.29	0.37		
20.61	0.77	0.55	0.89	0.56	0.29	0.50		
19.86	0.69	0.57	0.85	0.43	0.29	0.40		
19.16	0.72	0.23	0.78	0.26	0.24	0.39		
18.51	0.61	0.07	0.83	0.30	0.24	0.43		
18.20	0.55	0.07	0.79	0.52	0.25	0.36		
17.07	0.85	0.63	0.94	0.52	0.24	0.33		
16.06	0.31	0.14	0.82	0.75	0.23	0.48		
15.17	0.31	0.25	0.85	0.16	0.23	0.44		
14.37	0.52	0.34	0.90	0.37	0.26	0.57		
13.65	0.11	0.33	0.89	0.49	0.28	0.78		
13.00	0.43	0.49	0.78	0.74	0.32	0.85		
12.41	0.12	0.31	0.90	0.50	0.28	0.49		
11.87	0.24	0.13	0.72	0.81	0.35	0.53		
						0.51		

FOOT HILLS 15 AUG 1968 AM1 A2

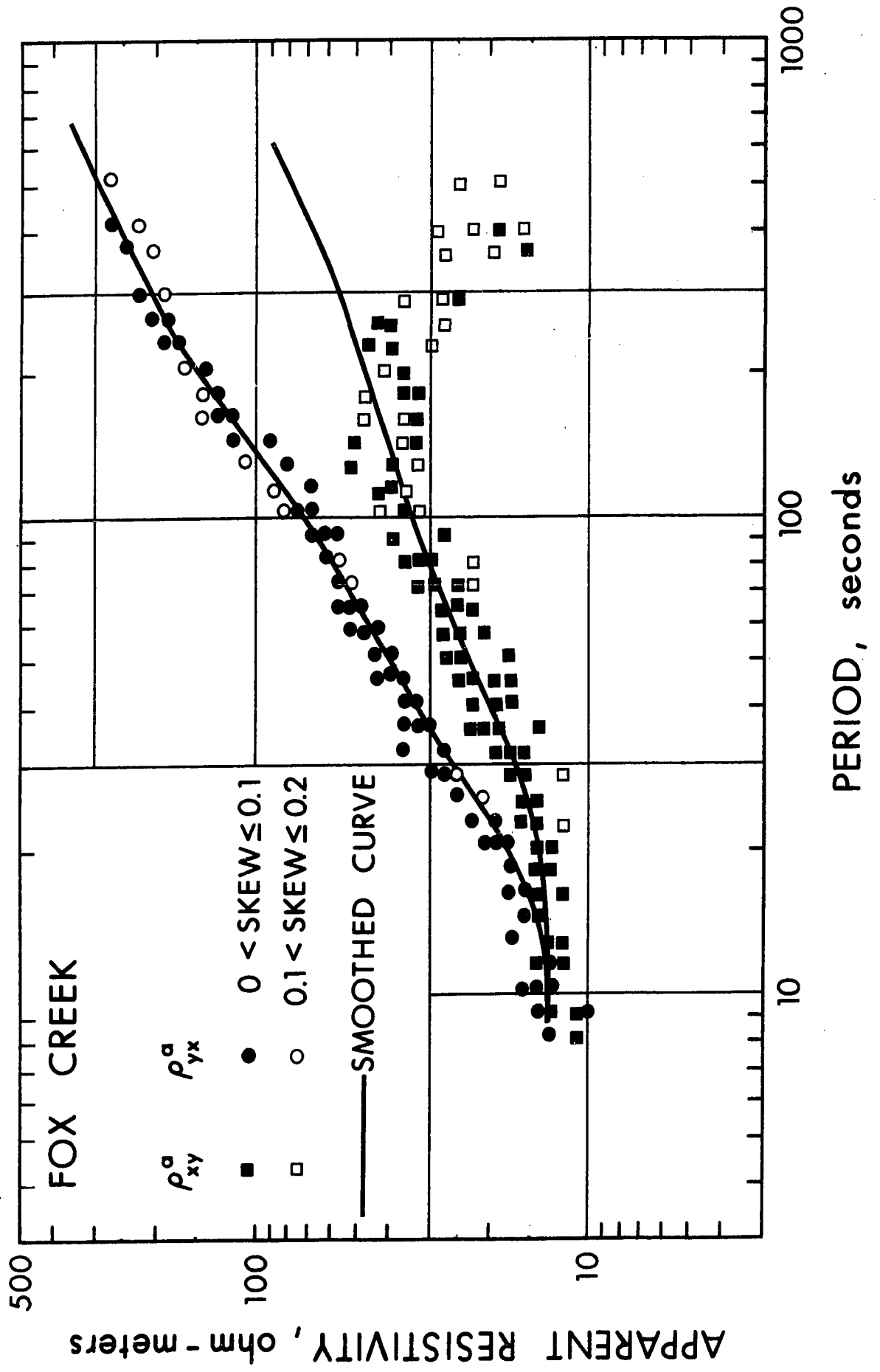
7. Fox Creek (Fig. 4.7)

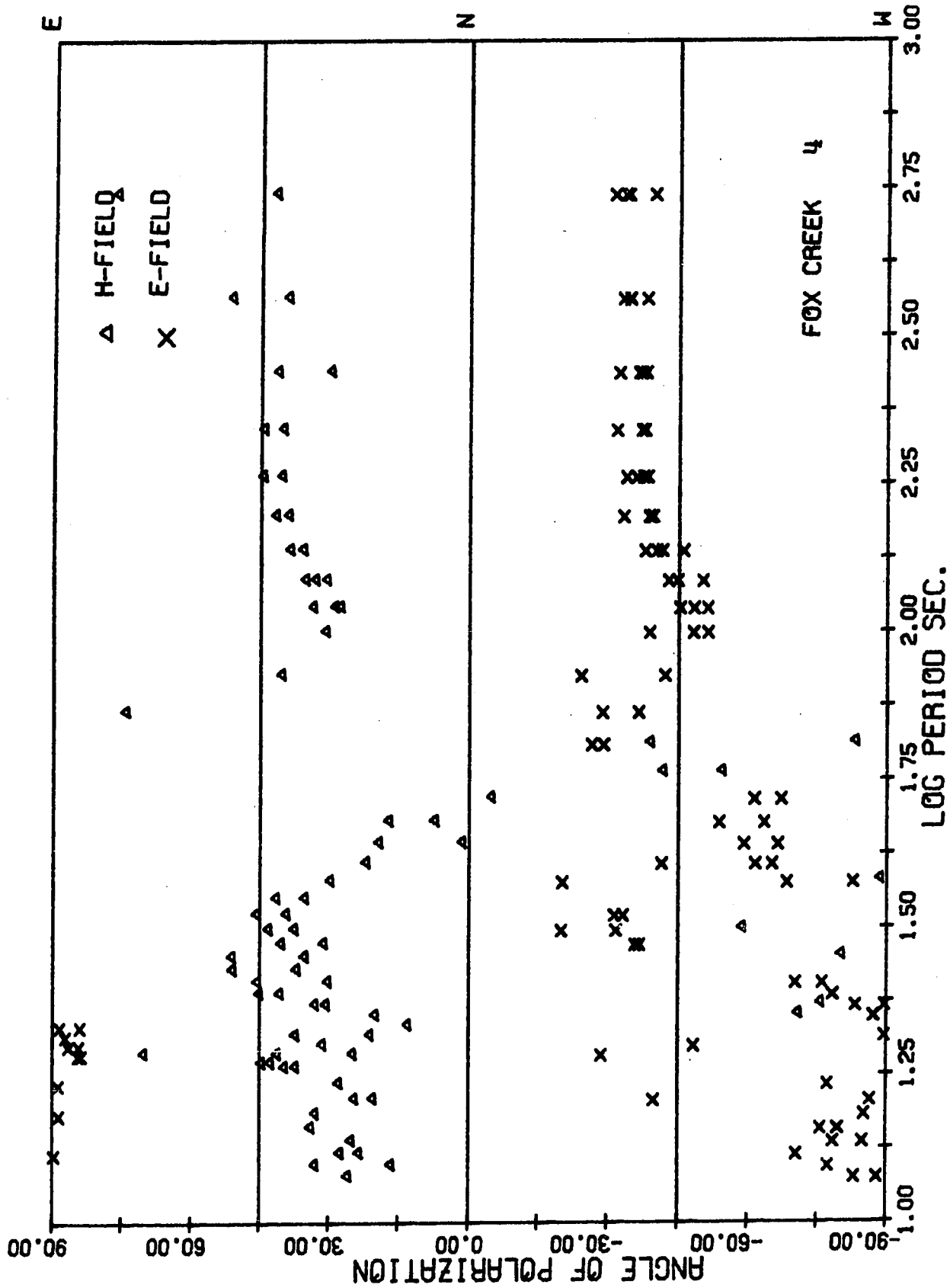
The rotated tensor apparent resistivities show an anisotropic behaviour for periods greater than 20 seconds, with ρ_{xy}^a values scattered for periods greater than 200 seconds. The ρ_{xy}^a values start to decrease for periods longer than 200 seconds. For short periods the apparent resistivity curves tend to approach 10 ohm-meters in value. The azimuth which tends to zero degrees for periods less than 10 seconds approaches $+60^\circ$ for longer periods. The angle of polarization of the telluric field is about $N35^\circ W$ for periods greater than 100 seconds but for short periods it is oriented along an east-west direction. The magnetic field is polarized along $N40^\circ E$ for longer periods and about $N30^\circ E$ for shorter periods.

Good coherencies between the vertical component of the magnetic field and the four horizontal components of the magnetotelluric field are obtained in the measuring directions, for long periods. For a rotation angle of $N50^\circ E$, $\text{coh } H_z E_x$ dropped to its minimum and $\text{coh } H_z E_y$ and $H_z H_x$ reached their maximum values implying a strike direction of $N40^\circ W$. $\text{coh } H_z H_x$ is high for all the periods for this rotation angle whereas $\text{coh } H_z E_y$ starts to decrease for periods less than 25 seconds. The amplitude ratio between H_z and H_y , for this rotation angle, varies with period from 0.3 to 0.6.

Figure 4.7: Magnetotelluric results for Fox Creek

- i. Tensor apparent resistivities in the principal directions.
- ii. Azimuth (the direction of minimum tensor apparent resistivity).
- iii. Polarization angles for telluric and magnetic fields.
- iv. Vertical magnetic field analyses results.





PERIOD SEC.	ROTATION ANGLE = N 0.0E				ROTATION ANGLE = N 50.0E				HZ/HY	HZ/HX	HZ/HY	HZ/HX
	COH HZ-EX	COH HZ-EY	COH HZ-HX	COH HZ-HY	COH HZ-EX	COH HZ-EY	COH HZ-HX	COH HZ-HY				
546.13	0.39	0.34	0.26	0.18	1.23	0.70	0.34	0.37	0.24	0.08	0.74	1.07
364.09	0.68	0.69	0.57	0.34	0.94	0.82	0.69	0.69	0.44	0.44	0.70	0.99
273.07	0.89	0.91	0.84	0.89	0.80	0.82	0.81	0.91	0.81	0.77	0.73	1.10
218.45	0.94	0.94	0.89	0.89	0.76	0.82	0.91	0.95	0.91	0.82	0.65	1.21
182.04	0.97	0.96	0.92	0.92	0.65	0.79	0.96	0.96	0.93	0.68	0.59	1.38
156.04	0.97	0.95	0.92	0.94	0.55	0.78	0.97	0.97	0.96	0.64	0.56	1.53
136.53	0.95	0.91	0.87	0.90	0.47	0.74	0.98	0.98	0.97	0.60	0.54	1.36
121.36	0.91	0.85	0.84	0.92	0.30	0.65	0.97	0.97	0.96	0.48	0.50	0.96
109.23	0.88	0.75	0.79	0.79	0.47	0.53	0.93	0.93	0.96	0.42	0.45	0.70
84.02	0.59	0.84	0.70	0.65	0.42	0.45	0.91	0.91	0.94	0.21	0.43	0.44
72.82	0.59	0.84	0.75	0.75	0.30	0.39	0.91	0.91	0.94	0.44	0.46	0.28
64.25	0.43	0.82	0.70	0.25	0.30	0.34	0.91	0.91	0.91	0.38	0.48	0.26
57.49	0.78	0.82	0.57	0.24	0.26	0.59	0.83	0.83	0.84	0.25	0.41	0.21
52.01	0.88	0.89	0.76	0.61	0.43	0.52	0.83	0.83	0.91	0.50	0.52	0.47
47.49	0.88	0.89	0.84	0.86	0.52	0.76	0.92	0.92	0.95	0.68	0.56	0.66
43.69	0.86	0.69	0.82	0.84	0.40	0.69	0.91	0.91	0.94	0.56	0.43	0.58
40.45	0.81	0.32	0.50	0.76	0.31	0.48	0.87	0.87	0.93	0.17	0.39	0.53
37.66	0.93	0.45	0.74	0.90	0.44	0.53	0.66	0.66	0.83	0.08	0.37	0.37
35.23	0.97	0.78	0.89	0.96	0.54	0.54	0.89	0.89	0.95	0.13	0.40	0.64
33.10	0.97	0.91	0.91	0.96	0.50	0.54	0.97	0.97	0.99	0.42	0.41	1.04
31.21	0.97	0.77	0.91	0.95	0.49	0.56	0.97	0.97	0.99	0.32	0.39	1.12
29.52	0.90	0.45	0.85	0.92	0.57	0.50	0.81	0.81	0.94	0.56	0.40	0.93
28.01	0.79	0.26	0.73	0.85	0.55	0.50	0.81	0.81	0.94	0.53	0.41	0.94
26.64	0.81	0.14	0.83	0.89	0.57	0.57	0.38	0.38	0.91	0.11	0.42	0.76
24.27	0.83	0.03	0.87	0.91	0.55	0.62	0.48	0.48	0.94	0.14	0.44	0.99
23.24	0.80	0.28	0.85	0.87	0.45	0.61	0.47	0.47	0.96	0.35	0.45	1.01
22.29	0.65	0.26	0.85	0.87	0.45	0.61	0.47	0.47	0.95	0.51	0.43	0.69
21.42	0.64	0.21	0.72	0.76	0.34	0.49	0.43	0.43	0.89	0.47	0.37	0.42
20.61	0.71	0.28	0.72	0.72	0.36	0.49	0.49	0.49	0.87	0.30	0.37	0.48
19.86	0.74	0.51	0.76	0.80	0.44	0.50	0.61	0.61	0.91	0.24	0.39	0.61
19.16	0.81	0.30	0.65	0.79	0.40	0.42	0.65	0.65	0.90	0.41	0.39	0.43
18.51	0.85	0.33	0.83	0.88	0.41	0.54	0.58	0.58	0.95	0.35	0.41	0.53
18.20	0.88	0.28	0.89	0.89	0.41	0.48	0.54	0.54	0.95	0.32	0.38	0.73
17.07	0.94	0.03	0.88	0.92	0.38	0.64	0.54	0.54	0.96	0.59	0.36	0.65
16.06	0.91	0.43	0.92	0.93	0.36	0.78	0.65	0.65	0.97	0.79	0.39	0.61
15.17	0.84	0.33	0.60	0.86	0.50	0.45	0.47	0.47	0.91	0.25	0.41	0.53
14.37	0.68	0.34	0.68	0.73	0.44	0.44	0.53	0.53	0.87	0.09	0.39	0.58
13.65	0.66	0.48	0.65	0.75	0.42	0.56	0.68	0.68	0.82	0.49	0.46	0.49
13.00	0.70	0.54	0.86	0.87	0.41	0.75	0.57	0.57	0.92	0.68	0.43	0.69
12.41	0.69	0.48	0.82	0.74	0.34	0.57	0.62	0.62	0.92	0.57	0.37	0.46
11.87	0.80	0.17	0.53	0.79	0.41	0.58	0.34	0.34	0.80	0.29	0.45	0.50

FOX CREEK 18 AUG 1968 PMI A1

FOX CREEK 18 AUG 1968 PMI A1

8. Gregg Lake

(Fig. 4.8)

The Gregg Lake station is situated within 40 miles of the central range of the Rocky Mountains which have a north-westerly strike in this area. The elevation of the station is about 4,000 feet and it is surrounded by mountains up to 6,000 feet in height.

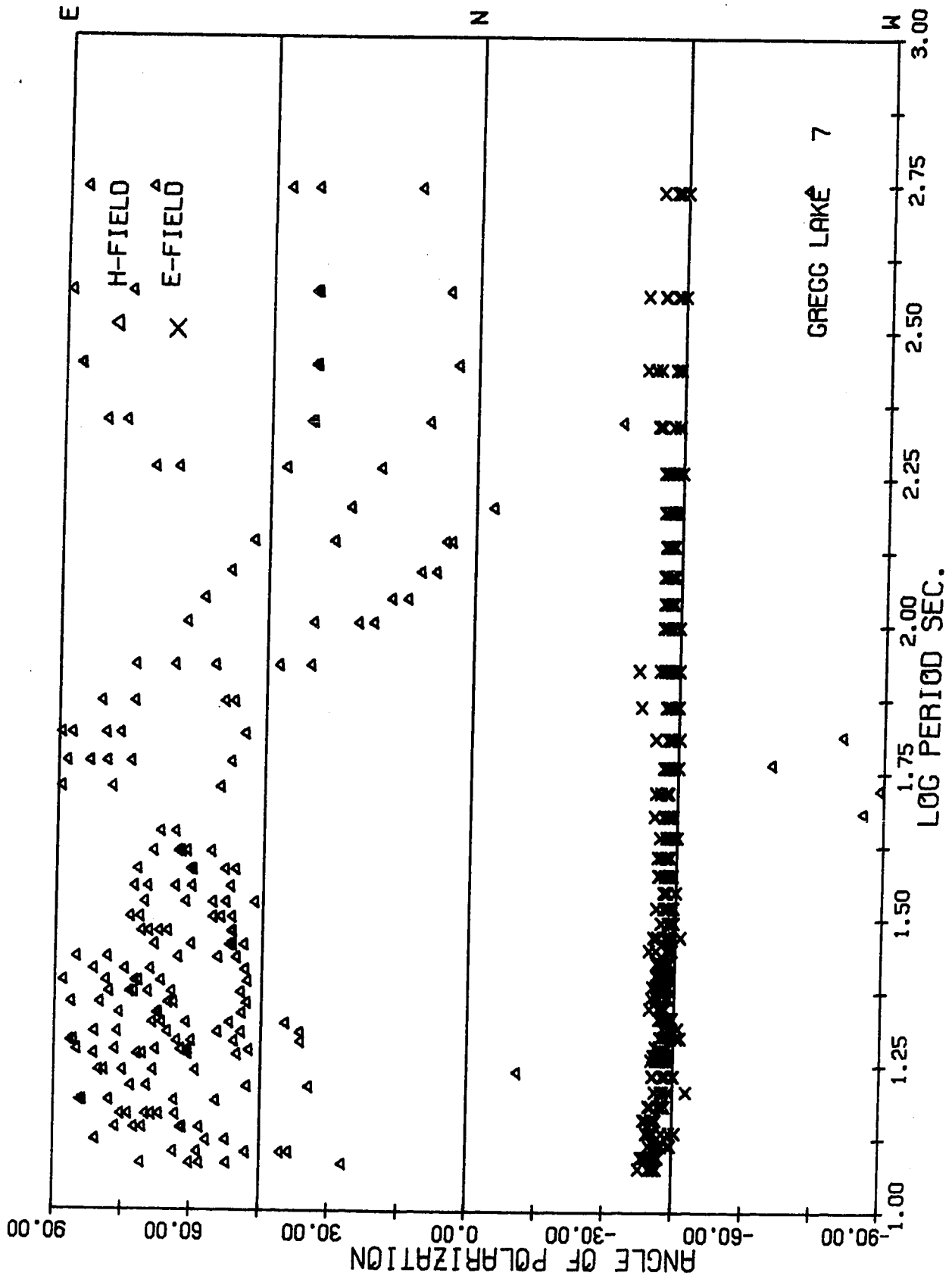
The coherencies between the orthogonal magnetic and telluric field components were low and the scalar resistivities were highly time dependent with much scatter. The tensor apparent resistivities had much scatter and did not satisfy the selection criteria and hence are not presented here.

The electric field is linearly polarized in the north-westerly direction. The angle of polarization of the magnetic field varied with period. It is approximately N30°E for long periods and about N65°E for shorter periods.

Significantly greater of H_z was observed for shorter periods than for longer periods. Coherency analyses show that H_z is coherent with E_x , E_y , H_x and H_y for shorter periods in the measuring directions, and for a rotation angle of N50°E the coherency between H_z-E_x and H_z-H_y dropped to their minimum whereas the coh $H_z E_y$ and the coh $H_z H_x$ showed an increase.

Figure 4.8: Magnetotelluric results for Gregg Lake

- i. Polarization angles for telluric and magnetic fields.
- ii. Vertical magnetic field analyses results.



ROTATION ANGLE = N 0.0E

PERIOD SEC.	COH			HZ-HY			HZ/HX			HZ/HY		
	HZ-EX	HZ-EY	HZ-HX	HZ-HY	HZ-HX	HZ-HY	HZ-HX	HZ-HY	HZ-HX	HZ-HY	HZ-HX	HZ-HY
546.13	0.31	0.34	0.19	0.38	1.45	1.52	0.38	0.42	0.93	1.17	1.52	0.38
364.09	0.30	0.37	0.52	0.42	0.93	1.17	0.42	0.34	0.34	1.03	1.17	0.42
273.07	0.24	0.34	0.69	0.34	0.73	1.03	0.34	0.36	0.65	0.82	1.03	0.34
218.45	0.27	0.36	0.65	0.34	0.61	0.82	0.34	0.41	0.51	0.67	0.82	0.34
182.04	0.29	0.41	0.51	0.23	0.56	0.67	0.23	0.44	0.29	0.57	0.67	0.23
156.04	0.31	0.44	0.51	0.12	0.57	0.69	0.12	0.49	0.34	0.66	0.69	0.12
136.53	0.31	0.49	0.34	0.15	0.66	0.86	0.15	0.42	0.40	0.81	0.86	0.15
121.36	0.34	0.42	0.40	0.52	0.81	0.88	0.52	0.42	0.28	0.78	0.88	0.52
109.23	0.58	0.42	0.28	0.95	0.79	0.78	0.95	0.53	0.31	0.70	0.78	0.95
99.30	0.67	0.53	0.31	0.87	0.91	0.70	0.87	0.68	0.57	0.73	0.70	0.87
84.02	0.73	0.68	0.57	0.74	0.72	0.73	0.74	0.65	0.41	0.64	0.73	0.74
72.82	0.74	0.65	0.41	0.72	0.64	0.89	0.72	0.74	0.56	0.63	0.89	0.72
64.25	0.78	0.74	0.56	0.82	0.55	0.63	0.82	0.78	0.73	0.63	0.63	0.82
57.49	0.75	0.78	0.53	0.75	0.54	0.60	0.75	0.73	0.53	0.54	0.53	0.75
52.01	0.77	0.73	0.53	0.74	0.54	0.60	0.74	0.82	0.83	0.87	0.60	0.82
47.49	0.85	0.82	0.83	0.88	0.68	0.87	0.88	0.51	0.60	0.97	0.87	0.88
43.69	0.59	0.51	0.60	0.61	0.68	0.97	0.61	0.57	0.42	0.85	0.97	0.61
40.45	0.64	0.57	0.42	0.62	0.47	0.68	0.62	0.87	0.70	0.86	0.68	0.62
37.66	0.88	0.87	0.70	0.86	0.47	0.68	0.86	0.82	0.81	0.90	0.68	0.86
35.23	0.90	0.82	0.68	0.90	0.41	0.57	0.90	0.71	0.48	0.70	0.57	0.90
33.10	0.86	0.81	0.68	0.88	0.42	0.70	0.88	0.67	0.57	0.85	0.70	0.88
31.21	0.71	0.67	0.57	0.85	0.48	0.68	0.85	0.64	0.67	0.79	0.68	0.85
29.52	0.76	0.64	0.67	0.79	0.63	0.59	0.79	0.59	0.63	0.75	0.59	0.79
26.01	0.83	0.59	0.52	0.54	0.73	0.75	0.54	0.70	0.70	0.77	0.75	0.54
26.64	0.87	0.70	0.57	0.70	0.70	0.77	0.70	0.86	0.62	0.65	0.77	0.70
25.40	0.89	0.86	0.59	0.90	0.62	0.59	0.90	0.85	0.49	0.63	0.59	0.90
24.27	0.87	0.85	0.79	0.86	0.49	0.63	0.86	0.91	0.59	0.61	0.63	0.86
23.24	0.94	0.92	0.86	0.91	0.59	0.61	0.91	0.88	0.44	0.57	0.61	0.88
22.29	0.85	0.88	0.88	0.71	0.48	0.65	0.71	0.65	0.50	0.53	0.65	0.71
21.42	0.75	0.82	0.81	0.65	0.50	0.67	0.65	0.81	0.55	0.53	0.67	0.65
20.61	0.84	0.83	0.89	0.81	0.55	0.60	0.81	0.90	0.68	0.60	0.60	0.81
19.86	0.69	0.75	0.85	0.91	0.78	0.78	0.91	0.78	0.49	0.52	0.78	0.91
19.16	0.78	0.69	0.79	0.90	0.68	0.67	0.90	0.92	0.49	0.52	0.67	0.90
18.51	0.89	0.78	0.77	0.92	0.49	0.52	0.92	0.86	0.48	0.51	0.52	0.86
18.20	0.92	0.88	0.86	0.94	0.76	0.55	0.94	0.73	0.63	0.66	0.55	0.94
17.07	0.82	0.74	0.73	0.93	0.48	0.55	0.93	0.83	0.63	0.66	0.55	0.93
16.06	0.92	0.88	0.70	0.83	0.63	0.66	0.83	0.70	0.72	0.49	0.66	0.83
15.17	0.68	0.55	0.70	0.72	0.49	0.54	0.72	0.69	0.53	0.49	0.54	0.72
14.37	0.72	0.69	0.67	0.73	0.53	0.49	0.73	0.59	0.70	0.64	0.49	0.73
13.65	0.70	0.59	0.70	0.72	0.42	0.64	0.72	0.82	0.76	0.71	0.64	0.72
13.00	0.91	0.75	0.82	0.92	0.76	0.70	0.92	0.86	0.71	0.57	0.70	0.92
12.41	0.86	0.82	0.78	0.91	0.66	0.70	0.91	0.90	0.66	0.70	0.70	0.91
11.87	0.90	0.86	0.90	0.91	0.66	0.70	0.91	0.86	0.66	0.70	0.70	0.91

GREGG LAKE 13 AUG 1968 PM2 B2

ROTATION ANGLE = N 50.0E

PERIOD SEC.	COH			HZ-HX			HZ-HY			HZ/HX			HZ/HY		
	HZ-EX	HZ-EY	HZ-HX	HZ-HY	HZ-HX	HZ-HY	HZ-HX	HZ-HY	HZ-HX	HZ-HY	HZ-HX	HZ-HY	HZ-HX	HZ-HY	
546.13	0.36	0.32	0.30	0.28	0.30	0.28	0.36	0.32	0.30	0.28	0.30	0.28	0.36	0.32	
364.09	0.55	0.33	0.48	0.48	0.60	0.48	0.55	0.29	0.60	0.48	0.48	0.48	0.55	0.33	
273.07	0.54	0.31	0.54	0.65	0.54	0.61	0.54	0.35	0.41	0.44	0.51	0.61	0.54	0.31	
218.45	0.53	0.38	0.25	0.22	0.25	0.22	0.53	0.38	0.25	0.22	0.25	0.22	0.53	0.38	
182.04	0.62	0.40	0.28	0.30	0.28	0.30	0.62	0.40	0.28	0.30	0.28	0.30	0.62	0.40	
156.04	0.71	0.35	0.42	0.52	0.42	0.52	0.71	0.35	0.42	0.52	0.42	0.52	0.71	0.35	
136.53	0.72	0.51	0.60	0.70	0.60	0.70	0.72	0.51	0.60	0.70	0.60	0.70	0.72	0.51	
121.36	0.58	0.72	0.71	0.25	0.71	0.25	0.58	0.72	0.71	0.25	0.71	0.25	0.58	0.72	
109.23	0.37	0.72	0.63	0.09	0.63	0.09	0.37	0.72	0.63	0.09	0.63	0.09	0.37	0.72	
99.30	0.34	0.77	0.77	0.38	0.77	0.38	0.34	0.77	0.77	0.38	0.77	0.38	0.34	0.77	
84.02	0.48	0.77	0.76	0.11	0.76	0.11	0.48	0.77	0.76	0.11	0.76	0.11	0.48	0.77	
72.82	0.46	0.84	0.91	0.41	0.91	0.41	0.46	0.84	0.91	0.41	0.91	0.41	0.46	0.84	
64.25	0.16	0.55	0.66	0.35	0.66	0.35	0.16	0.55	0.66	0.35	0.66	0.35	0.16	0.55	
57.49	0.62	0.62	0.58	0.20	0.58	0.20	0.62	0.62	0.58	0.20	0.58	0.20	0.62	0.62	
52.01	0.34	0.89	0.85	0.25	0.85	0.25	0.34	0.89	0.85	0.25	0.85	0.25	0.34	0.89	
47.49	0.35	0.87	0.86	0.24	0.86	0.24	0.35	0.87	0.86	0.24	0.86	0.24	0.35	0.87	
43.69	0.49	0.85	0.83	0.32	0.83	0.32	0.49	0.85	0.83	0.32	0.83	0.32	0.49	0.85	
40.45	0.30	0.71	0.79	0.08	0.79	0.08	0.30	0.71	0.79	0.08	0.79	0.08	0.30	0.71	
37.66	0.25	0.73	0.84	0.13	0.84	0.13	0.25	0.73	0.84	0.13	0.84	0.13	0.25	0.73	
35.23	0.26	0.78	0.64	0.28	0.64	0.28	0.26	0.78	0.64	0.28	0.64	0.28	0.26	0.78	
33.10	0.33	0.84	0.71	0.29	0.71	0.29	0.33	0.84	0.71	0.29	0.71	0.29	0.33	0.84	
31.21	0.30	0.90	0.84	0.24	0.84	0.24	0.30	0.90	0.84	0.24	0.84	0.24	0.30	0.90	
29.52	0.36	0.89	0.91	0.41	0.91	0.41	0.36	0.89	0.91	0.41	0.91	0.41	0.36	0.89	
28.01	0.35	0.94	0.96	0.27	0.96	0.27	0.35	0.94	0.96	0.27	0.96	0.27	0.35	0.94	
26.64	0.44	0.88	0.91	0.56	0.91	0.56	0.44	0.88	0.91	0.56	0.91	0.56	0.44	0.88	
25.40	0.56	0.80	0.85	0.46	0.85	0.46	0.56	0.80	0.85	0.46	0.85	0.46	0.56	0.80	
24.27	0.24	0.84	0.91	0.32	0.91	0.32	0.24	0.84	0.91	0.32	0.91	0.32	0.24	0.84	
23.24	0.61	0.72	0.95	0.02	0.95	0.02	0.61	0.72	0.95	0.02	0.95	0.02	0.61	0.72	
22.29	0.57	0.76	0.91	0.45	0.91	0.45	0.57	0.76	0.91	0.45	0.91	0.45	0.57	0.76	
21.42	0.37	0.87	0.92	0.06	0.92	0.06	0.37	0.87	0.92	0.06	0.92	0.06	0.37	0.87	
20.61	0.35	0.91	0.96	0.22	0.96	0.22	0.35	0.91	0.96	0.22	0.96	0.22	0.35	0.91	
19.86	0.21	0.80	0.91	0.17	0.91	0.17	0.21	0.80	0.91	0.17	0.91	0.17	0.21	0.80	
19.16	0.73	0.91	0.82	0.39	0.82	0.39	0.73	0.91	0.82	0.39	0.82	0.39	0.73	0.91	
18.51	0.50	0.63	0.75	0.39	0.75	0.39	0.50	0.63	0.75	0.39	0.75	0.39	0.50	0.63	
18.20	0.14	0.73	0.74	0.31	0.74	0.31	0.14	0.73	0.74	0.31	0.74	0.31	0.14	0.73	
17.07	0.32	0.68	0.74	0.46	0.74	0.46	0.32	0.68	0.74	0.46	0.74	0.46	0.32	0.68	
16.06	0.41	0.59	0.68	0.41	0.68	0.41	0.41	0.59	0.68	0.41	0.68	0.41	0.41	0.59	
15.17	0.88	0.87	0.90	0.41	0.90	0.41	0.88	0.87	0.90	0.41	0.90	0.41	0.88	0.87	
14.37	0.88	0.87	0.90	0.41	0.90	0.41	0.88	0.87	0.90	0.41	0.90	0.41	0.88	0.87	
13.65	0.88	0.87	0.90	0.41	0.90	0.41	0.88	0.87	0.90	0.41	0.90	0.41	0.88	0.87	
13.00	0.88	0.87	0.90	0.41	0.90	0.41	0.88	0.87	0.90	0.41	0.90	0.41	0.88	0.87	
12.41	0.88	0.87	0.90	0.41	0.90	0.41	0.88	0.87	0.90	0.41	0.90	0.41	0.88	0.87	
11.87	0.88	0.87	0.90	0.41	0.90	0.41	0.88	0.87	0.90	0.41	0.90	0.41	0.88	0.87	

GREGG LAKE 13 AUG 1968 PM2 B2

9. Meanook (Fig. 4.9)

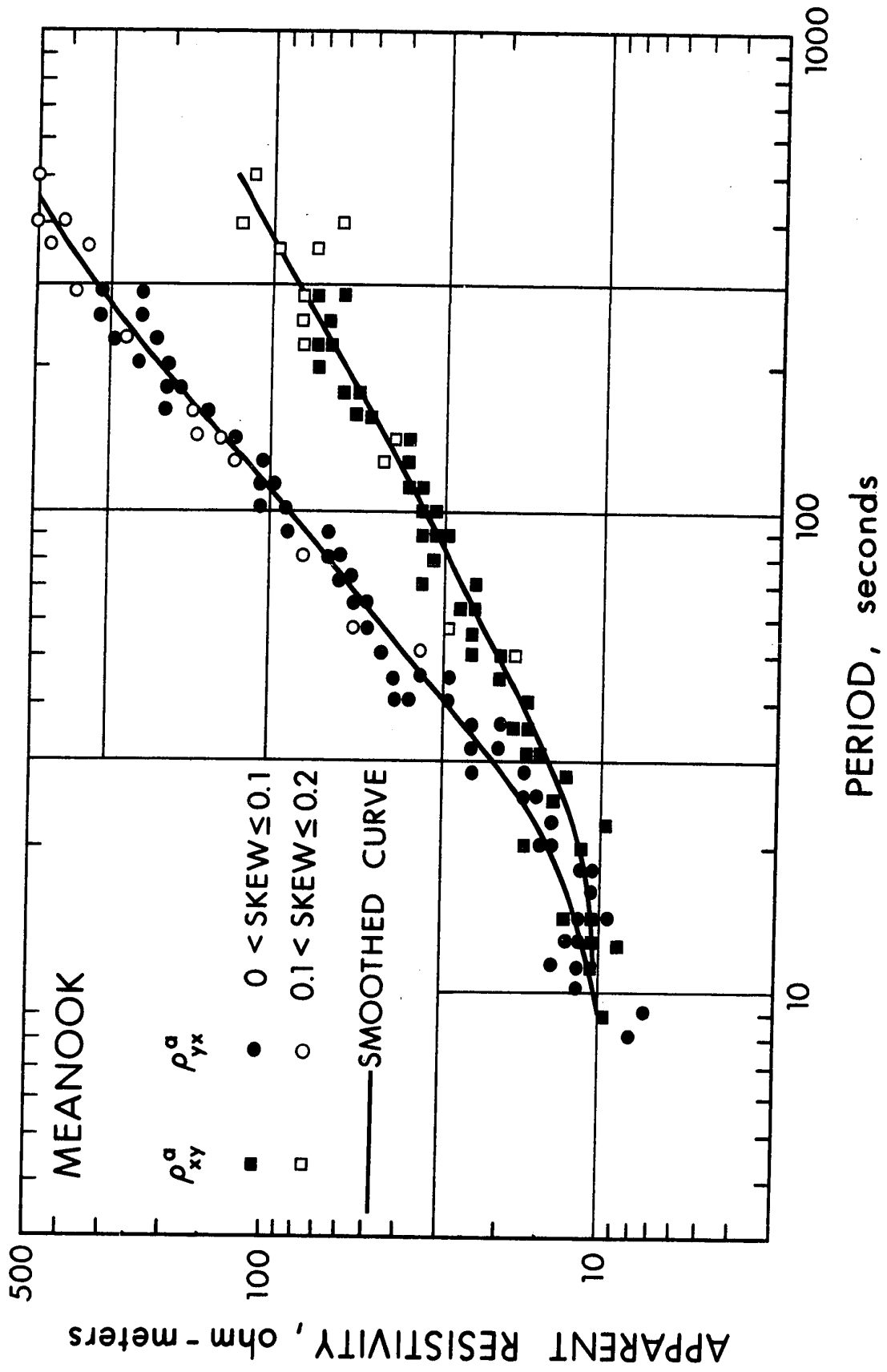
The Meanook magnetotelluric sounding site is situated within a few hundred feet of the Dominion Geomagnetic Observatory. Niblett and Sayn-Wittgenstein (1960) and Srivastava and Jacobs (1964) conducted magnetotelluric measurements and interpreted the scalar resistivities in terms of upper mantle conductivity anomalies. The tensor apparent resistivity curves from the present analyses show an anisotropic behaviour for periods greater than 30 seconds. The apparent resistivity estimates are smooth for skew less than 0.1 for long periods, but there is some scatter at the short-period end of the spectrum.

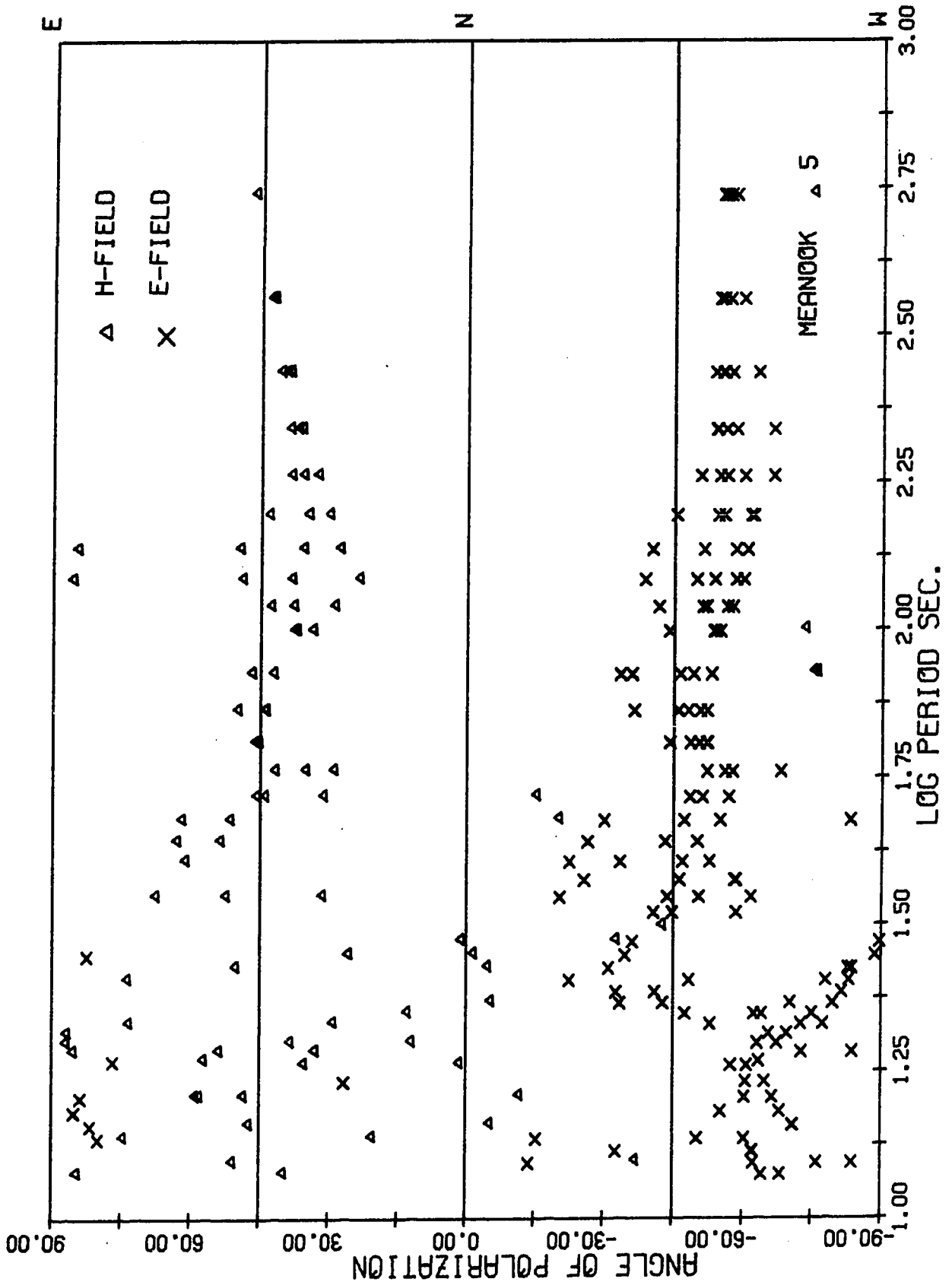
The azimuth of minimum resistivity is found to be about $+35^\circ$ for periods greater than 30 seconds and about $+15^\circ$ for shorter periods. There is much scatter in the angle of polarization of the magnetic and telluric fields for shorter periods, but for long periods the telluric field is polarized about $N55^\circ W$ whereas the magnetic field preferred $N35^\circ E$. The direction of maximum apparent resistivity and the angle of polarization of the telluric field are the same for these periods.

The vertical component of the magnetic field is coherent with the four horizontal components of magnetotelluric field in the measuring directions,

Figure 4.9: Magnetotelluric results for Meanook

- i. Tensor apparent resistivities in the principal directions.
- ii. Azimuth (the direction of minimum tensor apparent resistivity).
- iii. Polarization angles for telluric and magnetic fields.
- iv. Vertical magnetic field analyses results.





ROTATION ANGLE = N 0.0E

PERIOD SEC.	COH		COH		COH		HZ/HX	HZ/HY				
	HZ-EX	HZ-EY	HZ-HX	HZ-HY	HZ-EX	HZ-EY						
546.13	0.77	0.78	0.47	0.39	1.03	0.54	0.44	0.79	0.67	0.22	0.88	0.57
364.09	0.91	0.94	0.85	0.62	0.93	0.83	0.52	0.94	0.91	0.09	0.77	1.05
273.07	0.95	0.98	0.95	0.80	0.87	1.01	0.46	0.98	0.97	0.20	0.72	1.60
218.45	0.96	0.98	0.96	0.84	0.82	1.04	0.49	0.98	0.97	0.35	0.69	1.80
182.04	0.97	0.97	0.90	0.85	0.78	1.02	0.44	0.98	0.97	0.29	0.66	1.82
156.04	0.96	0.96	0.90	0.85	0.74	0.95	0.42	0.97	0.95	0.18	0.64	1.37
136.53	0.92	0.94	0.85	0.77	0.68	0.91	0.42	0.97	0.95	0.28	0.65	1.02
121.36	0.93	0.93	0.85	0.80	0.73	1.07	0.41	0.96	0.94	0.30	0.66	1.05
109.23	0.90	0.94	0.89	0.80	0.71	1.07	0.43	0.97	0.94	0.34	0.65	1.41
99.30	0.95	0.95	0.92	0.86	0.73	1.02	0.44	0.97	0.95	0.40	0.63	1.70
84.02	0.93	0.93	0.86	0.84	0.79	0.77	0.31	0.95	0.91	0.38	0.60	1.32
72.82	0.93	0.87	0.70	0.88	0.78	0.72	0.16	0.92	0.88	0.45	0.60	1.12
64.25	0.92	0.91	0.80	0.93	0.70	0.70	0.13	0.93	0.92	0.42	0.54	1.30
57.49	0.87	0.86	0.74	0.90	0.58	0.70	0.17	0.91	0.91	0.30	0.48	0.93
52.01	0.74	0.78	0.74	0.86	0.59	0.59	0.13	0.83	0.88	0.31	0.47	0.94
47.49	0.83	0.59	0.62	0.92	0.63	0.46	0.71	0.90	0.93	0.65	0.44	0.68
43.69	0.91	0.72	0.74	0.94	0.54	0.38	0.60	0.86	0.86	0.53	0.36	0.57
40.45	0.81	0.74	0.81	0.86	0.37	0.29	0.60	0.86	0.93	0.70	0.27	0.40
37.66	0.84	0.81	0.88	0.88	0.30	0.28	0.69	0.88	0.95	0.70	0.24	0.37
35.23	0.80	0.72	0.90	0.88	0.30	0.26	0.74	0.80	0.94	0.79	0.24	0.34
33.10	0.57	0.52	0.90	0.77	0.28	0.29	0.67	0.80	0.92	0.73	0.27	0.30
31.21	0.48	0.43	0.90	0.72	0.28	0.35	0.65	0.17	0.87	0.81	0.34	0.29
29.52	0.52	0.65	0.89	0.36	0.22	0.47	0.34	0.65	0.83	0.76	0.30	0.34
28.01	0.60	0.70	0.92	0.58	0.22	0.32	0.21	0.71	0.90	0.54	0.21	0.36
26.64	0.72	0.66	0.89	0.82	0.22	0.20	0.52	0.75	0.93	0.21	0.17	0.36
25.40	0.53	0.19	0.79	0.78	0.28	0.17	0.49	0.44	0.94	0.43	0.19	0.23
24.27	0.61	0.67	0.75	0.81	0.24	0.19	0.53	0.34	0.92	0.65	0.22	0.21
23.24	0.39	0.32	0.72	0.57	0.22	0.18	0.42	0.18	0.85	0.41	0.22	0.19
22.29	0.18	0.45	0.83	0.54	0.21	0.16	0.54	0.15	0.80	0.31	0.17	0.21
21.42	0.55	0.25	0.81	0.68	0.22	0.13	0.42	0.40	0.84	0.40	0.14	0.18
20.61	0.63	0.15	0.64	0.71	0.21	0.11	0.58	0.41	0.89	0.43	0.14	0.13
19.86	0.63	0.31	0.59	0.68	0.20	0.12	0.63	0.23	0.83	0.44	0.14	0.14
19.16	0.50	0.29	0.74	0.66	0.18	0.11	0.50	0.03	0.85	0.45	0.13	0.13
18.51	0.11	0.35	0.83	0.63	0.14	0.10	0.31	0.30	0.83	0.51	0.11	0.12
18.20	0.34	0.20	0.79	0.58	0.16	0.13	0.24	0.28	0.79	0.40	0.16	0.16
17.07	0.72	0.11	0.56	0.78	0.18	0.19	0.24	0.44	0.77	0.30	0.16	0.24
16.06	0.50	0.09	0.75	0.53	0.13	0.10	0.53	0.22	0.73	0.32	0.10	0.14
15.17	0.83	0.24	0.88	0.80	0.11	0.13	0.26	0.42	0.91	0.78	0.12	0.12
14.37	0.70	0.37	0.66	0.36	0.09	0.17	0.51	0.47	0.70	0.49	0.11	0.11
13.65	0.43	0.35	0.56	0.36	0.08	0.13	0.28	0.46	0.52	0.44	0.08	0.13
13.00	0.33	0.12	0.73	0.61	0.09	0.12	0.12	0.24	0.77	0.57	0.09	0.10
12.41	0.18	0.41	0.58	0.04	0.05	0.06	0.36	0.37	0.74	0.30	0.08	0.04
11.87	0.32	0.32	0.66	0.56	0.12	0.08	0.27	0.36	0.78	0.30	0.10	0.10

MEANOCK 3 JUNE 1969 PM B2

MEANOCK 3 JUNE 1969 PM 82

for long periods. For a rotation angle of $N40^{\circ}E$, $\text{coh } H_z E_x$ and $\text{coh } H_z H_y$ dropped to their minimum values and $\text{coh } H_z E_y$ and $\text{coh } H_z H_x$ reached their maximum values, which is consistent with a possible strike direction of $N55^{\circ}W$.

An aeromagnetic map which is available for this area shows a strong north-east trends a little to the east of the Meanook site.

Figure 4.9a: Aeromagnetic map for Meanook area

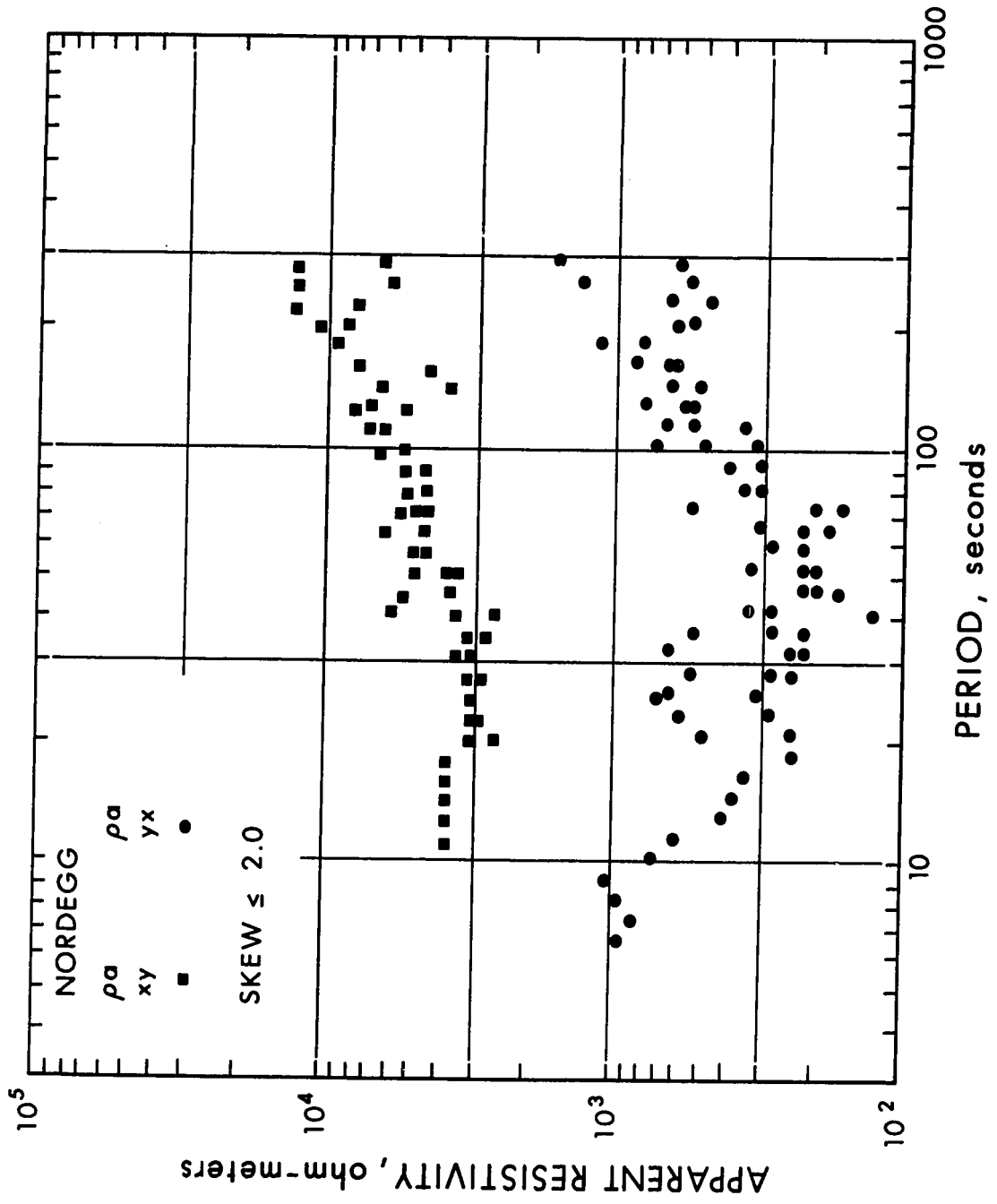
10. Nordegg (Fig. 4.10)

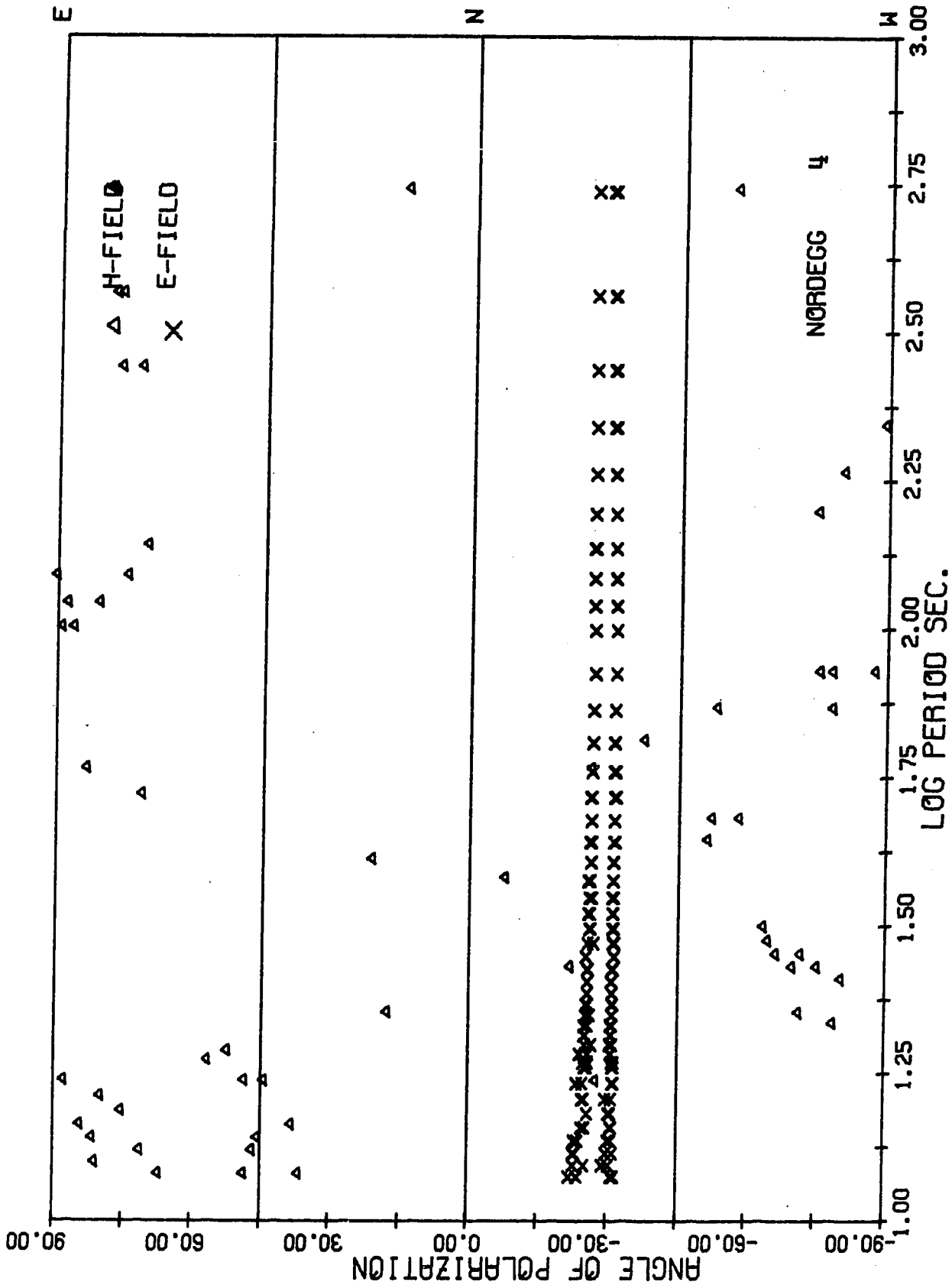
The Nordegg sounding site is in the foothills of the Rocky Mountains at an elevation of 4,500 feet. It is surrounded by mountains up to 6,000 feet high on all sides. Thirty miles to the west of the sounding site lies the first range of the Rocky Mountains with an elevation up to 10,000 feet. This and other ranges in the Rocky Mountains have a north-westerly trend in this area. Magnetotelluric measurements were made at this site during the 1968 and 1969 field seasons. The coherencies between the orthogonal components of the magnetic and telluric fields were low (<0.8) for both years' records. The coherency between the orthogonal components of the telluric field was very high. Predicted coherencies were good only for a couple of records for both these years and the skew values were greater than 1.0. Although the tensor apparent resistivity curves show anisotropic behaviour, it is not advisable to draw any conclusions from these results, because of high skew values. The azimuth for minimum resistivity was found to be $+90^\circ$ (not presented here).

The telluric field is linearly polarized about $N30^\circ W$, for both years, with slight deviation for 1969 records from 1968 records, which may be instrumental. There is much scatter in the angle of polarization of the magnetic field but it seems

Figure 4.10: Magnetotelluric results for Nordegg

- i. Tensor apparent resistivities in measuring directions.
- ii. Polarization angles for telluric and magnetic fields.
- iii. Vertical magnetic field analyses results.





ROTATION ANGLE = N 0.0E

PERIOD SEC.	COH		CCH		COH		HZ/HY	
	HZ-EX	HZ-EY	HZ-HX	HZ-HY	HZ-HX	HZ-HY	HZ/HX	HZ/HY
546.13	0.56	0.56	0.53	0.81	0.67	0.57	0.67	0.57
364.09	0.83	0.83	0.68	0.91	0.73	0.65	0.63	0.63
273.07	0.91	0.91	0.81	0.94	0.73	0.65	0.76	0.66
218.45	0.93	0.93	0.87	0.94	0.76	0.66	0.72	0.65
182.04	0.94	0.94	0.88	0.94	0.67	0.64	0.67	0.64
156.04	0.92	0.92	0.88	0.94	0.65	0.64	0.65	0.64
136.53	0.82	0.81	0.80	0.83	0.65	0.64	0.65	0.64
121.36	0.57	0.57	0.70	0.68	0.65	0.62	0.70	0.62
109.23	0.37	0.37	0.70	0.65	0.73	0.55	0.73	0.55
99.30	0.39	0.40	0.71	0.59	0.69	0.55	0.69	0.55
84.02	0.50	0.50	0.80	0.48	0.63	0.57	0.63	0.57
72.82	0.60	0.60	0.77	0.63	0.63	0.57	0.63	0.57
64.25	0.76	0.77	0.74	0.79	0.55	0.62	0.55	0.62
57.49	0.53	0.52	0.78	0.41	0.50	0.75	0.50	0.75
52.01	0.22	0.20	0.65	0.32	0.69	0.80	0.69	0.80
47.49	0.31	0.32	0.41	0.51	0.64	0.56	0.64	0.56
43.69	0.43	0.45	0.59	0.61	0.67	0.74	0.67	0.74
40.45	0.23	0.27	0.72	0.72	0.77	1.04	0.77	1.04
37.66	0.50	0.47	0.76	0.54	0.68	0.95	0.68	0.95
35.23	0.25	0.23	0.64	0.40	0.56	0.68	0.56	0.68
33.10	0.16	0.18	0.57	0.57	0.55	0.64	0.55	0.64
31.21	0.30	0.32	0.45	0.60	0.58	0.58	0.58	0.58
29.52	0.24	0.27	0.55	0.60	0.67	0.69	0.67	0.69
28.01	0.41	0.40	0.73	0.49	0.58	0.73	0.58	0.73
26.64	0.45	0.46	0.74	0.11	0.50	0.72	0.50	0.72
25.40	0.45	0.43	0.73	0.29	0.51	0.63	0.51	0.63
24.27	0.30	0.29	0.73	0.34	0.49	0.57	0.49	0.57
23.24	0.42	0.41	0.86	0.41	0.54	0.86	0.54	0.86
22.29	0.36	0.35	0.73	0.40	0.57	0.82	0.57	0.82
21.42	0.24	0.22	0.63	0.29	0.57	0.49	0.57	0.49
20.61	0.19	0.21	0.53	0.51	0.56	0.47	0.56	0.47
19.86	0.38	0.42	0.56	0.77	0.67	0.61	0.67	0.61
19.16	0.44	0.46	0.73	0.78	0.66	0.57	0.66	0.57
18.51	0.48	0.46	0.71	0.79	0.66	0.56	0.66	0.56
18.20	0.40	0.40	0.63	0.67	0.71	0.55	0.71	0.55
17.07	0.28	0.33	0.75	0.78	0.66	0.63	0.66	0.63
16.06	0.18	0.23	0.62	0.66	0.60	0.59	0.60	0.59
15.17	0.45	0.46	0.64	0.73	0.77	0.57	0.77	0.57
14.37	0.55	0.56	0.79	0.72	0.65	0.77	0.65	0.77
13.65	0.38	0.36	0.72	0.61	0.58	0.79	0.61	0.79
13.00	0.35	0.42	0.71	0.51	0.54	0.70	0.54	0.70
12.41	0.43	0.38	0.65	0.63	0.85	0.81	0.65	0.81
11.87	0.59	0.54	0.76	0.54	0.54	0.65	0.54	0.65

NORDEGG 2 AUG 1968 PM3 A1

ROTATION ANGLE = N 40.0E

PERIOD SEC.	COH		CCH		COH		HZ/HX		HZ/HY	
	HZ-EX	HZ-EY	HZ-HX	HZ-HY	HZ-HX	HZ-HY	HZ/HX	HZ/HY	HZ/HX	HZ/HY
546.13	0.56	0.56	0.41	0.80	0.41	0.80	0.41	0.80	0.79	0.52
364.09	0.83	0.83	0.73	0.79	0.73	0.79	0.73	0.79	0.75	0.55
273.07	0.91	0.91	0.87	0.86	0.87	0.86	0.87	0.86	0.83	0.60
218.45	0.93	0.93	0.91	0.91	0.91	0.91	0.91	0.91	0.85	0.61
182.04	0.94	0.94	0.93	0.92	0.93	0.92	0.93	0.92	0.84	0.59
156.04	0.92	0.92	0.93	0.90	0.93	0.90	0.93	0.90	0.84	0.56
136.53	0.82	0.82	0.91	0.77	0.91	0.77	0.91	0.77	0.83	0.55
121.36	0.58	0.57	0.92	0.51	0.92	0.51	0.92	0.51	0.74	0.58
109.23	0.36	0.37	0.93	0.29	0.93	0.29	0.93	0.29	0.67	0.63
99.30	0.38	0.39	0.90	0.31	0.90	0.31	0.90	0.31	0.67	0.59
84.02	0.49	0.50	0.87	0.45	0.87	0.45	0.87	0.45	0.74	0.53
72.82	0.60	0.60	0.86	0.61	0.86	0.61	0.86	0.61	0.75	0.51
64.25	0.76	0.76	0.79	0.74	0.79	0.74	0.79	0.74	0.76	0.49
57.49	0.54	0.53	0.88	0.60	0.88	0.60	0.88	0.60	0.79	0.49
52.01	0.24	0.21	0.87	0.19	0.87	0.19	0.87	0.19	0.89	0.65
47.49	0.30	0.31	0.80	0.29	0.80	0.29	0.80	0.29	0.85	0.49
43.69	0.41	0.43	0.85	0.38	0.85	0.38	0.85	0.38	0.81	0.63
40.45	0.22	0.24	0.83	0.42	0.83	0.42	0.83	0.42	0.76	1.05
37.66	0.52	0.49	0.77	0.60	0.77	0.60	0.77	0.60	0.80	0.77
35.23	0.27	0.24	0.76	0.31	0.76	0.31	0.76	0.31	0.65	0.58
33.10	0.13	0.17	0.81	0.09	0.81	0.09	0.81	0.09	0.60	0.59
31.21	0.29	0.31	0.77	0.19	0.77	0.19	0.77	0.19	0.62	0.54
29.52	0.24	0.25	0.81	0.49	0.81	0.49	0.81	0.49	0.73	0.64
28.01	0.42	0.41	0.84	0.48	0.84	0.48	0.84	0.48	0.68	0.58
26.64	0.44	0.45	0.75	0.52	0.75	0.52	0.75	0.52	0.68	0.51
25.40	0.46	0.44	0.82	0.26	0.82	0.26	0.82	0.26	0.64	0.50
24.27	0.30	0.30	0.88	0.49	0.88	0.49	0.88	0.49	0.54	0.51
23.24	0.43	0.42	0.88	0.58	0.88	0.58	0.88	0.58	0.58	0.75
22.29	0.37	0.35	0.76	0.36	0.76	0.36	0.76	0.36	0.58	0.79
21.42	0.24	0.23	0.66	0.13	0.66	0.13	0.66	0.13	0.54	0.51
20.61	0.17	0.20	0.75	0.13	0.75	0.13	0.75	0.13	0.53	0.49
19.86	0.36	0.39	0.76	0.51	0.76	0.51	0.76	0.51	0.56	0.76
19.16	0.44	0.44	0.81	0.47	0.81	0.47	0.81	0.47	0.48	0.98
18.51	0.49	0.47	0.82	0.48	0.82	0.48	0.82	0.48	0.50	0.93
18.20	0.39	0.41	0.75	0.39	0.75	0.39	0.75	0.39	0.53	0.75
17.07	0.25	0.29	0.88	0.26	0.88	0.26	0.88	0.26	0.53	0.89
16.06	0.15	0.20	0.81	0.28	0.81	0.28	0.81	0.28	0.60	0.64
15.17	0.44	0.45	0.76	0.59	0.76	0.59	0.76	0.59	0.56	0.72
14.37	0.55	0.55	0.83	0.09	0.83	0.09	0.83	0.09	0.54	1.20
13.65	0.36	0.38	0.82	0.21	0.82	0.21	0.82	0.21	0.57	0.83
13.00	0.32	0.32	0.78	0.38	0.78	0.38	0.78	0.38	0.53	0.72
12.41	0.43	0.42	0.76	0.12	0.76	0.12	0.76	0.12	0.70	1.07
11.87	0.61	0.57	0.75	0.36	0.75	0.36	0.75	0.36	0.47	0.88

NORDEGG 2 AUG 1968 PM3 A1

to be near an east-west direction for most of the period bands.

Coherencies between the vertical component of the magnetic field and E_x , E_y , H_x and H_y are high for periods greater than 100 seconds and for a rotation angle of $N40^\circ E$ the coh $H_z H_x$ reached their maximum without much change in other coherencies.

11. NSR Crossing (Fig. 4.11)

The station North Saskatchewan River Crossing (NSR Crossing) is located at the crossing of the North Saskatchewan River and the Banff-Jasper highway, in the central ranges of the Rocky Mountains. The station is surrounded by north-westerly striking mountain ridges with peaks up to 11,000 feet.

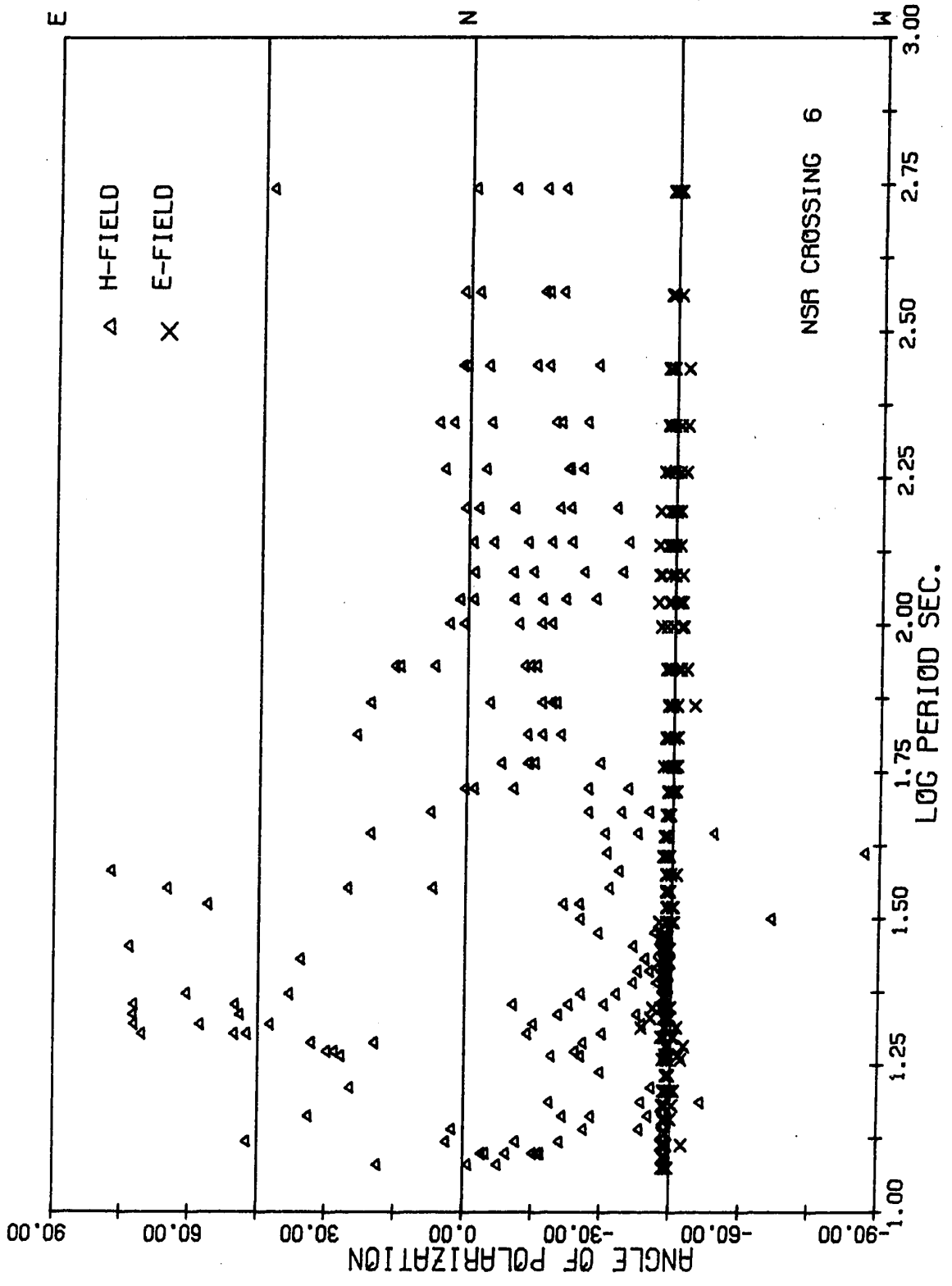
Very low amplitude magnetic signal was recorded at this site. The coherencies between the orthogonal components of telluric and magnetic fields were low (<0.7). The predicted coherencies were also low, and hence no reliable apparent resistivity curves were obtained for this site.

The polarization analyses of the magnetic and telluric field show that the telluric field is linearly polarized in north-westerly direction for all periods whereas the angle of polarization of the magnetic field is about $N20^{\circ}W$, for periods longer than 100 seconds, and very scattered for shorter periods.

Very low H_z activity was recorded at this site.

Figure 4.11: Magnetotelluric results for NSR crossing

- i. Polarization angles for telluric and magnetic fields.



12. Observatory (Fig.4.12)

Magnetotelluric results for the University of Alberta Geophysical Observatory were obtained both from 1968 and 1969 data. The skew values were high for this location. The rotated tensor apparent resistivities presented here, are for skew values less than or equal to 0.3. The apparent resistivity curves show an anisotropic behaviour for periods greater than 8 seconds but seems to converge for shorter periods. The ρ_{yx}^a value contain less scatter than ρ_{xy}^a values.

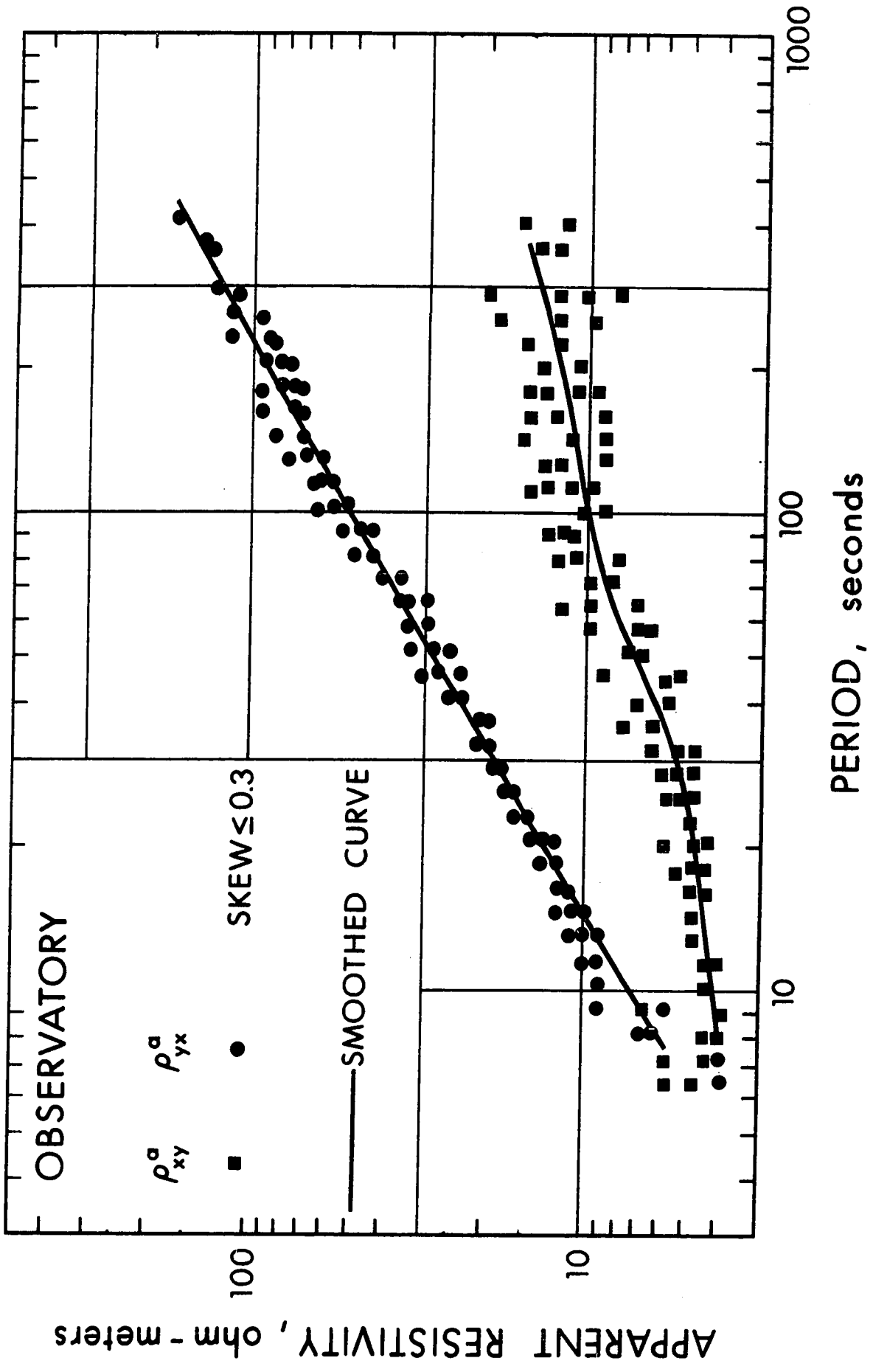
The azimuth for minimum resistivity changes from $+50^\circ$ for long periods to $+90^\circ$ for shorter periods. The angle of polarization of the telluric field is $N40^\circ W$ for long periods and there is much scatter for short periods but it is in between north and north-west. The magnetic field at $N30^\circ E$ direction for long periods. For short periods it scattered around $N35^\circ E$.

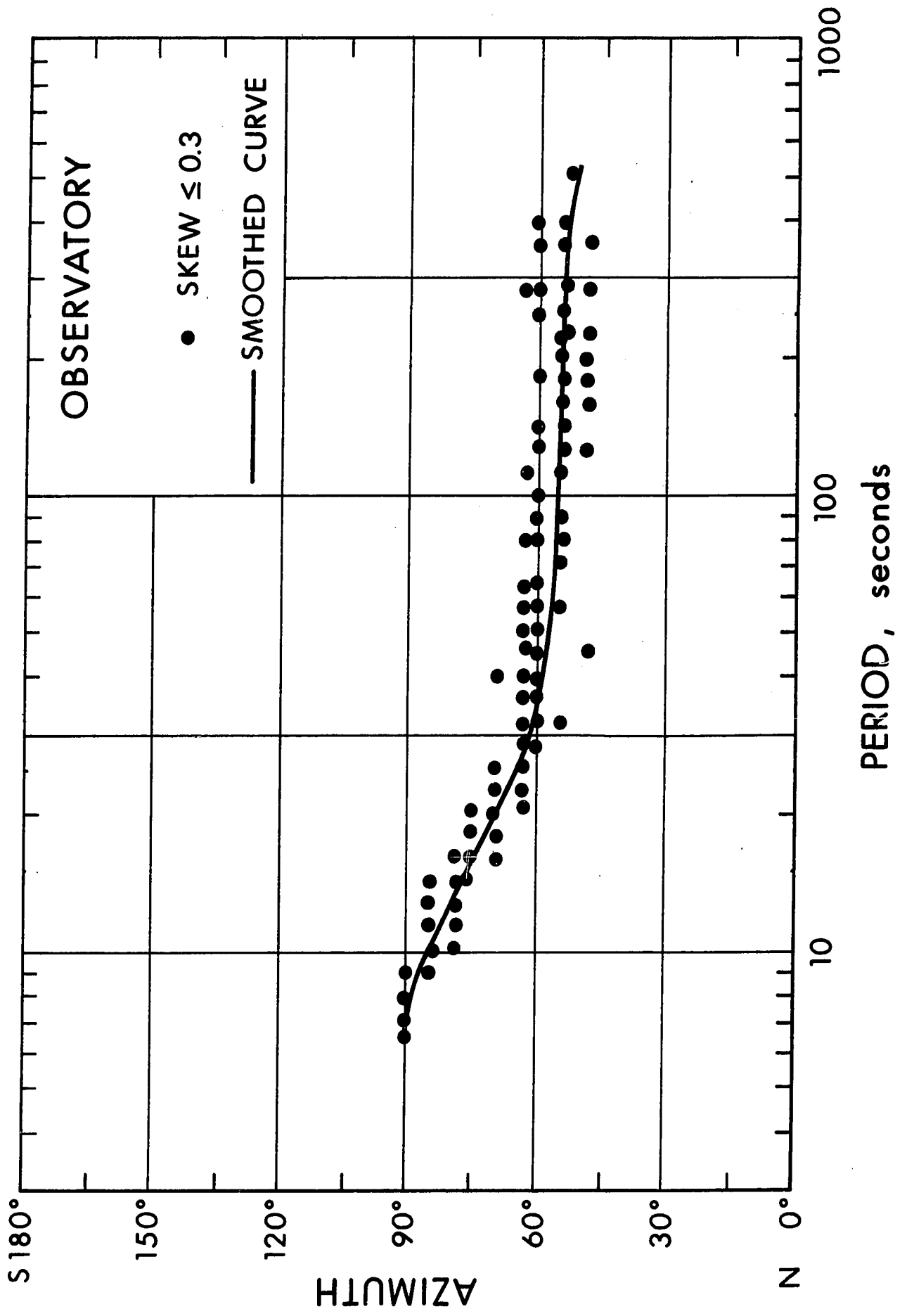
The direction of maximum resistivity and the angle of polarization of the telluric field coincide for longer periods.

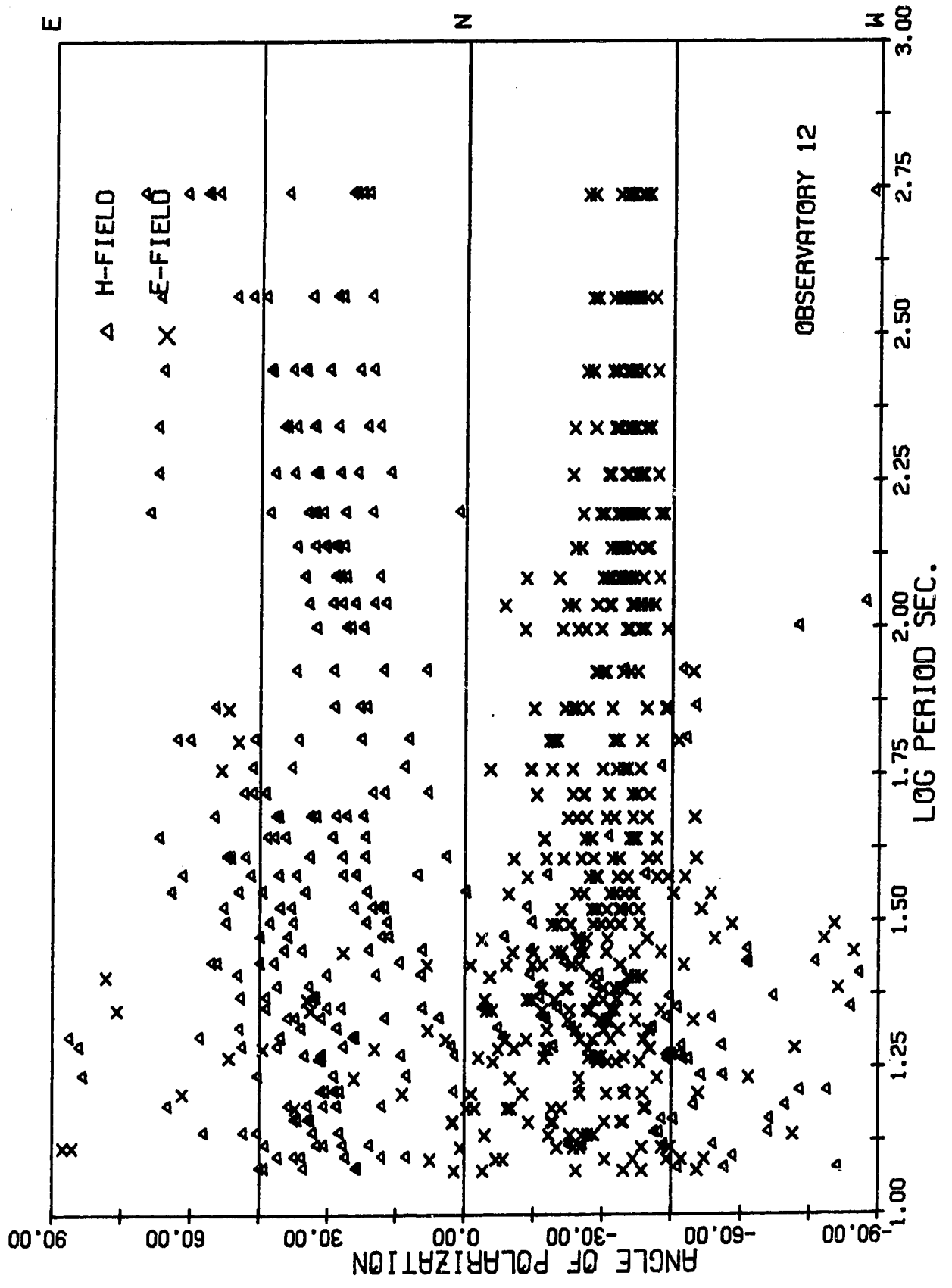
For data sets with reasonably good H_z for long periods, the coherency analyses show that H_z is coherent with the four horizontal components of the magnetotelluric field in measuring directions, and for a rotation angle of $N50^\circ E$, $\text{coh } H_z E_x$ and $\text{coh } H_z H_y$ dropped to their minima whereas other

Figure 4.12: Magnetotelluric results for Observatory

- i. Tensor apparent resistivities in the principal directions.
- ii. Azimuth (the direction of minimum tensor apparent resistivity).
- iii. Polarization angles for telluric and magnetic fields.
- iv. Vertical magnetic field analyses results.







ROTATION ANGLE = N 0.0E

PERIOD SEC.	COH HZ-EX	COH HZ-EY	COH HZ-HX	COH HZ-HY	HZ/HX	HZ/HY
546.13	0.73	0.73	0.78	0.52	1.14	0.95
364.09	0.86	0.87	0.81	0.67	0.86	0.84
273.07	0.91	0.93	0.87	0.77	0.70	0.76
218.45	0.92	0.94	0.90	0.84	0.58	0.67
182.04	0.94	0.96	0.93	0.88	0.47	0.60
156.04	0.95	0.96	0.93	0.88	0.41	0.59
136.53	0.95	0.95	0.93	0.84	0.37	0.60
121.36	0.92	0.90	0.90	0.74	0.34	0.62
109.23	0.89	0.85	0.85	0.64	0.31	0.58
99.30	0.84	0.81	0.81	0.62	0.27	0.49
84.02	0.66	0.59	0.57	0.68	0.22	0.26
72.82	0.63	0.33	0.42	0.66	0.16	0.16
64.25	0.66	0.33	0.34	0.71	0.20	0.13
57.49	0.69	0.29	0.41	0.66	0.28	0.19
52.01	0.43	0.67	0.76	0.17	0.23	0.36
47.49	0.70	0.68	0.75	0.48	0.18	0.27
43.69	0.51	0.52	0.72	0.23	0.17	0.19
40.45	0.55	0.51	0.71	0.46	0.18	0.24
37.66	0.61	0.46	0.56	0.50	0.15	0.17
35.23	0.62	0.58	0.62	0.57	0.09	0.10
33.10	0.50	0.64	0.67	0.48	0.07	0.08
31.21	0.32	0.39	0.42	0.28	0.07	0.08
29.52	0.19	0.07	0.14	0.26	0.08	0.10
28.01	0.29	0.15	0.22	0.40	0.09	0.10
26.64	0.31	0.17	0.19	0.31	0.12	0.13
25.40	0.36	0.21	0.24	0.33	0.15	0.17
24.27	0.10	0.20	0.17	0.10	0.08	0.11
23.24	0.35	0.12	0.26	0.49	0.09	0.12
22.29	0.19	0.13	0.30	0.33	0.10	0.17
21.42	0.44	0.24	0.47	0.39	0.14	0.20
20.61	0.21	0.38	0.38	0.23	0.13	0.20
19.86	0.19	0.38	0.30	0.22	0.11	0.13
19.16	0.31	0.28	0.28	0.31	0.08	0.09
18.51	0.17	0.11	0.14	0.20	0.07	0.11
18.20	0.26	0.13	0.23	0.27	0.07	0.10
17.07	0.25	0.09	0.24	0.32	0.07	0.10
16.06	0.16	0.24	0.29	0.12	0.08	0.13
15.17	0.31	0.61	0.50	0.25	0.09	0.12
14.37	0.26	0.15	0.09	0.27	0.08	0.11
13.65	0.11	0.20	0.15	0.19	0.09	0.08
13.00	0.13	0.22	0.16	0.06	0.06	0.09
12.41	0.11	0.17	0.15	0.14	0.07	0.12
11.87	0.15	0.21	0.24	0.22	0.08	0.14

OBSERVATORY 18 AUG 1968 PM 3

ROTATION ANGLE = N 50.0E

PERIOD SEC.	COH HZ-EX	COH HZ-EY	COH HZ-HX	COH HZ-HY	HZ/HX	HZ/HY
546.13	0.45	0.73	0.69	0.36	0.82	1.61
364.09	0.64	0.87	0.79	0.50	0.67	1.41
273.07	0.76	0.92	0.85	0.68	0.57	1.16
218.45	0.77	0.93	0.90	0.74	0.48	1.09
182.04	0.81	0.95	0.93	0.79	0.40	1.05
156.04	0.81	0.96	0.93	0.79	0.36	0.95
136.53	0.74	0.95	0.92	0.80	0.35	0.78
121.36	0.62	0.92	0.88	0.76	0.34	0.63
109.23	0.55	0.88	0.83	0.76	0.32	0.54
99.30	0.49	0.84	0.79	0.69	0.27	0.48
84.02	0.43	0.66	0.70	0.13	0.19	0.36
72.82	0.56	0.60	0.64	0.26	0.14	0.25
64.25	0.69	0.59	0.64	0.53	0.12	0.24
57.49	0.78	0.51	0.48	0.72	0.21	0.25
52.01	0.17	0.51	0.54	0.75	0.21	0.28
47.49	0.66	0.70	0.66	0.70	0.17	0.29
43.69	0.39	0.53	0.54	0.61	0.14	0.24
40.45	0.45	0.57	0.64	0.61	0.16	0.32
37.66	0.49	0.59	0.57	0.28	0.12	0.29
35.23	0.49	0.63	0.61	0.47	0.07	0.20
33.10	0.31	0.55	0.58	0.72	0.05	0.17
31.21	0.17	0.36	0.36	0.34	0.06	0.15
29.52	0.24	0.16	0.21	0.08	0.07	0.16
28.01	0.32	0.26	0.22	0.13	0.07	0.20
26.64	0.44	0.21	0.22	0.40	0.10	0.21
25.40	0.26	0.33	0.33	0.09	0.13	0.20
24.27	0.26	0.09	0.10	0.27	0.08	0.15
23.24	0.30	0.28	0.39	0.05	0.08	0.16
22.29	0.16	0.18	0.34	0.17	0.10	0.18
21.42	0.34	0.41	0.47	0.32	0.13	0.24
20.61	0.23	0.30	0.34	0.34	0.12	0.22
19.86	0.10	0.26	0.27	0.29	0.09	0.27
19.16	0.22	0.31	0.29	0.32	0.06	0.17
18.51	0.11	0.16	0.18	0.10	0.07	0.14
18.20	0.15	0.24	0.26	0.14	0.06	0.13
17.07	0.25	0.17	0.26	0.28	0.07	0.12
16.06	0.08	0.21	0.24	0.29	0.08	0.13
15.17	0.45	0.48	0.42	0.47	0.08	0.16
14.37	0.33	0.18	0.18	0.14	0.07	0.15
13.65	0.21	0.11	0.16	0.21	0.07	0.12
13.00	0.21	0.19	0.12	0.18	0.06	0.12
12.41	0.25	0.08	0.06	0.28	0.07	0.12
11.87	0.38	0.04	0.11	0.41	0.08	0.13

OBSERVATORY 18 AUG 1968 PM 3

coherencies were virtually unaffected.

The tensor apparent resistivity curves presented here are similar to the curves obtained in the measuring directions for 1966 data (Rankin and Reddy, 1969). The difference in the direction of principal axes obtained in both the cases may be due to change in the direction of magnetic field polarization, as well as less accurate analysis techniques applied to 1966 data.

13. Red Deer (Fig. 4.13)

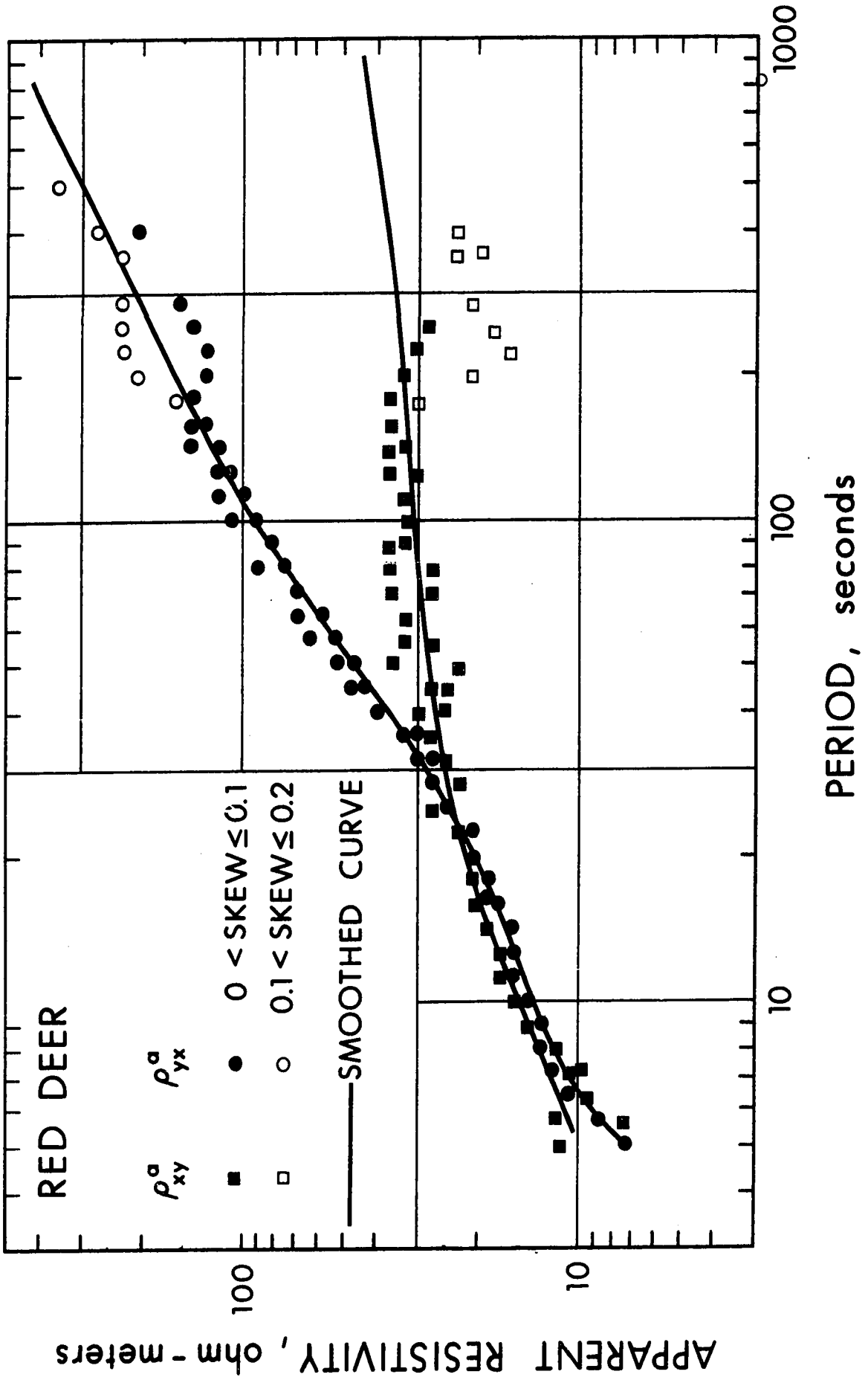
Magnetotelluric data for the Red Deer sounding site was collected by Dr. W. J. Peeples as a part of his magnetotelluric investigations in Southern Alberta. The tensor apparent resistivity curves show an anisotropic behaviour for periods greater than 40 seconds. The curves are isotropic for periods less than 40 seconds and seem to approach 10 ohm-meters for shorter periods. The minimum apparent resistivity estimates have much scatter for periods greater than 200 seconds.

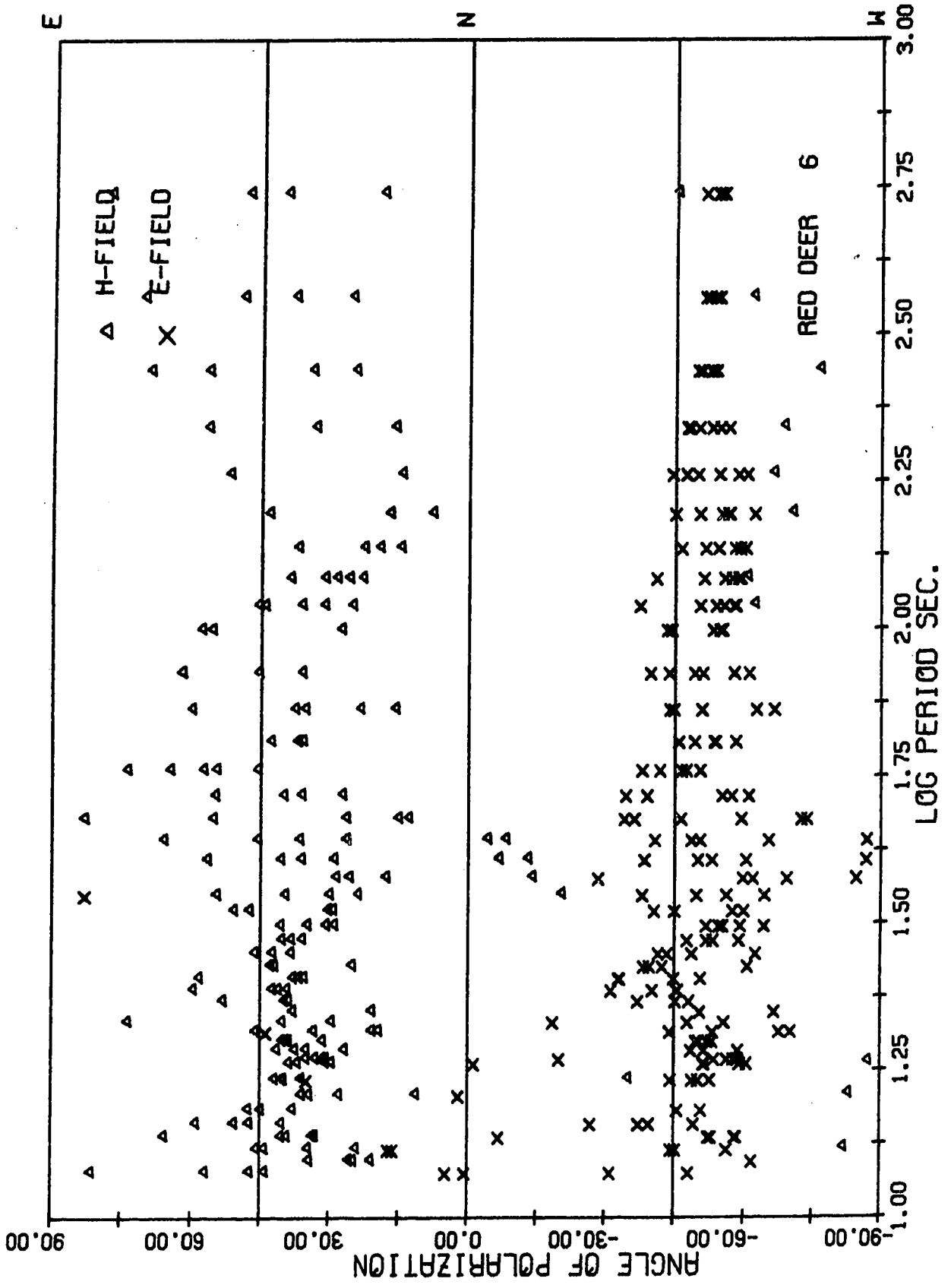
The azimuth for minimum resistivity is around $+40^\circ$ for periods greater than 40 seconds and varies between 0° and 90° for shorter periods. The angle of polarization of the electric field is about $N50^\circ W$ for the entire band with some scatter at the short period end. The average angle of polarization for magnetic field is around $N40^\circ E$, but there is much scatter. The magnetic and telluric fields are approximately orthogonal over the entire spectrum. The direction of maximum apparent resistivity and the average direction of telluric field are coincident.

The amplitude of the vertical component was low for this station. Coherency analyses show that H_z is more coherent with E_y and H_x than with E_x and H_y , for long periods, and for a rotation of $N30^\circ E$,

Figure 4.13: Magnetotelluric results for Red Deer

- i. Tensor apparent resistivities in the principal directions.
- ii. Azimuth (the direction of minimum tensor apparent resistivity).
- iii. Polarization angles for telluric and magnetic fields.
- iv. Vertical magnetic field analyses results.





ROTATION ANGLE = N 0.0E

PERIOD SEC.	COH HZ-EX	COH HZ-EY	COH HZ-HX	COH HZ-HY	HZ/HX	HZ/HY
546.13	0.29	0.46	0.72	0.40	1.44	1.23
364.09	0.57	0.72	0.69	0.26	1.05	1.12
273.07	0.69	0.80	0.69	0.37	0.84	1.21
218.45	0.73	0.81	0.77	0.45	0.70	1.37
182.04	0.77	0.86	0.85	0.56	0.63	1.32
156.04	0.72	0.87	0.86	0.52	0.58	0.99
136.53	0.52	0.72	0.77	0.32	0.47	0.65
121.36	0.52	0.62	0.69	0.40	0.33	0.50
109.23	0.54	0.64	0.71	0.43	0.30	0.54
99.30	0.59	0.72	0.78	0.50	0.31	0.53
84.02	0.45	0.58	0.58	0.41	0.31	0.41
72.82	0.35	0.39	0.40	0.37	0.23	0.29
64.25	0.19	0.12	0.18	0.25	0.27	0.33
57.49	0.24	0.24	0.37	0.22	0.23	0.23
52.01	0.29	0.68	0.74	0.37	0.26	0.28
47.49	0.39	0.84	0.86	0.50	0.29	0.53
43.69	0.44	0.85	0.86	0.52	0.24	0.36
40.45	0.61	0.91	0.91	0.62	0.19	0.28
37.66	0.44	0.84	0.87	0.34	0.19	0.38
35.23	0.23	0.25	0.38	0.22	0.18	0.20
33.10	0.32	0.15	0.29	0.29	0.14	0.14
31.21	0.17	0.42	0.45	0.15	0.11	0.13
29.52	0.42	0.61	0.63	0.39	0.10	0.11
28.01	0.18	0.57	0.61	0.14	0.12	0.14
26.64	0.38	0.25	0.32	0.39	0.15	0.15
25.40	0.37	0.31	0.29	0.36	0.13	0.09
24.27	0.22	0.22	0.26	0.22	0.10	0.07
23.24	0.02	0.36	0.44	0.04	0.10	0.08
22.29	0.14	0.57	0.65	0.10	0.11	0.13
21.42	0.09	0.62	0.65	0.10	0.10	0.13
20.61	0.21	0.54	0.57	0.23	0.08	0.11
19.86	0.36	0.54	0.58	0.34	0.11	0.14
19.16	0.54	0.69	0.70	0.50	0.10	0.14
18.51	0.24	0.54	0.52	0.25	0.09	0.12
18.20	0.12	0.48	0.46	0.16	0.08	0.09
17.07	0.22	0.48	0.51	0.23	0.08	0.09
16.06	0.27	0.64	0.65	0.26	0.07	0.08
15.17	0.40	0.71	0.73	0.43	0.08	0.08
14.37	0.36	0.67	0.73	0.36	0.10	0.10
13.65	0.36	0.70	0.71	0.39	0.08	0.09
13.00	0.40	0.58	0.57	0.44	0.07	0.07
12.41	0.45	0.67	0.64	0.48	0.09	0.10
11.87	0.41	0.66	0.70	0.43	0.07	0.07

RED DEER 23 MAY 1968 PMI

ROTATION ANGLE = N 30.0E

PERIOD SEC.	COH HZ-EX	COH HZ-EY	COH HZ-HX	COH HZ-HY	HZ/HX	HZ/HY
546.13	0.06	0.42	0.67	0.13	1.14	1.63
364.09	0.12	0.69	0.62	0.18	0.92	1.40
273.07	0.25	0.78	0.68	0.22	0.78	1.43
218.45	0.16	0.81	0.77	0.41	0.69	1.41
182.04	0.09	0.85	0.86	0.57	0.64	1.26
156.04	0.12	0.85	0.86	0.51	0.58	1.00
136.53	0.07	0.68	0.74	0.31	0.44	0.72
121.36	0.28	0.60	0.67	0.34	0.31	0.61
109.23	0.28	0.62	0.67	0.43	0.28	0.77
99.30	0.27	0.69	0.73	0.45	0.28	0.96
84.02	0.16	0.55	0.55	0.12	0.26	0.80
72.82	0.16	0.38	0.40	0.19	0.19	0.59
64.25	0.37	0.10	0.15	0.38	0.23	0.48
57.49	0.53	0.15	0.24	0.45	0.19	0.35
52.01	0.58	0.56	0.61	0.55	0.22	0.35
47.49	0.76	0.78	0.81	0.72	0.29	0.52
43.69	0.62	0.79	0.81	0.60	0.22	0.45
40.45	0.43	0.86	0.88	0.31	0.16	0.46
37.66	0.64	0.79	0.83	0.61	0.19	0.40
35.23	0.42	0.17	0.27	0.47	0.15	0.28
33.10	0.52	0.09	0.19	0.48	0.11	0.20
31.21	0.36	0.34	0.37	0.25	0.09	0.23
29.52	0.52	0.54	0.56	0.41	0.08	0.19
28.01	0.40	0.40	0.50	0.37	0.10	0.19
26.64	0.54	0.18	0.19	0.59	0.13	0.20
25.40	0.35	0.36	0.32	0.39	0.09	0.14
24.27	0.33	0.13	0.11	0.38	0.07	0.10
23.24	0.20	0.24	0.30	0.23	0.07	0.12
22.29	0.48	0.42	0.52	0.45	0.10	0.18
21.42	0.25	0.49	0.55	0.45	0.09	0.17
20.61	0.25	0.47	0.51	0.23	0.07	0.15
19.86	0.52	0.45	0.52	0.54	0.10	0.17
19.16	0.63	0.63	0.66	0.54	0.10	0.17
18.51	0.31	0.49	0.49	0.22	0.08	0.15
18.20	0.26	0.40	0.41	0.19	0.07	0.11
17.07	0.32	0.40	0.44	0.24	0.06	0.15
16.06	0.44	0.54	0.58	0.36	0.06	0.15
15.17	0.08	0.64	0.66	0.10	0.06	0.14
14.37	0.08	0.55	0.64	0.31	0.08	0.14
13.65	0.25	0.63	0.65	0.12	0.06	0.14
13.00	0.40	0.51	0.53	0.40	0.06	0.14
12.41	0.45	0.67	0.64	0.49	0.06	0.11
11.87	0.41	0.60	0.64	0.14	0.08	0.13

RED DEER 23 MAY 1968 PMI

$\text{coh } H_z E_y$ and $\text{coh } H_z H_y$ dropped to their minimum values, which are slightly lower than in the measuring directions. The other pairs are only slightly increased for this rotation.

$\text{coh } H_z E_y$ and $\text{coh } H_z H_y$ dropped to their minimum values, which are slightly lower than in the measuring directions. The other pairs are only slightly increased for this rotation.

14. Smoky Lake (Fig. 4.14)

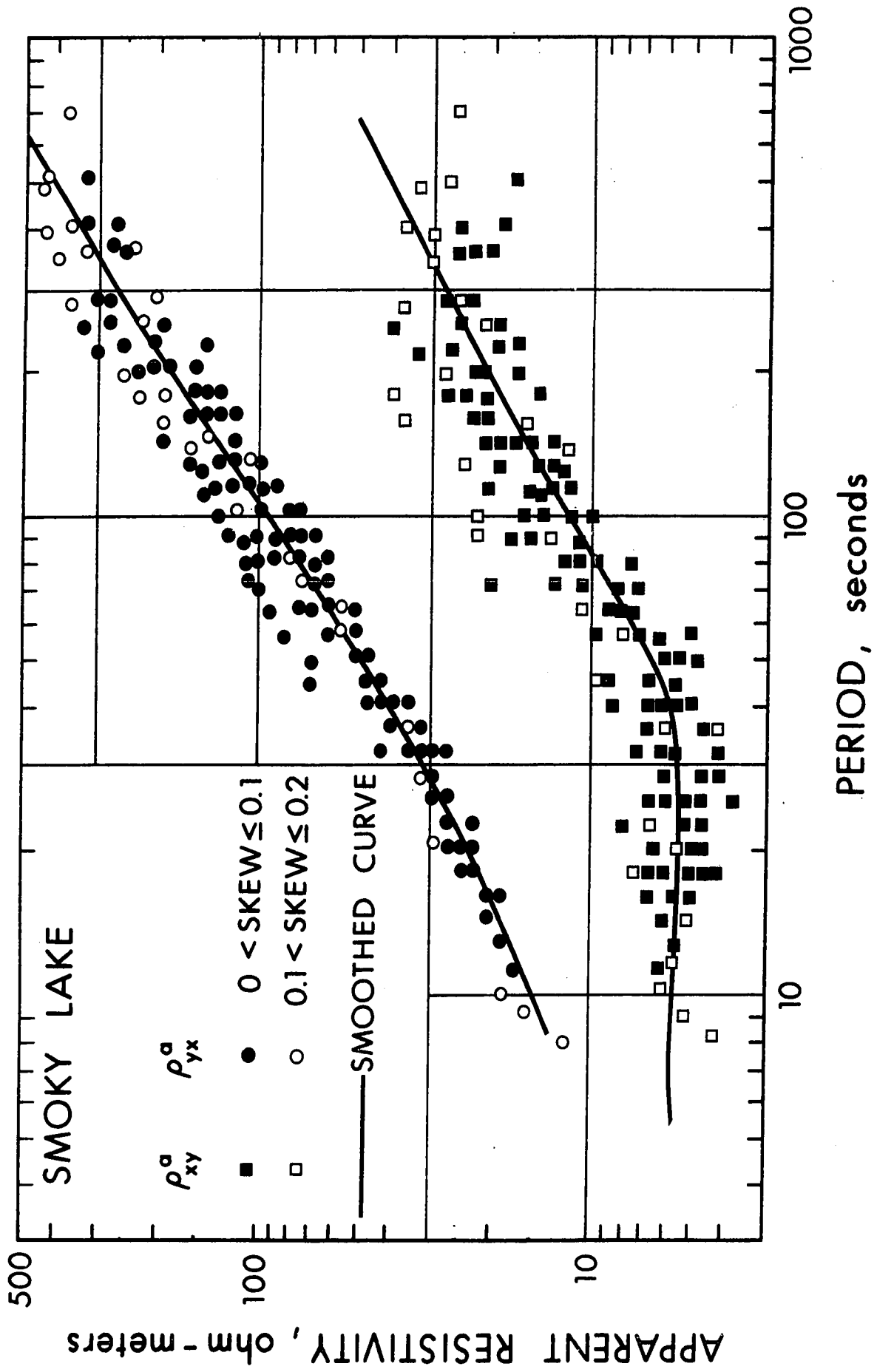
The tensor apparent resistivity curves in the principal directions show anisotropic behaviour for the entire spectrum with a greater degree of anisotropy at the long period end. The apparent resistivity estimates are relatively smooth, although ρ_{xy}^a have more scatter than ρ_{yx}^a values. The curves may converge for very short periods.

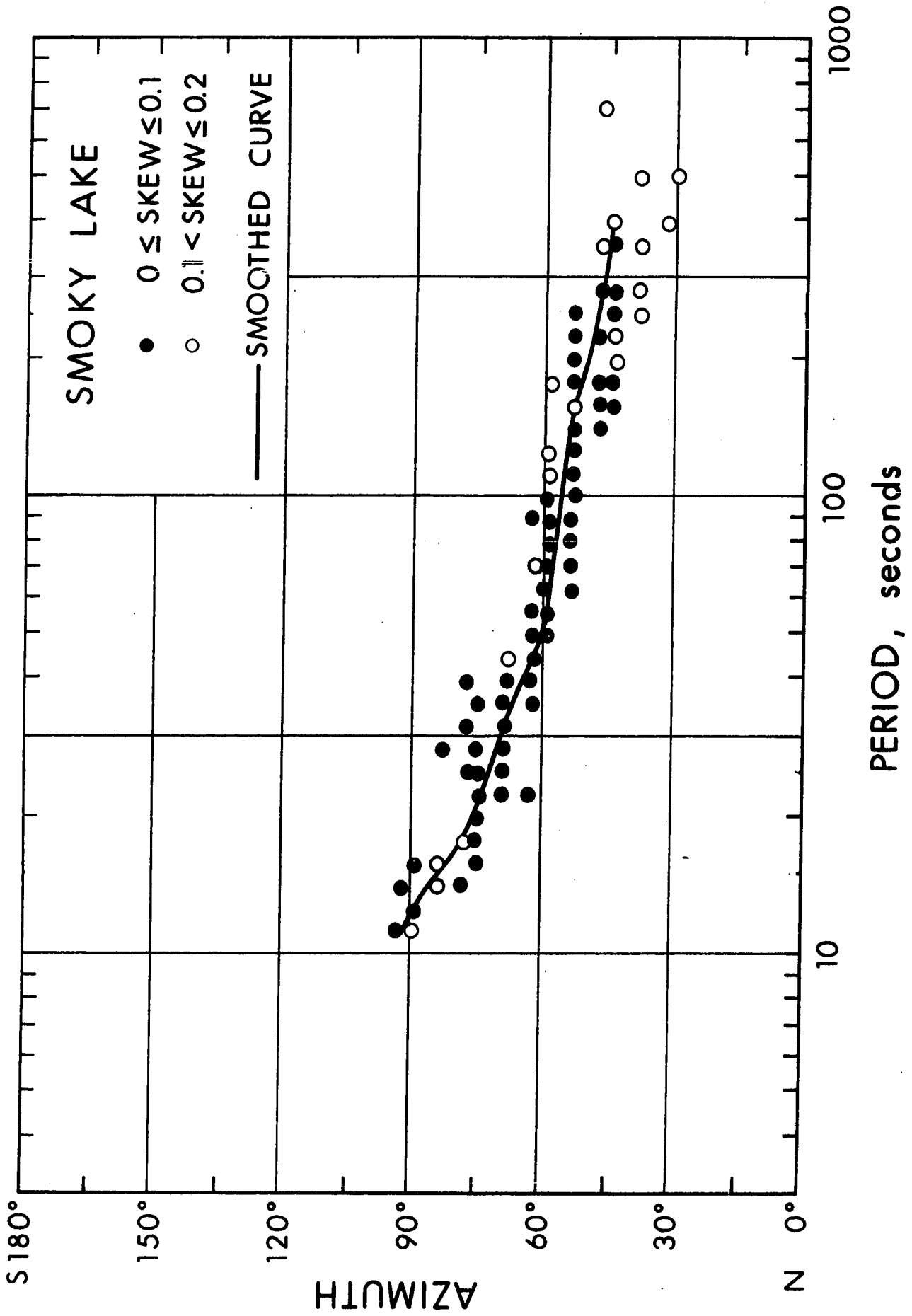
The azimuth of minimum apparent resistivity varies from $+90^\circ$ for 10 second period to $+30^\circ$ for 300 second period. The angle of polarization of the telluric field is around $N50^\circ W$ for long periods and tend towards $N25^\circ W$ for short periods. There is much scatter for short periods. The average direction for the magnetic field is $N20^\circ E$, but there is a considerable deviation from this direction.

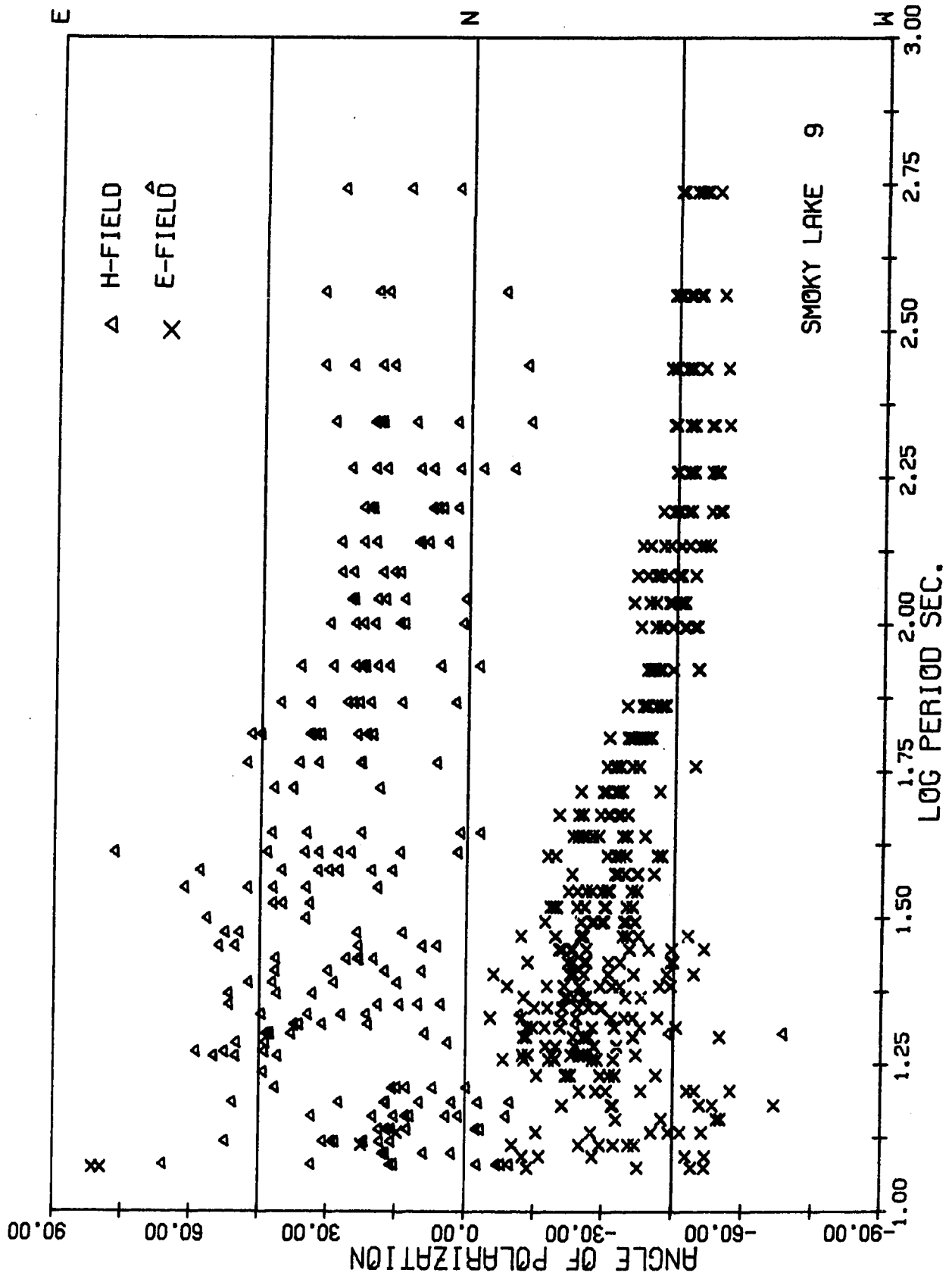
Coherency analyses of the vertical magnetic field with E_x , E_y , H_x and H_y show that H_z is highly coherent with E_x , E_y and H_x for periods greater than 50 seconds, in the measuring directions. For a rotation angle of $N50^\circ E$, $\text{coh } H_z E_x$ dropped to its minimum whereas $\text{coh } H_z E_y$ and $\text{coh } H_z$ remained more or less unchanged, implying a possible strike direction of $N40^\circ W$ for periods greater than 50 seconds.

Figure 4.14: Magnetotelluric results for Smoky Lake

- i. Tensor apparent resistivities in the principal directions.
- ii. Azimuth (the direction of minimum tensor apparent resistivity).
- iii. Polarization angles for telluric and magnetic fields.
- iv. Vertical magnetic field analyses results.







PERIOD SEC.	ROTATION ANGLE = N 0.0E				ROTATION ANGLE = N 50.0E				HZ/HX	HZ/HY
	COH HZ-EX	COH HZ-EY	COH HZ-HX	COH HZ-HY	COH HZ-EX	COH HZ-EY	COH HZ-HX	COH HZ-HY		
546.13	0.88	0.87	0.72	0.52	0.43	0.75	0.39	0.56	0.76	
364.09	0.95	0.95	0.89	0.75	0.64	0.96	0.60	0.52	1.00	
273.07	0.96	0.97	0.94	0.84	0.72	0.97	0.73	0.51	1.12	
218.45	0.94	0.96	0.94	0.80	0.72	0.95	0.80	0.48	0.98	
182.04	0.93	0.96	0.93	0.70	0.69	0.90	0.81	0.43	0.76	
156.04	0.92	0.96	0.93	0.66	0.61	0.91	0.77	0.39	0.61	
136.53	0.90	0.95	0.93	0.68	0.45	0.94	0.92	0.37	0.56	
121.36	0.93	0.95	0.93	0.77	0.28	0.94	0.77	0.37	0.61	
109.23	0.94	0.97	0.95	0.79	0.19	0.94	0.83	0.37	0.61	
99.30	0.93	0.97	0.96	0.70	0.23	0.96	0.83	0.37	0.61	
84.02	0.95	0.97	0.96	0.76	0.23	0.96	0.83	0.36	0.55	
72.82	0.94	0.96	0.89	0.71	0.48	0.96	0.80	0.30	0.51	
64.25	0.95	0.97	0.84	0.84	0.35	0.96	0.53	0.27	0.39	
57.49	0.97	0.95	0.88	0.89	0.65	0.97	0.26	0.22	0.40	
52.01	0.91	0.88	0.84	0.84	0.68	0.98	0.35	0.21	0.41	
47.49	0.87	0.87	0.79	0.63	0.51	0.93	0.50	0.19	0.26	
43.69	0.77	0.62	0.66	0.39	0.47	0.90	0.32	0.17	0.21	
40.45	0.82	0.73	0.79	0.57	0.35	0.79	0.38	0.19	0.17	
37.66	0.85	0.76	0.69	0.68	0.43	0.82	0.47	0.15	0.21	
35.23	0.83	0.70	0.61	0.77	0.50	0.86	0.20	0.12	0.16	
33.10	0.78	0.46	0.48	0.76	0.63	0.83	0.16	0.14	0.19	
31.21	0.65	0.46	0.49	0.61	0.63	0.85	0.16	0.14	0.19	
29.52	0.49	0.22	0.63	0.32	0.50	0.75	0.17	0.17	0.22	
28.01	0.40	0.18	0.46	0.30	0.44	0.65	0.11	0.16	0.22	
26.64	0.36	0.03	0.28	0.26	0.42	0.46	0.49	0.12	0.17	
25.40	0.61	0.09	0.43	0.47	0.42	0.36	0.38	0.09	0.22	
24.27	0.53	0.33	0.54	0.34	0.61	0.49	0.30	0.11	0.17	
23.24	0.35	0.16	0.30	0.32	0.28	0.55	0.30	0.12	0.15	
22.29	0.37	0.05	0.29	0.27	0.27	0.30	0.28	0.13	0.14	
21.42	0.50	0.11	0.27	0.36	0.42	0.27	0.06	0.12	0.15	
20.61	0.54	0.14	0.05	0.45	0.49	0.39	0.07	0.13	0.17	
19.86	0.36	0.21	0.07	0.30	0.46	0.40	0.42	0.16	0.22	
19.16	0.25	0.44	0.34	0.19	0.41	0.42	0.16	0.22	0.13	
18.51	0.48	0.17	0.36	0.18	0.25	0.38	0.13	0.28	0.15	
18.20	0.59	0.11	0.32	0.28	0.22	0.41	0.25	0.28	0.19	
17.07	0.23	0.08	0.10	0.22	0.46	0.46	0.18	0.19	0.17	
16.06	0.09	0.16	0.13	0.16	0.18	0.18	0.10	0.19	0.17	
15.17	0.28	0.09	0.10	0.16	0.18	0.10	0.12	0.19	0.25	
14.37	0.16	0.07	0.22	0.09	0.26	0.21	0.17	0.19	0.18	
13.65	0.06	0.05	0.23	0.24	0.16	0.11	0.16	0.22	0.38	
13.00	0.15	0.10	0.24	0.24	0.04	0.08	0.28	0.23	0.23	
12.41	0.16	0.16	0.16	0.16	0.11	0.18	0.22	0.28	0.31	
11.87	0.34	0.36	0.19	0.33	0.08	0.19	0.06	0.23	0.31	
					0.39	0.29	0.32	0.20	0.28	

SMOKY LAKE 6 JUNE 1969 PM A2

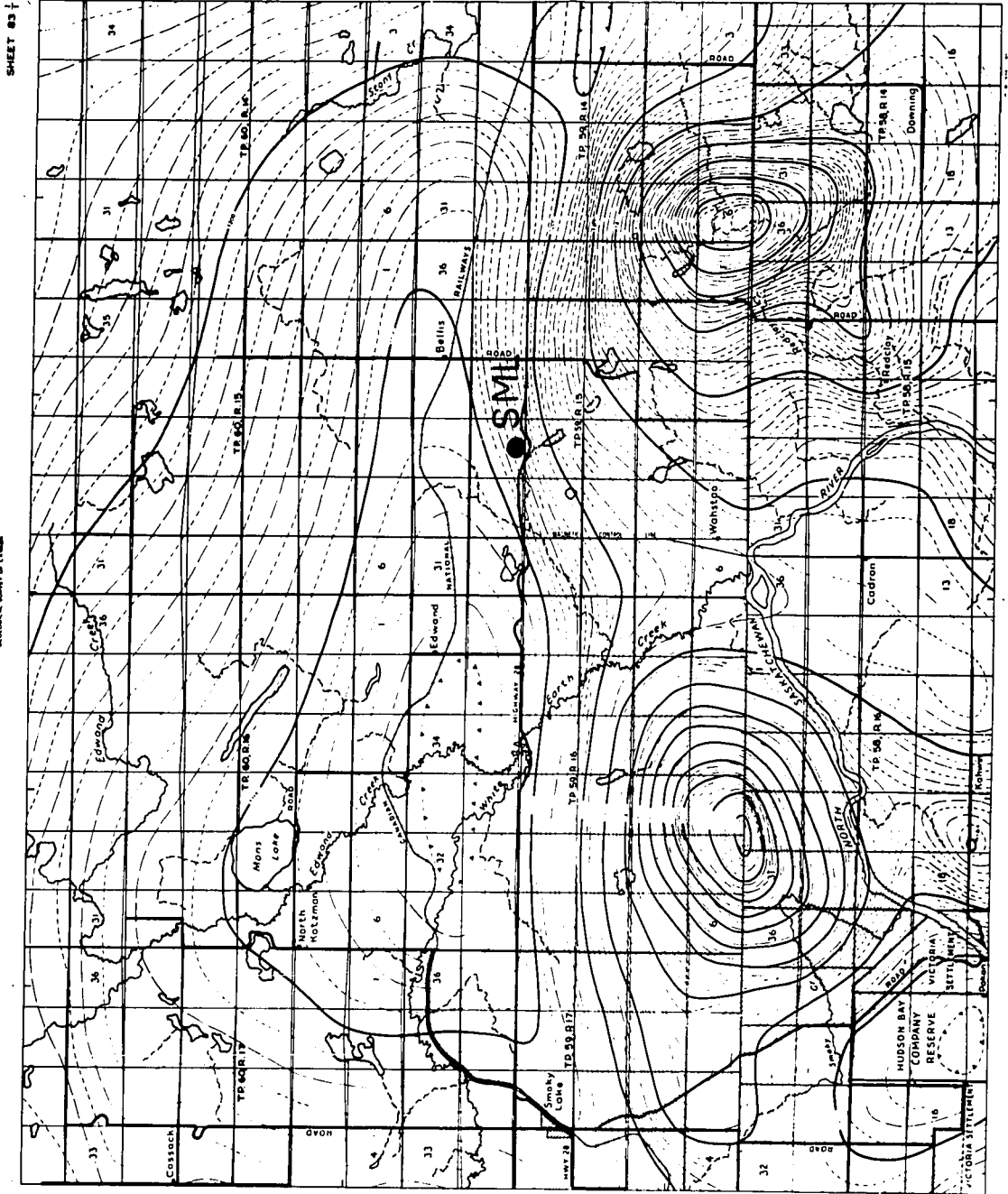
SMOKY LAKE 6 JUNE 1969 PM A2

An aeromagnetic map available for this area shows two very strong positive anomalies within five miles of the sounding site, one in south-east direction and the other in south-west direction. A weak east-west trending anomaly is present north of the sounding site.

Figure 4.14a: Aeromagnetic map for Smoky Lake area

Canada
DEPARTMENT
MINES AND TECHNICAL SURVEYS
GEOLOGICAL SURVEY OF CANADA

AEROMAGNETIC SERIES



SHEET 83

15. Two Hills (Fig. 4.15)

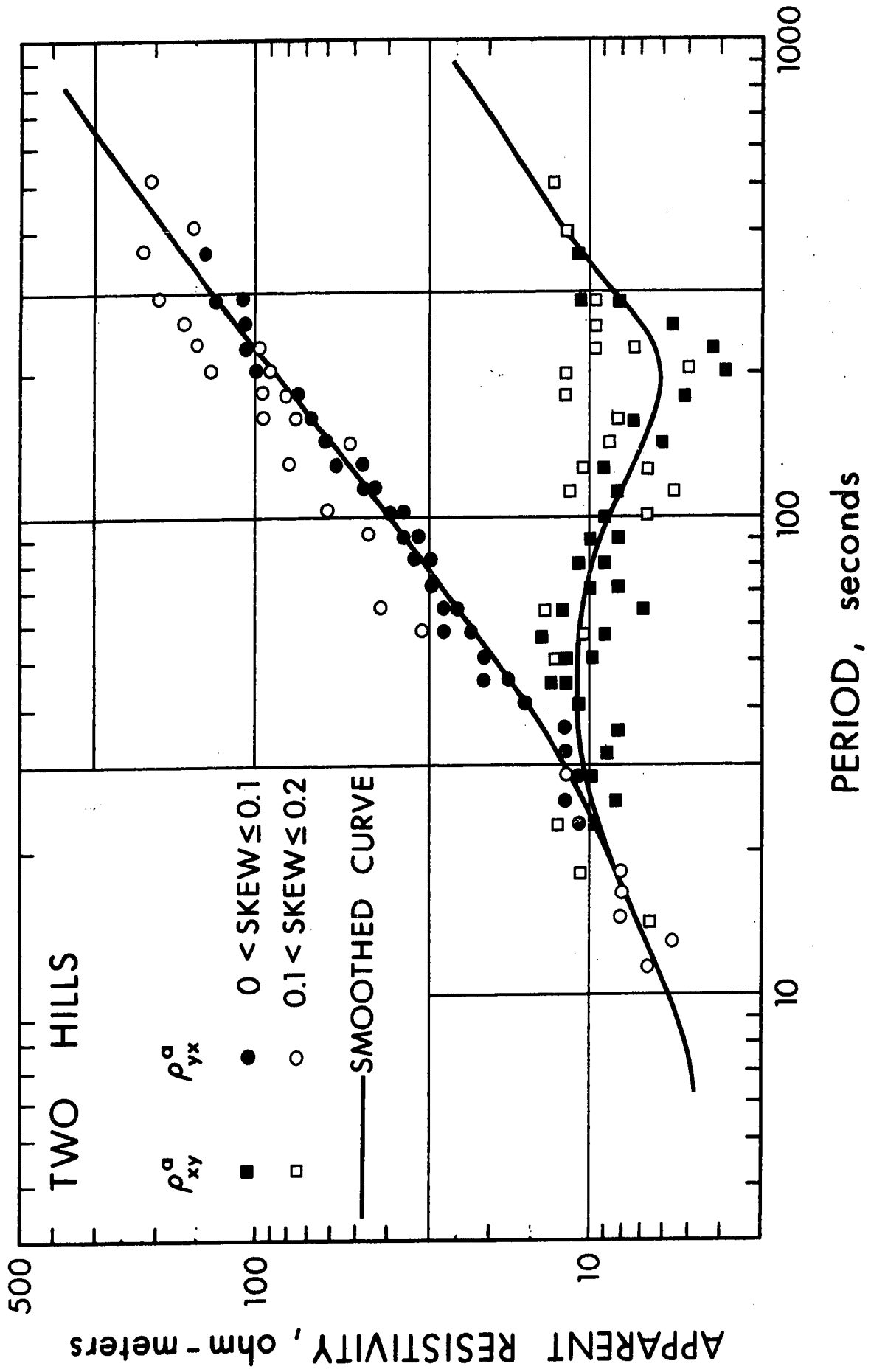
The tensor apparent resistivity curves in the principal directions show an anisotropic behaviour for periods greater than 30 seconds. The maximum apparent resistivity estimates are smooth compared with minimum apparent resistivity estimates which display considerable amount of scatter for periods greater than 100 seconds with lowest value around 200 second period band. For shorter periods the curves seem to approach asymptotically to 5 ohm-meters, indicating highly conductive surface layers.

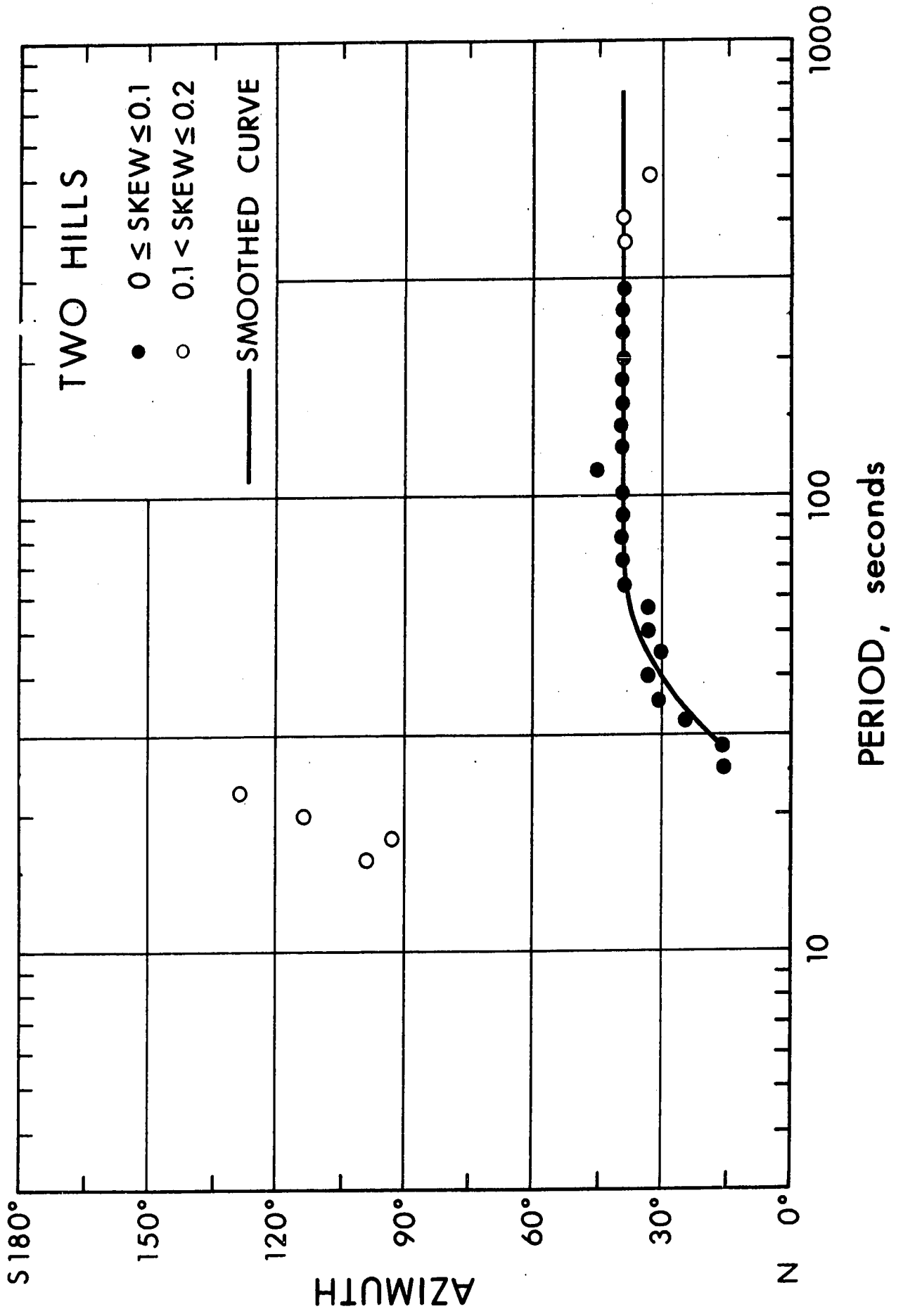
The azimuth for the minimum apparent resistivity is about $+40^\circ$ for periods greater than 50 seconds and tend toward zero degrees for short periods. The electric field is polarized about $N50^\circ W$ direction for long periods (> 200 seconds) and is about $N40^\circ W$ for short periods. The angle of polarization of the magnetic field is around $N20^\circ E$ for long periods and about $N40^\circ E$ for short periods. The electric and magnetic fields are close to orthogonality for short periods.

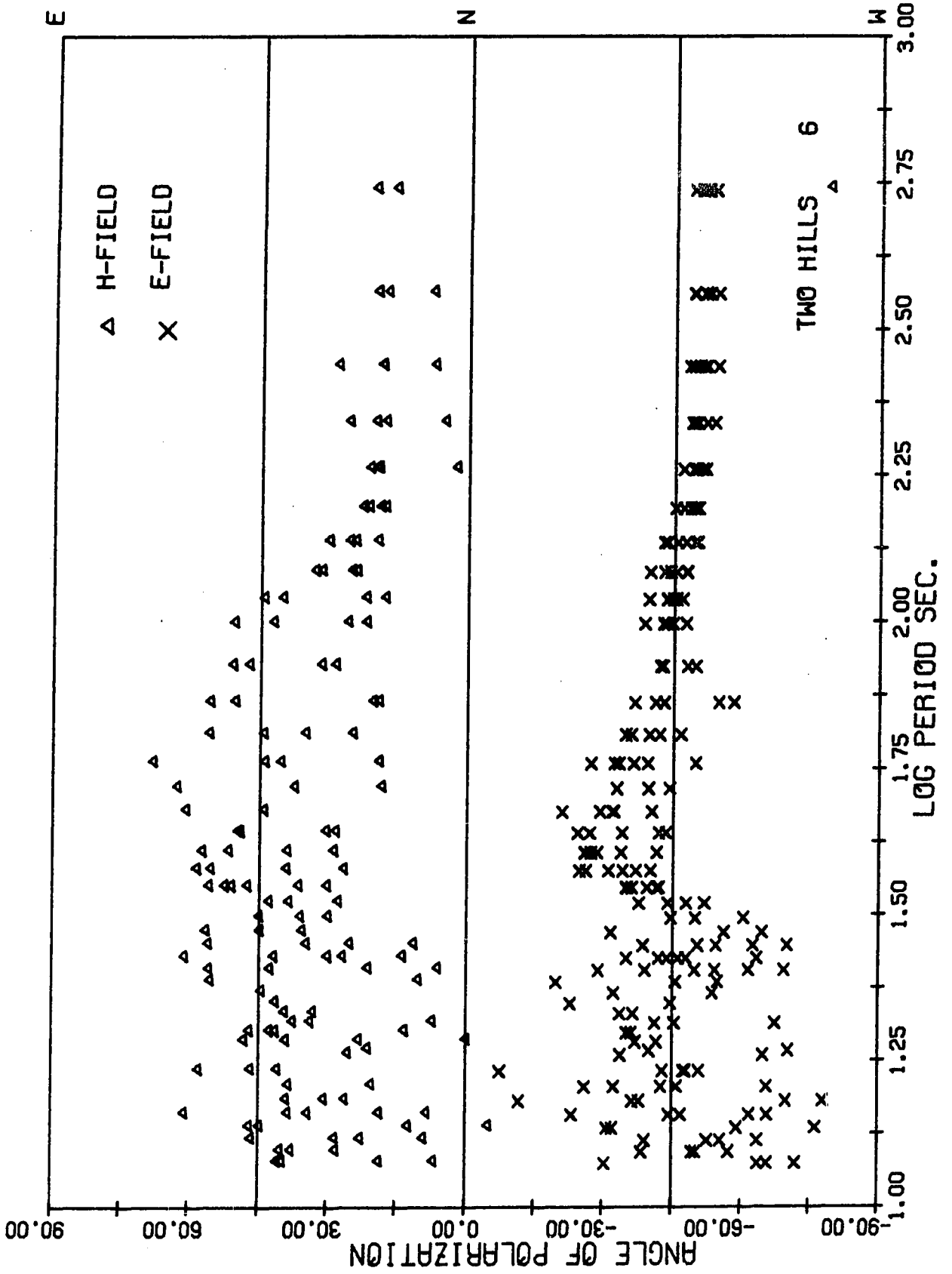
A low amplitude vertical magnetic field is observed for this station. The coherencies between $H_z - E_x$, $H_z - E_y$ and $H_z - H_x$ are greater than 0.8 for periods greater than 150 seconds, in

Figure 4.15: Magnetotelluric results for Two Hills

- i. Tensor apparent resistivities in the principal directions.
- ii. Azimuth (the direction of minimum tensor apparent resistivity).
- iii. Polarization angles for telluric and magnetic fields.
- iv. Vertical magnetic field analyses results.







ROTATION ANGLE = N 0.0E				ROTATION ANGLE = N 40.0E			
PERIOD SEC.	COH HZ-EX	COH HZ-EY	COH HZ-HX	COH HZ-HY	COH HZ-HX	COH HZ-HY	COH HZ-HY
546.13	0.85	0.90	0.88	0.65	0.63	1.24	0.84
364.09	0.86	0.92	0.94	0.62	0.58	1.37	0.76
273.07	0.81	0.89	0.93	0.48	0.53	1.14	0.56
218.45	0.82	0.90	0.91	0.45	0.47	0.96	0.35
182.04	0.85	0.92	0.92	0.60	0.42	1.01	0.33
156.04	0.93	0.90	0.90	0.56	0.40	0.86	0.51
136.53	0.74	0.82	0.83	0.44	0.38	0.62	0.20
121.36	0.67	0.67	0.68	0.55	0.35	0.52	0.36
109.23	0.67	0.69	0.65	0.73	0.30	0.36	0.44
99.30	0.72	0.73	0.68	0.79	0.28	0.31	0.44
84.02	0.62	0.49	0.32	0.76	0.30	0.29	0.56
72.82	0.61	0.29	0.22	0.74	0.34	0.31	0.78
64.25	0.67	0.23	0.52	0.78	0.41	0.35	0.89
57.49	0.69	0.17	0.50	0.79	0.46	0.31	0.89
52.01	0.59	0.37	0.07	0.73	0.36	0.24	0.88
47.49	0.61	0.17	0.17	0.70	0.30	0.21	0.79
43.69	0.54	0.14	0.31	0.56	0.19	0.17	0.79
40.45	0.58	0.45	0.53	0.64	0.18	0.16	0.66
37.66	0.66	0.31	0.40	0.72	0.19	0.15	0.76
35.23	0.51	0.27	0.16	0.66	0.21	0.18	0.60
33.10	0.33	0.56	0.52	0.54	0.17	0.18	0.53
31.21	0.56	0.70	0.66	0.75	0.19	0.20	0.53
29.52	0.82	0.90	0.88	0.91	0.22	0.23	0.66
28.01	0.83	0.85	0.78	0.88	0.27	0.22	0.85
26.64	0.86	0.84	0.73	0.89	0.26	0.19	0.81
25.40	0.77	0.77	0.69	0.85	0.23	0.19	0.83
24.27	0.64	0.56	0.43	0.73	0.20	0.16	0.75
23.24	0.41	0.34	0.28	0.50	0.15	0.16	0.47
22.29	0.62	0.28	0.32	0.55	0.20	0.27	0.62
21.42	0.71	0.24	0.25	0.66	0.25	0.28	0.65
20.61	0.50	0.23	0.20	0.49	0.19	0.21	0.48
19.86	0.54	0.16	0.13	0.55	0.21	0.22	0.52
19.16	0.26	0.17	0.15	0.22	0.17	0.23	0.16
18.51	0.40	0.19	0.21	0.40	0.16	0.29	0.32
18.20	0.45	0.13	0.14	0.49	0.19	0.26	0.15
17.07	0.53	0.53	0.52	0.59	0.25	0.42	0.34
16.06	0.05	0.37	0.34	0.28	0.25	0.38	0.50
15.17	0.31	0.57	0.61	0.52	0.24	0.63	0.37
14.37	0.22	0.19	0.31	0.43	0.32	0.45	0.26
13.65	0.35	0.39	0.38	0.73	0.36	0.89	0.34
13.00	0.35	0.38	0.23	0.61	0.62	0.89	0.15
12.41	0.10	0.24	0.43	0.78	0.78	0.85	0.29
11.87	0.33	0.35	0.56	0.82	0.58	0.67	0.15

TWO HILLS 17 JUNE 1969 AM D1

TWO HILLS 17 JUNE 1969 AM D1

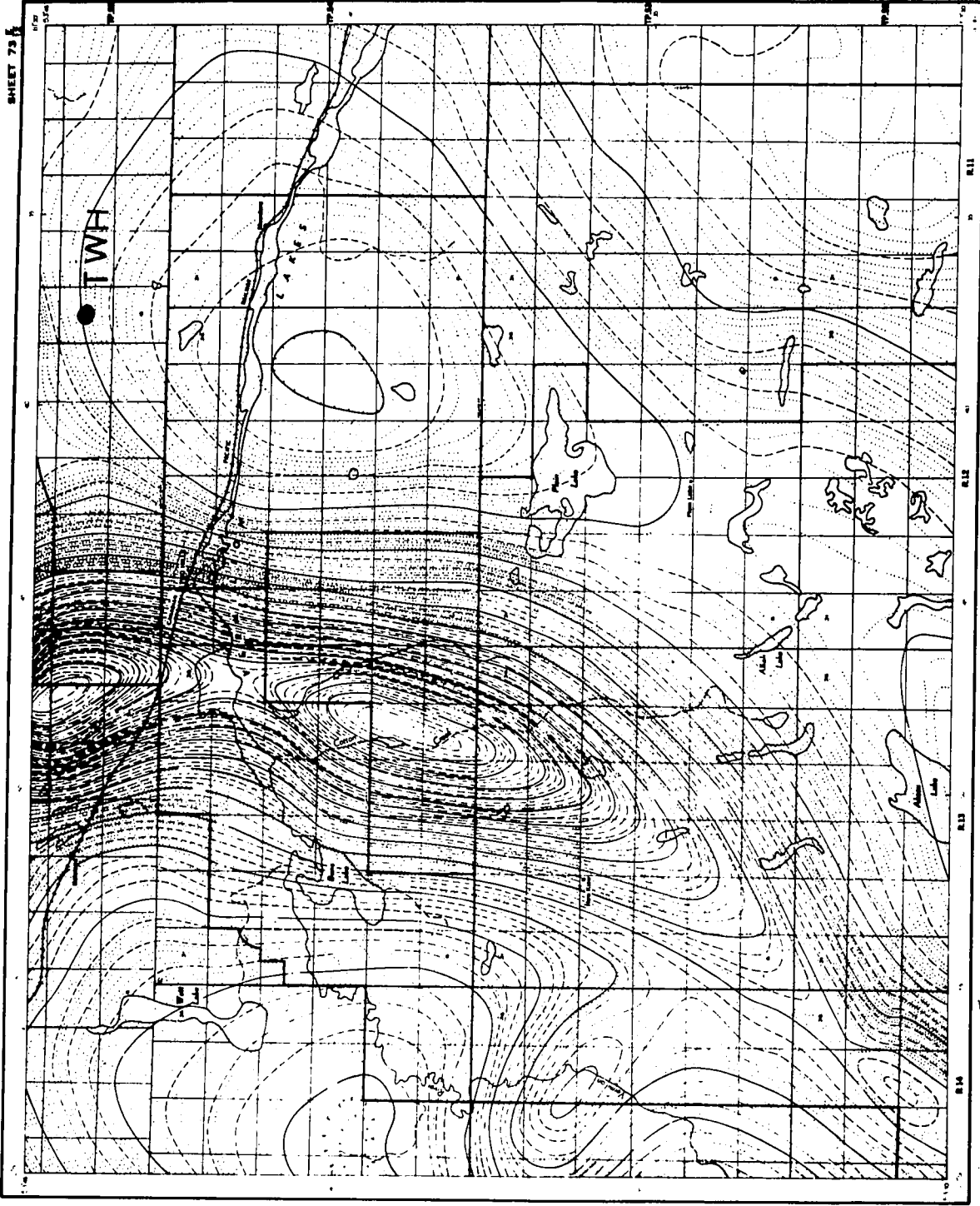
measuring directions and $\text{coh } H_z E_x$ dropped to its minimum for a rotation angle of N40°E.

The aeromagnetic map for this area shows a strong north-south lineament five miles west of the sounding site.

Figure 4.15a: Aeromagnetic map for Two Hills area

DEPARTMENT OF THE ARMY
ENGINEERING CENTER
WATERWAYS EXPERIMENTAL STATION
CORVALLIS, OREGON 97331

AEROMAGNETIC SERIES



SHEET 73

TWA

46°N
47°N
48°N
124°W
125°W
126°W

16. Vermilion (Fig. 4.16)

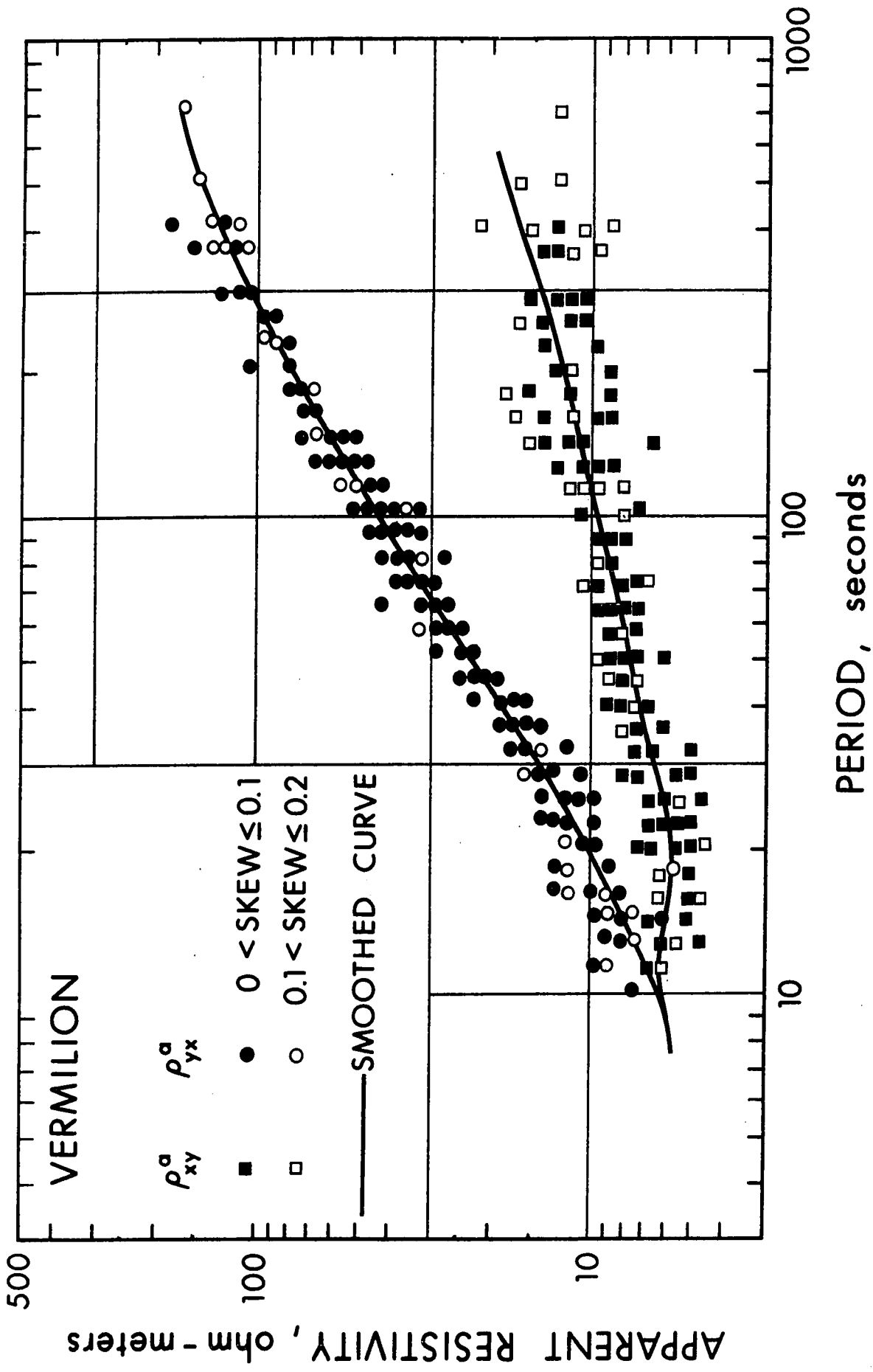
The Vermilion sounding site is located close to the Alberta-Saskatchewan provincial border. The thickness of the sediments at this site is about 2 km. The tensor apparent resistivity curves in the principal directions show an anisotropic behaviour for periods greater than 20 seconds, and seem to converge to 6 ohm-meters for shorter periods. The maximum apparent resistivities are relatively smooth compared to the minimum apparent resistivities, which have considerable scatter for periods greater than 100 seconds.

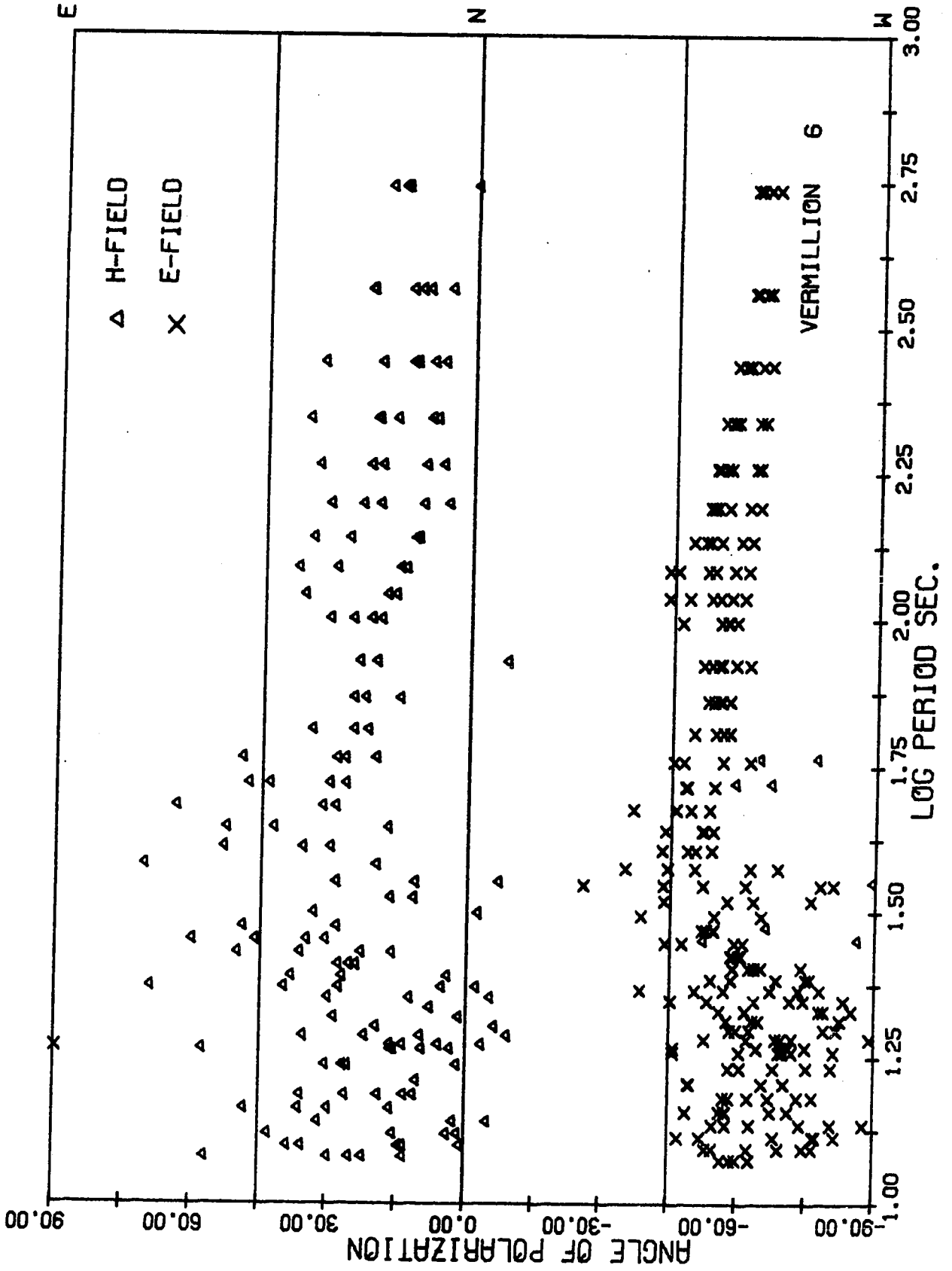
The azimuth for minimum apparent resistivity is about $+40^\circ$ for periods greater than 30 seconds and tend to shift towards $+15^\circ$ for shorter periods. The angle of polarization of the telluric field varies from $N40^\circ W$ for 40 seconds period to $N65^\circ W$ for periods about 300 seconds. For shorter periods the average direction of the telluric field is about $N70^\circ W$. The average direction of the magnetic field about $N20^\circ E$, with some scatter for short periods. The average directions of magnetic and telluric fields are orthogonal for short periods.

Low amplitude H_z is observed at this location. Coherency analyses for one record with significant H_z , for periods greater than 100 seconds, show that H_z is coherent with E_x , E_y , H_x and H_y in the measuring directions and for a rotation angle of $N50^\circ E$ the $\text{coh } H_z E_y$ and $\text{coh } H_z H_x$ improved a little with a slight drop in $\text{coh } H_z H_y$ and $\text{coh } H_z E_x$.

Figure 4.16: Magnetotelluric results for Vermilion

- i. Tensor apparent resistivities in the principal directions.
- ii. Azimuth (the direction of minimum tensor apparent resistivity).
- iii. Polarization angles for telluric and magnetic fields.
- iv. Vertical magnetic field analyses results.





ROTATION ANGLE = N 0.0E				ROTATION ANGLE = N 50.0E			
PERIOD SEC.	COH HZ-EX	COH HZ-EY	COH HZ-HX	COH HZ-EX	COH HZ-EY	COH HZ-HX	COH HZ-HY
546.13	0.65	0.59	0.72	0.50	0.62	0.71	0.49
364.09	0.75	0.67	0.72	0.50	0.72	0.76	0.49
273.07	0.85	0.77	0.79	0.65	0.82	0.86	0.45
218.45	0.89	0.83	0.82	0.73	0.87	0.90	0.46
182.04	0.91	0.83	0.82	0.73	0.87	0.90	0.44
156.04	0.93	0.81	0.82	0.64	0.88	0.91	0.50
136.53	0.92	0.78	0.84	0.59	0.87	0.86	0.56
121.36	0.90	0.76	0.85	0.60	0.85	0.85	0.52
109.23	0.88	0.72	0.80	0.49	0.82	0.84	0.52
99.30	0.84	0.64	0.69	0.43	0.76	0.78	0.48
84.02	0.78	0.56	0.53	0.21	0.68	0.73	0.28
72.82	0.75	0.36	0.36	0.21	0.56	0.62	0.14
64.25	0.50	0.26	0.28	0.21	0.38	0.34	0.10
57.49	0.71	0.66	0.64	0.39	0.70	0.70	0.10
52.01	0.66	0.69	0.66	0.39	0.70	0.72	0.37
47.49	0.66	0.66	0.64	0.46	0.68	0.72	0.48
43.69	0.60	0.51	0.51	0.20	0.58	0.62	0.13
40.45	0.42	0.27	0.21	0.08	0.40	0.41	0.05
37.66	0.23	0.25	0.24	0.20	0.26	0.29	0.16
35.23	0.33	0.24	0.23	0.12	0.29	0.29	0.21
33.10	0.18	0.11	0.09	0.16	0.12	0.12	0.14
31.21	0.32	0.36	0.28	0.36	0.34	0.31	0.26
29.52	0.50	0.46	0.36	0.12	0.25	0.24	0.14
28.01	0.27	0.19	0.21	0.27	0.23	0.24	0.11
26.64	0.25	0.23	0.26	0.12	0.23	0.24	0.11
25.40	0.54	0.47	0.50	0.48	0.49	0.50	0.40
24.27	0.38	0.49	0.46	0.30	0.45	0.41	0.39
23.24	0.49	0.50	0.45	0.30	0.52	0.48	0.22
22.29	0.39	0.37	0.35	0.06	0.40	0.46	0.25
21.42	0.26	0.18	0.25	0.11	0.23	0.39	0.05
20.61	0.51	0.52	0.54	0.11	0.53	0.53	0.37
19.86	0.18	0.22	0.18	0.16	0.22	0.21	0.17
19.16	0.16	0.17	0.07	0.11	0.18	0.08	0.07
18.51	0.20	0.23	0.23	0.17	0.24	0.22	0.18
18.20	0.32	0.32	0.34	0.22	0.34	0.34	0.26
17.07	0.25	0.20	0.24	0.09	0.24	0.36	0.12
16.06	0.60	0.50	0.37	0.25	0.59	0.58	0.24
15.17	0.27	0.24	0.15	0.31	0.22	0.12	0.36
14.37	0.20	0.29	0.19	0.22	0.25	0.15	0.16
13.65	0.13	0.26	0.32	0.38	0.17	0.17	0.40
13.00	0.16	0.13	0.18	0.16	0.14	0.09	0.17
12.41	0.44	0.32	0.27	0.16	0.40	0.35	0.05
11.87	0.34	0.16	0.02	0.08	0.27	0.24	0.42

VERMILION 12 JUNE 1969 PM B1

VERMILION 12 JUNE 1969 PM B1

CHAPTER 5
INTERPRETATION

5.1 Interpretation

The most important characteristics of the results presented in Chapter 4 are:

- 1) The tensor apparent resistivity curves in the principal directions for all the stations in the plains of central Alberta exhibit anisotropic behaviour.
- 2) The degree of anisotropy varies from station to station, with the maximum occurring at Bonnyville (2), a station close to the Canadian shield. The degree of anisotropy is a minimum for Carrot Creek (4), Camp Creek (3), Fox Creek (7) and for Meanook (9).
- 3) Higher than normal skew values in the plains are obtained for Donaldda (5) and the Observatory (13). In the foothills and the Rocky Mountains anomalously large skew (≥ 1.0) values are obtained.
- 4) The tensor apparent resistivity curves in the direction of the principal axis of maximum apparent resistivity are smooth compared to the curves along the principal axis of minimum resistivity.
- 5) The azimuth (the principal axis of minimum apparent resistivity) lies between $+30^\circ$ and $+60^\circ$ for periods greater than 30 seconds, for all the

stations in the plains. The azimuth is indeterminate for shorter periods, except for Smoky Lake (14), where the anisotropy exists even at shorter periods.

6) The electric field is linearly polarized about a north-westerly direction for periods greater than 30 seconds both at mountain stations and plain stations. For short periods the polarization of the electric field is less consistent, although it tends to lie in the north-west quadrant for most of the times for which the analyses were made.

7) The magnetic field tends to align in a north-north east direction for longer periods. For shorter periods there is a considerable variation in the angle of polarization of the ellipse. The magnetic field was elliptically polarized with an ellipticity less than 0.5 in most cases.

8) A significant vertical component of the magnetic field was observed for longer periods when the magnetic activity was high. H_z tends to be more coherent with the electric field component along the major axis of apparent resistivity and with the magnetic field component along the minor axis of the apparent resistivity than with the other components. This characteristic of

H_z is reversed or absent for stations in the foothills and mountains and also for Donaldda (5).

9) For the stations in the plains, the tensor apparent resistivities in the measuring directions (north-south and east-west) exhibited the smallest degree of anisotropy, except for Smoky Lake (14), where significant anisotropy was observed in measuring directions at short periods.

Tensor apparent resistivity curves along the major and minor axes of apparent resistivity and the directions of maximum apparent resistivity for all the twelve stations in the plains are presented in Figs. 5.1, 5.2 and 5.3 respectively.

The apparent resistivity curves in Fig. 5.1 show a wide spread from the high values at Bonnyville (2) to the low values at Two Hills (15). This effect may be due to variations in thickness and/or the resistivity contrasts. A set of theoretical apparent resistivity curves for a two layer earth model with varying thickness and resistivity of the first layer are presented in Fig. 5.4, as a comparison to the observed curves presented in Fig. 5.1.

Figure 5.1: Tensor apparent resistivity curves along the major axis of anisotropy for central Alberta.

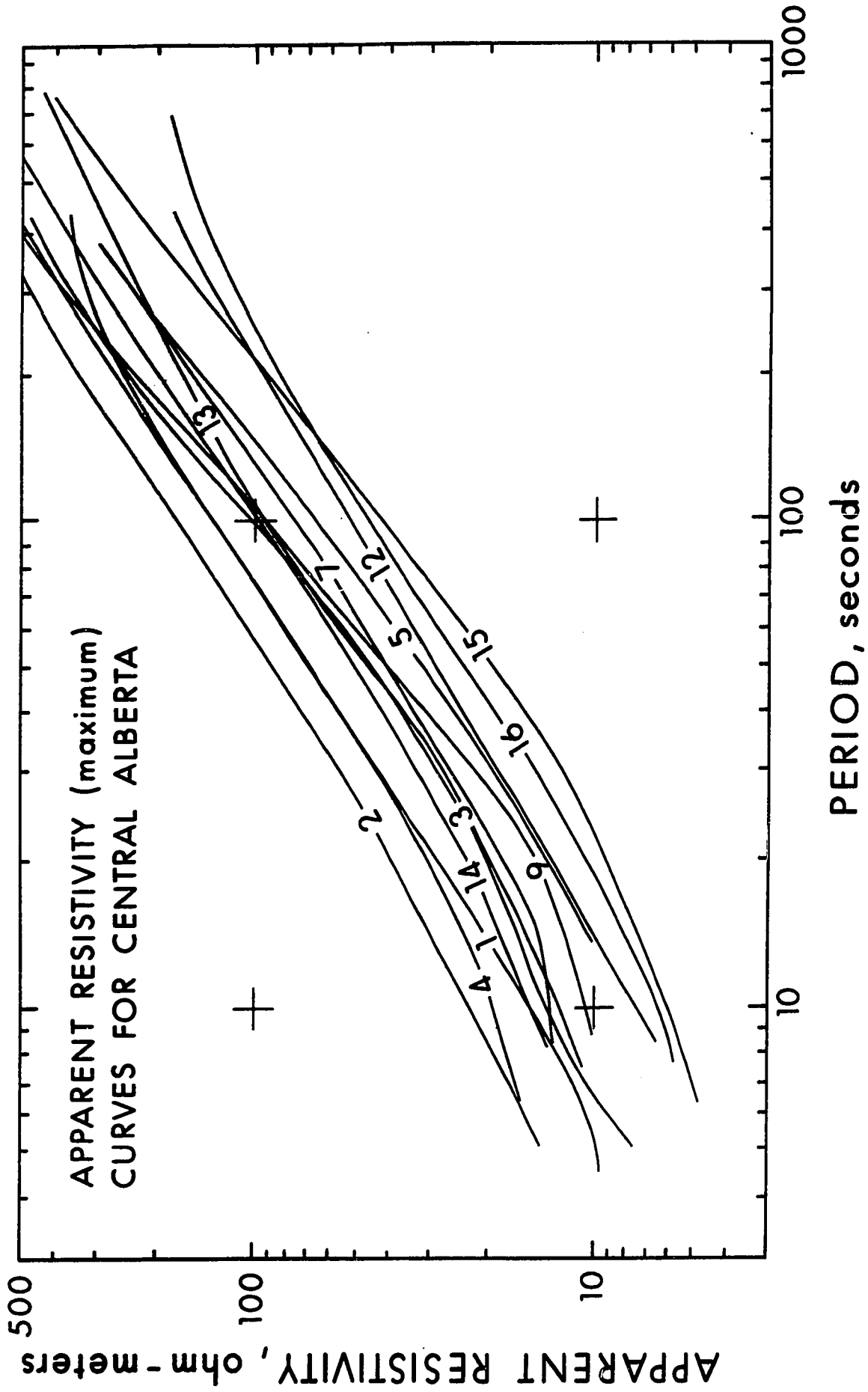


Figure 5.2: Tensor apparent resistivity curves along the minor axis of anisotropy for central Alberta.

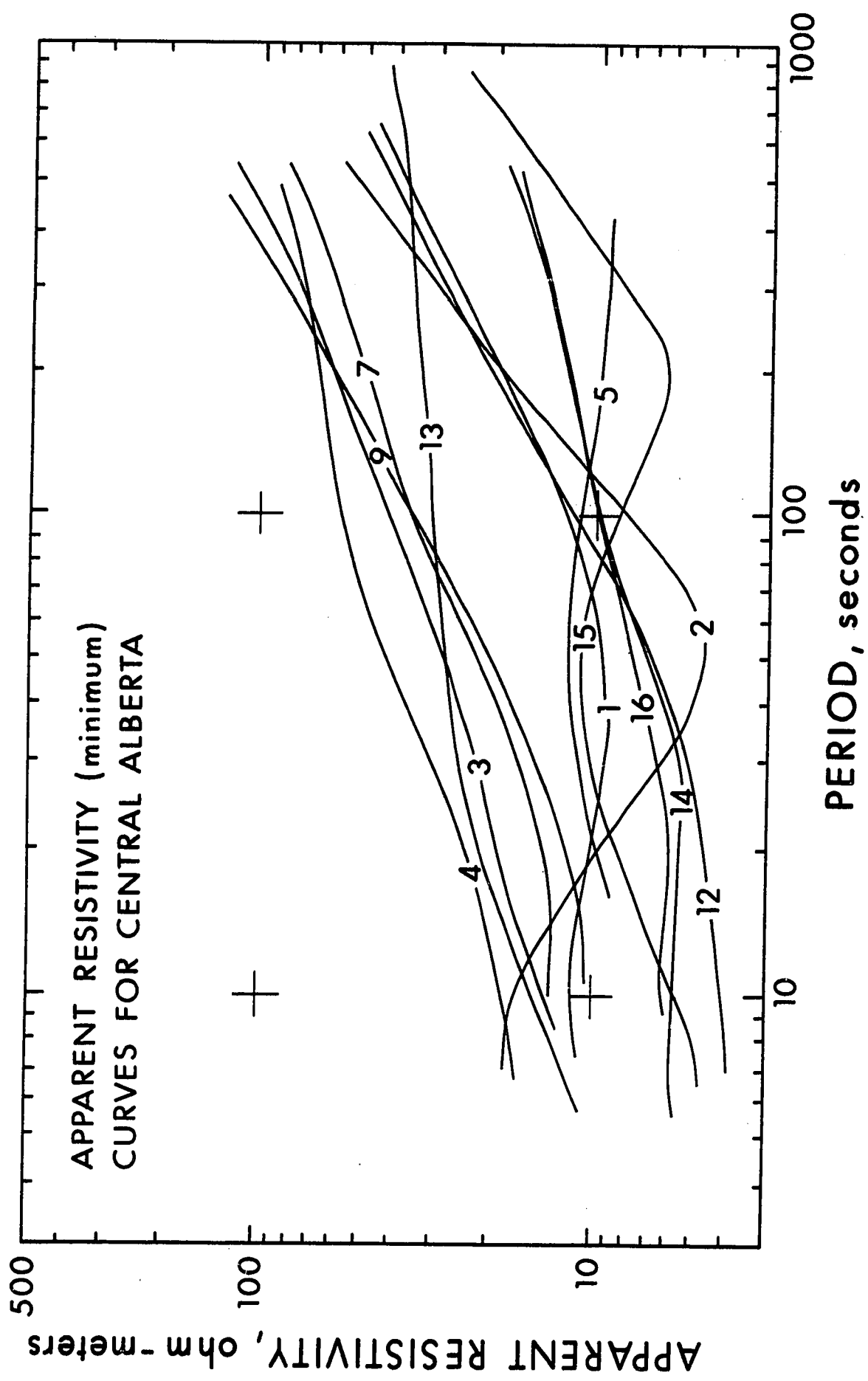


Figure 5.3: The directions of the maximum tensor apparent resistivity for central Alberta.

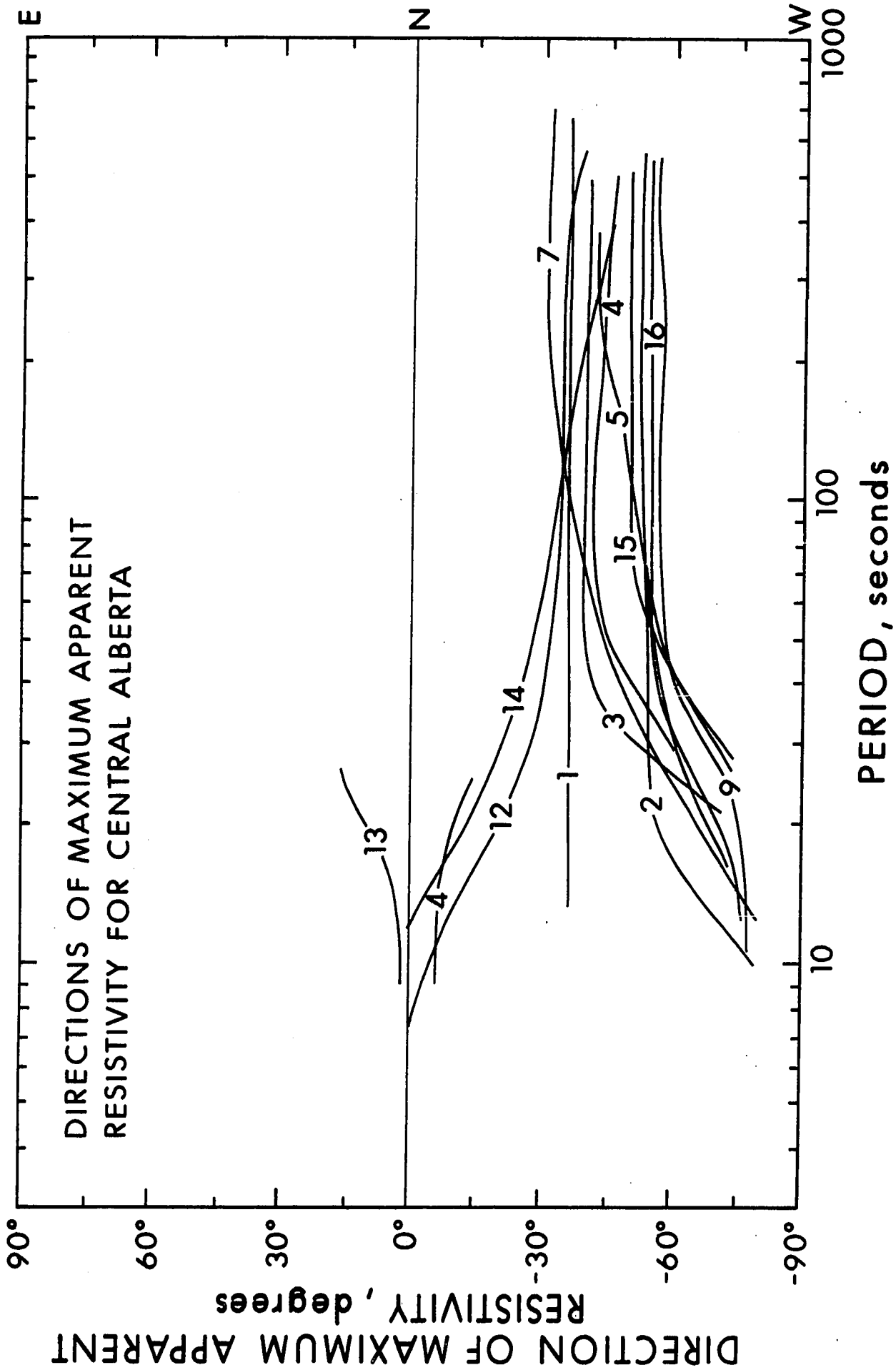
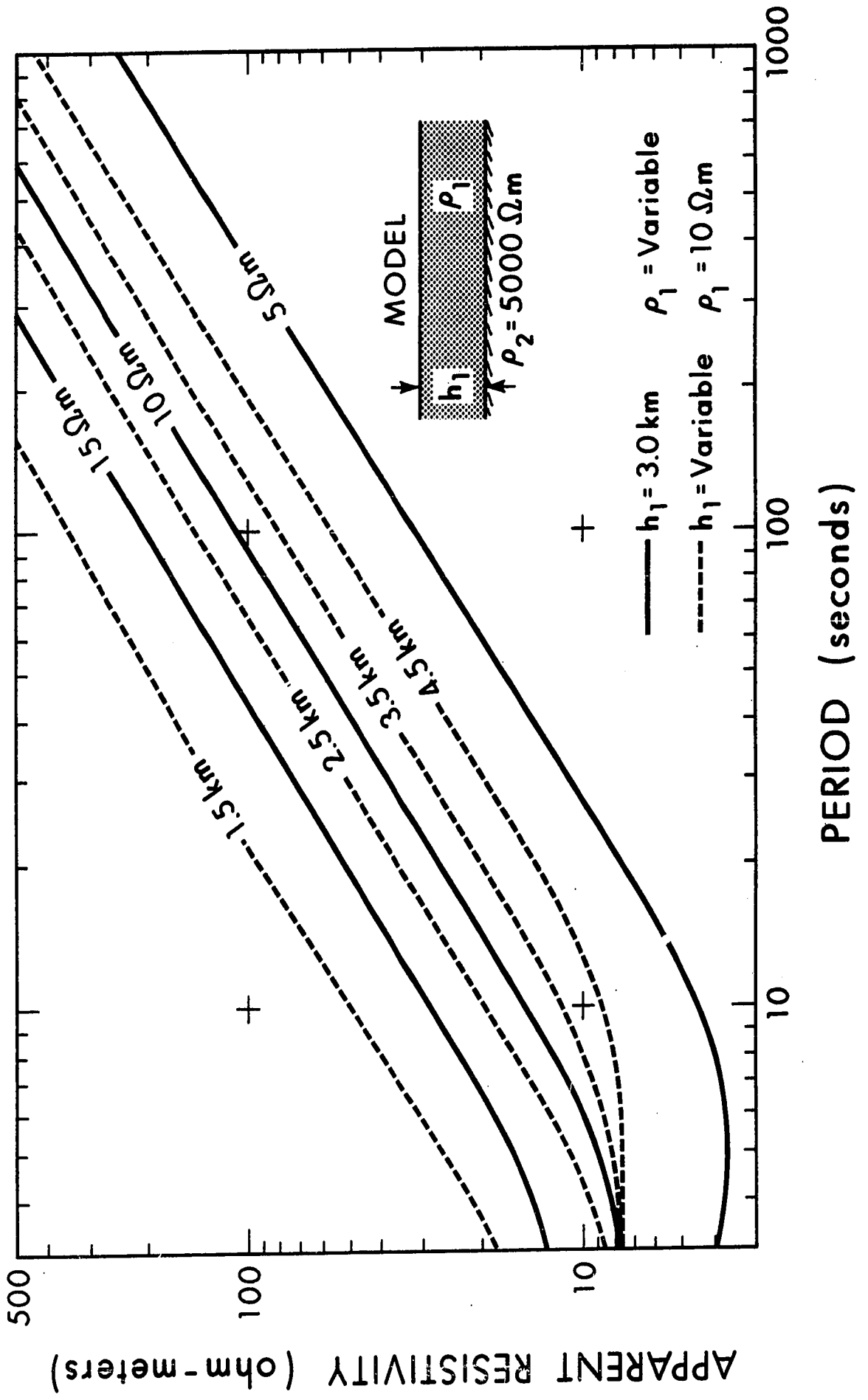


Figure 5.4: Theoretical apparent resistivity curves for a two layer earth model for various thicknesses and resistivities of the first layer.



Tensor apparent resistivity curves in the minor direction also show much variation (Fig. 5.2) from one station to another. For some stations (eg. Donalda, Red Deer) the curves continue to drop even at very long periods, for other stations they increase with period tending to approach asymptotically the curves along the major axis. There is much scatter in the minimum apparent resistivity values. For some stations, viz., Bonnyville and Two Hills, the apparent resistivities reached their lowest at intermediate periods.

The scatter in the apparent resistivities along the minimum resistivity axis is expected. Since the principal axes are chosen such that the diagonal terms of the tensor impedance matrix, $z_{x'x'}$ and $z_{y'y'}$, are a minimum (zero in the ideal case). Thus one can write as an approximation, in the principal direction (x' and y')

$$E_{x'} = z_{x'y'} H_{y'}$$

$$E_{y'} = z_{y'x'} H_{x'}$$

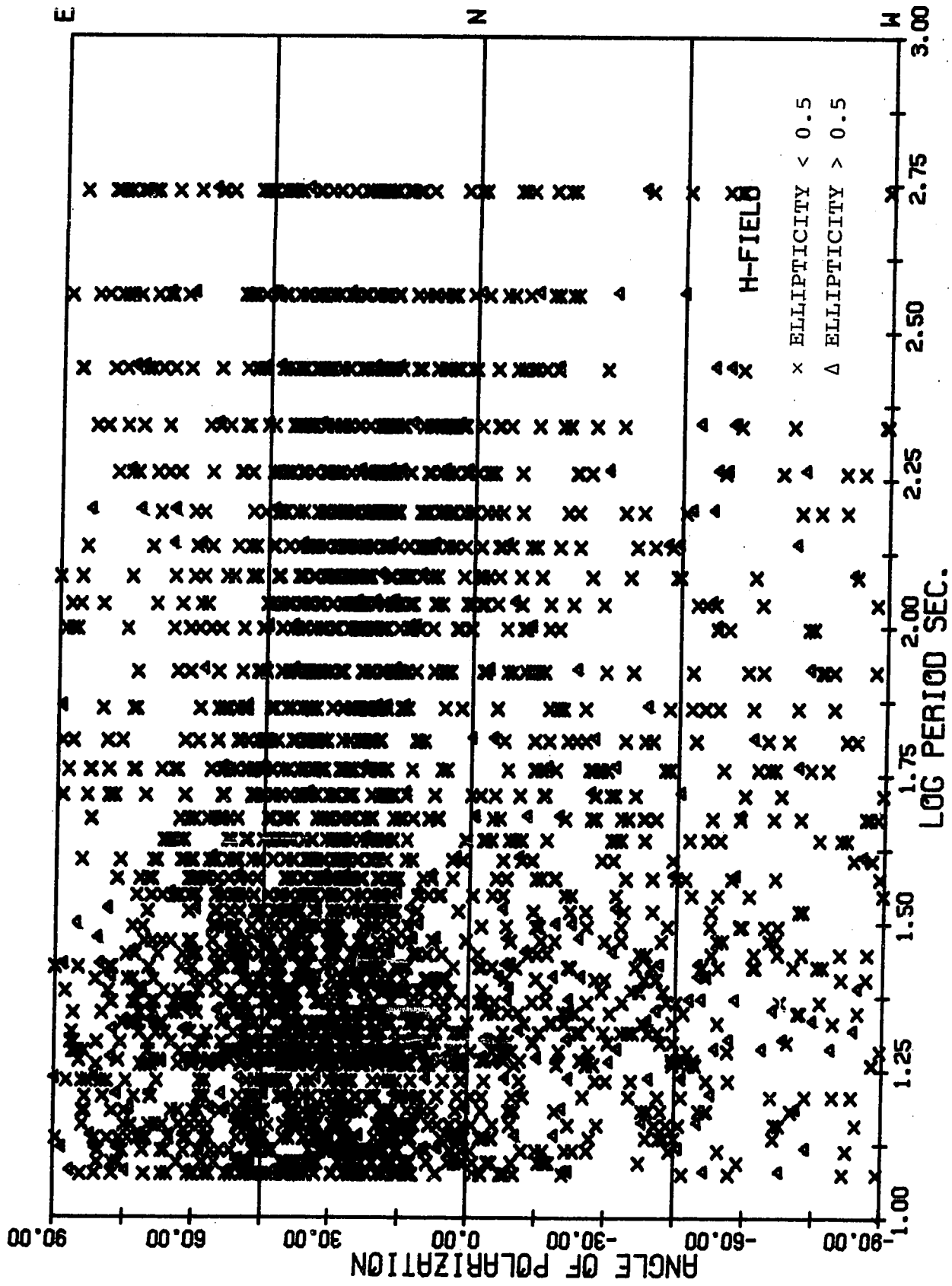
The maximum resistivity results from a larger value of E for any given value of the orthogonal component of H. Since the electric field is

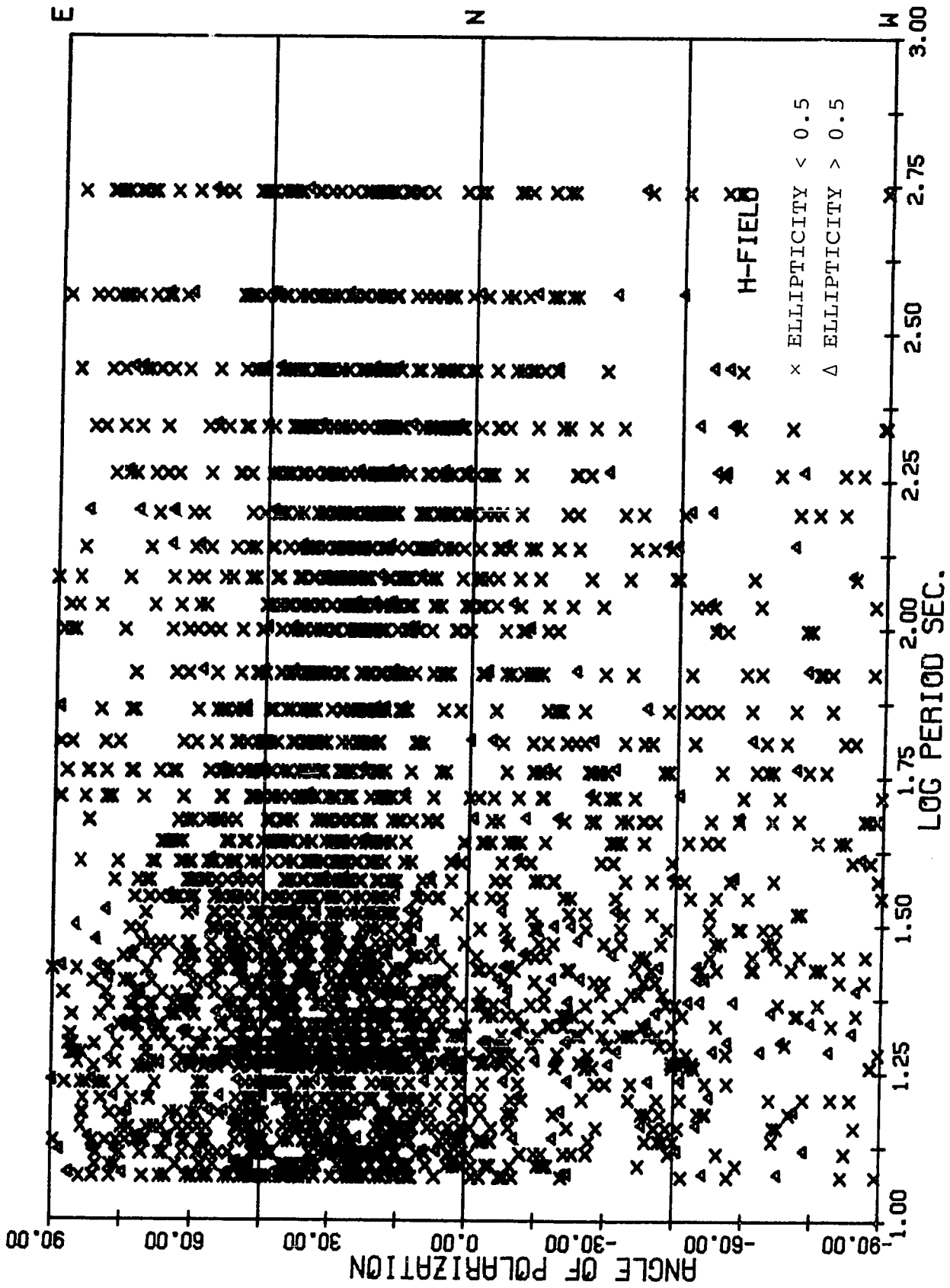
polarized with relatively small ellipticity, in most cases, approximately along direction of maximum apparent resistivity and H is polarized approximately orthogonal to E (close to the minimum apparent resistivity direction), both E_x , and H_y , are of low amplitude and hence the signal to noise ratio is poor. This results in a relatively large scatter in the apparent resistivity curves along x' .

The electric and magnetic field polarization angles for all the sixteen stations are plotted in Fig. 5.5 and 5.6 respectively. Different symbols are used to indicate the case of ellipticity less than 0.5 and greater than 0.5. There are only a few cases, generally for short periods, where the electric field has ellipticity greater than 0.5. The magnetic field has an average ellipticity larger than that of the electric field but also has only a few cases with ellipticity larger than 0.5. These plots indicate that for periods greater than 80 seconds the telluric field is polarized approximately northwest, most of the values lying within $\pm 20^\circ$ of this direction. For shorter periods there is a great deal more scatter with the direction lying mainly in the northwest quadrant. The magnetic field polarization angle is much more

Figure 5.5: Electric field polarization angles for central Alberta.

Figure 5.6: Magnetic field polarization angles
for central Alberta.





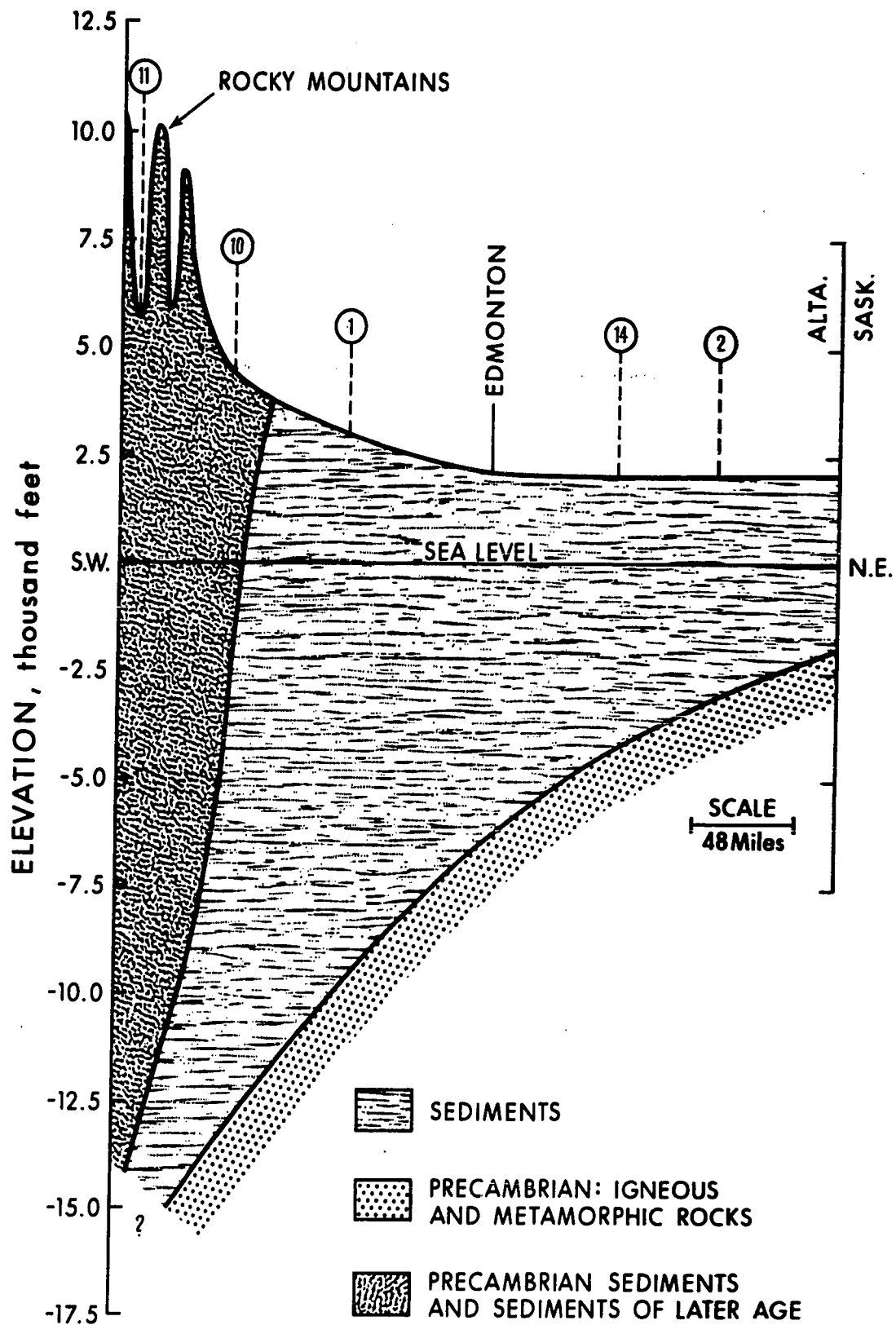
scattered with an average direction approximately north-north-east.

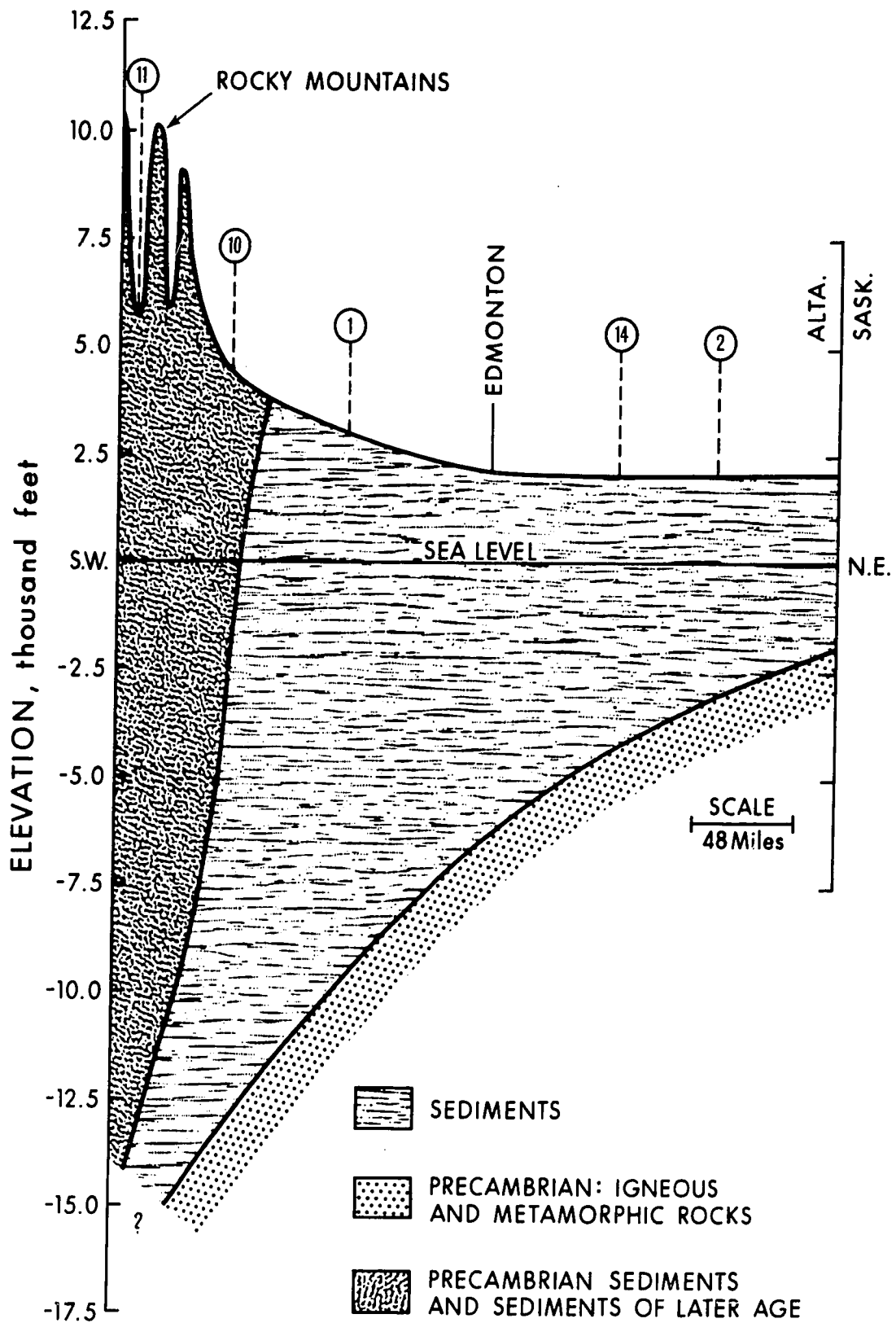
It is generally believed that the angle of polarization of the telluric field is mainly controlled by the local and/or regional geoelectric structures. The magnetic field polarization observed at the surface may be controlled by both the generating mechanism of geomagnetic pulsations and the geoelectric structure. Zybin (1967), Van'yan and Zybin (1967) made an extensive study on the effect of laterally inhomogeneous geoelectric structures on the magnetic field polarization and concluded that the preferred direction of polarization in the natural magnetic fields is determined by the geoelectric structure of the underlying medium and daily and seasonal variations in polarization are connected with micropulsation mechanisms. The magnetic field component parallel to the strike of the structure is unchanged (Section 2.5) whereas the magnetic field component normal to the strike is increased, resulting a change in the polarization characteristics of the total magnetic field, which is measured at the surface. A two dimensional structure tends to orient the magnetic field ellipse normal to its strike.

The main tectonic units of the region are oriented in a north-west direction parallel to the Rocky Mountains. A general cross section passing through Edmonton in a north easterly direction is presented in Fig. 5.7. The locations of five of the magnetotelluric sounding sites are also marked in the same figure.

Sedimentary rocks of low resistivity overlying a gently dipping highly resistive basement, blocked on the west by more resistive Precambrian metasediments and Phanerozoic sedimentary rocks belonging to the Rocky Mountains, constitute a major, north-west striking two-dimensional geoelectric structure. The resistivities of the individual layers of the sedimentary column vary from a few ohm-meters to approximately one hundred ohm-meters. The resistivities of the basement rocks may vary from several hundred ohm-meters to several thousand ohm-meters. No

Figure 5.7: A geological cross section along north-east and south-west passing through Edmonton, and approximate location of magnetotelluric sounding sites.





detailed knowledge is available on the resistivities of the rocks in the mountains and foothills, however, magnetotelluric measurements at Nordegg (Fig. 4.10) gave an average resistivity of a few thousand ohm-meters.

For a two-dimensional structure of the type described above, currents tend to flow more freely along the strike in the sedimentary basin producing a maximum electric field along strike for given resistivity. This may explain the north-westerly polarization of electric field (Fig. 5.4). The secondary magnetic field produced by induction trends normal to the strike and this secondary field together with the primary field produces a preferred direction about N25°E for the total magnetic field (Fig.5.5).

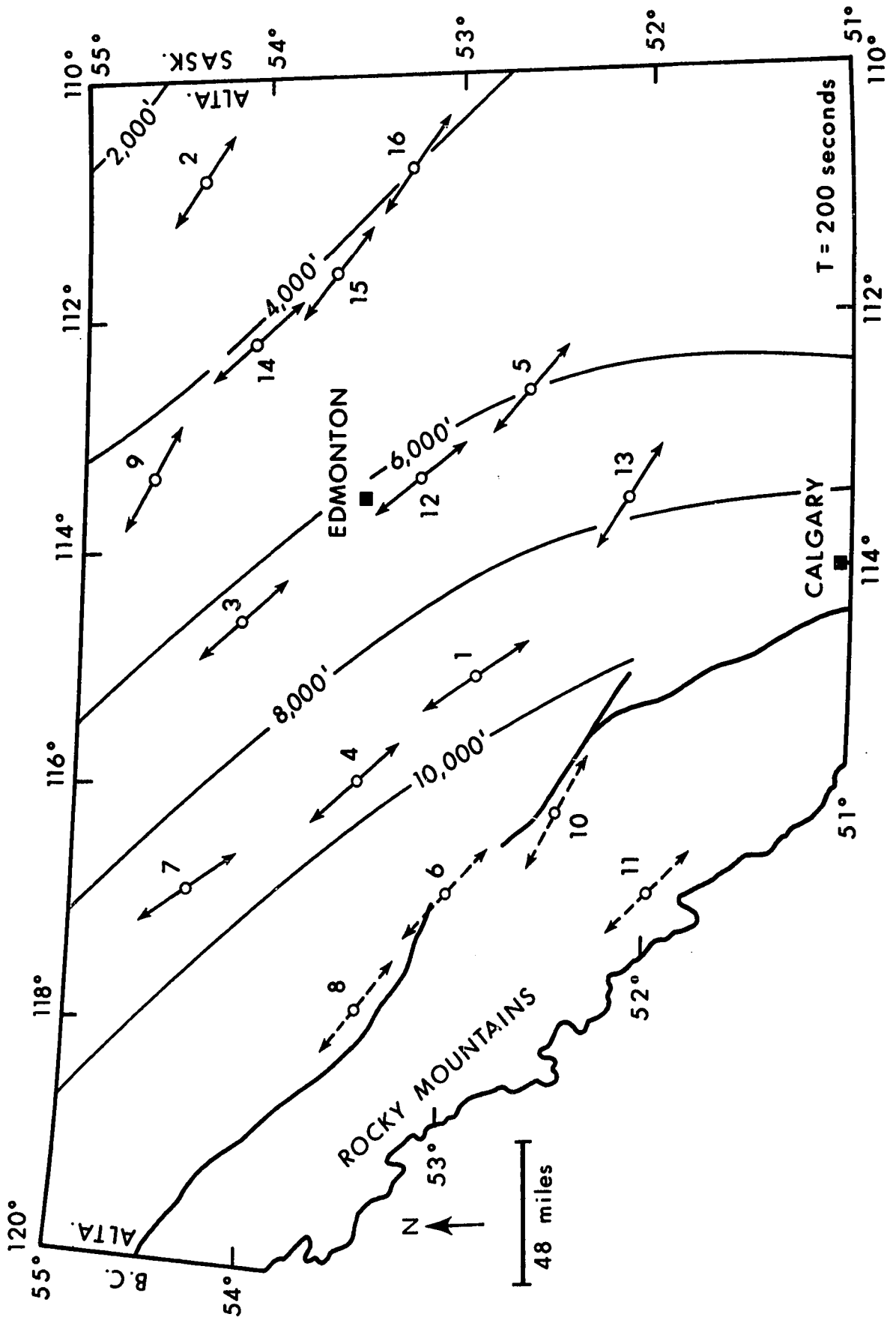
The coherency analyses involving the vertical component, H_z of the magnetic show that H_z is coherent with the electric field along the strike direction and with the magnetic field normal to the strike, which is consistent with the theory of the magnetotelluric fields for two-dimensional structures. The amplitude ratio between H_z and the magnetic field component normal to the strike was less than unity for most cases. The ambiguous results obtained with H_z for mountain stations and Donalda may be due

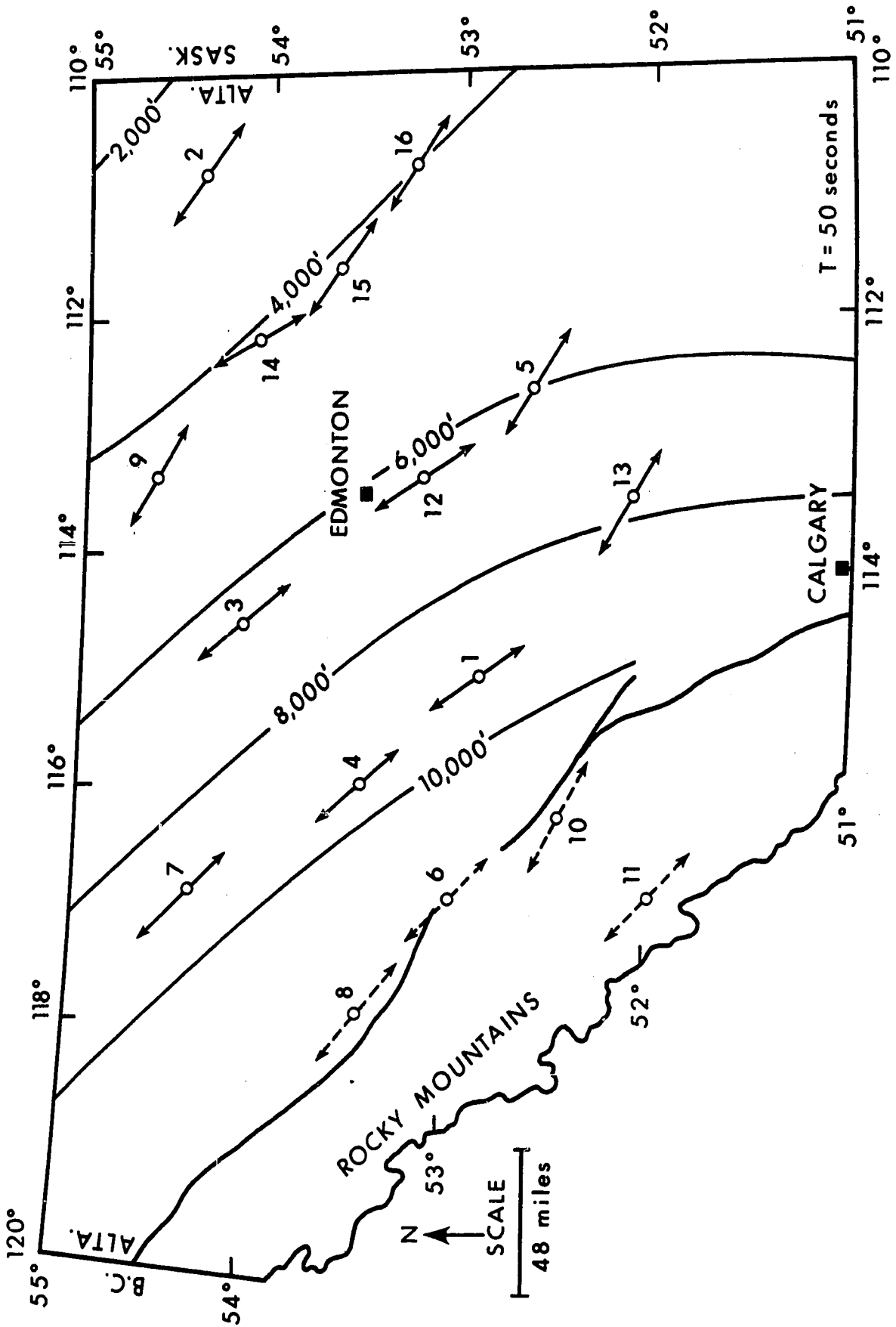
to a more complex geoelectric structure which also produces high skew values for these stations.

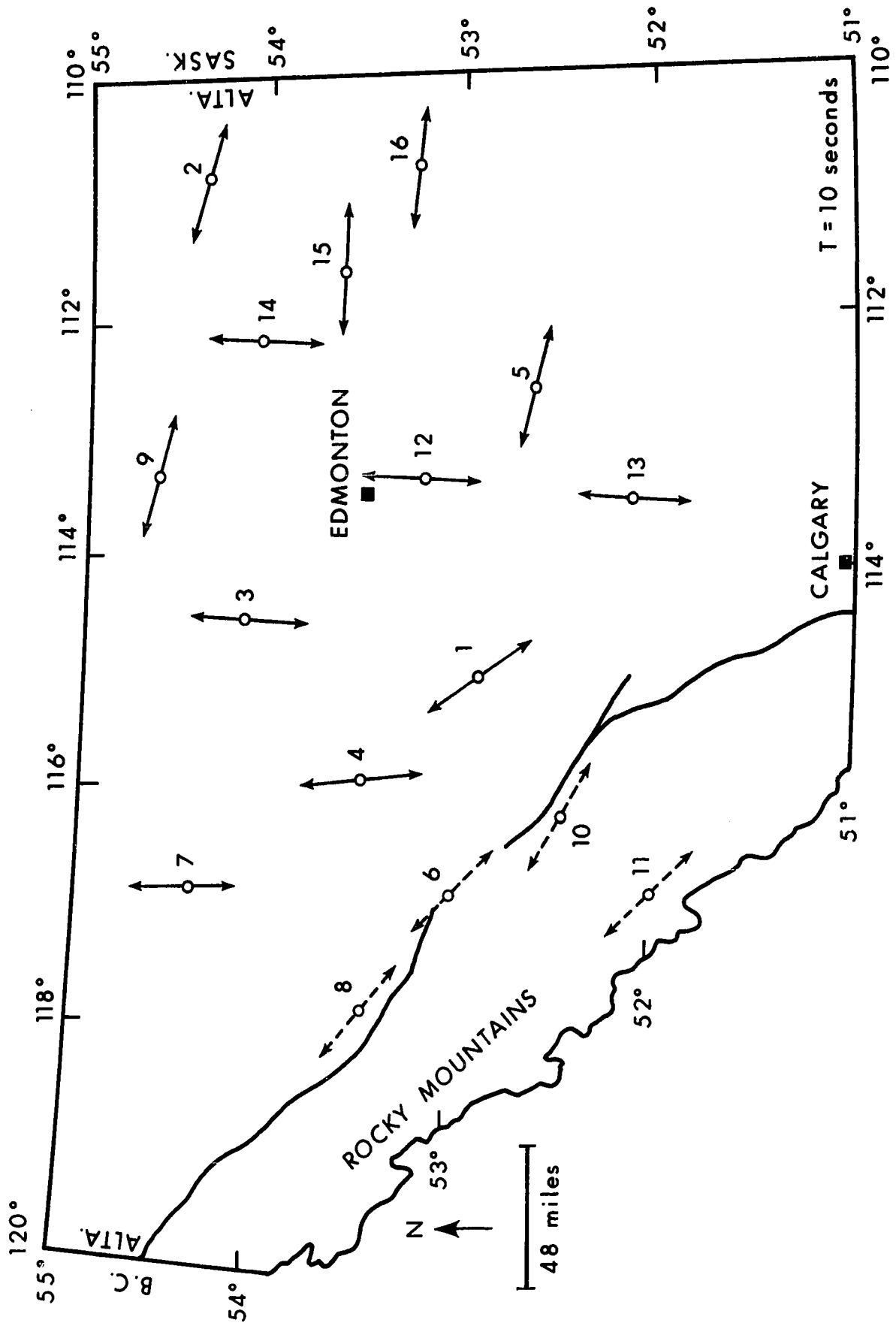
The anisotropy observed in the tensor apparent resistivity curves at each site may be due to 1) the anisotropy in the rocks below the sounding site and/or 2) lateral inhomogeneity due to structure, such as the one shown in Fig. 5.7. Anisotropies of various degrees have been observed in sedimentary rocks (Keller, 1968), but the existence of such anisotropies in igneous rocks is doubtful. According to Rankin and Reddy (1969) a resistivity contrast of 1 to 100 along the principal directions would be necessary in the basement and sub-basement rocks to explain observed anisotropies in central Alberta. It is most unlikely that the anisotropy shown by the apparent resistivity curves is due to the local anisotropy in true resistivity.

For the second alternative it will be useful to recall that for most of the stations in the plains, the skew values (<0.2) are consistent with a two-dimensional structure, which will be assumed that one that is presented in Fig. 5.7. In Fig. 5.8 are plotted the directions of maximum apparent resistivity for three periods, 200, 50 and 10 seconds. For the mountain stations the average angle of polarization of the

Figure 5.8: Directions of maximum tensor apparent resistivity for the central Alberta stations. (dashed arrows represent the polarization angles for telluric field).







telluric field is plotted, since no reliable apparent resistivity curves exist. These directions are approximately parallel to the strike for 200 and 50 second periods, and hence the curves of maximum and minimum resistivity can be associated with the electric and magnetic field polarizations respectively. The two southern most stations at Red Deer (13) and Donalda (5) are probably influenced by the Sweetgrass Arch (Fig. 5.6). For the 10 second period it can be seen that the results are scattered but the prevailing directions are close to the measuring directions which is consistent with an isotropic upper section (sedimentary) of the model.

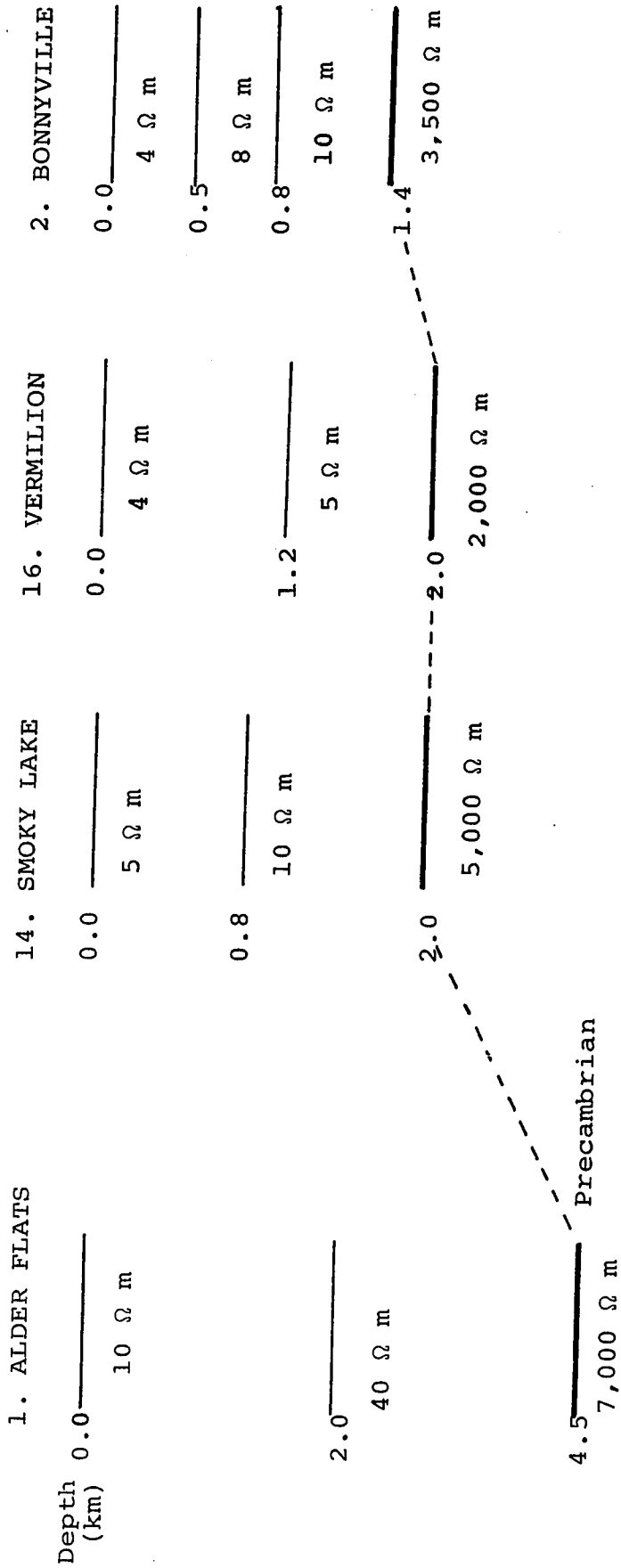
The two-dimensional example of Patrick and Bostick (1969) (Section 2.5) and also the work of Swift (1967), and Wright (1970), show that near surface geoelectric structures affect the H-polarization apparent resistivity curves even at very long periods (tens of thousands of seconds). However, in the results presented here the effect is limited to a few thousand seconds after which the apparent resistivity curves for H- and E-polarization tend to converge and approach asymptotically to the resistivities of bottom layers. Magnetotelluric measurements at longer periods are necessary to validate the above statement. Unfortunately no computational

results are available for the type of model presented in Fig. 5.7, except for some preliminary work by Peeples (personal communication) which demonstrates that this type of model yields apparent resistivities similar to the one presented in this thesis.

Lateral inhomogeneity in the case of E-polarization has less effect on the apparent resistivity curves than in the case for H-polarization. The curves for E-polarization may give an approximately valid vertical conductivity structure at a given site. Hence, an attempt is made to interpret E-polarization curves in terms of depth to the basement and resistivities of the basement and sedimentary rocks.

A one-dimensional model was derived for each of the four sounding sites, viz., Alder Flats (1), Bonnyville (2), Smoky Lake (14) and Vermilion (16). The depth to the basement is fairly well known for all the four sites. Well logs are available within a few miles of each of the sounding sites and these were used to check the thickness and the resistivities of the sedimentary layers. There are very thin highly resistive layers in the sedimentary section, but a study of various one-dimensional models with layers of various thickness and resistivities showed that the effect

Figure 5.9: One-dimensional models for four magnetotelluric sounding sites in central Alberta.

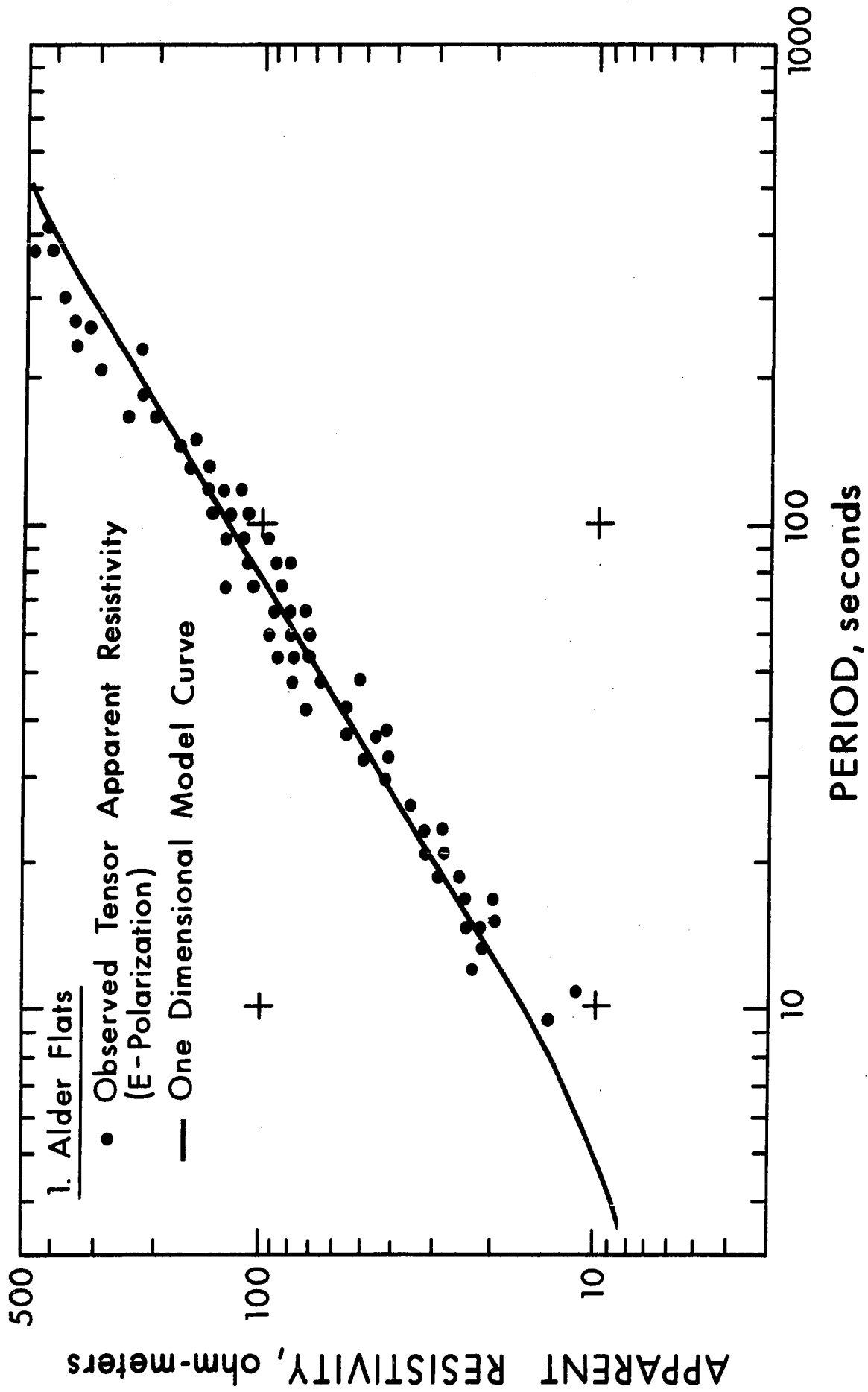


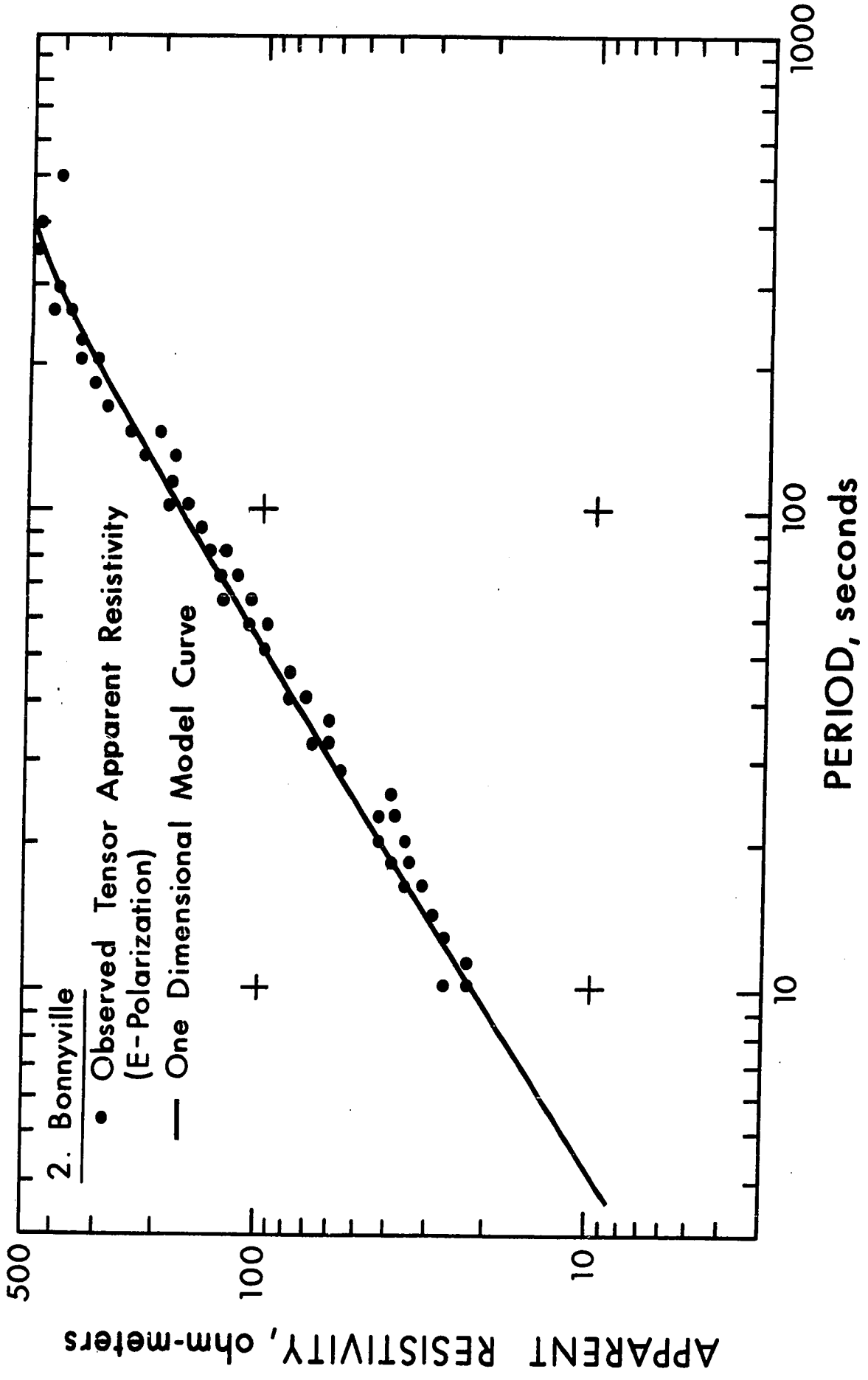
of thin layers such as are present in central Alberta is insignificant in comparison with the scatter in the data.

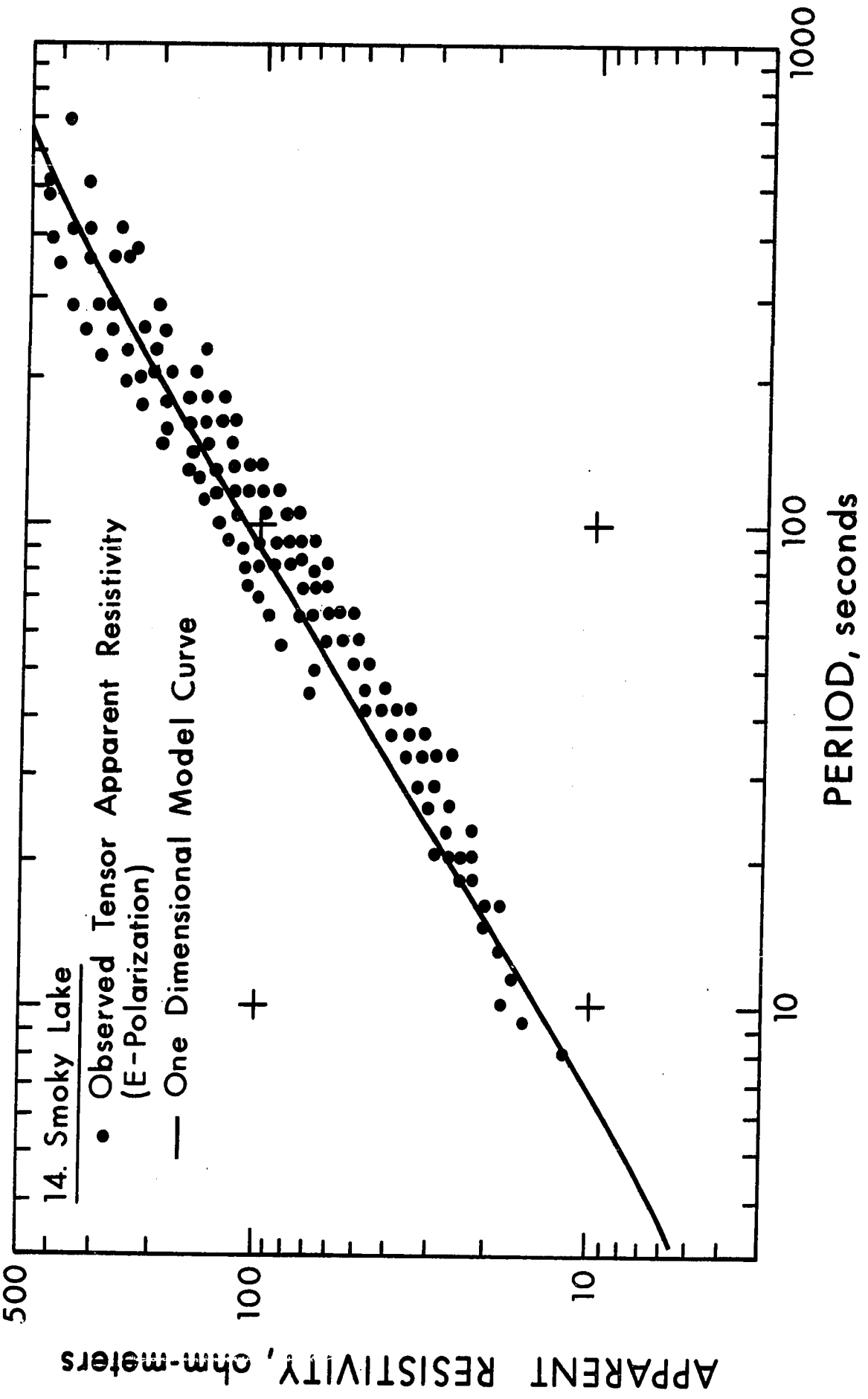
Several one-dimensional models were constructed for each site in order to match by trial and error to the observed tensor apparent resistivities for the E-polarization. Application of computer graphics, which has been tried at some stages of interpretation, or adopting inverse techniques will reduce the labour in obtaining a proper model. The one-dimensional models which gave curves in good agreement with the observed data for all the four stations are presented in Fig. 5.9. The model curves and the observed data are presented in Fig. 5.10.

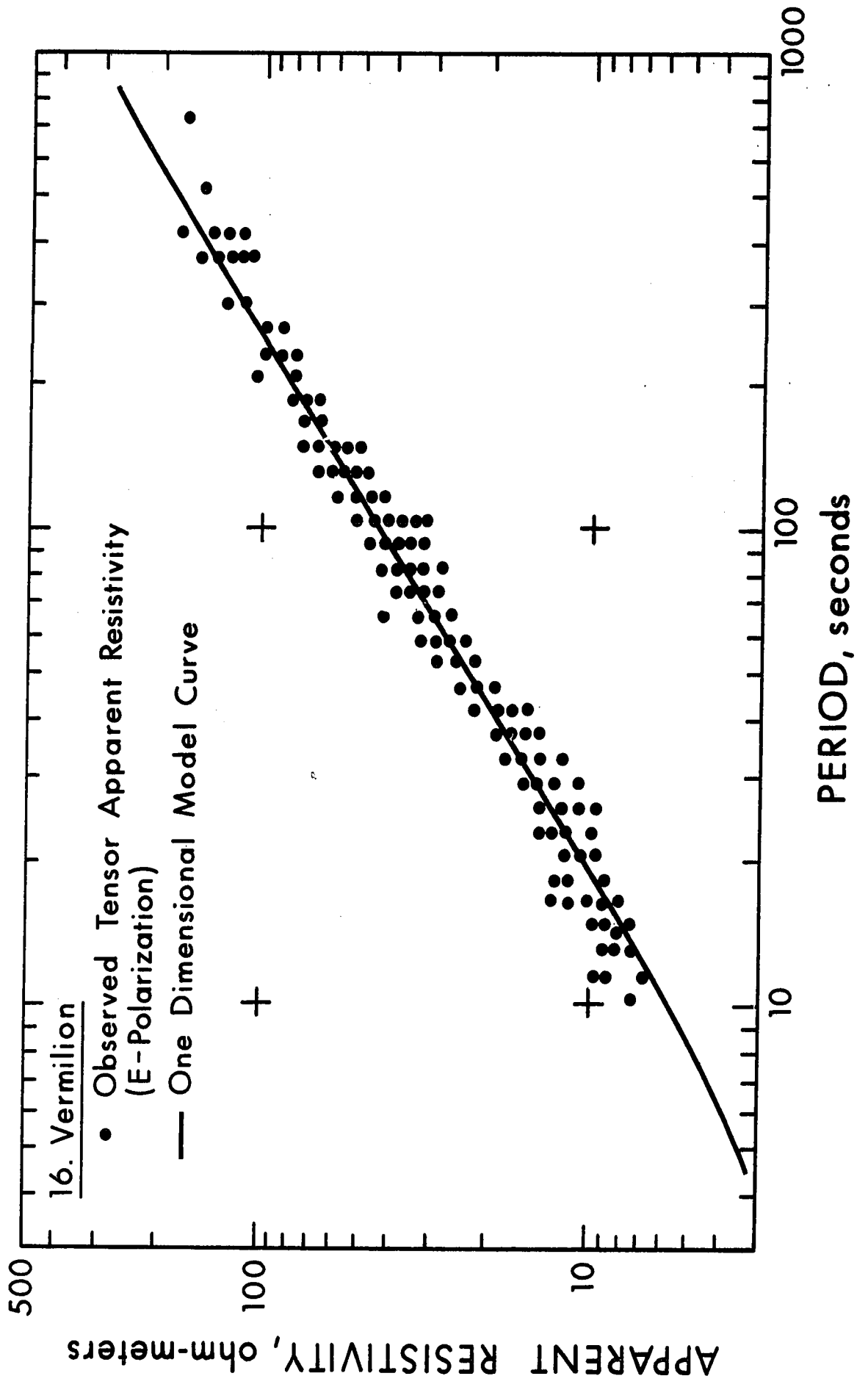
The models yielded a low resistive sedimentary section for Smoky Lake (14), Vermilion (16) and Bonnyville (2) and a more highly resistive sedimentary section for Alder Flats (1). This result is consistent with the well log data. The low resistivity for sedimentary column for Smoky Lake, Vermilion and Bonnyville may be due to relatively thin or absent Cambrian, Devonian and Mississippian formations, in these regions. The basement depths are read from well logs and used as invariant quantities in constructing models for each site. The different values for basement resistivities

Figure 5.10: One-dimensional model apparent resistivity curves and the observed apparent resistivity curves for E-polarization, for four magnetotelluric sounding sites in central Alberta.









at different locations may be due to lithological variations in the basement. Garland and Burwash (1959) predicted from gravity studies that these lithological variations extend up to 8 km in the basement.

The magnetotelluric data and the one-dimensional models presented here, validates the application of the magnetotelluric method for studying the basement profile as well as for studying local and regional geoelectric structures. The magnetotelluric theory for a layered earth model show that the results presented in Fig. 5.9 are not unique and the work on the effect of lateral inhomogeneities show that the apparent resistivity estimates for E-polarization cases will be greater than for one-dimensional models (see the examples in Section 2.5). If the magnetotelluric fields are affected to a significant extent by the lateral inhomogeneity of the type shown in Fig. 5.7, the basement and crustal resistivities must be lower than those obtained from one-dimensional theory.

5.2 Summary

The magnetotelluric results in central Alberta are affected by the geometry of the sedimentary basin and adjacent Rocky Mountains. The apparent resistivities for shorter periods, corresponding to a skin depth in the sediments, display no obvious anisotropy, indicating that the sedimentary section is free from both microscopic anisotropies and lateral inhomogeneities.

The varying degree of anisotropy from station to station may be due to local variations in basement composition and structure. The inconsistent results obtained in the Rocky Mountains are probably due to complexity in the local geology. An interpretation of these results will require further knowledge of the effects of three dimensional structure on magnetotelluric fields.

While a non-plane wave type source may contribute to the vertical component of the magnetic field, H_z , the high coherencies between H_z and the horizontal components of the magnetotelluric fields, particularly with telluric field components, indicates that H_z is a secondary, induced field and the plane wave approximation is valid.

For one-dimensional models deduced for the four stations, shown in Fig. 5.9 on the basis of E-polarization results, are consistent with the geological data, although these models are not unique. No evidence for a highly conducting layer corresponding to low velocity layer in the upper mantle is obtained from results of this work.

5.3 Suggestions for Future Work

The results of this work indicate that the magnetotelluric method has considerable potential for studying regional geoelectric structure as well as for mapping the basement in a sedimentary basin. An extension in the frequency would be most valuable for achieving this potential.

Present day modelling techniques for two-dimensional structures are computationally too expensive, for trial and error interpretation of magnetotelluric data. Hence, less expensive two-dimensional modelling techniques as well as knowledge of the effect of three-dimensional geoelectric structures on magnetotelluric fields, might make the magnetotelluric method an important tool in geophysical exploration.

The results presented here indicate that a study of source fields and the effect of complex geoelectrical structures on plane and non-plane wave sources are essential to the development of interpretation.

BIBLIOGRAPHY

- Adam, A., 1969, Appearance of the electrical inhomogeneity and anisotropy in the results of the complex electrical exploration of the Carpathian basin: Acta Geodaet., Geophys. et Montanist. Acad. Sci. Hung., Tomus 4, 187-197.
- Basham, P. W., 1967, Time domain studies of short period teleseismic P phases: Ph.D. thesis, University of British Columbia.
- Bendat, J. S., and A. G. Piersol, 1966, Measurements and analysis of Random Data: John Wiley & Sons, Inc., New York.
- Bingham, C., M. D. Godfrey and J. W. Tukey, 1967, Modern techniques of power spectrum estimation: IEEE Transactions on Audio and Electroacoustics, AU-15, 56-66.
- Blackman, R.B., and J. W. Tukey, 1958, The measurement of Power Spectra: Dover Publications, New York.
- Blake, J. R., and D. Swift, 1967, The magnetotelluric coast effect near a dyke or long promontory: Report No. UAGR-203, University of Alaska.

- Bostick, F. X., Jr., and H. W. Smith, 1962,
Investigation of large scale inhomogeneities
in the earth by the magnetotelluric method,
Proc. IRE, 50, 2339-2346.
- Burwash, R. A., 1957, Reconnaissance of surface of
Precambrian of Canada: Bull. Am. Assoc.
Petrol. Geologists, 41, 70-103.
- Burwash, R. A., 1965, Basement architecture of
Western Canada: Alta. Soc. Petrol. Geologists,
15th Annual Field Conference Guide Book.
280-288.
- Cagniard, L., 1953, Basic theory of magnetotelluric
method of geophysical prospecting: Geophysics,
18, 605-635.
- Campbell, W. H., 1966, A review of the equatorial
studies of rapid fluctuations in the earth's
magnetic field: Ann. Geophys. 22, 492-501.
- Campbell, W. J.; 1967, Geomagnetic pulsations: in
Physics of Geomagnetic Phenomena, Academic
Press, New York.
- Cantwell, T., 1960, Detection and analysis of low
frequency magnetotelluric signals: Ph.D.
thesis, M.I.T.
- Chetaev, D. N., 1960, The determination of the
anisotropy coefficient and the angle of
inclination of a homogeneous anisotropic
medium, by measuring impedance of the natural
electromagnetic field: Bull. Acad. Sci. USSR,
Geophys. Ser. 4, 12, 407-408.

- Chetaev, D. N., 1966, On the inverse problem in the theory of magnetotelluric prospecting: Akademia Nauk SSSR, Physocs of the Solid Earth, No. 9, 610-611.
- Cumming, G. L., and E. R. Kanasewich, 1966, Crustal Structure in Western Canada: Final report for AFCRL-66-519, University of Alberta.
- d'Erceville, I., and G. Kunetz, 1962, The effect of a fault on the earth's natural electromagnetic field: Geophysics, 27, 651-655.
- Dosso, H. W., 1966, Analog model measurements for electromagnetic variations near faults and dykes: Can. J. of Earth Sciences, 3, 287-303.
- Fowler, R. A., B. J. Kotick, and R. D. Elliott, 1967, Polarization analysis of natural and artificially induced geomagnetic micro-pulsations. J. Geophys. Res., 72, 2871-2883.
- Garland, G. D., and M. E. Bower, 1959, Aeromagnetic anomalies in northeastern Alberta: Oil Week, June 19, 32-40.
- Garland, G. D. and R. A. Burwash, 1959, Geophysical and petrological study of Precambrian of central Alberta: Bull. Am. Assoc. Petrol. Geologists, 43, 790-806.

- Garland, G. D., and T. F. Webster, 1960, Studies of natural electric and magnetic fields: J. of Res., N.B.S. Radio Propagation, 64D, 405-408.
- Gentleman, W. M., and G. Sande, 1966, Fast Fourier Transform for fun and profit: Fall Joint Computer Conf., AFIPS Proc., 29, 563-578.
- Haites, T., 1960, Trascurrent faults in Western Canada: Alberta Soc. Petrol. Geologists Jour., 8, 33-78.
- Hopkins, A. H., and H. W. Smith, 1966, An investigation of magnetotelluric method for determining subsurface resistivities: Report No. 140, EERL., University of Texas.
- Jacobs, J. A., Y. Kato, S. Matsushita and V. A. Troitskaya, 1964, Classification of geomagnetic micropulsations: J. Geophys. Res. 69, 180-181.
- Jacobs, J. A., and K. Sinno, 1960, World-wide characteristics of geomagnetic micropulsations: Geophys. J., 3, 333-353.
- Jenkins, G. M., and D. G. Watts, 1968, Spectral analysis and its applications: Holden-Day, Inc., San Franscisco.
- Jones, F. W., and A. T. Price, 1970a, The peturbations of alternating geomagnetic fields by conductivity anomalies: Geophys. J. (in press).

- Jones, F. W., and A. T. Price, 1970b, Geomagnetic effects of sloping and shelving discontinuities of earth conductivity: Geophysics (in press).
- Kanasewich, E. R., 1966, Deep crustal structure under the plains and Rocky Mountains: Can. J. Earth Sciences, 3, 937-945.
- Kato, Y., and T. Kikuchi, 1950, On the phase difference of the earth currents induced by changes of the earth's magnetic field: Parts I and II, Science Reports of Tohoku University, Series 5, Geophysics, 2, 139-145.
- Keller, G. V., 1968, Electrical prospecting for oil: Quarterly of the Colorado School of Mines, Vol. 63.
- Kovtun, A. A., 1961, The magnetotelluric investigation of structures inhomogeneous in layers: Bull. Acad. Sci. USSR, Geophys. Ser., 1085-1087.
- Kovtun, A. A. and N. D. Chicherina, 1969, Results of magnetotelluric studies in the Mid-Russian depression: in Magnetotelluric methods of structure studies of the earth's crust and upper mantle, Publishing House "NAUKA", Moscow.

- Madden, T. R., and P. Nelson, 1964, A defence of Cagniard's magnetotelluric method: Project NR-371-401, Geophysics Laboratory, M.I.T.
- Madden, T. R., and C. M. Swift, Jr., 1969, Magnetotelluric studies of the electrical conductivity structure of the crust and upper mantle: in *The earth's crust and upper mantle*, Geophysical monograph 13, Am. Geophys. Union, 469-479.
- Mann, J. E., 1965, The importance of anisotropic conductivity in magnetotelluric interpretation: *J. Geophys. Res.*, 70, 2940-2942.
- McCrossan, R. G., and R. P. Glaister, 1966, *Geological history of Western Canada: Alta. Soc. Petrol. Geologists, Calgary, Alberta.*
- Morrison, H. F., E. Wombell, and S. H. Ward, 1968, Analysis of earth impedances using magnetotelluric fields: *J. Geophys. Res.*, 73, 2769-2778.
- Nabetani, S., and D. Rankin, 1969, An inverse method of magnetotelluric analysis for a multilayered earth: *Geophysics*, 34, 75-86.
- Neves, A. S., 1957, *The magnetotelluric method in two-dimensional structures: Ph.D. thesis, M.I.T.*
- Niblett, E. R., and C. Sayn-Wittgenstien, 1960, Variations of electrical conductivity with depth by the magnetotelluric method: *Geophysics*, 25, 998-1008.

- O'Brien, D. P., and H. F. Morrison, 1967, Electro-magnetic fields in an n-layer anisotropic half-space: *Geophysics*, 32, 668-677.
- Parzen, E., 1961, Mathematical considerations in the estimation of spectra: *Technometrics*, 3, 167-189.
- Patrick, F. W., and F. X. Bostick, Jr., 1969, Magnetotelluric modeling techniques: Report No. 59, Electronics Research Center, The University of Texas at Austin.
- Paulson, K. V., 1968, The polarization and spectral characteristics of some high-latitude irregular pulsations: *Ann. Geophys.*, 24, 261-266.
- Peeples, W. J., 1969, Magnetotelluric profiling over a deep structure: Ph.D. thesis, University of Alberta.
- Pokityanski, I. I., 1961, On the application of the magnetotelluric method to anisotropic and inhomogeneous masses: *Bull. Acad. Sci. USSR, Geophys. Ser.*, 1050-1053.
- Price, A. T., 1962, The theory of the magnetotelluric method when source field is considered: *J. Geophys. Res.*, 67, 1907-1918.

- Praus, O., and V. Petr, 1969, Magnetotelluric calculations for the interaction of polarized fields with anisotropic layered media: *Can. J. of Earth Sciences*, 6, 759 - 769.
- Rankin, D., 1962, The magnetotelluric effect of a dyke: *Geophysics*, 27, 666-676.
- Rankin, D., G. D. Garland and K. Vozoff, 1965, An analog model for the magnetotelluric effect, *J. Geophys. Res.*, 70, 1939-1945.
- Rankin, D., and R. D. Kurtz, 1970, A statistical study of micropulsations polarizations: *J. Geophys. Res.* (in press).
- Rankin, D., and I. K. Reddy, 1969, A magnetotelluric study of resistivity anisotropy: *Geophysics*, 34, 438-449.
- Rankin, D., and I. K. Reddy, 1970, Polarization of the magnetotelluric fields over an anisotropic earth: *PAGEOPH*, 78, 58-65.
- Raspopov, O. M., 1968, Possible excitation mechanism of type Pi2 geomagnetic field pulsations: *Geomagn. and Aeronomy*, 8, 257-260.
- Richards, T. D., and D. J. Walker, 1959, Measurement of the thickness of the earth's crust in the Albertan plains of Western Canada: *Geophysics*, 24, 262-284.

- Rikitake, T., 1950, Electromagnetic induction within the earth and its relation to the electrical state of the earth's interior: Bull. Earthq. Res. Inst. Tokyo, 28, 45-98.
- Rikitake, T., 1951, Changes in earth currents and their relation to the electrical state of the earth's crust. Bull. Earthq. Res. Inst., Tokyo, 29, 270-275.
- Sims, W. E. and F. X. Bostick, Jr., 1969, Methods of magnetotelluric analysis: Report No. 58, Electronics Research Center, The University of Texas at Austin.
- Sinha, A. J., 1969, The magnetotelluric effect in an inhomogeneous and anisotropic earth: Geoprospection 7, 9-28.
- Srivastava, S. P., 1965, Methods of interpretation of magnetotelluric data when source field is considered, J. Geophys. Res., 70, 945-954.
- Srivastava, S. P., and J. A. Jacobs, 1964, Determination of the resistivity distribution at Meanook, Alberta, Canada, by the magnetotelluric method: J. Geomag. Geoelect., 15, 280-288.

- Srivastava, S. P., J. L. Douglass and S. H. Ward,
1963, The application of magnetotelluric and
telluric methods in central Alberta:
Geophysics, 28, 998, 1008.
- Swift, C. M., Jr., 1967, A magnetotelluric inves-
tigation of an electrical conductivity
anomaly in the Southwestern United States,
Ph.D. thesis, M.I.T.
- Takacs, E., 1969, The orientation of the magneto-
telluric impedance ellipses: Acta Geodaet.,
Geophys. et Montanist. Acad. Sci. Hung,
Tomus 4, 415-423.
- Tikhonov, A. N., 1950, Determination of the electrical
characteristics of deep layers of the
earth's crust, Dok. Akad. Nauk., USSR, 73,
295-297.
- Tikhonov, A. N. and M. N. Berdichevskii, 1966,
Experience in the use of magnetotelluric
methods to study the geologic structure of
sedimentary basins: Bull. Acad. Sci., USSR,
Earth Physics, 93-97.
- Van'yan, L. L., and K. Yu. Zybin, 1967, The effect
of geoelectric inhomogeneities on the
polarization of geomagnetic micropulsations.
Bull. Acad. Sc. USSR, Earth Physics, 804-808.

- Volker, H., 1968, Observations of geomagnetic pulsations Pc3, 4 and Pi2 at different latitudes: *Ann. Geophys.*, 24, 245-252.
- Vozoff, K., R. M. Ellis, and M. D. Burke, 1964, Telluric currents and their use in petroleum exploration: *Bull. Am. Assoc. Petrol. Geologists*, 48, 1890.
- Vozoff, K., H. Hasegawa, and R. M. Ellis, 1963, Results and limitations of magnetotelluric surveys in simple geologic situations: *Geophysics*, 28, 778-792.
- Vozoff, K., A. Orange and H. S. Lahman, 1969, Magnetotelluric deep earth resistivity at eight U.S. "Type-locations": Report No. RU68011, Geoscience Incorporated, Cambridge, Massachusetts.
- Wait, J. R., 1954, On the relation between telluric currents and the earth's magnetic field: *Geophysics*, 19, 281-285.
- Wait, J. R., 1962, *Electromagnetic waves in stratified media*: Pergamon Press, Inc., New York.
- Weaver, J. T., The electromagnetic field within a discontinuous conductor with reference to geomagnetic micropulsations near a coast line, *Can.J.Phys.*, 41, 484-495.

- Wiese, H., 1962, Geomagnetische Tiefemtellurik, Teil I, Geofisica Pura E. Applicata, 51, 59-78.
- Wright, J. A., 1969, The magnetotelluric and geomagnetic response of two-dimensional structures: GAMMA, 7, Inst. Geophysik Meteorologie, Tech. Univ. Braunschweig.
- Wright, J. A., 1970, Anisotropic apparent resistivities arising from non-homogeneous two-dimensional structures: Can.J. of Earth Sciences, 7, 527-531.
- Wu, F. T., 1968, The inverse problem of magnetotelluric sounding: Geophysics, 33, 972-979.
- Zybin, K. Yu., 1967, On the polarization characteristics of middle latitude geomagnetic pulsations: Indian J. of Met. and Geophys. 18, 349-354.

APPENDIX I

The magnetic and electric field components in the m^{th} layer (2.3-4) can be expressed in matrix form, as

$$[F_m] = [A_m] [C_m] ,$$

where column vectors $[F_m]$ and $[C_m]$, and the 4×4 matrix $[A_m]$ are defined as

$$[F_m] = \begin{bmatrix} H_{x,m} \\ H_{y,m} \\ E_{x,m} \\ E_{y,m} \end{bmatrix} , \quad [C_m] = \begin{bmatrix} A_{1,m} \\ B_{1,m} \\ A_{2,m} \\ B_{2,m} \end{bmatrix}$$

$$[A_m] = \begin{bmatrix} a_{11,m} & a_{12,m} & a_{13,m} & a_{14,m} \\ \vdots & & & \vdots \\ a_{41,m} & \text{---} & \text{---} & a_{44,m} \end{bmatrix}$$

and the elements of $[A_m]$ are:

$$a_{11,m} = \exp(-k_{2,m} \delta_m) \cos \theta_m , \quad a_{12,m} = \exp(k_{2,m} \delta_m) \cos \theta_m$$

$$a_{13,m} = -\exp(-k_{1,m} \delta_m) \sin \theta_m , \quad a_{14,m} = -\exp(k_{1,m} \delta_m) \sin \theta_m$$

$$a_{21,m} = \exp(-k_{2,m} \delta_m) \sin \theta_m , \quad a_{22,m} = \exp(k_{2,m} \delta_m) \sin \theta_m$$

$$a_{23,m} = \exp(-k_{1,m} \delta_m) \cos \theta_m , \quad a_{24,m} = \exp(k_{1,m} \delta_m) \cos \theta_m$$

$$a_{31,m} = \frac{k_{2,m}}{\sigma_{2,m}} a_{21,m} \quad a_{32,m} = \frac{k_{2,m}}{\sigma_{2,m}} a_{22,m}$$

$$a_{33,m} = \frac{k_{1,m}}{\sigma_{1,m}} a_{23,m} \quad a_{34,m} = \frac{-k_{1,m}}{\sigma_{1,m}} a_{24,m}$$

$$a_{41,m} = \frac{-k_{2,m}}{\sigma_{2,m}} a_{11,m} \quad a_{42,m} = \frac{k_{2,m}}{\sigma_{2,m}} a_{12,m}$$

$$a_{43,m} = \frac{-k_{1,m}}{\sigma_{1,m}} a_{13,m} \quad a_{44,m} = \frac{k_{1,m}}{\sigma_{1,m}} a_{14,m}$$

and $\delta_m = z - z_{m-1}$.

At the boundary, $z = z_m$ the tangential components of electric and magnetic fields are equal and thus:

$$[\Lambda_m]_{z=z_m} [C_m] = [\Lambda_{m+1}]_{z=z_m} [C_{m+1}]$$

The elements of the matrix $[\Lambda_{m+1}]$ are similar to the elements of $[\Lambda_m]$, but with subscripts $m+1$. At $z=z_m$,

$$\delta_m (=z-z_{m-1}) \rightarrow 0.$$

The coefficient vector $[C_m]$ in the m^{th} layer is now written as:

$$[C_m] = [A_m]_{z=z_m}^{-1} [A_{m+1}]_{z=z_m} [C_{m+1}]$$

$$= [X_m] [C_{m+1}]$$

$$\text{where } [X_m] = [A_m]_{z=z_m}^{-1} [A_{m+1}]_{z=z_m}$$

Applying the boundary conditions at each horizontal interface, the coefficient vector $[C_1]$, in the first layer can be written as:

$$[C_1] = [R] [C_{n+1}] \quad (A1)$$

where $[C_{n+1}]$ is the coefficient vector in the $(n+1)^{\text{th}}$ layer and

$$[R] = [X_1] [X_2] [X_3] \dots [X_n].$$

Since the $(n+1)^{\text{th}}$ layer is assumed to be of infinite thickness, the coefficients $\beta_{1,n+1}$ and $\beta_{2,n+1} \rightarrow 0$, and

$$[C_{n+1}] = \begin{bmatrix} A_{1,n+1} \\ 0 \\ A_{2,n+1} \\ 0 \end{bmatrix}$$

Expanding (A1), one gets:

$$\begin{array}{lll} A_{1,1} = r_{11} & A_{1,n+1} + r_{13} & A_{2,n+1} \\ B_{1,1} = r_{21} & A_{1,n+1} + r_{23} & A_{2,n+1} \\ A_{2,1} = r_{31} & A_{1,n+1} + r_{33} & A_{2,n+1} \\ B_{2,1} = r_{41} & A_{1,n+1} + r_{43} & A_{2,n+1} \end{array}$$

where

$A_{1,1}$, $B_{1,1}$, $A_{2,1}$ and $B_{2,1}$ are the coefficients in the first layer and r_{11} , r_{21} , r_{41} and r_{43} are the elements of the matrix [R], which are dependent on geometrical and electrical properties of the layers.

APPENDIX II
SPECTRAL ANALYSIS

The formulae used to compute the auto and cross power spectral density estimates are summarized here. Detailed derivation of these formulae can be obtained from Blackman and Tukey (1958), Bendat and Piersol (1966), Gentleman and Sande (1966), Bingham et al. (1967), and Jenkins and Watts (1967).

Consider a sample record $x(t)$ of finite length T , with N , even numbers of equally sampled points and Δ the time interval between two successive points. The transformed data values are then given by

$$x_n = x(n\Delta) \quad n = 1, 2, \dots, N$$

For any point t in the interval $(0, T)$ one obtains by Fourier series representation

$$x(t) = A_0 + \sum_{k=1}^{N/2} A_k \cos \frac{2\pi kt}{T} + \sum_{k=1}^{N/2-1} B_k \sin \frac{2\pi kt}{T},$$

and for n^{th} sampled point

$$x_n = x(n\Delta) = A_0 + \sum_{k=1}^{n/2} A_k \cos \frac{2\pi kn\Delta}{N} + \sum_{k=1}^{N/2-1} B_k \sin \frac{2\pi kn\Delta}{N}$$

$$B_k \sin \frac{2\pi kn\Delta}{N}$$

The coefficients A_k and B_k are given by

$$A_0 = \frac{1}{N} \sum_{n=1}^N x_n = \bar{x} = 0$$

$$A_k = \frac{2}{n} \sum_{n=1}^N x_n \cos \frac{2\pi kn\Delta}{N} \quad k = 1, 2, \dots, \frac{N}{2}-1$$

$$A_{N/2} = \frac{1}{N} \sum_{n=1}^N x_n \cos \pi n\Delta$$

$$B_k = \frac{1}{N} \sum_{n=1}^N x_n \sin \frac{2\pi kn\Delta}{N} \quad k = 1, 2, \dots, \frac{N}{2} - 1.$$

The estimated (raw) autocorrelation function at the displacement $T = r\Delta$ is defined by the formula

$$\hat{R}_x(\tau) = \hat{R}_x(r\Delta) = \frac{1}{N} \sum_{n=1}^{N-r} x_n x_{n+r} \quad r = 0, 1, 2, \dots, m$$

where $\tau = r\Delta$, r is the lag number and m is the maximum lag number. \hat{R}_x is the raw estimate of true autocorrelation R_x . The autocorrelation function may take on negative as well as positive values of τ , and

$$R_x(-\tau) = R_x(\tau).$$

A normalized value of autocorrelation function is obtained by dividing $\hat{R}_x(\tau)$ by $\hat{R}_x(0)$, where

$$\hat{R}_x(0) = \frac{1}{N} \sum_{n=1}^N (x_n)^2 = x^2$$

The autocorrelation functions can be computed more efficiently from the Fourier transforms using the relationship (Gentleman and Sande, 1966)

$$\hat{R}_x(r) = \frac{1}{N} C(r)$$

$$C(r) = \sum_{n=1}^N x(r) x(n-r) = \frac{1}{N} \sum_{k=1}^N X^*(k)$$

$$X(k) \exp\left(\frac{2\pi ikr}{N}\right)$$

where X is the Fourier transform of $x(t)$ and $*$ implies complex conjugate.

Power spectral density estimates

The power spectral density estimates can be obtained from the correlation function

$$S_x(f) = \int_{-\infty}^{\infty} R_x(r) \exp(-2\pi ifr) dr \quad -\infty < f < \infty$$

Since only the positive frequencies are of physical interest, the physically realizable spectrum is defined as two times $S_x(f)$ for positive frequencies only. For discrete case

$$\hat{P}_X(f) = 2\Delta \left[\hat{R}_x(0) + 2 \sum_{r=1}^{m-1} \hat{R}_x(r) \cos\left(\frac{\pi r f}{f_c}\right) + \right.$$

$$\left. \hat{R}_x(m) \cos\left(\frac{\pi m f}{f_c}\right) \right] \quad 0 \leq f \leq f_c$$

where $f_c = \frac{1}{2\Delta}$, Nyquist frequency,

and $f = \frac{k f_c}{m} \quad k = 0, 1, 2, \dots, m.$

k is the frequency index also called the harmonic number. We can also write \hat{P}_X as a function of frequency index

$$\hat{P}_X(k) = 2\Delta \left[\hat{R}_x(0) + 2 \sum_{r=1}^{m-1} \hat{R}_x(r) \cos\left(\frac{\pi r k}{m}\right) + \right.$$

$$\left. (-1)^k \hat{R}_x(m) \right]$$

Smoothed power spectral estimates can be obtained by multiplying correlation function with appropriate weighting function. The smoothed spectral estimates are written as

$$PX(k) = 2\Delta [R_x(0) + 2 \sum_{r=1}^{m-1} R_x(r) D(r) \cos \frac{\pi rk}{m}]$$

where $D(r)$ is any lag window. The Parzen (1961) lag window with the weighting functions

$$\begin{aligned} D(r) &= 1 - 6 \left(\frac{r}{m}\right)^2 + \left(\frac{6|r|}{m}\right)^3 & |r| &= 0, 1, \dots, \frac{m}{2} \\ &= 2 \left(1 - \left[\frac{|r|}{m}\right]^3\right) & |r| &= \frac{m}{2} + 1, \dots, m \\ &= 0 & |r| &> m \end{aligned}$$

is used in this thesis.

Cross power spectral density estimates

Consider a second record $y(t)$ of the same length as $x(t)$ with same number of sampled points and same sampling interval. The sampled cross correlation functions of $x(t)$ and $y(t)$ are defined as

$$\hat{R}_{xy}(r) = \frac{1}{N} \sum_{n=1}^{n-r} x_n y_{n+r}$$

$$\hat{R}_{yx}(r) = \frac{1}{N} \sum_{n=1}^{n-r} y_n x_{n+r}$$

In terms of the convolution,

$$\hat{R}_{xy}(r) = \frac{1}{N} C_{xy}(r)$$

where $C_{xy}(r)$, the convolution of $x(t)$ with $y(t)$, and is defined as

$$C_{xy}(r) = \sum_{A=1}^N x(r) y(n-r)$$

$$= \frac{1}{N} \sum_{k=1}^N X^*(k) Y(k) \exp\left(\frac{2\pi i n k}{N}\right) .$$

By the odd symmetry of cross correlation function

$$R_{xy}(r) = R_{yx}(-r) = R_{xy}^*(-r).$$

The even and odd parts of the cross correlation function as

$$A_r = \frac{1}{2} [R_{xy}(r) + R_{yx}(r)] \quad \text{even.}$$

$$B_r = \frac{1}{2} [R_{xy}(r) - R_{yx}(r)] \quad \text{odd.}$$

Cross power spectral density $P_{XY}(f)$ is a complex function,

$$P_{XY}(f) = C_{XY}(f) - i Q_{XY}(f)$$

where $C_{XY}(f)$ is called co-spectral density function and $Q_{XY}(f)$ is called the quadrature spectral density function. The raw estimates of co- and quadrature spectral density functions are

$$\hat{C}_{XY}(k) = 2\Delta \left[A_0 + 2 \sum_{r=1}^{m-1} A_r \cos\left(\frac{\pi r k}{m}\right) + (-1)^k A_m \right]$$

$$\hat{Q}_{XY}(k) = 4\Delta \sum_{r=1}^{m-1} B_r \sin\left(\frac{\pi r k}{m}\right)$$

and the smoothed estimates are

$$CXY(k) = 2\Delta \left[A_0 + 2 \sum_{r=1}^{m-1} A_r D(r) \cos \left(\frac{\pi rk}{m} \right) \right]$$

$$QXY(k) = 4\Delta \sum_{r=1}^{m-1} B_r D(r) \sin \left(\frac{\pi rk}{m} \right)$$

where $D(r)$ is the lag window. The smoothed cross amplitude spectrum estimate is

$$AXY(f) = [CXY(f) + QXY(f)]^{1/2}$$

and the smoothed phase spectral estimate is

$$\phi_{XY}(f) = \tan^{-1} \left[\frac{QXY(f)}{CXY(f)} \right] .$$